PHOTOCALORIMETRY: DEVELOPMENT OF METHODS TO ASSESS THE PHOTOSTABILITY OF PHARMACEUTICAL COMPOUNDS

By

MEENA DHUNA

A THESIS SUBMITTED TO THE SCHOOL OF PHARMACY, UNIVERSITY OF LONDON IN PARTIAL FULFILMENT OF THE REQUIREMENTS FOR THE DEGREE OF DOCTOR OF PHILOSOPHY

THE SCHOOL OF PHARMACY
UNIVERSITY OF LONDON

JULY 2008

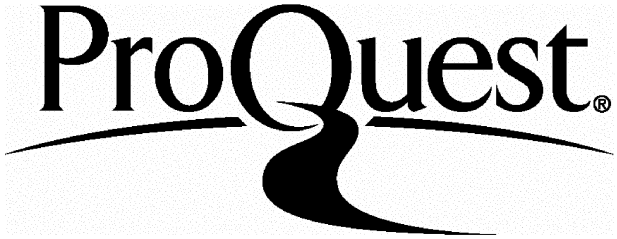

Declaration

This thesis describes research conducted in the School of Pharmacy, University of London, between 2004 and 2008 under the supervision of Dr. Simon Gaisford and Prof. Anthony Beezer. I certify that the research described is original and that any parts of the work that have been conducted by collaboration are clearly indicated. I also certify that I have written all the text herein and have clearly indicated by suitable citation any part of this dissertation that has already appeared in publication.

Meena Khurana. — 31st July 2008

Signature **Date**

Abstract

The main focus of the research presented in this thesis is to develop a robust and easy-to-use photocalorimeter to allow a quantitative assessment of the photostability of pharmaceutical compounds. As a result, a novel photocalorimeter was successfully developed. Initially a Xe-arc lamp was used as a light source, but this was found to be problematic, rendering quantitative analysis of data challenging. A novel approach using light-emitting diodes (LEDs) as a light source was developed; this approach demonstrated much potential in photostability testing. Using the prototype systems a suitable method to allow measurement of the radiant energy delivered to the sample during a photochemical process was investigated. The best system appeared to be the photodegradation of 2-nitrobenzaldehyde (2NB). Although promising as a test and reference reaction, it was found that 2NB was sensitive to non-photochemical processes and the reaction was complex which means further work on its application in this area must be undertaken.

The application of chemometric analysis as an approach to interpret complexity in Isothermal Calorimetric data was then studied. A three-step consecutive reaction was used to demonstrate the applicability of principal component analysis to determine the number of reaction steps and reaction parameters in a process.

The application of photocalorimetry for the study of a known photosensitive drug, nifedipine was investigated. The photolysis of nifedipine in solution was studied under full spectrum lighting and under specific wavelengths for the determination of causative wavelength (s). The data showed the photodegradation of nifedipine to be particularly sensitive at 360 nm. No significant photosensitivity was detected above 370 nm.

Finally a novel autobalance power supply, currently under development, designed to improve the performance of the photocalorimeter is described.

~ Acknowledgements ~

First and foremost I would like to express my deepest and heart-felt gratitude to my supervisors Dr. Simon Gaisford and Prof. Tony Beezer for their guidance, encouragement and inspiration throughout the course of this PhD project. I feel privileged to have had the opportunity to work with such high calibre academics and would like to thank them for all their support and providing me with opportunities to present my work at numerous international conferences.

I would also like to express my gratitude towards the following people who have contributed tremendously to this project; Prof. Joe Connor, Mr. David Clapham (GSK supervisor) and Dr. Mike O'Neill for their useful advice and informative discussions, Mr. John Frost for his engineering expertise in the construction of the optical assemblies, Mr. Chris Courtice for his electronics expertise in the development of the LED system, and GSK for financial support. Many thanks to my colleagues and friends; Diane, Fang, Hisham, Peng, Emma, Matt, Hala, Mo, Da, Tiago, Reshma and Ahmed for their many words of encouragement, particularly in times of despair and hurdles faced during my PhD.

I am forever indebted to the love, support and blessings of my dearest Mother and Father to whom I dedicate this PhD, for the hard work I have encountered over the past three years is insignificant to the many years of hard work they have endured with me during my studies. They have been the pinnacle of my strength throughout my studies and have always believed in me. Many thanks to all my family and a special thank you to the Sehdev family for their ample love and support.

Finally, I would like to thank my beloved fiancé Gagandeep Sehdev for his unconditional love, support and understanding. Thank you for your immense encouragement and for the countless times you have been there for me in every possible way, especially to share all the highs, and lows, experienced throughout this PhD. You are my perfect life partner and I truly love and respect you with all my heart. I look forward to sharing the rest of my life with you and to the start of a new beginning...

Meena Dhuna, July 2008

FOR MY PARENTS

All that I am, or hope to be, I owe to my angels – Mother and Father.

- Contents -

CHAPTER 1: INTRODUCTION

CHAPTER 2: PHOTOCALORIMETRY: DESIGN AND DEVELOPMENT

CHAPTER 3: ACTINOMETRY

CHAPTER 4: CHEMOMETRIC APPROACH TO COMPLEXITY

- List of Figures -

CHAPTER 1: INTRODUCTION

CHAPTER 2: PHOTOCALORIMETRY: DESIGN AND DEVELOPMENT

CHAPTER 3: ACTINOMETRY

CHAPTER 4: CHEMOMETRIC APPROACH TO COMPLEXITY

CHAPTER 5: APPLICATIONS

CHAPTER 6: SUMMARY AND FUTURE WORK

- List of Tables -

CHAPTER 1: INTRODUCTION

CHAPTER 2: PHOTOCALORIMETRY: DESIGN AND DEVELOPMENT

CHAPTER 3: ACTINOMETRY

CHAPTER 5: APPLICATIONS

- List of Abbreviations -

ΔH	Change in enthalpy
ΔS	Change in entropy
ΔG	Change in Gibbs free energy
ΔU	Change in internal energy
ϕ	Quantum yield
λ	Wavelength
[ ]	Concentration
2NB	2-nitrobenzaldehyde
API	Active Pharmaceutical Ingredient
A_0	Initial amount of reactable material
A	Cross-sectional area of solution exposed
c	Speed of light
DSC	Differential Scanning Calorimetry
dq/dt (Φ)	Thermal power
dx/dt	Rate of change in quantity of products
E_a	Activation energy
E_λ	Energy of a photon of wavelength λ
EDTA	Ethylenediamine tetraacetic acid
ESR	Electron Spin Resonance
Eqn.	Equation
Fig.	Figure
F_o	Photon flux
h	Hours

h	Planck's constant
HPLC	High Performance Liquid Chromatography
I_o	Irradiance
IC	Isothermal Calorimetry
ICH	International Conference on Harmonisation
I_f	Forward current
IR	Infra-red
IUPAC	International Union of Pure and Applied Chemistry
J	Joule
K	Kelvin
k	Rate constant
LED	Light-Emitting Diode
LCMS	Liquid Chromatography-Mass Spectrometry
LHS	Left hand side
mcd	millicandela
µW	Micro-Watt
min	Minutes
N_A	Avogadro's number
n	Order of reaction
nm	Nanometers
NMR	Nuclear Magnetic Resonance
PCA	Principal Component Analysis
P	Pressure
Q	Total heat evolved or absorbed by a process
q	Time dependent heat-output

R	Gas constant
REF	Reference
R_s	Resistance
s	Seconds
SPD	Spectral Power Distribution
TAM	Thermal Activity Monitor
T	Temperature
t	Time
UV	Ultra-Violet
VIS	Visible
V	Voltage
V	Volume
V_f	Forward voltage
V_s	Power supply max voltage
W	Watts
w	Work done
x	Amount of material reacted
Xe	Xenon

- Chapter One -

Introduction

1. Overview

One of the major challenges currently facing the pharmaceutical industry is the lack of a general analytical tool that will allow the determination of the rate of reaction for a wide range of materials, particularly in solid-state systems, during a photochemical process. Most analytical approaches are hampered by a lack of reliable instrumentation and rapid testing protocols since the measurement of photostability is commonly made separately from the irradiation of the sample. Such methods are not ideal, however, since the stability data are not obtained in real-time. Moreover, it is the case that the vast majority of pharmaceutical photostability assays require a solid drug to be dissolved into a solution phase before any stability data can be obtained. However, with this the ideal of real-time data collecting without removing any solid-state history of the sample has been lost. This increases both experimental complexity and the number of assumptions that must be made for the determination of stability. The analytical challenge is, therefore, to be able to measure the stability data in real-time, without altering the nature of the sample, over a short experimental time in order to predict long term stability. One such technique that can be used to achieve this is photocalorimetry, primarily because the experimental measurements (changes in heat) are made directly as the photosensitive material in a solution-phase, semi-solid or solid-state system is irradiated, and in combination with appropriate data analysis methodologies, allows for the derivation of thermo-kinetic information to monitor photodegradative processes.

It is, therefore, the main objective of the research, reported here, to be able to develop a robust, compact and easy-to-use photocalorimeter to allow for the quantitative assessment of the photostability of pharmaceutical compounds.

The relevant background information on photostability testing, principles of calorimetry and details of how the technique can be adapted to monitor photodegradation materials (photocalorimetry) are all introduced in this chapter. Subsequently, a comprehensive account on the development of a novel LED photocalorimeter, the final design of which was arrived at through a series of iterative prototype designs, is detailed in Chapter 2. Details of the instrument design, technicalities, operation and performance are also given along with developments and modifications made to achieve the final design. Following the construction of a compact irradiation apparatus, the development of

suitable methods for measuring the amount of light delivered to a sample were investigated in Chapter 3. For this, the potential of 2-nitrobenzaldehyde, a chemical actinometer, was studied for use as a chemical test and reference reaction as a means to validate the performance of the instrument.

For any reaction that takes place in the calorimeter a certain degree of complexity should be expected since heat is ubiquitous and, therefore, the calorimeter measures *all* thermal processes that occur, without discriminating between individual processes. This renders the quantitative interpretation of calorimetric data cumbersome. Chapter 4 therefore focuses on the application of chemometric analysis as an approach to deconvolute the processes that exist into their individual reaction steps in order to aid interpretation of complexity in Isothermal Calorimetric data. Theoretical considerations for the determination of reaction parameters such as reaction enthalpy (ΔH) and rate constants (k) are discussed.

The final stage of the project was then to demonstrate the applicability of the photocalorimeter with a well-known photosensitive drug, nifedipine i.e. a real-life photolabile system. Chapter 5 investigates the photodegradation of nifedipine in a solution phase and describes the work conducted to analyse 'causative wavelengths' (a specific wavelength or a particular wavelength range of light at which photochemistry occurs) of the drug sample; an area that is of particular interest industrially.

In essence, the aims and objectives of this thesis are to;

- Build a robust and easy-to-use photocalorimeter; one with potential use for the routine screening of API's (active pharmaceutical ingredients) for the assessment of photostability
- Validate the performance of the photocalorimeter by quantification of the amount of light delivered to a sample through the development of a suitable chemical test and reference reaction
- Apply chemometric analysis to multi-component systems for the quantitative interpretation of complex Isothermal Calorimetric data
- Investigate the photostability of a known photosensitive compound and screen for its causative wavelength(s) across the UV-VIS region

1.1 An Introduction to the Importance of Pharmaceutical Stability Testing

For many years, the stability of drugs and drug products has been an area of research that has received great practical interest.[1] The extent of degradation can be influenced by a number of factors such as chemical degradation i.e., oxidation, hydrolysis or reduction; photodegradation from UV light, mechanical degradations such as compression, shearing or stretching, thermal degradation etc. For example, esters such as aspirin and procaine are susceptible to solvolytic breakdown, whilst oxidative decomposition occurs for substances such as ascorbic acid. Any of the forms of degradation can cause a change in the chemical and physical state of the material. A combination of these stresses can add further complexity to the physicochemical characteristics of the product. For the myriad of materials that exist, a change in the chemical or physical state may be obvious, for example, rusting of a metal, or discolouring of paint, etc. In such instances a major consideration that must be taken into account in determining if a physical or chemical change is of importance is the length of time over which such a change occurs. This is intuitively defined as the rate of reaction, and is dependent on how fast or slow a reaction process is. For example, the oxidation of iron under ambient conditions is a slow reaction which can take several years. Conversely, the combustion of butane in a fire is a reaction that takes place in fractions of a second. In other cases, a change can be more serious resulting in a danger to health, such as in the case of pharmaceutical preparations, which can result in a reduction in useful properties and loss in quality. Usually a loss of drug potency is observed, and this can have a detrimental effect on the quality and, more seriously, safety of the substance. It is therefore imperative to identify degradation products and pathways to minimise or prevent the occurrence of any pernicious processes. The rate of degradation, therefore, must be determined to ensure stability over an acceptable period of time (product shelf-life). The product shelf-life is given in the form of an expiration date on the final product which is required to assure that drug products have the identity, purity, structure and quality described on the label and package throughout its period of use under the storage conditions stated.

In order for a suitable shelf life to be determined, there are various stages of testing that are considered. During preformulation studies the drug undergoes a series of different stability tests to address its sensitivity toward many factors (temperature, light,

humidity, etc) and to determine the stability of the drug over a long period of time (shelf-life). Under normal conditions, such tests may take months, or years, before any degradation occurs. Necessarily, stability tests are often performed under "accelerated or stressed" conditions i.e., elevated temperature or high relative humidity. Such tests inevitably include photostability studies and are the primary focus of the research presented in this thesis.

Until recently, however, there was no established guideline for photostability testing of drugs. As a result, testing procedures varied significantly among pharmaceutical laboratories with every single issue being confronted in an independent manner.[2-6] This is reflected in a large discrepancy in photostability data as a result of the diverse approaches taken towards photostability testing in the absence of regulatory guidelines. Consequently, there is no general consensus on factors such as sample presentation, radiation source, spectral exposure levels, exposure time, and dosage-monitoring devices. Such variations make it difficult to correlate photostability results among different research groups. In October 1993, the "Stability Testing of New Drug substances and Products" guideline was recommended for adoption by the International Conference on Harmonisation (ICH). The European Union, Japan and USA agreed to the harmonisation tripartite guideline which described the procedures for investigating the effects of temperature and humidity without testing for light-induced processes during stability studies. More recently, photostability testing within the pharmaceutical industry has become a requirement by the regulating authorities and has evolved rapidly, particularly since the publication of the ICH Q1B guideline on "Photostability Testing of New Drug Substances and Products" was implemented in Europe in 1996[7] and in USA and Japan in 1997.[8] The guidelines attempted to better standardise photostability practices from a global perspective although in practice can lead to various interpretations and results.[9] Several attempts have also been made to provide an overview of the practical interpretation of the guidelines and offer important insights into satisfying the test requirements.[10-14] The most recent guidelines "Photostability testing of new active substances and medicinal products" issued by ICH in 2002, state that light testing should be an integral part of stress testing.

At present, however, there is no requirement for quantification since the photostability testing involves giving a simple pass/fail (stable/unstable) type decision as a means of

screening drug candidates early in the development process, giving no information about the kinetics of the process or about the factors that influence photostability. Therefore there is a need in the pharmaceutical industry, at present, to have a general analytical tool in place that is able to measure photostability of a drug substance, or drug product, as part of a routine screening process, in a manner which is rapid and cost-effective, using a minimum number of samples and operator time. The analytical challenge is, therefore, to address this knowledge gap, through the work presented in this thesis, focussing specifically on photostability testing, for the reasons given above.

1.2 An Introduction to the Photostability of Pharmaceutical Compounds

It has been well documented that the degradation of pharmaceuticals under ultraviolet-visible (UV-VIS) photon exposure can alter the properties of different drug substances and drug products.[15] Evidence of such photochemical damage is observed by the bleaching of coloured compounds, such as paints and textiles, or as a discolouration of colourless products. For example, a street map or magazine left in a car below the rear window will undergo a noticeable colour change within a few weeks as a result of direct exposure to UV radiation in sunlight. This is caused by the photochemical decay of cellulose fibres, from which paper is made, which react with water (naturally present in the fibrous cellulose) and atmospheric oxygen. The interaction between the oxygen and water, upon exposure to sunlight, leads to the formation of hydrogen peroxide resulting in a gradual oxidative breakdown of the cellulose. Consequently, since oxygen and moisture cannot be eliminated, every precaution has to be taken to prevent the exposure of valuable articles of paper or cellulose fibre to UV radiation with appropriate packaging. Similarly, pharmaceuticals are no exception and require appropriate measures of protection against light exposure.

For pharmaceuticals, the most critical effect of photodecomposition is a loss of potency of the drug product. This can result, eventually, in a therapeutically inactive drug product, or worse, the formation of phototoxic products during storage and administration. The inactive drug product can still act as a source of free radicals or form in-vivo phototoxic metabolites. As a result, the drug can still cause photo-induced side effects after administration if the patient is exposed to light (photosensitisation).[16]

In drug formulations, light does not only lead to the photodegradation of the active drug substance, but it can also alter the physicochemical properties of the product e.g., the product can become discoloured or cloudy in appearance, a loss in viscosity or a change in the dissociation rate may be observed or a precipitate may be formed on dissolution. Thus, it is important that an appropriate assessment of photostability is performed for a number of reasons;[17] to determine whether the drug is stable in a particular formulation and package;[18,19] to determine the effects that light sources of different wavelengths produce; to determine if other factors like oxygen, pH, or heavy metals produce different effects; and to estimate the potential in-vivo photosensitisation of a drug from its in-vitro photochemical behaviour.[3]

The European Pharmacopoeia prescribes light protection for a number of medical drugs. The number of photosensitive drugs is steadily increasing; consequently new compounds are frequently being added to the list of photolabile drugs. Therefore, knowledge concerning photodegradation behaviour is of growing importance. Nowadays, however, there are also legal requirements concerning unknown impurities and the structural elucidation of degradation products. This means that knowledge of photo-instability of a drug substance alone is not sufficient and there is a strong demand to characterise the photodecomposition products and photochemical pathways. Moreover, there is a need to investigate potential photo-induced side effects and determine whether their cause is due to toxic photodegradation products or due to in-vivo reactions such as photosensitisation. Although many drugs are found to decompose on exposure to light the practical consequences may not necessarily be the same for all compounds. Some drugs will decompose by only a small percentage after several weeks exposure, while other substances (such as derivatives of the drug nifedipine – an extremely photolabile drug substance) have a photochemical half-life of only a few minutes.[20] Establishing the kinetics of a degradative process plays an important part in characterising the nature of the photoinstability. The rate of a reaction is determined with the objective of establishing its dependence on concentration. Knowledge of this assists in deciding the development strategy of a drug formulation and in identifying any limitations that the degradation rate places on the product.

1.2.1 Current Analytical Methods for Photostability Testing of Pharmaceuticals

As highlighted earlier, an assessment of photostability is required as it provides a means of screening drug candidates early in the development process, and allows identification of photolabile drugs and photoproducts prior to a scale-up investment in development and testing. Following the identification of a photolabile drug, it may be possible to develop a strategy for modification of its molecular structure, provide appropriate photo-protection of some kind, or further development of the photolabile drug may be abandoned if stabilisation is unsuccessful. To help identify such photosensitive drugs, a number of analytical techniques can be employed. Ideally, the technique used must permit the separation, detection and quantification of all degradation products, even at very low levels. In the cases of unknown impurities, the analytical method must provide as much qualitative information as possible. Since there is no general analytical procedure yet in place, the assessment of photostability remains a complex problem.

Most analytical instruments employed in the measurement of photostability are separate from that where sample irradiation takes place i.e., the sample may be situated in a photostability chamber for a known period of time and is irradiated using a particular light source. The irradiation should, ideally, be performed in wavelength regions and intensities that relate to real conditions i.e. natural sun light. The sample is then analysed using a specific analytical technique, such as chromatography or spectroscopy, and photodegradation products are then analysed at particular time intervals. There are many types of analytical instruments widely available that are capable of determining the rates of degradation. Each of these analytical instruments has been specially designed for a particular function and therefore varies in sensitivity and versatility. High Performance Liquid Chromatography (HPLC)[21-23] and spectrophotometry[24] are the most common analytical techniques currently utilised for monitoring photodegradation processes.

Spectrophotometry is a relatively rapid and simple technique. Sample solutions are directly exposed to a source of radiation in a quartz cell. A portion of the incident radiation is absorbed by the sample; the remainder is transmitted to a detector and subsequently analysed in the same cell obviating the need for further dilution or treatment. The degradation products can be quantified providing there is a significant absorption change and little interference from degradation products. Chromatographic

analysis such as HPLC is predominant in the pharmaceutical industry to assess drug photostability. This is primarily attributed to the technique's high separation ability, high degree of accuracy and precision, particularly in quantification, and the availability of a wide variety of sensitive and specific detectors that accompany it. The technique is, therefore, commonly used to determine the rate of reactions by kinetic analysis.

There are many issues associated with such methods for stability testing of drug substances and products. A major drawback is the inability to collect long-term stability data in "real-time" as the photoreaction proceeds. Chromatographic techniques are insensitive to small changes in concentration as it requires that samples are taken for analysis at regular intervals because continuous analysis of a photodegradation process is not possible. A kinetic study, therefore, would demand a long observation period making it difficult to achieve reliable results if the degradation rate of the reaction was slow. HPLC requires that all components must be in solution; a solid-state drug substance necessarily is dissolved in a suitable solvent and may exhibit totally different properties from the original solid-state system since dissolution of the sample before analysis removes any solid-state history. This has an additional requirement that the act of dissolution of the compound does not cause further degradation before the assay is complete. In the majority of cases, such a technique is time consuming, labour intensive, due to extensive sample preparation, and involves destructive and invasive sampling techniques. Examples of other techniques[22,25,26] reported for photostability studies include; infra-red spectroscopy (IR),[27,28] nuclear magnetic resonance (NMR),[29] electron spin resonance (ESR),[30] liquid chromatography-mass spectrometry (LCMS)[31] and colorimetry,[32] but these also suffer limitations similar to those already mentioned above.

Because of the limitations of current analytical techniques, it is highly desirable to develop techniques that can directly analyse photolytic processes that occur within the "real" system, in a non-invasive manner to elucidate photostability data so as to predict a product's shelf-life. In order to achieve this, knowledge of the kinetics and thermodynamics of the degradative reactions are required. Most analytical instruments, mentioned above, that can quantitatively analyse a reaction will yield only kinetic information, thus, other types of analysis are required to enable the reaction to be fully and properly characterised.

Calorimetry is one such technique that has found value for recognising subtle differences in a reaction that are not apparent using any other technique. This is because calorimetry exploits thermodynamic parameters common to all reactions, that is, the changes in enthalpy (ΔH) that accompany all reactions and physical processes under constant pressure conditions. A calorimeter is therefore a reporter of heat and records the changes in heat content of a sample. The change can be monitored as a function of time so the rate of reaction can also be determined. In effect, the calorimeter is capable of yielding both thermodynamic and kinetic parameters during any chemical or physical process. Calorimetry is adopted as the principle technique herein and is adapted to allow for the study of photostability of pharmaceuticals.

In order to understand the principles of calorimetry, it is necessary to appreciate the basic requirements that must be met if a reaction is to proceed and the changes that accompany a physico-chemical process.

1.3 Requirements for a Reaction

If a reaction in its simplest form is considered, reactant A forms product B. The reaction proceeds only if there is a reaction pathway available. In some cases, only one reaction pathway may exist, but for many reactions there may be a number of different pathways and the reaction mechanism may become complex. In any case, there are three criteria that must be fulfilled before a reaction can proceed *via* a particular pathway; the reaction must be mechanically, kinetically, and thermodynamically feasible. If any of the requirements are not met then the system is stable and reaction will not take place. If conditions are altered, e.g., temperature, pressure, etc., then this can result in an unstable system and a reaction may be able to take place.

1.3.1 Mechanistic factors

The first requirement relates to the physical properties of the molecule or substance undergoing a reaction. For this, the reactants must possess the ability to interact with other species. In the absence of any interaction products will not be formed. The reactant must contain reactable groups of the correct physical form, i.e. the correct chemical bonds within specific orientations, correct energy, etc., to allow interaction with reactable groups of other compounds.

1.3.2 Thermodynamic factors

The second requirement is that a reaction be thermodynamically feasible. Thermodynamics is concerned with the study of transformation of energy. Most chemical and physical processes are associated with an exchange of heat energy between a *system* and its *surrounding*. Everything in the universe except the system under study is known as *surroundings*. The system is separated from the remainder of the universe by a *boundary*. It is across this boundary that an exchange of *work*, *heat* or *matter* may take place. If a boundary allows energy (work and heat) and/or matter to be exchanged with its surrounding then the system is described as *open*. If energy can be transferred through the boundary, but not matter, then the system is *closed*. If neither

matter nor energy can be transferred through the boundary then the system is *isolated* i.e., the system is completely isolated in every way from its surrounding.

The basic concepts of thermodynamics are work, energy and heat. Energy is the capacity of a system to do work and it is when the energy of a system changes, as a result of a temperature difference between it and its surrounding, that the energy change occurs by a transfer of heat. The loss of heat from a system is described by an *exothermic* process (and, hence, a change in heat is given a negative sign), and if the system gains heat, it is described by an *endothermic* process (where the heat change is given a positive sign).

The observations made using calorimetry are based upon the laws of thermodynamics. The first law of thermodynamics states that;

"Energy can be changed from one form to another, but it cannot be created nor destroyed" and thus *"the internal energy of the system is constant unless it is altered by doing work or by heat."*

The first law can be stated mathematically as;

$$\Delta U = q + w \qquad \text{Eqn. 1.1}$$

where ΔU is the change in the internal energy (U is the total energy content of a system known as its internal energy), q represents the transfer of heat to and from the system, and w is the work done on or by the system.

If a system is kept under constant pressure, the enthalpy (H) is a direct measure of the heat content. The enthalpy is related to the internal energy and the work done by the system in expansion against the atmosphere, $P\Delta V$, by;

$$H = U + PV \qquad \text{Eqn. 1.2}$$

where P is the pressure and V is the volume of the system. Note that calorimeters measure heat as a change in enthalpy, not a change in internal energy.

The second law of thermodynamics deals with the direction of spontaneous change and governs if a reaction takes place or not. This is determined by considering the Gibbs function (ΔG), also termed Gibbs free energy. Developed by an American mathematical

physicist, Josiah Willard Gibbs, in the 1870s the Gibbs function is the most fundamental thermodynamic parameter in any chemical reaction. It is comprised of two terms; a change in enthalpy (ΔH) and a corresponding change in entropy, (ΔS) at constant pressure conditions **only**. The feasibility of a reaction is dependent on the balance between ΔH and ΔS and is governed by ΔG, and is described by Equation 1.3.

$$\Delta G = \Delta H - T\Delta S \qquad \text{Eqn. 1.3}$$

For a reaction to take place ΔG must be negative, however, it is not an indication that the reaction **will** take place at a given temperature and neither is it an indication of the rate at which that reaction will occur. A negative value of ΔG suggests only that a reaction is thermodynamically feasible. A positive ΔG is unfavourable and the reaction will not occur under the defined conditions. In terms of enthalpy an exothermic reaction ($-\Delta H$) is favoured as the reactant forms the product. The measurement of disorder is known as the entropy where a positive entropy change ($+\Delta S$) indicates an increase in the disorder of the system. This is a favourable condition which determines if a reaction is spontaneous as governed by the second law of thermodynamics, which states;[33]

"Any spontaneous process that occurs in a system will lead to an increase in the total entropy of the system."

A spontaneous process is one that occurs naturally; without any intervention. A high and negative value of ΔG favours a spontaneous reaction. Reactions that are spontaneous are often exothermic but the enthalpy change of the system does not determine spontaneity. It is only spontaneous if the entropy term is positive i.e. the $T\Delta S$ term is larger than the ΔH term. Equilibrium thermodynamics however, gives no information concerning the rate of reaction, i.e. the ΔG value can indicate if the reaction is spontaneous, but does not indicate the rate at which equilibrium is achieved nor the mechanisms by which the reaction occurs.

1.3.3 Kinetic factors

The third requirement concerns the kinetic feasibility of the reaction and is determined by the reaction rate. The rate of a reaction can vary from very fast to very slow and,

between these limits, there is a range of rates that, in principle, is measurable. If the reaction is extremely slow then the rate can be regarded as negligible since the extent of degradation is far too small to reach detectable levels under storage conditions. The maximum extent of degradation allowable is usually 5% in two years (equating to a half-life of 27 years, assuming the reaction follows first order kinetics).[34]

There are three main parameters that govern the rate of the reaction; the quantity of reactants available for reaction, the fraction of the quantity available for the reaction that possess sufficient energy to overcome the activation energy (E_a) barrier, and lastly, the order of the reaction (n). The relationship between the fraction of molecules that can react, the order of reaction and the total number of molecules that could react is described by Equation 1.4.

$$\frac{dx}{dt} = k(A_0 - x)^n \qquad \text{Eqn. 1.4}$$

Where; k is the rate constant, (A_0-x) is the quantity of material that is available for the reaction at time t, and n is the order of the reaction. It should be noted that n may have any value; integral or non-integral.

In order for a reaction to occur, the molecules must collide in the correct orientation and possess a certain minimum amount of energy, known as the activation energy (E_a) to overcome a barrier to reaction if the reaction is to proceed. E_a is typically provided by the heat of a system i.e. as the translational, vibrational and rotational energy of each molecule, although sometimes by light or electrical fields. The rate of a reaction (Equation 1.4) has a dependence on temperature, which is solely provided from the rate constant. Generally, the rate constants of most chemical reactions increase rapidly as the temperature is raised. For solution phase reactions, a rise of 10°C near room temperature can cause the rate of a reaction to, typically, double or treble.[35] This is because an increased proportion of the reactant molecules (A_0-x) possess sufficient (kinetic) energy that is greater than E_a. Figure 1.1 illustrates the relationship between E_a, and reaction enthalpy change, ΔH, for an exothermic and endothermic reaction. If E_a is very large, only a small proportion of molecules have enough energy to react so the reaction proceeds very slowly i.e. the greater the energy barrier the harder it becomes for an interaction to occur. If, however, E_a is very small, most of the molecules have sufficient

energy to react and the reaction proceeds very rapidly. ΔH gives no information concerning *how far* a reaction goes towards completion. The fact that a certain minimum energy is needed to initiate most reactions is well demonstrated by fuels and explosives. These usually require a small input of energy to start their extremely exothermic reactions.

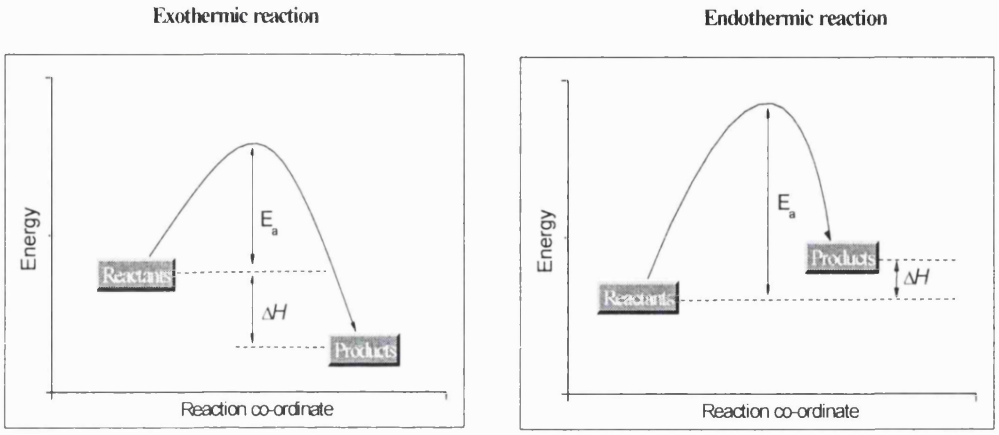

Figure 1.1: Graphical representation of activation energy

The relationship between the activation energy, temperature and the rate constant is described by the Arrhenius equation (Equation 1.5).

$$k = Ae^{\frac{-E_a}{RT}} \qquad \text{Eqn.1.5}$$

Logarithmic form;

$$\ln k = \ln A - \frac{E_a}{RT} \qquad \text{Eqn.1.5.1}$$

Where; A, the Arrhenius constant, can be regarded as a pre-exponential factor. E_a is the activation energy, R is the universal gas constant and T is the absolute temperature (in Kelvin, K).

The Arrhenius equation is adopted for the determination of solution phase or solid-state stability under "accelerated conditions" and is achieved by extrapolation outside the experimental range of data obtained at elevated temperatures, since it would be impractical in most cases to wait the several years it may require for degradation

products to reach detectable levels under storage conditions. The activation energy of the reaction is determined at the higher temperatures and the Arrhenius relationship is employed to calculate the degradation rates at any desired (lower) temperature *via* extrapolation of data. The method is valid **only** if the mechanism of degradation remains constant over the temperature of both the experiment and the extrapolation. If the Arrhenius relationship deviates from linearity outside the experimentally determined region then there may be a change in mechanism and the method is invalidated.

The final parameter that influences the rate of a reaction is the order of reaction (n) which is a power function and is related to the contribution that the reactant makes to the rate of reaction. Consider the following simple reaction;

$$aA + bB \rightarrow cC + dD$$

It may be the case experimentally that the rate of reaction is directly proportional to the concentration of A raised to the power a; Rate α $[A]^a$. Similarly, if the rate of reaction is proportional to the concentration of B then it is raised to the power b; Rate α $[B]^b$. For example, a reaction order of one (first order) can be expressed as Rate α [A]. If the reaction order is two (second order), then the reaction rate is proportional to the concentration of reactant available squared and expressed as Rate α $[A]^2$. The overall rate equation can be written as;

$$\text{Rate} \alpha [A]^a [B]^b$$

The rate of reaction at a given time is then described by;

$$\text{Rate} = k[A]^a [B]^b$$

In the example given above, the reactants A and B are raised to the power of exponents a and b, respectively, which define the reaction order. The order of a reaction depends on the reaction mechanism i.e., the sequence of elementary steps that take place. The overall reaction order (n) is the summation with respect to the individual components, i.e. $n = a + b$. Note that the order of the reaction is not the same as the molecularity of the reaction which provides information about the number of molecules that take part in an individual step within the overall reaction mechanism. A reaction, therefore,

proceeding from A to B must possess a reaction mechanism and be thermodynamically and kinetically observable. The reaction will proceed only when these three criteria have been met.

Reaction kinetics is the study of reaction rates and its dependence upon concentrations of the species involved. During a chemical reaction, the concentration (for a solution phase system) or quantity (for a solid-state reaction) of reactants decreases with time, whilst the concentration/quantity of the final product(s) increases with time. The average rate of reaction in terms of a specific reactant or product within any given interval of time is defined as the change in concentration (or quantity) of that reactant or product (d[ ]) that occurs within the given time interval (dt), as described in Equation 1.6.

$$\text{Rate} = -\frac{\text{d[reactant]}}{\text{dt}} \quad \text{or} \quad \text{Rate} = \frac{\text{d[product]}}{\text{dt}} \qquad \text{Eqn. 1.6}$$

The reaction rate at any time, t, can be calculated from the concentration *vs* time curve. This is achieved by drawing tangents to the curve and calculating the slope at that time. Such a process can be laborious and inaccurate, particularly for slow reactions. (Note, for negative slopes, the sign is changed when reporting the rate so that all reaction rates are positive).

In effect, it is more appropriate to employ specific rate equations applicable to the process under investigation. Rate equations can be derived for most chemical processes. Such equations relate the rate of reaction at any time t to the concentration of the reactants and products present at that time. Alternatively they can relate the rate of reaction directly to time. For both cases the relationship is expressed through the rate constant (k).

There are two types of rate equation; the **differential rate equation** and the **integrated rate equation**. The former express the rate of reaction as a function of **concentration** and the latter expresses it as a function of **time**. Most reactions follow either zero-, first, or second-order kinetics, and thus obey a specific kinetic scheme. Third-order reactions are rare and will not be discussed here. The differential and integrated rate expressions commonly used to describe the three simple reaction orders are represented in Table 1.1.

Table 1.1: Differential and Integrated rate expressions for different reaction schemes

Overall reaction order	Differential rate form	Integrated rate form	Linear plot to determine *k*
Zero	$-\frac{d[A]}{dt} = k$	$[A] = [A_0] - kt$	$[A]$ *vs* t
First	$-\frac{d[A]}{dt} = k[A]$	$\ln[A] = \ln[A_0] - kt$	$\ln[A]$ *vs* t
Second	$-\frac{d[A]}{dt} = k[A]^2$	$\frac{1}{[A]} = \frac{1}{[A_0]} + kt$	$\frac{1}{[A]}$ *vs* t
nth	$-\frac{d[A]}{dt} = k[A]^n$	$\frac{1}{[A]^{n-1}} = \frac{1}{[A_0]^{n-1}} + (n-1)kt$ [Except first order]	$\frac{1}{[A]^{n-1}}$ *vs* t

A zero-order reaction (i.e. n=0) has a rate that is independent of the concentration of the reactant (s) i.e. increasing the concentration of the reacting species will not speed up the rate of reaction. Typically, zero-order reactions are found when a material required for a reaction to proceed (such as a surface or catalyst) is saturated by the reactants. A reaction is zero-order if a concentration *vs* time plot yields a straight line. The slope of the resulting line is the zero-order rate constant (k).

A first-order reaction (i.e. n=1) depends on the concentration of only one reactant (a unimolecular reaction). A plot of ln[A] against time is linear with a slope equal to $-k$.

A second order reaction (i.e. n=2) depends on the concentration of one second-order reactant or two first-order reactants e.g. [A] and [B] thus overall n=2. A plot of 1/[A] against time is linear with a slope equal to k.

1.4 Calorimetry

Calorimetry (derived from *calor*, Latin, meaning **heat** and *metry*, Greek, meaning **measurement)** is defined as the measurement of heat. A calorimeter, thus, is a device

that can measure the heat change by a reaction as it proceeds. The change in heat can be measured over time, which can yield information not only on the heat change (thermodynamics) but also on the rate of a reaction (kinetics). Since most chemical and physical changes are accompanied by a change in heat content, or enthalpy, it is possible, in principle, to study all chemical reactions using this technique. Calorimetry is, thus, an extremely useful tool that can be used to monitor homogeneous and heterogeneous reactions, such that both thermodynamic and kinetic information may be obtained.

An early practical application in the realm of calorimetry was pioneered by Lavoisier and Laplace[36] who designed a simple calorimeter with the notion to study the respiration of a guinea pig. The calorimeter consisted of a sample cell, surrounded by ice, which was contained in an insulating jacket. A guinea pig was placed in an insulated box packed with ice. Any heat evolved from the guinea pig's enthalpy of metabolism melted a certain quantity of the surrounding ice. The resulting water was collected, through a small outlet in the bottom of the calorimeter, and weighed (Figure 1.2). The heat evolved calculations were based on Black's prior discovery of latent heat – nowadays this term is generally obsolete and instead the modern practice is to use enthalpy of transformation. With knowledge of the quantity of water produced and the latent enthalpy of fusion of water required to produce that amount of water, it is possible to determine the equivalent heat output, Q, (in Joules) for the process. By knowing the body-mass of the guinea pig, the change of enthalpy for metabolism could then be determined (in kJ kg^{-1}). This is a thermodynamic term, although it alone does not give any useful information about the thermodynamic reactivity of molecules. This is because it is not possible to make direct comparisons in enthalpy between two reactions unless the reagents in both reactions have the same molecular weight. It is also possible to derive kinetic information from this process. If the mass of water collected was recorded periodically as a function of time (min), then the rate of metabolism could be measured (J min^{-1}) consequently, giving a thermodynamic and kinetic evaluation for respiration. At the end of the experiment the guinea pig was released unharmed, demonstrating that calorimetry can be a non-invasive and non-destructive technique.

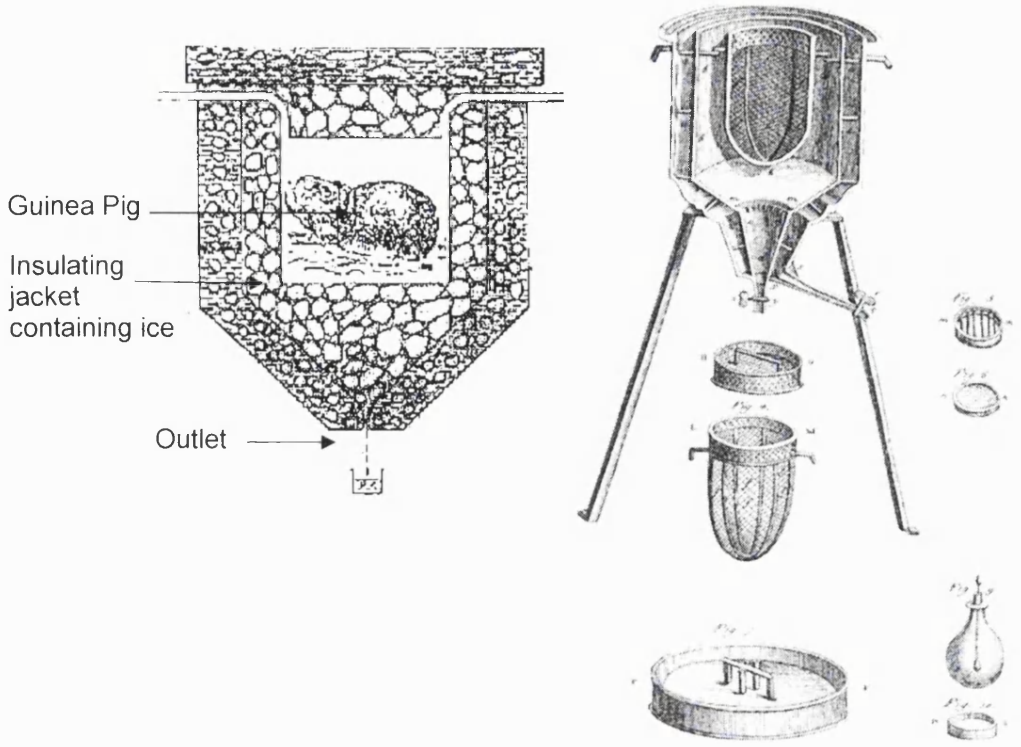

Figure 1.2: Schematic representations of the first ice calorimeter[36]

Nowadays, through the considerable advances made in the technology of calorimeters, there are several types of calorimeters commercially available. Microcalorimeters, designed for measuring in the micro-Watt range, are among the common type utilised and can be categorised into three measuring priniciples:[37]

1. **Adiabatic microcalorimeters** – there is no heat exchange between the calorimetric vessel and its surroundings. These conditions are achieved by ensuring insulation between the two entities. In most cases, semi-adiabatic (or isoperibol) microcalorimeters are used since, in practice, true adiabatic conditions are difficult to obtain which results in some heat-leak to the surroundings. In this case, it is necessary to apply corrections to allow the return of accurate data.

2. **Power compensation microcalorimeters** – the heat removed or gained during an exothermic or endothermic process, respectively, is balanced by an opposing

electrical power; usually by using the Peltier effect current, such that the calorimetric vessel is maintained at a given temperature.

3. **Heat conduction microcalorimeters** – any heat produced or absorbed in a reaction flows to, or from, a surrounding "heat sink" which acts to maintain the system at a constant temperature. These types of microcalorimeters are known as isothermal. The "Peltier effects plates" (thermopiles) are used as sensors for the heat flow between the calorimetric vessels and surrounding heat sinks.

Isothermal heat conduction microcalorimetry is the principal microcalorimeter that has been used throughout the studies presented herein.

1.4.1 The Principles of Isothermal Microcalorimetry

Isothermal microcalorimeters are surrounded by a heat sink that acts to maintain the system at a constant temperature. Any heat produced or absorbed by the sample is quantitatively exchanged with the heat sink (water bath). The microcalorimeter is used in a differential mode, where a thermal energy change creates a small temperature difference relative to the heat sink which forces heat to flow, either to, or from, the heat sink, depending on whether the reaction being followed is exothermic or endothermic. The magnitude of the temperature difference is directly proportional to the heat-flow and thus to the rate of the process under study. The thermopiles situated around the sample are extremely sensitive, and are used to ensure the heat-flow is measured and quantified. The potential generated by the thermopiles is then amplified and recorded as heat-flow (dq/dt, thermal power in Watts) and is measured as a function of time.

There are a number of isothermal microcalorimeters available, one such instrument is the Thermal Activity Monitor, or **TAM**, manufactured by ThermoMetric AB (Järfalla, Sweden).

The TAM is a multichannel microcalorimeter comprised of four separate channels, and is therefore capable of measuring four separate experiments simultaneously (Figure 1.3). The principle of operation is simple; each channel has two identical chambers

adjacent to each other; a reference (right-hand side) and a reaction/sample (left-hand side) chamber. Generally an inert material, of similar heat capacity and quantity to the sample, is placed in the reference chamber. The relative heat-flow between the two sides is measured (differential mode) where it can be assumed that, ideally, no reaction occurs from the inert material, i.e. zero heat-flow, or it has a extremely slow and unenergetic reaction, beyond the capacity of the TAM to measure, and therefore does not produce a detectable calorimetric signal. The measured heat-flow is thus solely attributed to the sample reaction taking place. Very sensitive thermopiles surround each chamber and are used to detect any thermal power that arises between the sample and reference sides.

Each chamber is capable of accepting glass or stainless steel ampoules (typically 3 – 20 mL capacity). Typically, disposable glass ampoules and stainless steel ampoules are utilised. All four channels are immersed in a closed thermostated water bath (ca. 20 L). The temperature of the water bath can be finely set (within the range +5°C to 95°C) and is regulated by a series of thermostats and heaters, which continually operate to maintain a constant temperature. Generally, at ambient temperature, the long-term baseline stability is within 1 x 10^{-7} W and has a nominal stability of ± 0.0001 K over a period of 24 hours providing the room temperature does not fluctuate more than ± 1°C.[38,39] The baseline stability is typically better than ± 0.1 μW over 12 hours and ± 0.2 μW for larger channels. The whole system is thus maintained in isothermal conditions, and helps achieve high sensitivity and good long-term stability to measure small heat-flow changes.

Figure 1.4 illustrates a single sample chamber inside the calorimeter. The ampoule is lowered into the central chamber and heat from the reaction flows from the sample to the heat sink, or from the heat sink to the sample, depending on whether the reaction occurring is exothermic (positive signal) or endothermic (negative signal). Note: by convention the enthalpy of heat loss is exothermic, denoted by a negative signal, and an endothermic response is represented by a positive signal as measurements are made from the view point of the system. The calorimeter, however, reports a heat gain (positive) or heat loss (negative) signal from the perspective of the surroundings and not by the system under study.

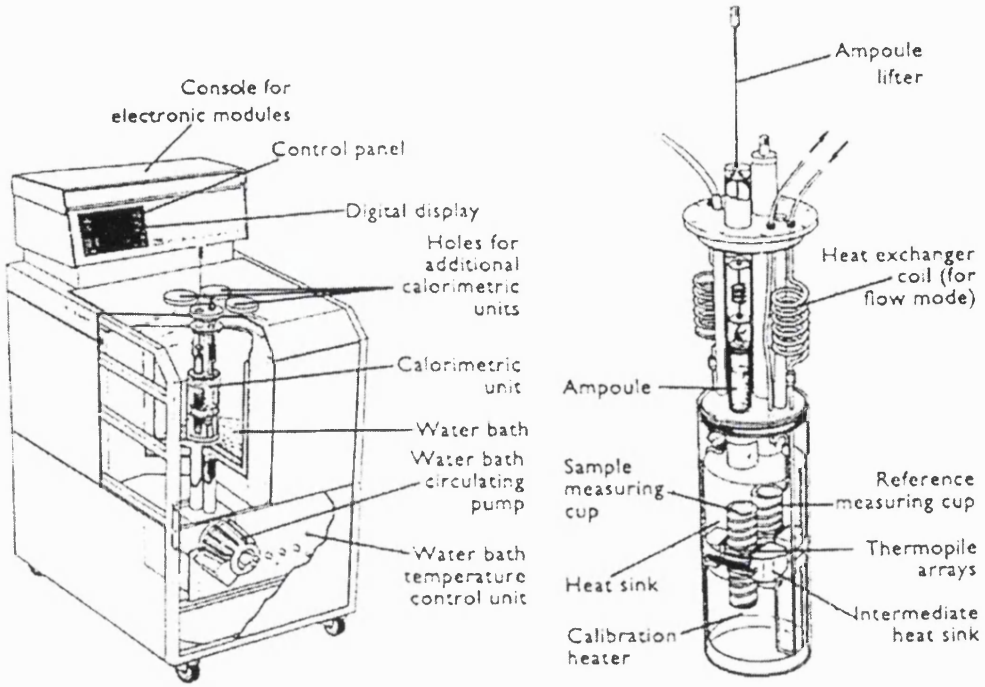

Figure 1.3: The Isothermal Microcalorimeter, TAM (left) and a calorimetric unit (right). *Source*: Courtesy of Thermometric AB.

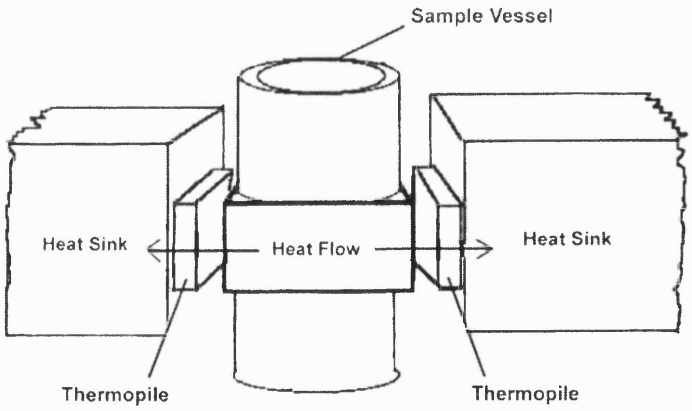

Figure 1.4: The heat sinks surrounding the sample vessel. The thermopiles connect the sample vessel to the heat sink. *Source*: Courtesy of Thermometric AB.

The instrument is calibrated, usually by means of an electrical calibration, prior to sample measurement, which can be set over a range of sensitivity scales; 3, 10, 30, 100, 300, 1000 or 3000 μW.[40]

The TAM confers several advantages over other techniques; it has a combination of versatility and sensitivity making it superior to many other analytical instruments. For example, it has been reported that the TAM is 10,000 fold more sensitive than a commercial Differential Scanning Calorimetry (such as a Perkin Elmer, DSC 7).[34] Its high sensitivity comes from having an accurate and precise control of temperature, such that materials can be studied at ambient temperatures and the reaction environment can be precisely controlled (pH, partial pressure, humidity etc).[37,39,41] It has been claimed that the TAM has sufficient sensitivity to monitor slow reactions with lifetimes lasting up to 10,000 years, and it has also been reported that the instrument can discriminate between a reaction that has a first order rate constant of 1×10^{-11} s^{-1} and 2×10^{-11} s^{-1} after the collection of 50 hours of data.[42,43] Such a versatile system can be used together with insertion vessels of different designs and functions ranging from simple closed ampoules to stirred vessels fitted with injection tubes, devices facilitating dissolution, electrodes, or optical cables. It is the latter design type that forms the focus of this research.

The instrument has the ability to detect, and potentially quantify, the changes in a wide range of materials. For this, there are two requisites; firstly, the sample must produce a sufficient quantity of heat that can be detected by the thermopiles, and, secondly, the sample (or a representative proportion of it) must fit within the calorimetric vessel. The TAM is non-invasive and non-destructive to the sample and so the reaction under study is not influenced by the calorimeter, nor does the sample require any special treatment or preparation prior to analysis. The instrument is also invariant to the physical form of analysis; the sample can be solid, in solution, gaseous or a combination of all phases. This unique quality allows complex heterogeneous systems to be studied. Furthermore, unlike other analytical techniques (e.g. UV spectroscopy), neither colour, optical transparency nor the absence of suspended matter are requirements. Since the calorimeter records measurements as a function of time, it is possible to capture data in real-time, in a rapid manner, making it possible for small changes (both chemical and physical) to be detected over a period of time.

1.4.2 Analysis of Calorimetric Data

The TAM reports the heat flow for a reaction as $\frac{dq}{dt} \equiv \boldsymbol{\Phi}$, which is the rate of change in **heat-output** or **thermal power**, and is measured in Watts (Js^{-1}) per unit time (seconds). A plot of $\boldsymbol{\Phi}$ against time shows the change in thermal power as a function of time for the process (power-time curve) under study. The time dependent heat-output, $\boldsymbol{q}$, is the enthalpy change for the reaction at any time, t, and can be calculated by integration of the area under the power-time curve. Integration of the power-time curve can therefore yield two types of data; heat flow (a kinetic term) and the time dependent reaction enthalpy change (a thermodynamic term). In solution phase reaction systems, for any reaction that has gone to completion ($t = \infty$), the **total heat output** from the reaction can be denoted $\boldsymbol{Q}$; similarly heat that is evolved or absorbed at **any particular time point, *t***, can be denoted $\boldsymbol{q}$. Both terms; Q and q, can be derived simply by integrating the area under the Φ vs t curve for $t = 0$ to $t = \infty$ and $t = 0$ to $t = t$ respectively.

The magnitude of the total heat output, Q, is dependent upon two factors; the energetics of the process and the amount of material available for the reaction. A reaction that has gone to completion must be equal to the product of the enthalpy of reaction, ΔH, and the number of moles of material reacted, A_0. This relationship is given by Equation 1.7.

$$Q = A_0 \Delta H \qquad \text{Eqn.1.7}$$

This can be rearranged to give Equation 1.7.1;

$$\Delta H\left(\text{J mol}^{-1}\right) = \frac{Q(\text{J})}{A_0(\text{mol})} \qquad \text{Eqn.1.7.1}$$

In cases where A_0 or Q is unknown, the determination of enthalpy change can become a little more difficult. Q can, in principle, be detected by the integration of the entire heat output, although A_0 may not be known.

At any time during the reaction, the amount of material (in moles) that has reacted can be denoted by x, Equation 1.8;

$$q = x\Delta H \qquad \text{Eqn. 1.8}$$

Equation 1.8.1 follows;

$$x = \frac{q}{\Delta H} \qquad \text{Eqn. 1.8.1}$$

Both x and q are time dependent variables; both equal zero at $t = 0$. For a reaction that goes to completion, this approach makes it is possible to determine the percentage of reaction completed at any time, t, by taking fractional areas. The value of Q is, thus, equal to the integrated area under the power-time curve for a reaction that has gone to completion.

If a simple mono-molecular kinetic expression for a solution phase system, $A \rightarrow B$ reaction, is considered; using Eqn. 1.4,

$$\frac{dx}{dt} = k(A_0 - x)^n \qquad \text{Eqn. 1.4}$$

then substituting $q/\Delta H$ for x gives Equation 1.9, as described by Willson *et al.*[42]

$$\frac{dq}{dt} \equiv \Phi \cdot \frac{1}{\Delta H} = k\left(A_0 - \frac{q}{\Delta H}\right)^n \qquad \text{Eqn. 1.9}$$

This expression can be rearranged to form the basic calorimetric equation;

$$\Phi = k\Delta H\left(A_0 - \frac{q}{\Delta H}\right)^n \qquad \text{Eqn. 1.10}$$

Similarly, if Equation 1.4 is substituted with $Q/\Delta H$ for A_0 and $q/\Delta H$ for x and, following rearrangement gives;

$$\Phi = k\Delta H^{n-1}(Q-q)^n \qquad \text{Eqn. 1.11}$$

Equation 1.11 is in differential form and can be integrated to determine the quantity of material remaining as a function of time, Equation 1.12;

$$(Q-q) = \left[kt\Delta H^{1-n}(n-1) + Q^{1-n}\right]^{\frac{1}{1-n}} \qquad \text{Eqn. 1.12}$$

Note that integration of Equation 1.12 is valid for all simple solution phase reactions, except that of first order.

The integral of Equation 1.12 can then be substituted into Equation 1.11 to provide a relationship between power and time i.e. the calorimetric signal, Equation 1.13:

$$\Phi = k\Delta H^{1-n}[kt\Delta H^{1-n}(n-1) + Q^{1-n}]^{\frac{n}{1-n}} \qquad \text{Eqn. 1.13}$$

The above equation describes the calorimetric data that derive from reactions which follow the general rate expression for any simple single-step reaction such as that given in Equation 1.4.

It is important to note, particularly in the derivation of calorimetric equations for solution phase reactions, that the terms A_0 and x in the above equations are **quantity** related terms and so reflect the amount of the material in moles and not in terms of concentration (mol dm^{-3}). This means that the rate constant will not contain any concentration related units. Hills[44] pointed out the importance of introducing the volume term, V, as a separate variable in data fitting and that care should be exercised in reporting the correct units of data. In order for the rate constant and the reaction enthalpy to be in conventional units the calorimetric equation must contain the initial concentration of reactable material and the volume of the solution that is loaded into the calorimetric ampoules, as given in Equation 1.14.

$$\Phi = k\Delta HV\left(A_0 - \frac{q}{\Delta HV}\right)^n \qquad \text{Eqn 1.14}$$

In 1995, Willson *et al*[42] presented a new method to improve the versatility of the interpretation of calorimetric data and the reaction kinetics obtained through a process of **iteration**. The calorimetric data obtained can be entered into a suitable mathematical software package, such as Origin™ and fitted into Equation 1.13 using Willson's process of iteration. In 2001, Beezer *et al*[45] developed a new **direct calculation** method to determine the reaction parameters in complex systems.

1.4.2.1 Solid-state reactions

The kinetic processes by which solid state reactions occur are significantly different from those of solution phase reactions (as described above). Typically, solution phase systems are homogenous and very uniform. Solid systems, however, are heterogeneous and the particles can be very irregular and contain defects. The analysis of solid-state systems is generally more complex than that for solution phase systems. The general equation that can be used to describe most solid-state reactions is known as the Ng equation[46] (Eqn. 1.15).

$$\frac{d\alpha}{dt} = k(1-\alpha)^n(\alpha)^m \qquad \text{Eqn. 1.15}$$

where α is the fractional extent of reaction at time t, k is the rate coefficient and has the units s^{-1}, and m and n are fitting constants, which are related to the reaction mechanisms, not reaction orders.

The calorimetric form of the Ng equation can be used to describe calorimetric data from a solid-state reaction, which conforms to a Ng model.[47] The fractional extents of the reaction (α) can be given in terms of the number of Joules of heat released by the reaction process (Eqn. 1.16).

$$\frac{dq}{dt} = \Phi = kQ\left[1-\left(\frac{q}{Q}\right)\right]^n\left(\frac{q}{Q}\right)^m \qquad \text{Eqn. 1.16}$$

where Q is the total number of joules involved in the reaction to time, $t=\infty$ (i.e. completion of the reaction) and q is the number of joules evolved up to any time t.

The need to determine parameters n and m in addition to k and ΔH increases the demand on the iterative process. Unlike solution phase systems, the problem associated with solid-state reactions is that the fitting parameters (n and m) expressed in Eqn. 1.16 are not usually integral and the equations are complex. Consequently, it is recommended that a direct calculation method for solid-state reactions is used for the analysis of the calorimetric data. The fitting parameters m and n can be determined using a technique of data pairing. This uses values of Φ and q for paired time points throughout the power-time curve (Φ-t) during the observation period.

Once the parameters, m and n, are calculated from the data paired values (Φ-t) a value for Q must then be determined. Note it is not possible to measure this value experimentally because the rates of reaction associated with solid-state reactions are generally very slow. The value for Q can, thus, also be determined through analysis of paired data points. If Eqn. 1.16 is written for two data points and a ratio between them is formed then this gives;

$$\frac{\Phi_1}{\Phi_2} = \frac{(1-q_1/Q)^n (q_1/Q)^m}{(1-q_2/Q)^n (q_2/Q)^m} \qquad \text{Eqn. 1.17}$$

If the values for q_1 and q_2 are then selected such that q_2 is a known factor of q_1 (for example, q_2 is equal to cq_1 (hence $q_2/q_1 = c$) and setting R as:

$$R = \left(\frac{\Phi_1}{\Phi_2}(c)^m\right)^{1/n} = \frac{(1-q_1/Q)}{(1-cq_2/Q)} \qquad \text{Eqn. 1.18}$$

Eqn.1.18 can then be solved to determine Q as:

$$Q = \frac{q_1(cR-1)}{(R-1)} \qquad \text{Eqn. 1.19}$$

With knowledge of Q, m and n allows calculation of k for each value of Φ:

$$k = \frac{\Phi}{Q\left[1-(q/Q)\right]^{n}(q-Q)^{m}} \qquad \text{Eqn.1.20}$$

This method does, however, have limitations. One issue is how much data is required (i.e., the minimum fraction of reaction) for a successful determination of Q and hence α (equal to q/Q)) at any time t and then to determine k and hence the reaction lifetime.

The use of data simulation to establish the minimum value for α (i.e. (q/Q)) for given values of m and n allows characterisation of the model system. Mathematical programmes such as Mathcad© have been used to allow data simulation for the values m, n, Q and k, for solid state reactions where Q ranged from 10 to 10,000 J; the rate coefficient, k, ranged from 10^{-4} – 10^{-8} s^{-1} and values for m and n between 0 and 1.[48,49] The data were given in the form of Φ *vs* q for a range of values of α up to a maximum of α = 1. Data analysis was then performed using Willson's[50] algorithm written in Microsoft Excel®, which allowed for the determination of Q for varying ratios of Φ_2/Φ_1 (where Φ_2 was fixed as the value of Φ when α is at a maximum). It is possible to determine α value as small as around 0.01 (when Q is assigned a value of 100 J) and, thus, it is possible to recover the correct values for the target parameters. It should be noted that for successful analysis, the ratio of Φ_2/Φ_1 should be as large as possible and the analysis becomes more difficult as the value of Φ_1 approaches Φ_2 (i.e. Φ_2/Φ_1 approaches 1). The separation required between Φ_1 and Φ_2 depends on the values of Q and α. If Q is small then α must be large enough to allow sufficient separation between Φ_1 and Φ_2. The maximum required value of α depends on the value of Q; the maximum value of α required for satisfactory analysis is 0.1 for solid-state reactions with values of Q as low as 2 J. Note, there is no method available, at present, to integrate the calorimetric form of the Ng equation such that it can be cast in terms of time.

All the method of analysis described so far using the iterative process and direct calculations method are useful for the quantitative analysis of complexity, both in solution[42,51,52] and solid states[49]. However, all these methods suffer a common drawback; they all require prior knowledge of the reaction mechanism. If there is only one reaction step occurring in the process then this is not a major problem and the

equations described above can be used to quantitatively determine the reaction parameters. The difficulty in analysing data arises when reactions comprising of multiple steps are studied. This is severely limiting for successful analysis to those methods described above in cases where there is no prior knowledge of the reaction mechanism. It is possible to systematically fit the data to increasingly complex kinetic models until a fit is obtained. Such an approach, however, is extremely time consuming and requires the derivation of many complex equations. It is also necessary to impose a model on the system. Since calorimeters measure *all* the thermal events, without discrimination, the resultant calorimetric data will reflect *all* the thermal processes form each mechanistic step. Therefore, without prior knowledge of the reaction mechanism, the quantitative interpretation of calorimetric data can be very complex in multi-component systems. One approach of determining individual reaction steps comprising a complex reaction is the application of chemometric analysis. Chapter 4 discusses the potential application of chemometric techniques such as principal component analysis (PCA) as an approach to deconvolute complex reaction processes into their individual components and the interpretation of complex Isothermal Calorimetric data for the determination of reaction parameters such as reaction enthalpy (ΔH) and rate constants (k) are described.

On the whole, it has been described above that calorimetry has found much value for the analysis of pharmaceuticals and is unique among many analytical techniques. Therefore, the set of qualities offered from calorimetry makes it an ideal candidate for the direct study of photochemical reactions for a range of materials. This technique is known as Photocalorimetry and is discussed below.

1.5 Photocalorimetry: Basic Concepts and Principles

Photocalorimetry has been under development for many years and is considered as an extension of classical calorimetry for the study of the combined effects of heat and radiation.[53-56] Many different types of photocalorimeters have been developed for different purposes and their application has covered many fields ranging from microbiology, organic chemistry, to materials science. It is the availability of a wide variety of thermo-kinetic information from the calorimetric data that makes it possible

for such information to be exploited for the development of photocalorimetric studies. However, to observe slow and low-energetic reactions very few instruments have been developed (as detailed below). In such cases, the sensitivity and stability of the instrument would be of great importance. The successful application of such a technique can offer the advantage of being able to monitor both fast and very slow processes and has the capability to study the kinetics and mechanisms of complex systems.

In general, the basic components of a photocalorimeter are comprised of a:

- 'standard' calorimeter – contains the sample and reference to provide actual measurement
- light delivery system – lamp source, power supply, filters or monochromators and appropriate optics for beam steering
- connection between both the calorimeter and light delivery system
- recording device – normally a PC with suitable software

An illustration of a basic setup is represented in Figure 1.5.

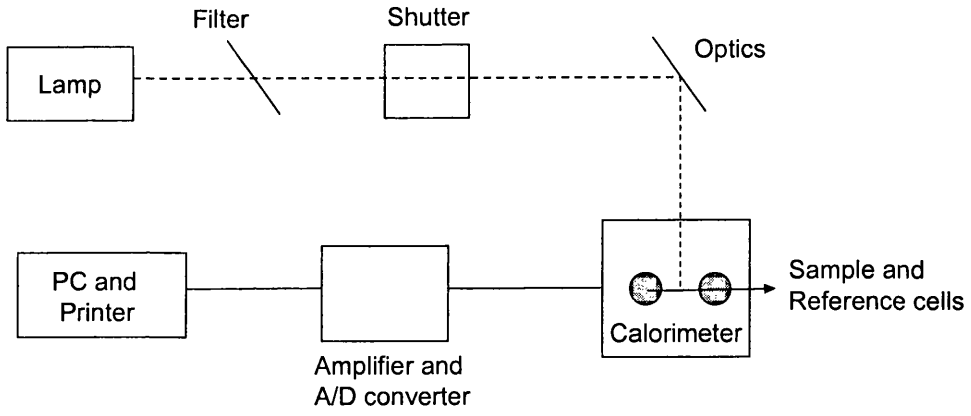

Figure 1.5: Schematic of the basic components of a photocalorimeter

There are two main methods used to introduce light into a calorimetric vessel; the first, through a window made from glass or quartz, the other method is by use of light guides consisting of fibres, fibre bundles or solid rods, (which can be made from a polymer, quartz or glass). Nowadays liquid-filled flexible tubes are also available. These are further discussed in Chapter 2. Flexible light guides can offer a great advantage for instrument design and use. However, light transmission through a flexible guide may vary significantly if its shape is changed. It is, therefore, essential that the light guide has a well-defined and fixed position in the instrument.

In a photocalorimeter, a reaction is initiated when a sample is irradiated, by light of an appropriate wavelength from an external source, directly into the calorimeter via flexible fibre optic light guides. All the light entering the calorimeter cell is either absorbed by the sample or by the walls of the calorimetric vessel. In the case of an inert substance (reference), all the light energy is converted into heat and the calorimeter measures the total light energy flux into the cell. If however, the light induces a photochemical reaction in the sample, an additional heat of reaction is observed, over and above the incident light energy itself. This causes the signal in the sample side in the calorimeter to be out of balance with that of the reference side. Thus, by comparison of the photochemically active substance with some suitable inert reference, and by determining the extent of the light-induced reaction, it is possible to measure directly: (1) the change in heat energy (enthalpy) of the sample produced by the isothermal photochemical transformation and (2) the amount of material, in moles, transformed in the reaction.[54]

In a reference experiment the total amount of radiation, E_p, supplied to the photo-inert substance is quantitatively transformed into heat, Q', and measured by the calorimeter, as represented in Equation 1.21.

$$E_p = Q' \qquad \text{Eqn. 1.21}$$

Note; Equation 1.21 is only valid for the simplest case where no heat losses occur.

During a photochemical experiment, which now contains the photolyte under study, the same amount of radiant energy is supplied to the calorimeter in conditions as close as

possible to those in the blank experiment. In this case, however, a photochemical reaction does take place as shown below.

$$A + \ldots\ldots \xrightarrow{h\nu} A^{*} + \ldots\ldots \longrightarrow B + \ldots$$

$$\text{Reactants} \xrightarrow{h\nu} \text{Products}$$

The photolyte, A, is activated by the radiation and it goes from the ground to an excited state A^{*}, which then undergoes the reaction.

In a photochemical experiment, a certain amount of radiation, E_p, is quantitatively transformed to heat energy, Q (associated with the formation of the products during the reaction) and measured by the calorimeter. An ideal situation, as that represented by a reference experiment (Eqn. 1.21), only occurs where *all* the light energy is transformed to heat. Components, such as stirrers, light guides, etc, in the photocalorimetric system, can cause some loss of the incident radiation should be accounted for.

1.5.1 History and Development of Photocalorimetry

Interest in the thermodynamic examination of materials sensitive to light using calorimetric techniques has increased significantly since the late 1930's. The first use of the photocalorimeter was reported by Magee *et al*, 1939.[57] It was designed for the thermal determination of the quantum efficiency of photosynthesis in algae (*Chlorella pyrenoidosa* or *Chlorella vulgaris*). The photocalorimeter was comprised of a thermopile heat-conduction calorimeter using a small thin-walled quartz cell mounted in an aluminium container with a double thermostat bath. A multi-junction thermocouple was used; one thermopile was used as a sensor for the heat-flow, the other for the measurement of light transmittance. A schematic of the instrument is shown in Fig. 1.8.

The determination of the thermal efficiency of photosynthesising algae was conducted using a 500 *W* projection lamp which introduced light through the front wall of the quartz cylinder. The thermal efficiency was calculated based on the rate of heat absorption by the process of respiration and photosynthesis. The net amount of radiation dissipated as heat by the algae per unit time was then calculated between the two processes.

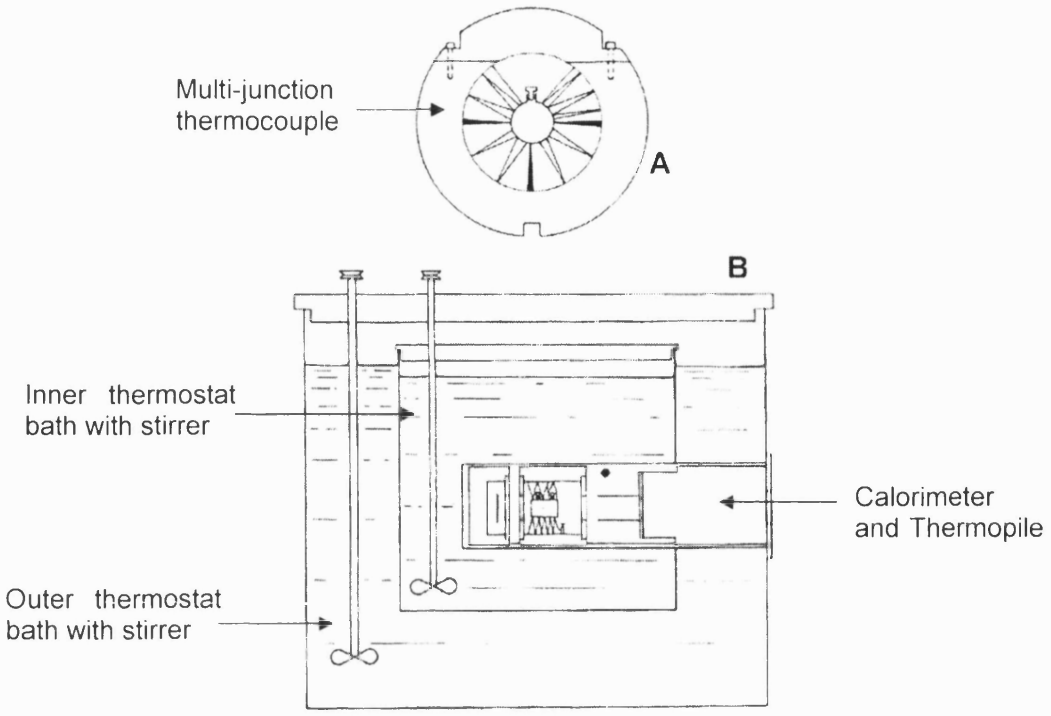

Figure 1.6: The first photocalorimeter designed by Magee *et al* (1939)[57]; A: end view, B: side view in thermostat

The same apparatus was later used to study the quantum yields and the influence of oxygen in the kinetics of the photobromination of hydrocarbons.[58] Although the apparatus was used to determine the overall enthalpy change associated with photochemical reactions and to study the photochemical quantum yields of the organism, its design was elaborate and lacked determination of long-term stability.

After thirty years, photocalorimetry steadily started to be developed. In the late sixties, Seybold *et al* (1969)[59] investigated the quantum yield of fluorescent dyes using a semi-adiabatic double calorimeter. One of the calorimetric vessels was charged with fluorescent solution and the other vessel was charged with a black solution to allow the measurement of the transmitted light.

It was during the eighties when development of photocalorimeters rapidly increased and the technique was applied to different fields. Many of the instruments developed during

allow irradiation of the sample. These were particularly important in the studies concerning photopolymerisation.[60-64]

In 1977, Olmsted *et al*[65-68] made further improvements to Seybold's photocalorimeter. The fluorescence quantum yields were measured in a similar manner as reported by Seybold (1969)[59] but solutions were prepared using spectrophotometric techniques. A Dewar calorimetric vessel was equipped with quartz windows to allow passage of light from a 75 *W* Hg lamp source. A similar instrument was designed for photon flux measurements of solutions.[67,68] It consisted of a Dewar vessel equipped with quartz optical windows, a magnetic stirrer which assured thermal uniformity of the solution, a calibration heater and a thermistor used as a temperature sensor.

In 1978, Adamson *et al* (1978)[69] reported on a photocalorimeter, similar to the Olmsted instrument, for the determination of enthalpies of photolysis of *trans*-azobenzene, ferrioxalate and cobaltioxalate ions, hexacarbonylchromium and decarbonyldihenium. The apparatus (depicted in Figure 1.7) included a glass reaction vessel and double-wall container fitted with quartz windows for the incident light beam. Adamson and co-workers used the instrument, with slight modifications, to further study a series of other systems.[70-74]

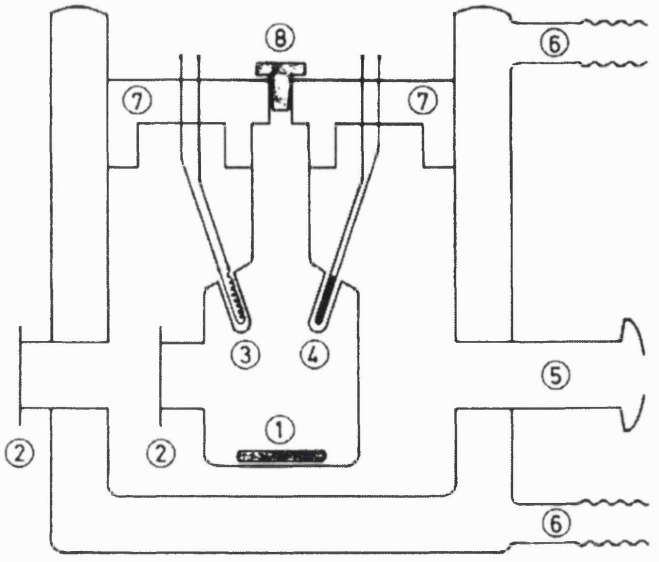

Figure 1.7: Photocalorimeter designed by Adamson *et al* (1978)[69]: 1) Magnetic stirrer bar; (2) Quartz windows; (3) Calibration heater; (4) Thermistor; (5) to Vacuum pump; (6) to Thermostat; (7) Metal cover; (8) Cap to inner cell.

The photocalorimeteric procedure, using the instrument shown above, allowed determination of the light-induced enthalpy change of a reaction as follows; in the case where the light of flux F^0 (Js^{-1}) is absorbed by a solution, yet no photochemical reaction occurs, the energy appears as heat, F^0t (where t is the time of irradiation in seconds). However, in the occurrence of a photo-induced reaction, the observed rate of heat production will be of a different value, F, and the quantity $(F^0 - F)t$ gives the enthalpy change associated with the amount of reaction that has occurred. The ΔH of the reaction can thus be calculated by $(F^0 - F)/n$ (where n is the number of moles reacted per second). It should be noted that the terms $F^0 - F$ are proportional and not direct measurements of heat (J). A particular drawback to this instrument was that it suffered in precision since its application was dependent upon the difference in heat $(F^0 - F)$ and if ϕ (the quantum yield for the photoreaction) is small, this technique could also be insensitive.

During the same period interest in photocalorimetry was fast evolving. The use of optical light guides, rather than windows made of glass or quartz, was becoming a more

popular method to introduce light into the calorimetric vessel. A major advantage was its practical applicability; optical light guides usually have a small aperture making them more suitable for use with microcalorimeters.

The first report of the use of optical light guides as a means to introduce light into a calorimetric vessel was by Schaarschmidt and Lamprecht[75-77] who described two different calorimeters fixed with two light guides designed for studies of living yeast cells. The first design comprised of a quartz light guide, 10 *mm* diameter, used to investigate the sensitivity of yeast cells to UV radiation. The second design was fitted with two thin light guides, 1 *mm* diameter, into a twin isothermal microcalorimeter. The vessel was not designed as a photocalorimetric vessel, but its purpose was for the simultaneous determination of heat production and optical densities of yeast cell suspensions. A schematic of the instrument is represented in Figure 1.8.

McIlvaine and Langerman (1977)[78] used a semi-adiabatic titration calorimeter fitted with a 6.5 *mm* fibre bundle in their calorimetric measurements of luminescent bacteria. The light generated by the micro-organisms was transmitted by the light guide to a photomultiplier. Although not strictly a photocalorimeter since there is no irradiation system, the work is still of relevance. Langerman (1978)[79] also described a similar instrument, where the calorimetric vessel was fitted with fibre optics, which was used for the simultaneous determination of heat evolution and light production.

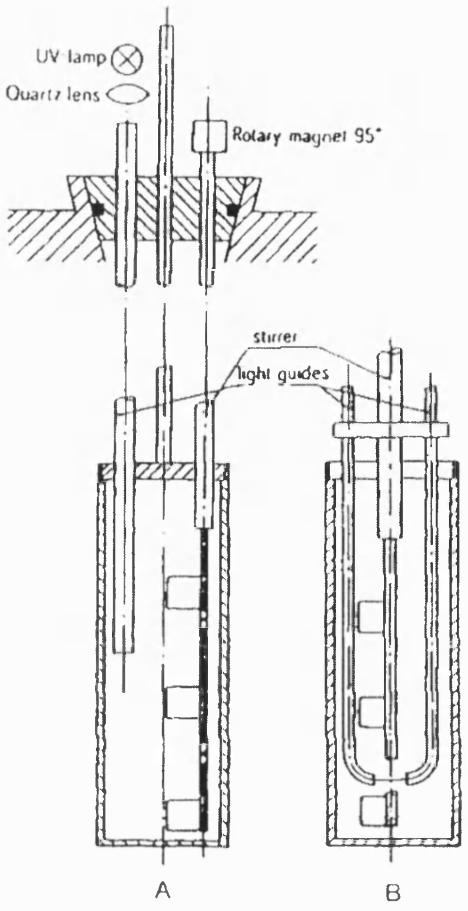

Figure 1.8: Photocalorimeter designed by Schaarschmidt and Lamprecht *et al* (1973); [75] (A): photocalorimetric vessels (B): vessel for simultaneous measurement of heat flow and optical density.

Different types of photocalorimeters have been used to study the chemistry of vision, including a typical solution-reaction microcalorimeter (LKB Producter batch microcalorimeter, now known as a TAM ThermoMetric AB, Järfalla, Sweden). Cooper and Converse (1976)[80] transformed a LKB batch microcalorimeter into a photocalorimeter by fitting it with quartz optical fibre light guides for their study of the photochemistry of *rhodopsin*. A schematic of their assembly is shown in Figure 1.9. The optical system comprised of a 200 *W* Hg-Xe arc lamp, a monochromator and glass fibre bundles.[81-83]

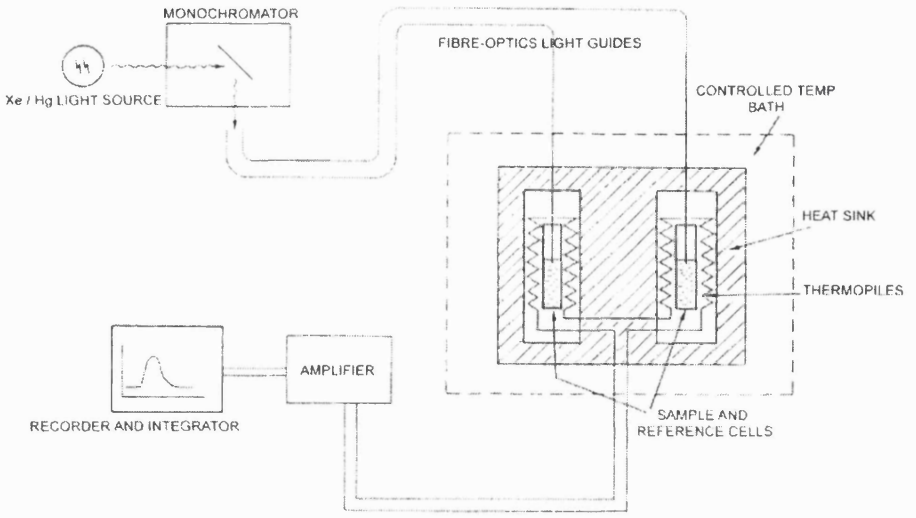

Figure 1.9: Photocalorimeter designed by Cooper and Converse (1976)[80].

In recent years, thermopile heat conduction type microcalorimeters have been applied to photocalorimeteric studies. The commercial TAM is available as a modular system with several channels (as shown previously in Figure 1.3). Because of a combination of versatility and sensitivity, the TAM makes a more superior choice for photocalorimetric measurements over a conventional DSC.[84] Many types of calorimetric vessels, such as steel ampoules, perfusion-titration vessels, etc, can be incorporated into the calorimetric channels making it suitable for photocalorimeteric work.

An application of this was reported in 1990[53] where two twin calorimeters (LKB Thermometric 2277 or TAM, Jarfalla, Sweden) were fitted with six optical cables of single fibres of 1 *mm* diameter, i.e. two channels were operated simultaneously. The optical cables guided light from a 100 *W* tungsten lamp through a monochromator. The beam was split between two calorimetric vessel (three cables were inserted in each vessel) of the two twin calorimeters. One vessel, a stirred perfusion/titration vessel, was used for the measurement of the thermal power during a photochemical reaction. The other served as a photo-inert reference, using a simple calorimetric vessel. The differential signal was recorded for each of the two twin calorimetric vessels. The

design, shown in Figure 1.10, was typical of solution photocalorimeters believed to be useful in the study of different plant materials.[85]

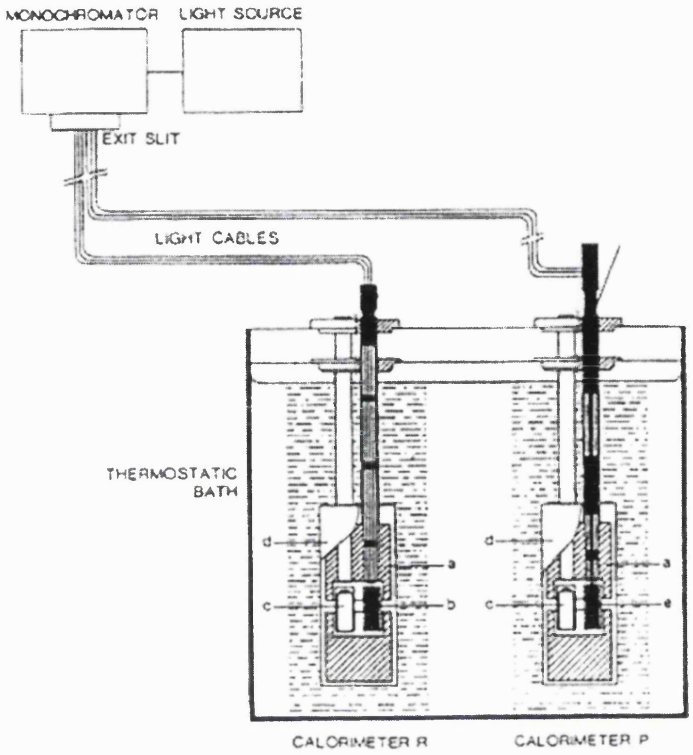

Figure 1.10: Photocalorimeter designed by Teixeira and Wadso (1990)[53]. Calorimeter R: vessel for photochemical reactions; Calorimeter P: vessel for photo-inert reactions; a) heat sinks; b) photo-inert light absorption vessel; c) calorimetric reference "vessel"; d) steel can; e) photochemical reaction "vessel". Note: the thermopiles and parts of the heat sink surrounding the vessel are not shown

Subsequent work followed where the same kind of twin microcalorimeter and photochemical reaction vessel was used.[86,87] In this instance only one of the four chambers, i.e. one channel, of the TAM was utilised, as shown in Figure 1.11. Three optical cables were inserted into each vessel; the photo-inert vessel and perfusion-titration (sample) vessel. The perfusion-titration vessel was a modified version of the

vessel.[53] These modifications were made in order to improve the baseline stability. The photoinert vessel is used as the reference, quantitatively transforming the entire incident light. The sample vessel containing the light guides is charged with the solvent. The position of the optical fibres is adjusted to maintain a stable baseline with and without illumination. In such conditions, the same heat output is measured in both vessels, thus the net output is zero.

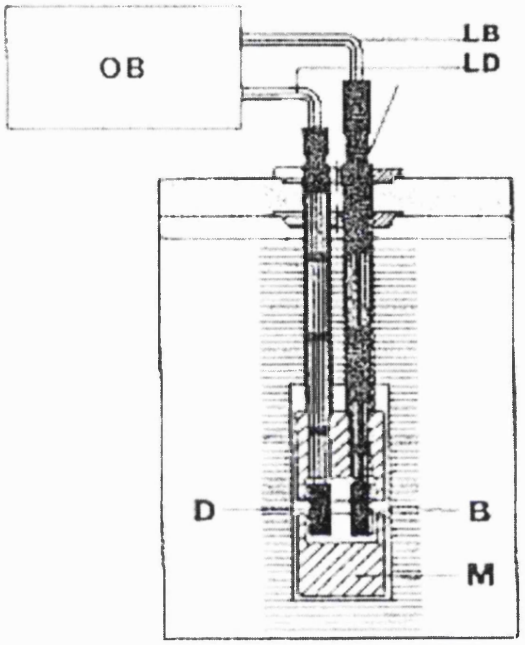

Figure 1.11: TAM photocalorimeter (one channel operation); (OB): optical bench; (D): photoinert vessel; (B): perfusion titration vessel; (M): an ampoule channel in an twin calorimeter; (LD): three optical cables inserted into vessel D; (LB): three optical cables inserted into vessel B.

The instruments described so far have been designed specifically for a number of purposes and their application has been related to different fields such as biology and pure chemistry (namely organic and inorganic). Although these instruments were built for different measurements, their basic mechanical design is similar and closely related to that of the novel photocalorimeter described herein.

1.5.1.1 Applications in Pharmaceutics

Calorimetric and in particular photocalorimetric techniques are particularly useful to study reactions which are too slow for the observation under thermal activation conditions, but can be sufficiently activated by irradiation. In general, there is a lack of instrumentation available for the observation of slow and low energetic reactions. Such an instrument would require particular attention to the sensitivity and stability of the apparatus. In recent years, this issue was addressed by Lehto *et al* (1999).[88] A photocalorimeter was constructed which was designed potentially to monitor slow and low-energetic photoreactions in application to pharmaceuticals of both solid and solution forms. The photocalorimeter consisted of an irradiation cell coupled with a TAM 2277 and was used with the commercial 4 mL ampoule microcalorimetric unit.

The apparatus (Figure 1.12) comprised of a 75 *W* Xe-arc lamp which was used to introduce light through a grating monochromator via an assembly of focusing mirrors and a shutter. The light entry was split into two parts through two identical 1*mm* optical light cables and introduced into the calorimetric vessels. One of the vessels is used as a photocalorimetric vessel that responded to both the thermal activity of the photosensitive reaction and adsorption of the light. The other vessel served as a reference vessel that responds solely on the light adsorption.

The instrument was used for photodegradation studies of photolabile compounds; nifedipine and L-ascorbic acid, at different wavelengths in solution and solid state.[89] The measurements were conducted using two technically identical irradiation cells that were positioned in the sample sides of two separate twin calorimetric units. Although no significant quantitative data were obtained, the technique offered a rapid and versatile method to study the photosensitivity of materials in any state.

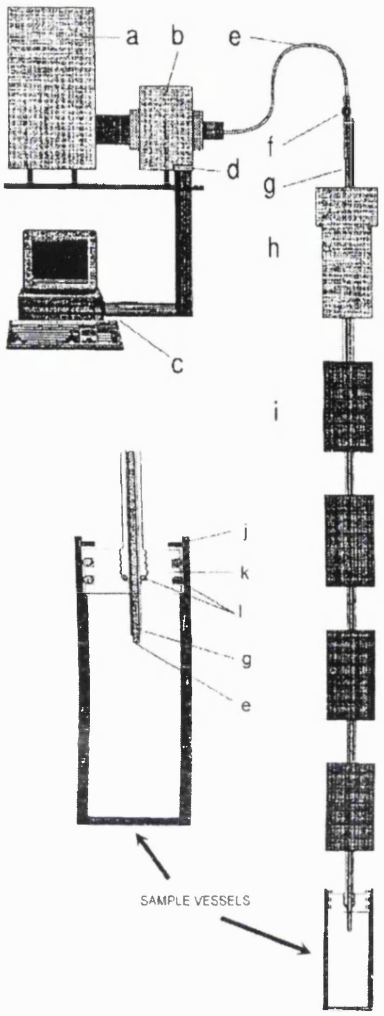

Figure 1.12: Schematic of an irradiation cell constructed by Lehto *et al* (1999)[88]. The beam from the monochromator is split into two parts and conducted into identical irradiation cells; (a): lamp house; (b): monochromator; (c): PC; (d): step motor; (e): light cable; (f): SMA connector; (g): insertion tube for light cable; (h): plastic holder; (i): heat exchanger; (j): locking ring; (k): teflon lid; (l): O-ring.

More recently, a photocalorimeter was constructed by Morris[56] which aimed to perform photostability testing of pharmaceuticals to yield both qualitative and quantitative data in solution and solid-state materials. Its design was based on the work of Lehto *et al* (1999).[88] The photocalorimeter was equipped with a high-intensity light (300 W xenon arc lamp) from which light irradiated a sample through a monochromator. This allowed

the different wavelengths of light contributing to photodegradation to be analysed selectively. The light then passed via a trifurcated cable of optical fibres; two of the cables led into the sample and reference cells of a commercial TAM, and the third could be connected to a spectroradiometer enabling direct quantitative measurement of the amount of light being delivered to photochemical sample in "real time". The flexible optical cables were contained in a stainless steel light guide. This ensured the optic cables were fixed in position relative to each other, since any changes in the orientation, shape and position of the cables may significantly vary the light transmittance. Furthermore, well defined light guides were used to ensure the optic cables were at a fixed distance apart to allow an easy and consistent entry into the calorimetric unit.

Figure 1.13 depicts a schematic of the instrument design. Note; the monochromator is not shown. The monochromator stands as a separate accessory and can be incorporated as part of the system during measurement.

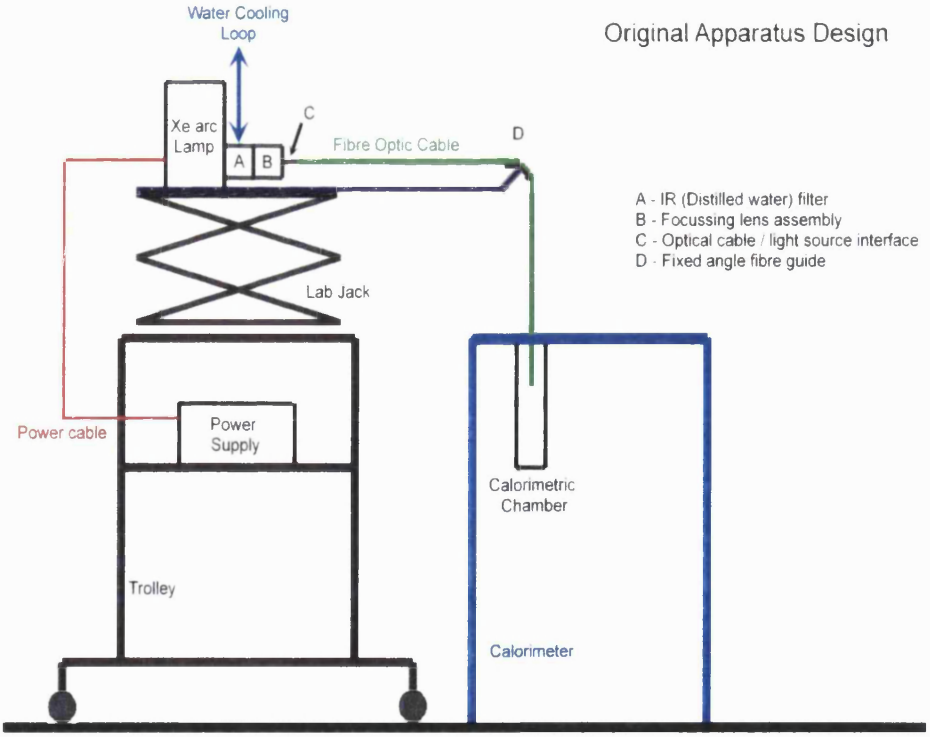

Figure 1.13: Schematic design of Morris' (2004) photocalorimeter[56]

The instrument was designed to study the rate of photodegradation for a wide range of pharmaceuticals, which can be used to yield information on the kinetic and thermodynamic parameters for both solid and solution phase systems. The suitability of the photodegradation of 2-nitrobenzaldehyde and photoreduction of potassium ferrioxalate – an IUPAC recommended chemical calibrant – were investigated for validating photoreactions in solution phase systems. The photodegradation of nifedipine was also proposed as a calibrant in the solid-state.

It is the photocalorimeter design of Morris[56] that forms the basis of the instrument developed during this project. The instrument design and test applications are further detailed in Chapter 2, 3 and 5. The former project, conducted by Morris[56], was originally based at the University of Greenwich, UK. Thereafter, the photocalorimeter was transported, to its current location; The School of Pharmacy, University of London, UK for further developmental work. This research follows on from Morris'[56] work, and extends on developments through design considerations to improve the performance of the instrument.

Details of the instrument design, technicalities, operation and performance are given in Chapter 2 along with developments and modifications made to the system as the project progressed.

1.6 Summary

This thesis is primarily concerned with the development of a novel photocalorimeter to study the photostability of pharmaceutical compounds. In order to assess the photostability of a material, for the predication of shelf life for instance, something about the kinetics and thermodynamics of the degradative reactions must be known.

Calorimetry is widely recognised as an alternative to classical analytical techniques, for example, HPLC and spectrophotometry. Such techniques can be time consuming, require extensive sample preparation, and involve destructive and invasive sampling techniques. Calorimetry, on the other hand, offers many advantages; it is invariant to physical form, rapid, non-invasive, non-destructive to the sample, and offers availability of a wide variety of thermo-kinetic information from calorimetric data in real-time. These qualities set the technique apart from most other analytical techniques commonly used for stability studies. The extension of calorimetry to monitor photodegradative processes is therefore particularly interesting because the combined effects of heat and radiation can be studied.

Subsequent chapters will show the development of a novel photocalorimeter and how thermo-kinetic information can be exploited from the calorimetric data to monitor photostability of pharmaceuticals. This is considered through the development of a chemical test and reference reaction, 2-nitrobenzaldehyde, and the photodegradation of nifedipine in a solution phase system.

1.7 References

1 Carstensen, J.T., and Rhodes, C.T. (2000) *Drug Stability Principles and Practices*, Marcel Dekker

2 Anderson, N.H., Johnston, D., McLelland, M.A., and Munden, P. (1991) Photostability testing of drug substances and drug products in UK pharmaceutical laboratories. *J.Pharm.Biomed.Anal* 9, 443-449

3 Tonnesen, H.H. (1991) Photochemical degradation of components in drug formulations. I. An approach to the standardization of degradation studies. *Pharmazie* 46, 263-265

4 Tonnesen, H.H., and Karlsen, J. (1995) Photochemical degradation of components in drug formulations. III. A discussion of experimental conditions. *Pharmeuropa* 7, 137-141

5 Tonnesen, H.H., and Moore, D.E. (1993) Photochemical degradation of components in drug formulations. *Pharm.Tech.Int* 5, 27-33

6 Piechocki, J.T. (1998) Principles of chemical actinometry. In *Drugs photochemistry and photostability* (Albini, A., and Fasani, E., ed.), The Royal Society of Chemisty

7 ICHQ1B. (1997) Photostability Testing of New Active Substances and Medicinal Products. *EMEA*, CPMP/ICH/2791/2795

8 ICHQ1B. (1997) Photostability Testing of New Drug Substances and Products. *Fed. Reg.* 62 (95), 27115-27122

9 Sequeira, F., and Vozone, C. (2000) Photostability studies of drug substances and products. Practical implications of the ICH guideline. *Pharm.Tech* 24 (8), 30-35

10 Piechocki, J.T., Wolters, R.J. (1993) Use of actinometry in photolysis stability studies. *Pharm.Tech* 17, 46-52

11 Piechocki, J.T., Wolters, R.J. (1994) Light stability studies: A misnomer. *Pharm.Tech* 18, 60-65

12 Nema, S., Washkuhn, R.J., and Beussink, D.R. (1995) Photostability testing: an overview. *Pharm.Tech.* 19 (3), 170-185

13 Thatcher, S., Mansfield, R.K., Miller, R.B., Davis, C.W., and Baertschi, S.W. (2001) "Pharmaceutical photostability" A technical guide and practical interpretation of the ICH guideline and its application to pharmaceutical stability - Part I. *Pharm.Tech* 25 (3), 98-110.

14 Thatcher, S., Mansfield, R.K., Miller, R.B., Davis, C.W., and Baertschi, S.W. (2001) "Pharmaceutical photostability" A technical guide and practical interpretation of the ICH guideline and its application to pharmaceutical stability - Part II. *Pharm.Tech* 25 (4), 58-64

15 Moore, D.E. (1987) Principles and practice of drug photodegradation studies. *J.Pharm.Biomed.Anal* 5 (5), 441-453

16 Tonnesen, H.H. (2004) *Photostability of drugs and drug formulations*, CRC press

17 Tonnesen, H.H. (2001) Formulation and stability testing of photolabile drugs. *Int.J.Pharm.* 225, 1-14

18 Aman, W., and Thoma, K. (2002) The influence of formulation and manufacturing process on the photostability of tablets. *Int.J.Pharm.* 243, 33-41

19 Templeton, A.C., Xu, H., Placek, J., and Reed, R.A. (2005) Implications of photostability on manufacturing, packaging, storage, and testing of formulated pharmaceutical products. *Pharm.Tech.*, 68-86

20 Thoma, K., and Klimek, R. (1991) Photostabilization of drugs in dosage forms without protection from packaging materials. *Int.J.Pharm.* 67, 169-175

21 Andrisano, V., Bertucci, C., Battaglia, A., and Cavrini, V. (1999) Photodegradation studies on Atenolol by liquid chormatogrpahy. *J.Pharm.Biomed.Anal* 21, 851-857

22 Andrisano, V., Bertucci, C., Battaglia, A., and Cavrini, V. (2000) Photostability of drugs: photodegradation of melatonin and its determination in commercial formulations. *J.Pharm.Biomed.Anal* 23, 15-23

23 Brisaert, M., and Plaizier-Vercammen, J. (2000) Investigation on the photostability of a tretinion lotion and stabilisation with additives. *Int.J.Pharm.* 199, 49-57

24 Majeed, I.A., Murray, W.J., Newton, D.W., Othman, S, and Al-turak, W.A. (1987) Spectrophotometric study of the photodecomposition kinetics of nifedipine. *J.Pharm.Pharmacol* 39, 1044-1046

25 Chang, H., Su, Y., and Chang, S. (2006) Studies on photostability of butyrylated, milled wood lignin using spectroscopic analyses. *Polymer Degradation and Stability* 91, 816-822

26 Teraoka, R., Otsuka, M., and Matsuda, Y. (2004) Evaluation of photostability of solid-state nicardipine hydrochloride polymorphs by using Fourier-transformed reflection-absorption infrared spectroscopy-effect of grinding on the photostability of crystal form. *Int.J.Pharm.* 286, 1-8

27 Chen, X., Peng, X., Cui, Z., Wang, B., Wang, L., and Zhang, R. (2006) Photostabilities of novel heptamethine 3H-indolenine cyanine dyes with different N-substituents. *J.Photochem.Photobiol A:Chem* 181, 79-85

28 Lipson, S.M., O'Brien, D.F., Byrne, H.J., Davey, A.P., and Blau, W.J. (2000) Investigation of efficiency and photostability in polymer films. *Synthetic Metals* 111-112, 553-557

29 Breier, A.R., Nudelman, N.S., Steppe, M., and Schapoval, E.E.S. (2008) Isolation and structure elucidation of photodegradation products of fexofenadine. *J.Pharm.Biomed.Anal* 46, 250-257

30 Chen, D., Zhou, J., Tian, Q. (1996) Mechanisms and structures of free radicals in the photoreaction processes of o-substituted nitrobenzaldehydes. *Journal of Photochemistry and Photobiology A: Chemistry* 98, 21-26

31 Silchenko, S., Schöneich, C., Carlson, B.J., and Stella, V. J. (2003) Photostability of 2-hydroxymethyl-4,8-dibenzo[1,2-b:5,4-b']dithiophene-4,8-dione (NSC 656240), a potential anticancer drug. *Int.J.Pharm.* 264, 97-105

32 Kojima, T., Onoue, S., Katoh, F., Teraoka, R., Matsuda, Y., Kitagawa,S., and Tsuhako, M. (2007) Effect of spectroscopic properties on photostability of tamoxifen citrate polymorphs. *Int.J.Pharm.* 336, 346-351

33 Atkins, P.W. (1994) *Physical Chemistry*, 5th Ed. Oxford University Press

34 Buckton, G., Beezer A.E. (1991) The applications of microcalorimetry in the field of physical pharmacy. *Int.J.Pharm.* 72, 181-191

35 Cox, B.G. (1994) *Modern liquid phase kinetics*, Oxford University Press

36 Lavoisier, A.L., and De Laplace, P.S. (1784) Memoir of heat. *Histoire de l'Academie Royale des Sciences* 1780, 355

37 Wadso, I., Goldberg, R. N. (2001) Standards in isothermal microcalorimetry (IUPAC technical report). *Pure.Appl.Chem* 73, 1625-1639

38 Backman P, B.M., Briggner LE, Hagg S, Hallen D, Lonnbro P, Nilsson SO, Olofsson G, Schon A, Suurkuusk J, Teixeira C, and Wadso I. (1994) A system of microcalorimeters. *Pure & Appl Chem* 66 (3), 375-382

39 Suurkuusk, J., and Wadso, I. (1982) A multichannel microcalorimetry system. *Chem Scripta* 20, 155-163

40 Technical Specification, Thermometric AB, Note 22016.

41 Wadso, L. (2001) The isothermal heat conduction calorimeter: a versatile instrument for studying processes in physics, chemistry and biology. *J.Chem.Edu.* 78, 1080-1086

42 Willson, R., Beezer, A., Mitchell., J.C., and Watson, L. (1995) Determination of thermodynamic and kinetic parameters from isothermal heat conduction microcalorimetry: applications to long-term reaction studies. *J.Phys.Chem* 99, 7108-7113

43 Willson, R.J. (1995) Ph.D Thesis. University of Kent, UK.

44 Hills, A.K. (2001) Ph.D Thesis. University of Kent

45 Beezer, A., Morris, A.C., O'Neill, M.A.A., Willson, R.J., Hills, A.K., Mitchell, J.C., and Connor, J.A. (2001) Direct determination of equilibrium thermodynamic and kinetic parameters from isothermal heat conduction microcalorimetry. *J.Phys.Chem B* 105, 1212-1215

46 Ng, W.L. (1975) Thermal decomposition in solid-state. *Aust.J.Chem* 28, 1169-1178

47 Beezer, A.E., Gaisford, S., Hills, A.K., Willson, R.J., Mitchell, J.C. (1999) Pharmaceutical microcalorimetry: applications to long-term stability studies. *Int.J.Pharm.* 179, 159-165

48 Beezer, A., O'Neill, M.A.A., Urakami, K., Connor, J.A., and Tetteh, J. (2004) Pharmaceutical microcalorimetry: recent advances in the study of solid-state materials. *Therm.Acta* 420, 19-22

49 O'Neill, M.A.A., Beezer, A.E., Morris, A.C., Urakami, K., Willson, R.J., Connor, J. (2003) Solid-state reactions from isothermal heat conduction microcalorimetry: Theoretical approach and evaluation via simulated data. *J.Therm.Anal.Cal.* 73, 709-714

50 Willson, R.J., and Beezer, A.E. (2003) A mathematical approach for the calculation of reaction order for common solution phase reactions. *Therm.Acta* 402, 75-80

51 O'Neill, M.A.A. (2005) Recent Developments for the Analysis of Data Obtained from Isothermal Calorimetry. *Curr.Pharm.Biotechnol.* 6, 205-214

52 Skaria, C.V., Gaisford, S., O'Neill, M.A.A., Buckton, G., Beezer, A.E. (2005) Stability assessment of pharmaceuticals by isothermal calorimetry: two component systems. *Int.J.Pharm.* 292, 127-135

53 Teixeira, C., Wadso, I. (1990) A microcalorimeter system for photochemical processes in solution. *J Chem Therm* 22, 703-713

54 Teixeira, C., and Wadso, I. (1994) Solution photocalorimeters. *Netsu Sokutei* 21, 29-39

55 Teixeira, C. (1999) Photocalorimetry: methods and applications. 105-136

56 Morris, A.C. (2004) Ph.D Thesis. University of Greenwich, Kent, UK.

57 Magee, J.L., DeWitt, T.W., Smith, E.C., and Daniels, F. (1939) A photocalorimeter: The quantum efficiency of photosynthesis in aglae. *J.Am.Chem.Soc.* 61, 3529-3533

58 Magee, J.L., Daniels, F. (1940) The heat of photobromination of the phenyl methanes and the cinnamic acid, and the influence of oxygen. *J.Am.Chem.Soc.* 62, 2825-2833

59 Seybold, P.G., Gouterman, M., and Callis, J. (1969) Calorimetric, photometric and lifetime determinations of fluorescein dyes. *Photochem.Photobiol.* 9, 229-242

60 Appelt, B.K., and Abadie, M.J.M. (1985) Thermal analysis of photocurable materials. *Polym.comp.* 25, 931-933

61 Appelt, B.K., and Abadie, M.J.M. (1988) Calorimeteric characterisation of photosensitive materials. *Polym.Eng.Sci.* 28, 367-371

62 Abadie M.J.M., A.B.K. (1989) Photocalorimetry of light-cured dental composites. *Dent.Mater* 5, 6-9

63 Hoyle, C.E. (1992) Calorimetric analysis of photopolymerization. *Radiation curing* 3, 57-133

64 Lecamp, L., Youssef, B., Bunel, C.,. (1997) Photoinitiated polymerization of a dimethacrylate oligomer: 1. Influence of photoinitiator concentration, temperature and light intensity. *Polymer* 38, 6089-6096

65 Mardelli, M., and Olmsted III, J. (1977) Calorimetric determination of the 9, 10-diphenyl-anthracene fluorescence quantum yield. *J.Photochem* 7, 277-285

66 Magde, D., Brannon, J. H., Cremers, T. L., Olmsted III, J. (1979) Absolute luminescence yield of cresyl violet. A standard for the red. *J.Phy.Chem* 83, 696-699

67 Olmsted III, J. (1979) Photon flux measurements using calorimetry. *Rev.Sci.Instrum.* 50, 1256-1259

68 Olmsted III, J. (1980) Photocalorimetric studies of singlet oxygen reactions. *J.Am.Chem.Soc.* 102, 66-71

69 Adamson, A.W., Vogler, A., Kunkely, H., and Wachter, R. (1978) Photocalorimetry. Enthalpies of photolysis of *trans*-azobeneze, ferrioxalate and cobaltioxalate ions, chromium hexacarbonyl, and dirhenium decarbonyl. *J Am Chem Soc.* 100, 1298-1300

70 Nakashima, M., and Adamson, A.W. (1982) Photocalorimetry. 2. Enthalpies of ligand substitution reactions of some group 6 metal carbonyl complexes in solutions. *J.Phy.Chem* 86, 2905-2909

71 Nakashima, M., and Adamson, A.W. (1982) Photocalorimetry. 3. Enthalpies of substitution reactions of some Cr (III) Ammines and Cr (III) and Co (III) Cyano complexes in aqueous solution. *J.Phy.Chem* 86 (2910-2912)

72 Harel, Y., and Adamson, A.W. (1986) Photocalorimetry. 4. Enthalpies of substitution reactions of Rhodium (III) and Iridium (III) Pentaammine Halides and of Ruthenium (II) Hexaammine. *J.Phy.Chem* 90, 6690-6693

73 Harel, Y., and Adamson, A.W. (1986) Photocalorimetry. 5. Enthalpies of reaction of $M_2(CO)_{10}$ (M = Mn, Re) compounds with Iodine in Cyclohexane solution at 25°C. *J.Phy.Chem* 90, 6693-6696

74 Harel, Y., and Adamson, A.W. (1987) Photocalorimetry. 6. Enthalpies of isomerization of Norbonadiene and of substituted Norbonadienes to corresponding Quadricyclenes. *J.Phy.Chem* 91, 901-904

75 Schaarschmidt, B., and Lamprecht, I. (1973) UV-irradiation and measuring of the optical density of microorganisms in a microcalorimeter. *Experientia* 29, 505-506

76 Schaarschmidt, B., and Lamprecht, I. (1986) Simultaneous measurements of heat production and optical density in oscillating reactions. *Thermochima Acta* 105, 205-213

77 Lamprecht, I., Schaarschmidt, B., and Plesser, Th. (1987) Extended batch calorimetry on periodic chemical reactions. *Thermochima Acta* 119, 175-187

78 McIlvaine, P., and Langerman, N. (1977) A calorimetric investigation of the growth of the luminescent bacteria beneckea harveyi and photobacterium leiognathi. *Biophy.J.* 17, 17-25

79 Langerman, N. (1978) The simultaneous determination of heat changes and light production. *Meth.Enzymol.* LVIII (57), 540-549

80 Cooper, A., and Converse, C.A. (1976) Energetics of primary process in visual excitation: Photocalorimetry of rhodopsin in rod outer segment membranes. *Biochem.* 15, 2970-2978

81 Cooper, A. (1979) Energy uptake in the first step of visual excitation. *Nature* 282, 531-533

82 Cooper, A. (1982) Calorimetric measurements of light induced processes. *Meth.Enzymol.* 88, 667-673

83 Cooper, A., Dixon, S.F., Tsuda, M. (1986) Photoenergetics of octopus rhodopsin. *Eur.Biophys.J* 13, 195-201

84 Beezer, A.E., Willson, R.J., Mitchell, J.C., Hills, A.K., Gaisford, S., Wood, E., and Connor, J.A. (1998) Thermodynamic and kinetic parameters from isothermal heat conduction microcalorimetry. *Pure Appl.Chem* 70, 633-638

85 Wadso, I. (1995) Microcalorimetric techniques for the investigation of living plant materials. *Thermochima Acta* 250, 285-304

86 Dias, A.R., Minas Da Piedade, M.E., Simoes, J.M., Simoni, J.A., Teixeira, C., Diogo, D., Yan, Y.M., and Pilcher, G. (1992) Enthalpies of formation of *cis*-azobenzene and *trans*-azobeneze. *J.Chem.Therm.* 24, 439-447

87 Dias, P.B., Teixeira, C., Dias, A.R., Simoni, J.A., and Simoes, J.M. (1994) Photomicrocalorimetry: photosubstitution of carbonyl by phosphites in [Mn (n^5-$C_5H_4CH_3$)$(CO)_3$]. *J.Organomet.Chem.* 482, 111-118

88 Lehto, V.P., Salonen, J., and Laine, E. (1999) Real time detection of photoreactivity in pharmaceutical solids and solutions with isothermal microcalorimetry. *Pharm.Research* 16, 368 - 373

89 Lehto, V.P., Salonen, J. and Laine, E. (1999) A microcalorimetric study on the role of moisture in photolysis of nifedipine powder. *J.Therm.Anal.Cal.* 56, 1305-1310

- Chapter Two -

Photocalorimetry:

Design and Development

2. Introduction

The aim of this chapter is to provide a comprehensive account on the development of a novel photocalorimeter (Mark III) which was built through a series of iterative prototype designs. Details of the instrument design, technicalities, operation and performance are given along with developments and modifications made to the system as the project progressed. Over the course of the project two prototype designs were built. The original design was developed by Morris[1] and forms the basis of the subsequent re-designed photocalorimeters reported herein. For clarity, reference to each design will be given as Mark I, II or III where the original photocalorimeter, that is the design of Morris[1], is referred to as Mark I. The re-designed instrument (beam splitting design) is referred to as Mark II, and the final design (LED photocalorimeter) is referred to as Mark III.

2.1 The Original Photocalorimeter (prototype Mark I)

The design of the Mark I photocalorimeter was briefly outlined in Chapter 1. Figure 2.1 gives detail of the instrument design. Since the photocalorimeter was transported from one location to another, it was imperative that the instrument was assembled and set-up correctly prior to analysis as any change to the geometry of the apparatus can lead to differences in the light transmittance. It is therefore important that the instrument's geometry is securely fixed for consistency in data.

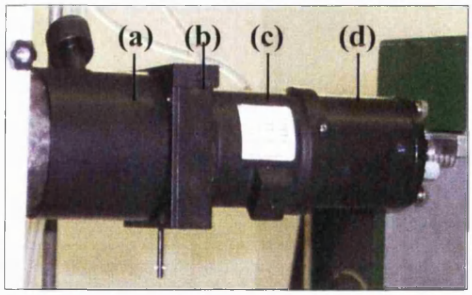

Figure 2.1a: (a): IR filter; (b): shutter; (c): cooling system; (d): focusing lens assembly

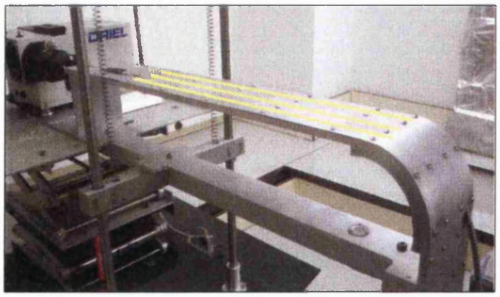

Figure 2.1b: Optical cables contained within stainless steel light guide (indicated in yellow)

Figure 2.1: The Mark I photocalorimeter and components[1]; (A): lamp housing fitted with a 300 W Xe Arc lamp; (B): filter/lens assembly; (C): plastic shrouding surrounding light guide; (D): hand-wound lab jacks; (E): optical cables lowered into TAM calorimetric unit. Note: monochromator not shown.

The Mark I photocalorimeter utilised a 300 W xenon (Xe) arc lamp (ozone free) from which light irradiated through a collimating lens and IR filter into a flexible bundle of optical fibres. The bundle of optics was trifurcated; one branch led into the sample cell and one into the reference cell of a TAM 2277, and the third could be connected to an external radiometer. Assuming an equal division of light between the three branches, the radiometer allowed precise measurement of the light power irradiating the sample cell.

The calorimetric cells were standard stainless steel TAM ampoules (20 mL) and the fibre-optic bundles were mounted through the ampoule lids. Individual fibre-optic cables are relatively fragile and the amount of light transmitted is dependent upon the angle through which the bundle turns. The flexible bundles were long (1 m length) and mounted in a stainless steel light guide (Fig. 2.1b) to which the calorimetric cells were attached. This ensured the optic cables were fixed in position relative to each other and kept in the same orientation to ensure a repeatable geometry to provide consistency in performance. The metal light guide was encased in a detachable plastic shroud designed to insulate the optic cables and minimise data fluctuations generated by heat conduction since the calorimeter is sensitive to even minute heat flow changes. Two mechanical hand-wound lab jacks mounted one on another were situated beneath the lamp housing and components allowing the apparatus to be vertically raised and lowered for sample loading and unloading, respectively. The light source components were placed onto a heavy duty trolley (100 kg) designed to support the weight of the light source equipment and to match the vertical height of the TAM. Figure 2.1 illustrates the photocalorimeter and its design components. A monochromator stands as a separate accessory and could easily be incorporated as part of the assembly for selective wavelength studies.

Having reassembled the instrument, the first step was to investigate the baseline response when the calorimetric cells were situated in the calorimeter. The baseline stability of the Mark I photocalorimeter was monitored in two ways; one to assess the response of the system without subjecting the calorimetric cells to light (light off), and two, to assess the calorimetric response with the input of light (light on). In any case, in a differential system if the heat-flow on the sample and reference side is of equivalence then, ideally, there should be no net signal and hence result in a zero-power signal on the TAM. It was hoped that the Mark I photocalorimeter would respond in such a manner.

2.1.1 Investigating Baseline Stability of Mark I – Light off

Previously, one of the fundamental problems experienced by Morris[1] with this system was that of achieving a stable and zero-baseline. It proved problematic to combine the sensitivity of the TAM with a large mass of stainless steel light source equipment.

Initial tests performed showed baseline outputs to be non-zero and arbitrary. The values reported were irreproducible, varying from ~40 μW to ~300 μW, and not zero as anticipated. One attempt to reduce the irreproducibility revealed that shielding the optic cables with foam based sheets (green shroud in Fig. 2.1) provided some level of protection against external factors (such as the influence of air-conditioning in the laboratory) from interfering with the calorimetric output. This was shown to have a marked response on the system reducing the baseline signal by ~33%. However, this shielding was still not sufficient enough for a zero baseline to be achieved suggesting the system was still subject to heat loss.

To assess if this was still the case even after re-location of the instrument and now in a laboratory without air-conditioning, initial trials were made using the following procedure to assess baseline stability with the light off.

2.1.1.1 Method

All experiments were performed at 298 K in a 2277 TAM (Thermometric Ltd), unless otherwise stated. Electrical calibration checks (3000 μW) were performed periodically on the TAM. All data were recorded on the dedicated software package Digitam 4.1™ and analysed using Microcal Origin Pro 7.0™, unless otherwise stated.

Two empty 20 mL stainless steel calorimetric ampoules were used throughout, unless otherwise stated. The ampoules were washed in ethanol and dried each time prior to use. Each ampoule was clipped securely using a circlip onto the end of a sample and reference fibre optic cable. The ampoules were lowered into the TAM using the hand-wound lab jacks and held in equilibrium for 30 minutes to allow the signal to settle from a thermal shock before being lowered further into the measuring position. The calorimetric response was then recorded and the baseline data were collected. Five experiments were run in this manner and data were collected for approximately 2 hours. The experimental set up remained unchanged for each experiment. Linear regression fittings were performed on the data for the individual runs where the fit linear analysis function on Microcal Origin Pro 7.0™ was used to determine the average power signal after the signal reached plateau.

2.1.1.2 Results and Discussion

Figure 2.2 is typical of the baseline response in the calorimeter. The data obtained though linear regression fitting is represented in Table 2.1. NB. All standard deviations reported throughout were calculated using $x\sigma_{n-1}$ function with a 68% confidence limit (indicated as ± value alongside mean value).

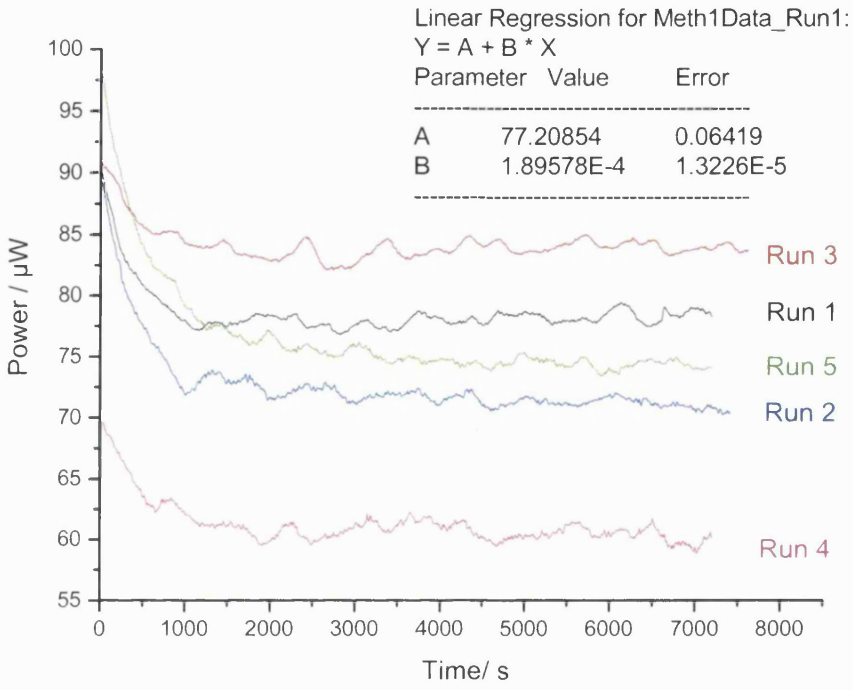

Figure 2.2: Comparison of baselines using the Mark I Photocalorimeter with the light off

Table 2.1: Calorimetric outputs derived through linear regression fitting

Run	Power output/ µW
1	77.2
2	72.6
3	83.0
4	61.3
5	76.2
Mean ± SD	**74.1 ± 8.1**

Initial trials were not promising, a significant problem being that it proved impossible to get a repeatable baseline signal with the light off. The power outputs obtained concur with previous observations,[1] in that a non-zero and irreproducible baseline is exhibited.

An initial thermal shock was observed for approx. the first 1500 seconds of data recording ranging from ~70 μW to ~98 μW. After the effects of the thermal shock the baseline settled to a plateau, as seen after ca. 1500 seconds, the offset equilibrium was reached. The power signals were arbitrary and varied from ~60 μW to ~85 μW with an average offset of **74.1 ± 8.1 μW** derived though linear regression fitting. In a differential system, ideally, a zero baseline signal would indicate equivalence in heat-flow of the sample and reference. Clearly, this was not the case and the irreproducible nature of the baselines suggested there was a significant loss of heat from the calorimeter during measurement. Furthermore, it was not possible even to zero the baseline signal by manual adjustment using the voltage signals of the amplifiers since the magnitude of the signal was far too large and outside the adjustable range of the amplifiers. This immediately indicated that there were problems with equivalence (of geometry) of the sample and reference sides and/or heat losses through conduction and convection. The magnitude of the irreproducibility of the baseline signals would make it difficult/impossible to determine accurate power signals for a sample undergoing a photo-reaction. It was, therefore, essential to address this issue and it became necessary to consider various design elements to ensure the repeatability of the baseline signal. (Section 2.1.3 details the various design considerations that were implemented in order to achieve this). Moreover, further problems arose when the system was subjected to light input (illustrated in Figure 2.3). This issue is discussed further in greater detail in section 2.1.2 and section 2.1.3).

2.1.2 Investigating Baseline Stability of Mark I – Light on

The instrument's response with the light on was tested. Several light on/off tests were conducted to assess the repeatability of the signal with the light on and off using the following method.

2.1.2.1 Method

Two empty 20 mL stainless steel ampoules were lowered into the TAM and held in equilibrium for 30 minutes before being lowered into the measuring position. The

calorimetric response was then recorded until a stable baseline was achieved. The Xe arc lamp (set to 240 W) was ignited and allowed to warm up for 1 hour[2] to minimise photon fluctuations before the ampoules were irradiated. The light was then switched on/off periodically by opening/closing of the shutter. The output with the "light on" was recorded until a stable baseline was attained. The light was then turned off i.e., the shutter was closed, and the "light off" output was recorded until a stable baseline was returned. The light was turned on and off three times to assess baseline repeatability.

2.1.2.2 Results and Discussion

Figure 2.3 is typical of the signal obtained for a single light on/off test and is typical of the baseline response when the system is irradiated with high-intensity light. Immediately, it was observed that turning the light on/off had a significant impact on the TAM output in that there was a considerable deflection from the original baseline (light off) and the signal settled to a new baseline upon irradiation (not zero as hoped in the case of a well balanced system). Such a response was typical and also observed by Morris.[1]

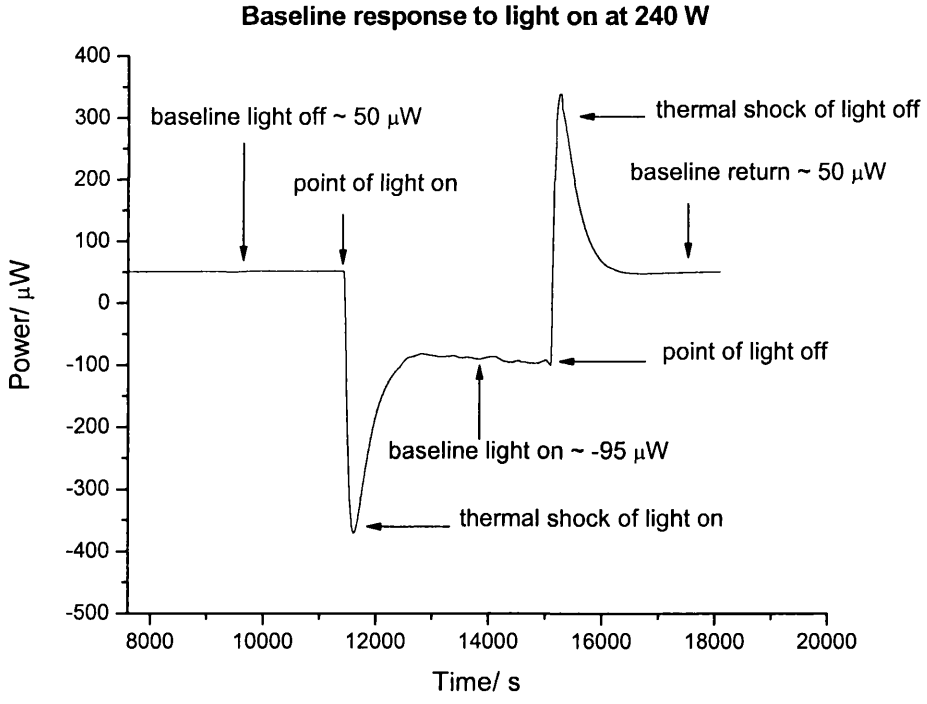

Figure 2.3: Baseline response to light on and off

As shown in Figure 2.3, the baseline initially settled to approx. 50 μW. A thermal shock was observed as the light was turned on and then the signal reached a minimum (lasting approx. 30 minutes) before recovering and settling to a new baseline of approx. -95 μW. The light was then switched off and a positive thermal shock was observed before the signal equilibrated to its original baseline value of approx. 50 μW. The light was switched on and off a two times further to assess the repeatability of the signal (Figure 2.4).

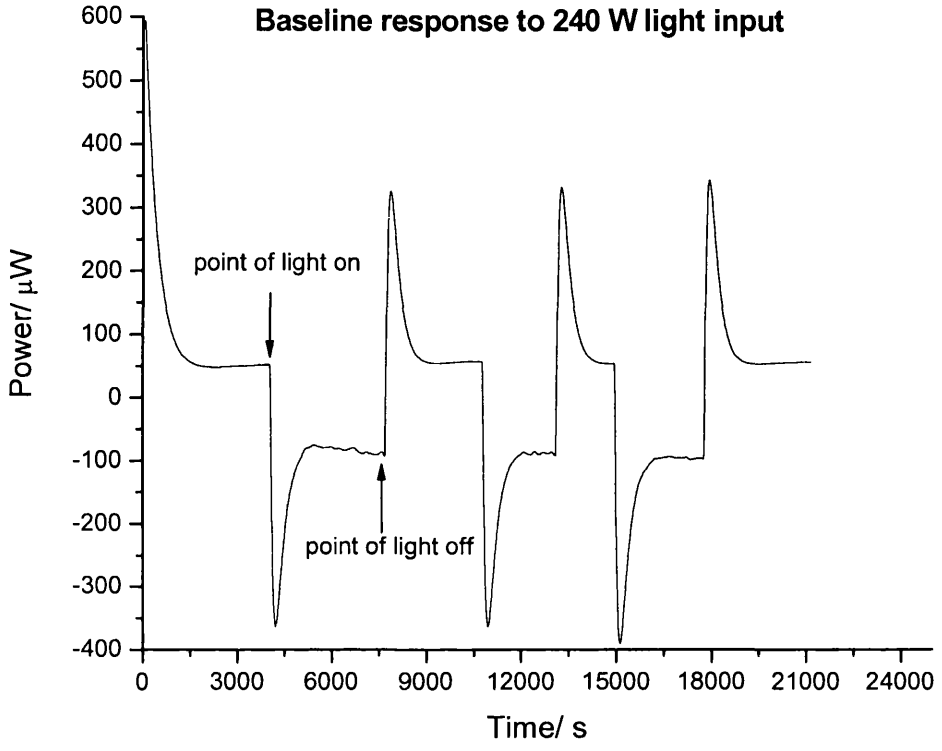

Figure 2.4: Baseline response to repeat light on and off test

In each case the repeatability of the signal when the light was switched on or off was fairly consistent; an average baseline signal of **54.02 ± 2.68 μW** was derived when the light was switched off, and with the light on the signal settled to a baseline of ca. -90 μW giving an average deflection of **-91.09 ± 4.29 μW** giving an overall deflection of ca. -145 μW. Such a difference is immediately indicative of an imbalance in the light delivery from the pair of fibre optics. A deflection of -145 μW suggested there is a greater proportion of light being delivered in the reference side. Ideally, if the amount of light output from each cable were equivalent then the net signal would be zero. Clearly,

this was not the case and there was a significant difference in the input from each cable. In combination, the magnitude of the irreproducibility of the baseline signals may preclude using the instrument for samples producing small powers (note that the standard specifications for a TAM, using micro-Watt amplifiers, is a noise of ±2 μW and a baseline drift over 8 h of ±2 μW for a 20 mL channel).[3] It was therefore essential to implement some design changes in order to try and minimise the baseline deflection so that it is as close to a zero value as possible, and, moreover, to ensure that reproducible outputs (within an acceptable range) are obtained each time the ampoules are lowered into and raised from the TAM. Further design modifications were therefore considered and implemented.

The immediate challenges, then, were to redesign the instrument in two phases:

- To obtain a zero baseline with the light off
- To obtain a zero baseline with the light on

2.1.3 Design Considerations and Modifications

One of the main causes of the irreproducible outputs was the way in which the system was designed. Dealing with the inability to attain a zero baseline first, it was clear (from the irreproducible data and through observation of the way the ampoules fit into the TAM) that the primary problem was the fixed geometry of the sample and reference ampoules relative to each other. The two ampoules could not be lowered into the TAM properly and independently as the raising/lowering process of the ampoule was very much dependent on the mechanical hand-wound lab jacks. This meant that the sample and reference ampoules were kept in a fixed position relative to the base of the calorimetric unit and hence any ill-alignment and/or imbalance between the two sides would therefore also be fixed and difficult to control. The original reason for fixing the geometry was to keep the fibre-optic bundles in a consistent position because of their fragility, but this became a limiting drawback on the instrument's flexibility and ability to align the ampoules correctly in the TAM. The irreproducible and non-zero outcomes were a result of an imbalance in the position of the ampoules relative to the base of the calorimetric channel and it was the case that one ampoule was sat in a higher position

than the other within the channel. As a result, there was a noticeable gap between the top of the column insert and calorimetric unit when situated in the measuring position. The impact this had was that the instrument was subjected to a significant proportion of heat loss through air conduction and/or convection from the calorimetric chamber. Unless aligned perfectly with the TAM, it would always be the case with this particular design, that one ampoule would sit higher in its channel than the other and, consequently, result in inconsistent data. It was therefore imperative to reconsider the instrument design to provide better control of the lowering and alignment of the ampoules into the TAM in order to counteract the imbalance of the fit and reduce heat escape.

In order to try and improve the baseline stability various design elements were revised and re-designed. The first approach was to break the fixed geometry of the sample and reference ampoules allowing each ampoule to be inserted independently, as well as simultaneously, into the TAM so that to ensure the fit was adequately air tight. Modifications were also made to the various supporting lids surrounding the metal column which contained the fibre-optic cable. The original column used in the Mark I is depicted in Figure 2.5.[1]

The fibre-optic cable is situated inside the metal column and it is surrounded with plastic support lids at upper and lower ends of the column. Plastic fittings (spacers) were also placed at defined intervals down the length of the vertical section of the column to minimise the effect of air conduction within the calorimetric chamber, the construction of which were based on the design of commercially available perfusion shafts manufactured by Thermometric AB, Jarfalla, Sweden.[4] The supporting lids at the lower end of the column were fixed in place and allowed for a 20 mL ampoule to be freely suspended. It was because of the fixed position of the supporting lids that it was not possible to adjust the position of the ampoule relative to the base of the calorimetric chamber. This lead to an inequivalence in alignment between the sample and reference sides which resulted in the irreproducible nature of the baselines (as previously shown in Figure 2.2). Necessarily, modifications were made and a new column with better supporting lids was constructed, as shown in Figure 2.6.

All engineering work was undertaken at The School of Pharmacy, University of London.

Figures 2.5 to 2.6b show a comparison of the original and re-designed column. A schematic diagram of the modified column is also illustrated in Figure 2.7.

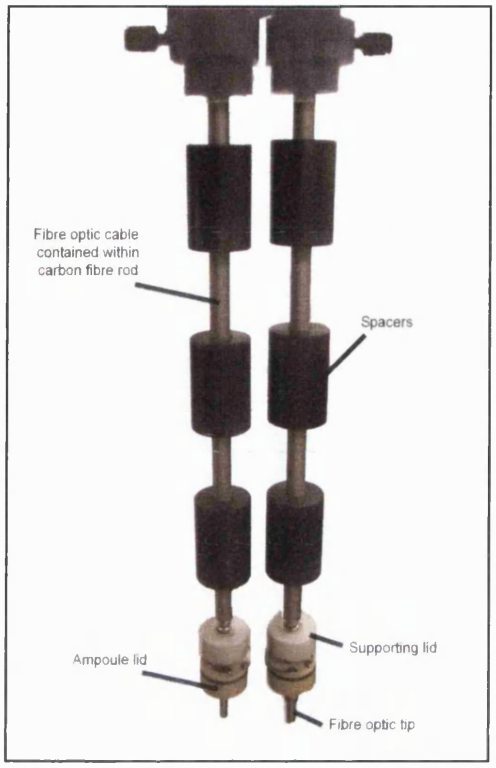

Figure 2.5: Original column[1]

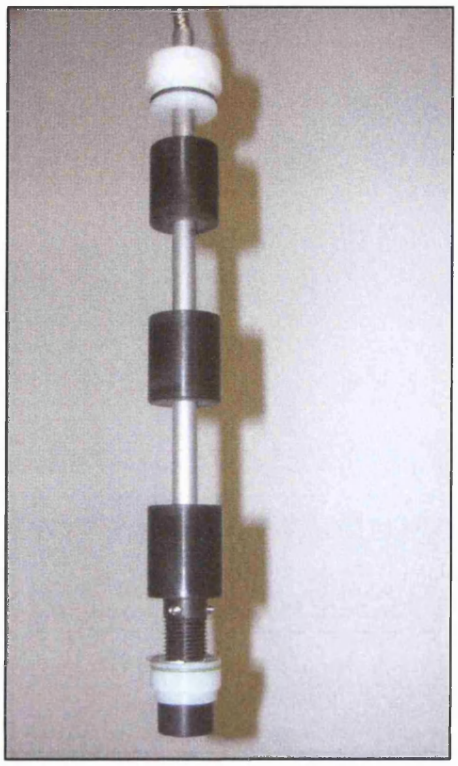

Figure 2.6: Re-designed column

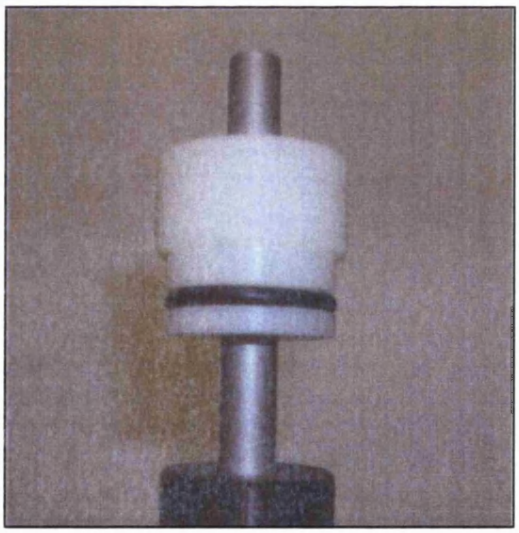

Fig 2.6a: Supporting lid at top of column

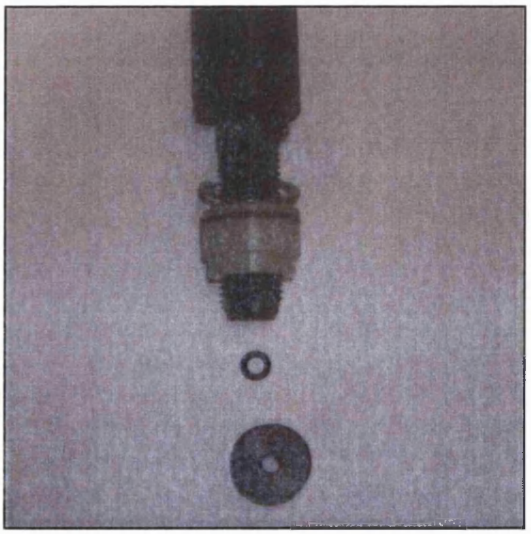

Fig 2.6b: Supporting lids at end of column

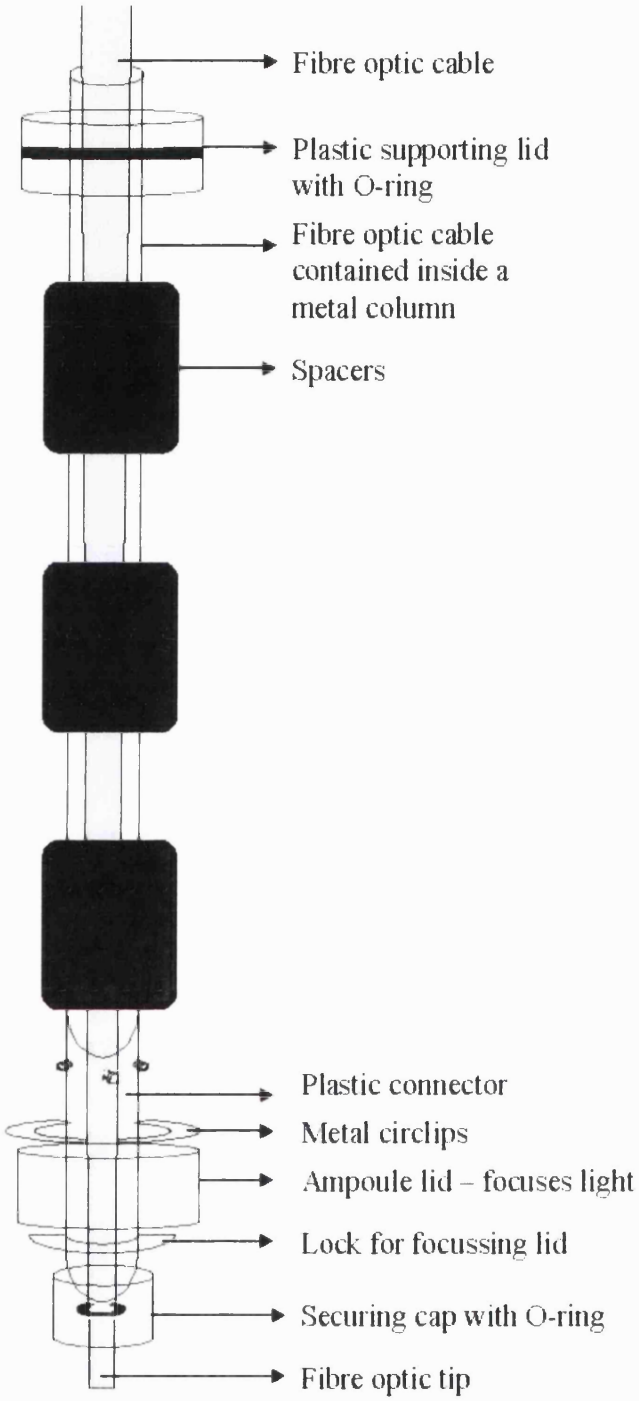

Figure 2.7: Schematic diagram of the modified column with components

Specially-made plastic supporting lids were made using black glass filled Nylon 66 (purchased from RS components) since it is unaffected by UV light. These were designed to allow a better fit of the fibre optic cable into the ampoule with a number of adjustable features to control the position of the ampoule in the TAM and the light focus across the base of the ampoule. The plastic support lid at the top of the column is adjustable so that the ampoule can be adequately lowered and firmly situated at the bottom of the channel before the lid is secured in position. It is fitted with a rubber O-ring (Fig. 2.6a) to create an air-tight seal around the top of calorimetric chamber and the column to help reduce heat losses. The lower end of the column was fitted with a plastic connector which was screwed onto the cable sheathing. The connector was machined with threads to allow the position of the ampoule lid to be adjusted. It was thus possible to control the distance of the fibre optic-tip, and hence light intensity and focus, relative to the base of the ampoule by adjusting the height of the ampoule on the connector i.e., positioning the ampoule lid down towards the lower end of the column increases the distance between the optic-tip and the ampoule base, consequently, increasing the area of light exposure across the base of the ampoule, and reducing the light intensity, and vice versa. Such focussing adjustments were not possible with the original column. The ampoule lid is fitted with an O-ring to ensure an air tight interface with the ampoule. To ensure the focus of the light remained unchanged throughout the sample loading and unloading process and that the lid was held firmly in place, a lock ring was placed below the ampoule lid. A metal circlip was used to secure a 20 mL ampoule in place. A screw cap (with an O-ring) at the bottom of the column was used to fix the position of the cable so that the fibre optic-tip was always at a fixed distance relative to the base of the ampoule.

Having broken the fixed geometry of the sample and reference sides and with the new adjustments now in place, it was no longer necessary to use the hand-wound lab jacks to lower/raise the ampoules vertically in/out of the TAM since each ampoule could now be lowered autonomously. Thus upon lowering one could ensure that both the ampoules were sat wholly on the base of the calorimetric chamber. The fibre optic cables were kept in the same light guide (Figure 2.1b) as in the original setup and remained unchanged since it is important, for accuracy, that the fibre optic bundles are kept in the same orientation at all times during measurements. Using this set-up the baseline response with the light off was assessed.

2.1.3.1 Investigating baseline stability after modifications (light off)

The calorimetric output using the re-designed column was monitored with the light off. The experimental procedure was set up in the same manner as that already described (section 2.1.1) with the exception of the superfluous hand-wound lab jacks. Both ampoules were lowered independently, and simultaneously, into the calorimetric channel and held in equilibrium (30 minutes) using a specially made metal bar which clipped directly onto the sample and reference column inserts (Figure 2.8). The bar was positioned midway on both columns to allow ampoules to situate in equilibrium before being removed to lower the ampoules into measuring position post 30 minutes. A bar was also attached above the upper lid on the column to ensure ampoules were held at a fixed distance apart relative to each other as they were simultaneously lowered into the TAM. A polystyrene case was placed over the top of the channel and column inserts as a temporary means to provide a shroud around the top of the TAM chamber and to protect against external factors such as temperature, humidity, etc. The shroud was removable to allow easy access to the cables and ampoules.

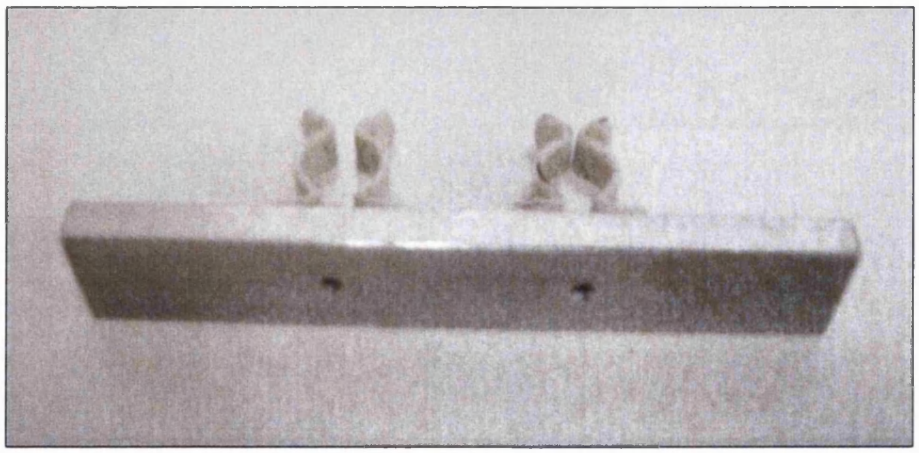

Figure 2.8: Metal support bar used to position ampoules in equilibrium

Figure 2.9 shows the impact of the design changes on the calorimetric output and are compared to the baselines using the original design. Five experimental runs for each design are compared below. Data representing the original design are recalled from data represented in Figure 2.2 for comparison purposes.

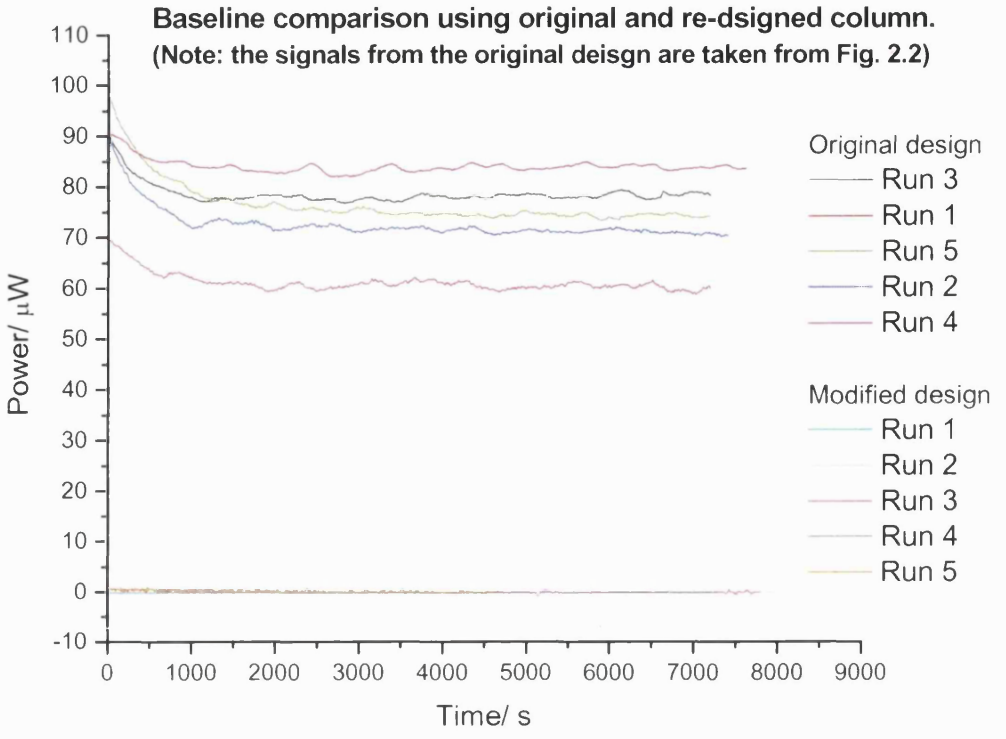

Figure 2.9: Comparison of baselines using the original and re-designed column with the light off

The heat-flow signals from use of the re-designed column were extremely encouraging and clearly had a significant impact on the baseline as indicative in Figure 2.9. The modifications made a dramatic improvement on the baseline stability and reproducibility reducing the signal by **99%** to give an average baseline value of **0.5 ± 0.3 µW** derived through linear regression (cf. to **74.1 ± 8.1 µW** with the original design). The signal can be finely adjusted to zero using the amplifier zero dial setting. This was not possible with the earlier design since the magnitude of the signal was far greater than the capacity of the amplifier to attenuate the signal. Thus, the TAM itself, effectively acts as a null adjust to ensure a balance in the heat flow signal between the sample and reference. This demonstrates that the design changes implemented are working effectively in minimising heat escape from the TAM and thus, with a better design system and sufficient insulation in place, the photocalorimeter is capable of producing a zero baseline signal in both a reproducible and consistent manner.

An example of a typical baseline signal obtained with the re-designed column is represented in Figure 2.10. The red dashed line represents a zero baseline.

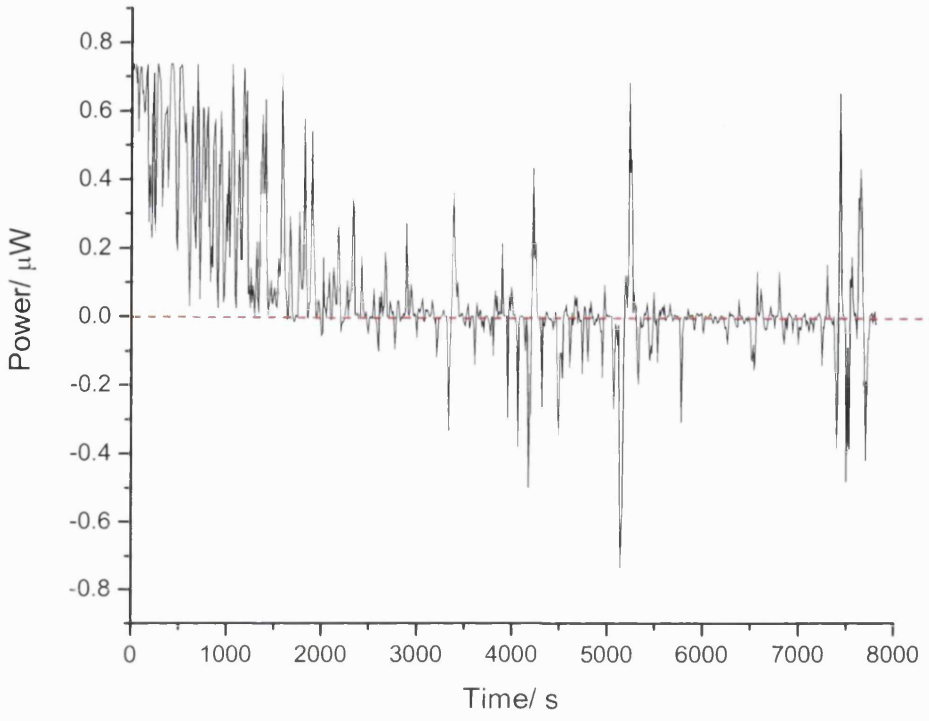

Figure 2.10: Example of a typical baseline signal using the modified column

The baseline was recorded over a period of 2 hours. The observed drift during the first 2000 seconds was a maximum of +0.736 µW and a minimum of -0.057 µW. After this period, the baseline settled to a plateau and an absolute maximum of +0.736 µW and minimum of -0.736 µw arising from the short-term spikes. An average baseline signal of +0.314 µW is derived in this case and is much lower than the range. Even if the absolute values were taken in the worst case, then it can be seen that the stability and noise over the defined observation period is within ±1 µW declared well within the manufacturers quoted specifications of ±2 µW for a 20 mL capacity.[3]

The design changes implemented have made an immense improvement on the calorimetric output making it possible to attain a zero baseline with the light off. Having established a zero baseline with the light off, the next stage was to turn attention to the instrument's inability of achieving a zero baseline with the light on.

2.1.3.2 Investigating the effect of light after modifications

As highlighted previously (Section 2.1.2) switching the light on introduced further problems to the baseline as a result of an imbalance in the amount of light delivered through the sample and reference optic cables. Using the same procedure (as described earlier in section 2.1.2) the system's response to the influence of light was investigated to see if there were any improvements from the design changes that had already been implemented. Five experiments were conducted to assess the reproducibility and repeatability of the signal. For reproducibility, a new experiment was set-up each time by loading and unloading empty ampoules. The repeatability was assessed by switching the light on and off at least in duplicate in each experiment. Figure 2.11 is typical of the calorimetric output obtained when the light is turned on.

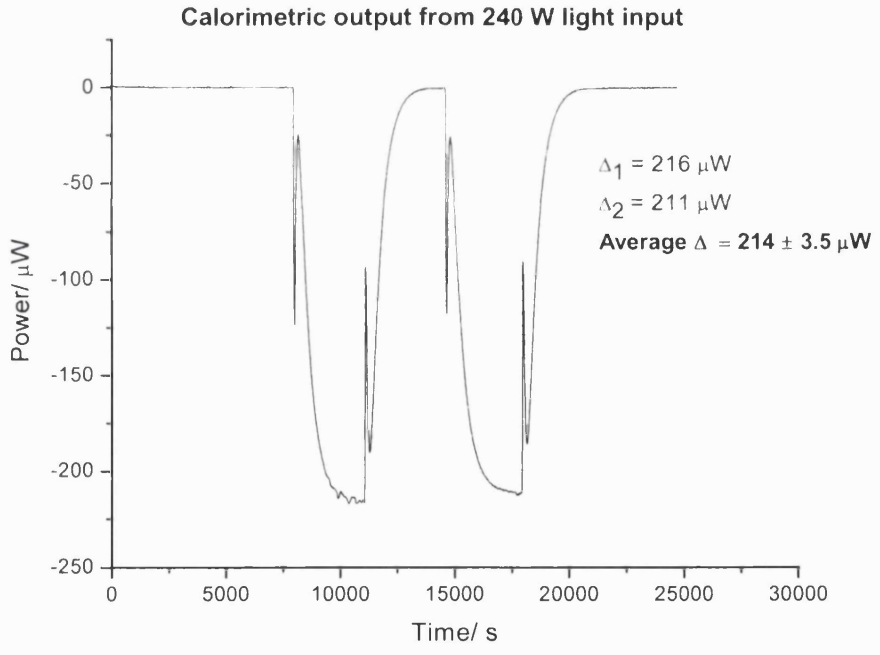

Figure 2.11: Typical calorimetric output from 240 W light input

The output clearly indicated there is still an imbalance in light from each optic cable. Table 2.2 summaries the offset values obtained from five experimental measurements.

The values were ~ 211 μW to ~ 227 μW with an average baseline deflection of **217 ± 5.8 μW** as observed across a series of light on/off tests. In all cases, the experiment began with a stable zero signal (ca. -0.24 ± 0.35 μW) for the pair of empty ampoules. At the point of light input, the system experiences a thermal shock between ~ 100 μW to ~ 125 μW, due to intense heat generated by the lamp source, before settling at a baseline of about ~ -220 μW. When the light is switched off a similar thermal shock is observed before the signal reached its original baseline.

Table 2.2: Comparison of 5 calorimetric outputs with 240 W light input

Experiment	Power output/ μW	
	Δ_1	Δ_2
1	212	213
2	216	211
3	219	218
4	216	211
5	226	227
Mean ± SD	**217 ± 5.8**	

The offsets were larger in this case than compared with those observed prior to making the design changes on the column (cf. ~ -145 μW), possibly because any changes in the geometry of the instrument can alter the light transmission. The repeatability and reproducibility of the signal is fairly consistent, however, the magnitude of the deflection is far too large making it difficult or impossible to determine the instrument's performance particularly if the sample generated small powers. Thus it was essential to implement further design changes principally to attenuate the light input by some means so to balance the light input through the sample and reference cable. Before doing so, a further experiment was conducted using the third cable (of the trifurcated cable serving as a reference to an external actinometer) in order to ascertain if the third cable could provide a better match of the light throughput when used in conjunction with either the sample or reference optic cable. The third cable was substituted for each of the two cables in turn to find the best matched pair. Conventionally, the sample cable is situated in the left hand side (LHS) of the TAM chamber and the right hand side (RHS) is occupied by the reference cable. The third cable was alternated so that it occupied both the LHS and RHS with its corresponding sample or reference cable. Figure 2.12 shows

an example of the calorimetric response when the third cable replaced the sample cable on the LHS and the reference cable remained on the RHS.

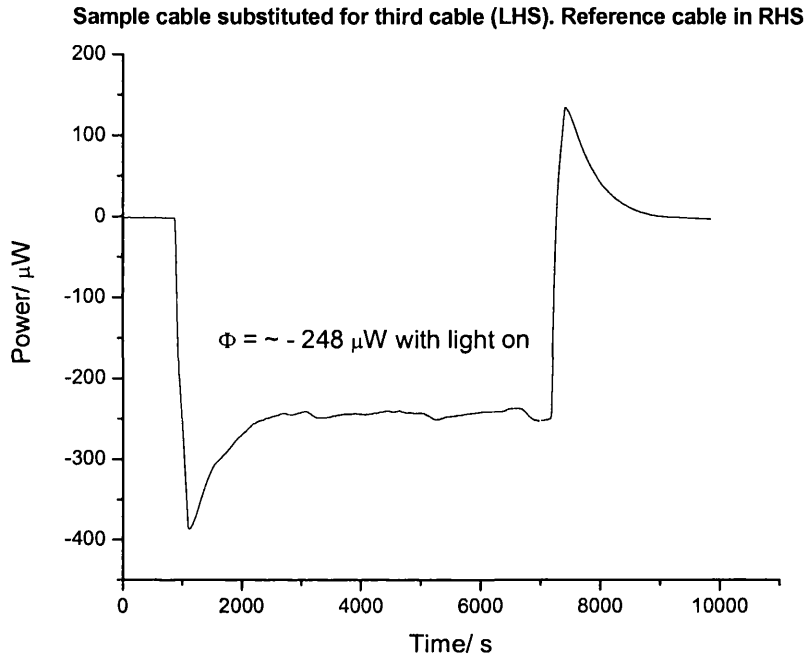

Figure 2.12: Plot to show effect of substituting the sample cable with the third cable

The imbalance of the amount of light delivered through the third cable was greater than the sample and reference ones indicating that there was far less light transmitted by the third cable than the sample and reference cable. It was also noted visually that the light from the third cable was far less intense compared with the two other cables. This was observed as a pale yellow footprint reflected from a white background as opposed to a bright footprint produced by the sample and reference cables. This was also in agreement with previous work[1] where the spectral distribution of the light output from the three cables was compared and showed that the two optical cables already in use i.e., sample (LHS) and reference (RHS) cables, were the pair that were best matched. Thus, the effect of imbalance in light transmitted from the fibre optic cables was already minimised.

On the whole, if the irreproducibility of a baseline signal with the light on is far greater than the signal of a reaction then this would inevitably make it impossible to validate the performance of the instrument. For this reason, further design changes were necessary. This led to the construction of a novel photocalorimeter – Mark II, the design, construction, and operation of which is explained in greater detail below in section 2.2.

2.2 Re-Designed Photocalorimeter (Prototype Mark II)

Having successfully dealt with the issue of the baseline stability with the light off, the focus was now to deal with the inability to obtain a zero baseline with the light on. In a calorimetric measurement, differences in the heat flow signals may be observed in cases where the fibre-optic cable is not positioned properly in regard to the exit slit, for instance, or if there is any movement to the position of the cable during measurement. As a consequence energy differences of the light quantity between the sample and reference side may be observed. Furthermore, energy differences can arise in cases where there is inequality in the distribution of a split beam. Such differences can commonly arise in the use of multi-branch fibre bundles. The trifurcated fibre bundle (utilised in the original photocalorimeter) had one common end, which connected directly to the light source, and then split at a junction into three branches (Figure 2.11). Even though the bundles of fibre are designed to produce evenly divided outputs, in principle, this can be difficult to achieve due to reflection, packing fraction losses etc., and only a certain amount of the total incident radiation is transmitted through each branch (approximately 27% according to the manufacturer[2]). Moreover, the bundles are sensitive to position changes. Changing the position of the common end, relative to the exit slit, or any of the branches will change the position of the output beam distribution and power. Therefore it is important to avoid movement of the bundle during measurements. This essentially put a constraint on the system since there was no feature to control the quantity of light delivered to any of the three branches in order to compensate for any differences that may have risen. In order to overcome this obstacle the light delivery system was completely re-designed to allow better control, adjustment and focus of the light quantity in each ampoule. Two major changes were proposed and implemented:

- The trifurcated fibre bundles were replaced with an optical beam splitter
- The fibre-optic cables were replaced with liquid-filled light guides

The optical beam splitter assembly is comprised of a set of mirrors and lenses used to split and direct light (as opposed to the split at the trifurcated junction used previously) into the sample and reference ampoules via its respective optic cable. The large metal light guide supporting the fibre bundles thus became superfluous and it was possible to attach two individual liquid-filled light guides directly onto the end of the beam splitter assembly. Liquid light guides offer many advantages over fibre-optic bundles (explained in section 2.2.1) and were chosen as a better suited alternative. To address the issue of light control and adjustability, shutters and focussing assemblies were incorporated into the design. These were positioned beneath the optical beam splitter to control the light power of each beam. A basic schematic of the proposed re-design is illustrated in Figure 2.13. The basic components consist of; a Xe arc lamp as an irradiation source, Infra-red (IR) filter, optical beam splitter (containing a polka-dot beam splitter and first surface mirror), shutters and focussing assembly, and liquid-filled light guides. Details of all components used in the construction of the optical assembly are given in section 2.2.1.

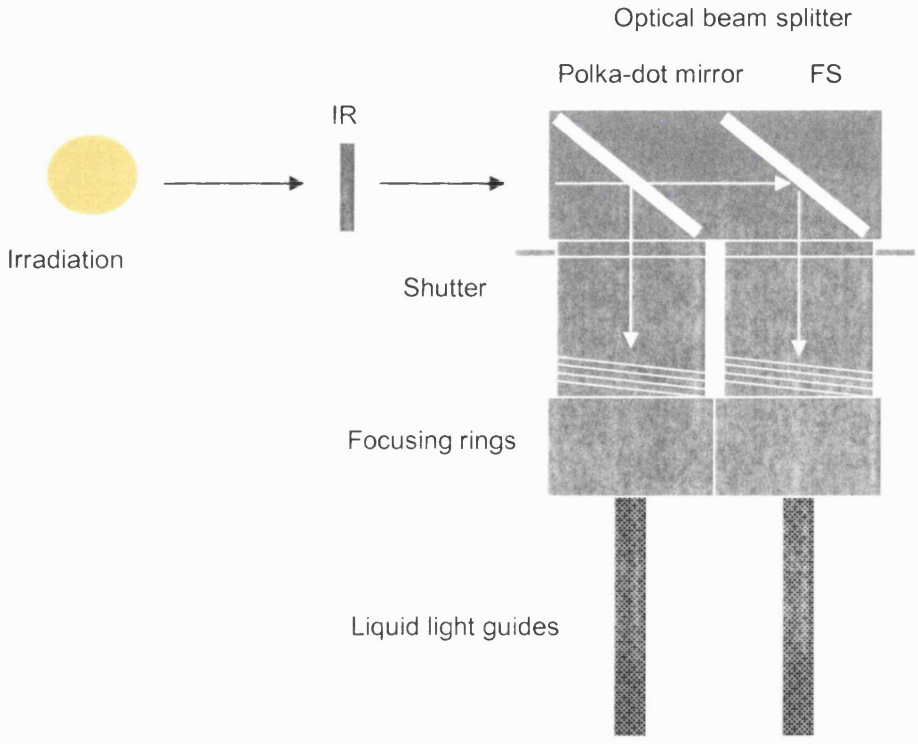

Figure 2.13: A basic schematic of the proposed instrument re-design

A key feature of this design was to be able to control the delivery of light in each of the ampoules. This is something which was not possible to achieve with the earlier prototype, nor that with any existing photocalorimeters to date published in literature. The re-designed photocalorimeter was built to control better the light energy input into the system. This is achieved firstly by the use of an optical beam splitter assembly. It consists of a polka-dot beam splitter which splits the light beam into two equal arrays; 50% of the light is reflected at a 90° angle and is passed via a liquid light guide into one of the ampoules, the remaining 50% of the light is transmitted through to a front surface mirror, creating a 90° bend in light path, and subsequently enters the other ampoule via a liquid–filled light guide. Shutters positioned beneath the mirrors can be adjusted on each side to control the entry of each beam. The focus of the light can then be manipulated by fine adjustment of the focussing rings situated just above the liquid light guide. These permit further control of the amount of light entering each cell, in that the distance of the end of the light guide can be altered relative to base of the ampoule to allow an even spread of light across the ampoule base. The light guides are locked into position, using a locking ring, and fed through the centre shaft of a metal column. The column is surrounded by various support lids (as described earlier, section 2.1.3) which fix the position of the cable in place to ensure that the liquid-filled tip is always at a fixed distance relative to the base of the ampoule.

2.2.1 Various Design Components

The 300 W Xe arc lamp, O_3 free (model No. 6258), lamp housing (model No. 66902), liquid-filled light guides (model No. 77554), and digital power supply (model 69910) were purchased from LOT-Oriel™ Ltd, UK. All optical components were purchased from Edmund Optics™ Ltd, UK; polka-dot beamsplitter (part No. A46-461), first surface mirror (part No. A31-422), plano-convex lenses, anti-reflection coated (part No. A46-267), and plano-concave lenses (part No. A08-026).

The optical beam splitting assembly was specially constructed and engineered at The School of Pharmacy, University of London, UK.

The various components used in the construction of the Mark II photocalorimeter offer several benefits;

2.2.1.1 Xenon (Xe) arc lamp

The photocalorimeter was equipped with a 300 W Xe arc lamp (ozone free) as a radiation source (pictured in Fig. 2.14). Xe lamps are the basis for international standards because their Spectral Power Distribution (SPD) is characteristic of a smooth continuum that covers the UV-VIS and short IR range similar to that of the solar spectrum which makes them ideal for UV photochemistry and spectroscopy applications.

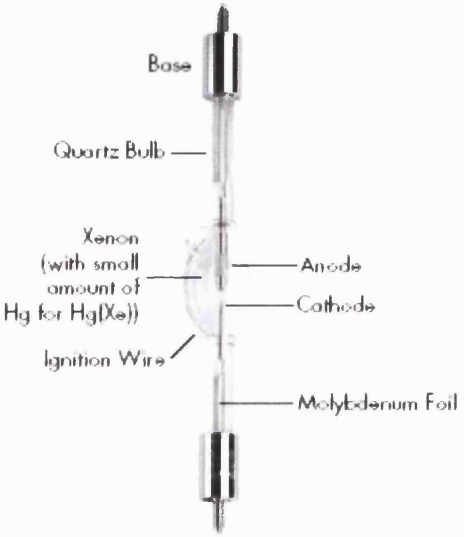

Figure 2.14: Construction of a Xe arc lamp

The lamp is simple in construction and utilises a fused quartz envelope with thorium-doped tungsten electrodes to enhance electron emissions between the anode and cathode. Note that fused quartz is the only economically feasible material currently available that can withstand the high pressure and high temperature present in an operating lamp while still being optically clear. The quartz bulb is filled with purified xenon gas which is maintained at a high internal pressure (approx. 8 - 10 bar) in order to achieve maximum efficiency. This can triple during operation due to the high operating temperature of the lamp. Because of the small arc region (approx. 5mm gap length or less) between the two electrodes, the lamp can generate extremely bright and high intensity radiance in the UV-VIS making them very suitable to create a collimated beam. They are therefore valued not only for their high correlation with solar radiation but also for their high intensity which translates into reduced testing times. The lamp has an average lifetime of ~900 h at its rated power and is typically defined as the average number of hours for a lamp's visible output to fall 75% of the initial value.[2] A new bulb was assembled in its lamp housing (Fig. 2.15). The image of arcs was aligned to create a collimated beam of light using the reflector and focussing adjustments on the lamp housing prior to measurements[5]. Heat sensitive paper was used as an indicator to centre the collimated beam of light. The light causes an imprint (black mark) on the paper from where the

heat is produced. This type of paper can commonly be found in superstores (receipt paper) utilised in modern cash registers.

Note: Some lower power xenon lamps can be operated in a horizontal position. For the purpose of this particular construction, a vertical lamp was best suited.

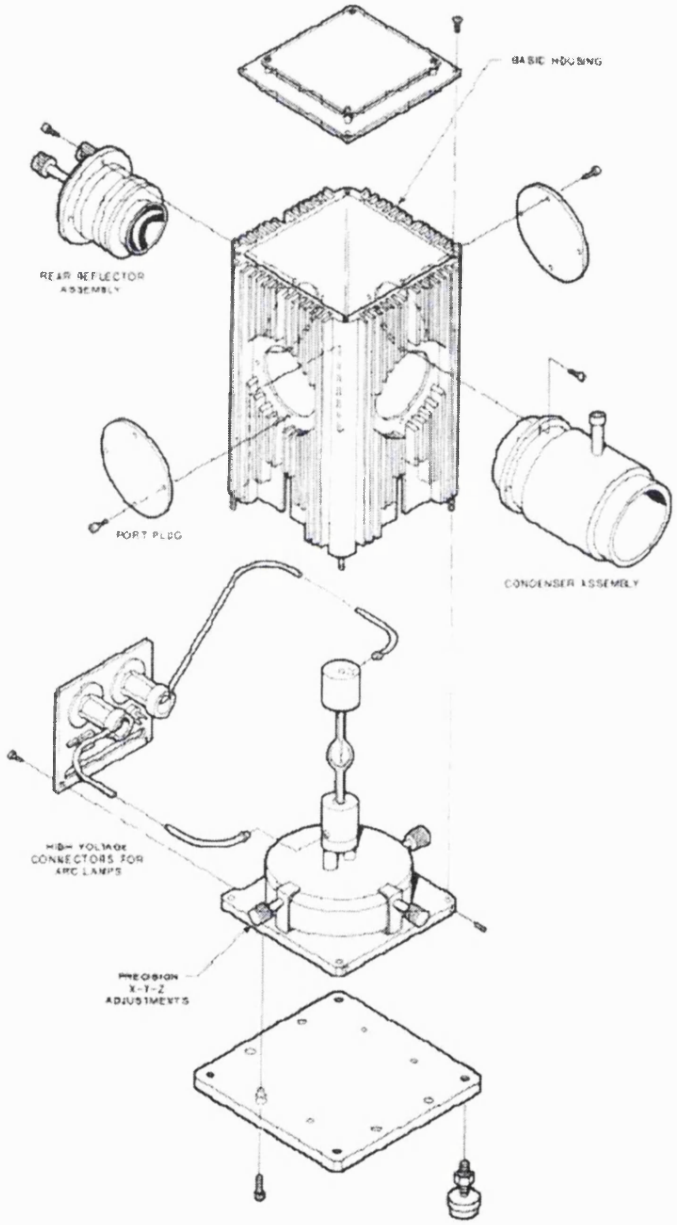

Figure 2.15: Exploded view of a typical lamp housing with an arc lamp

The lamp housing is common to all types of lamps. A time elapsed indicator contained on the housing provides an account of the remaining lamp life. The condenser assembly is designed to produce a collimated beam. There is also a focussing lever which can be altered to adjust the position of the lens to produce a converging and diverging beam if required. For the purpose of this system, the beam of light was collimated before it entered through a shutter and an Infra-red (IR) filter. The shutter is used to prevent the sample from irradiation without extinguishing the irradiation source i.e., the lamp can be ignited for a sufficient period of time to allow it to 'warm up' before sample exposure. The IR filter (Fig. 2.16) utilises distilled water to remove emissions of IR light produced from the irradiation source. A water-cooling jacket surrounds the exterior of the filter, which allows cold distilled water to be pumped around the filter-casing. This is because the high pressure levels of an operating lamp are related to high operating temperatures and, thus, demands the need for a water cooling system.

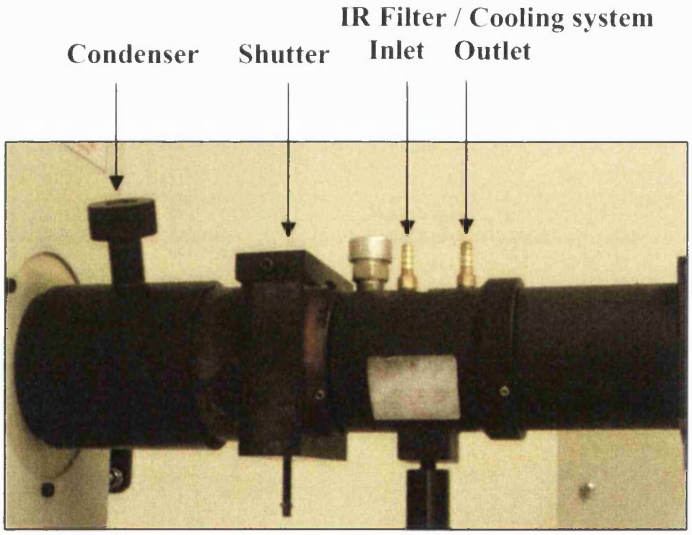

Figure 2.16: IR filter / Water cooling system

2.2.1.2 Power Supply

A digital series arc lamp power supply was used to supply constant power to the Xe lamp. Note: the lamp can be operating in two modes; constant power and constant voltage. Fig. 2.17 shows a typical digital power supply suited for use with 200 to 500 W

Xe arc lamps. The power output rating varies from 160 to 600 W. For a 300 W lamp, the power supply allows the lamp to be operated at ± 20% of its rating i.e. 240 W to 360 W.[2] Typically, an operating power of 240 W was set and the desired value was pre-selected before the lamp was ignited.

Figure 2.17: Digital Power Supply used to provide constant power to the lamp

2.2.1.3 Liquid-filled light guides

The bundles of fibre optic cables were replaced with two single branched liquid-filled light guides in order to maximise light transmission (Fig. 2.18). The liquid light guides (3 mm core diameter, 1 m length) have excellent overall UV transmission covering a range of 300 to 650 nm in the UV-VIS region. The liquid-filled light guides consist of a pressurised tube comprising of Teflon cladding and are flexible in nature. The inner core is filled with a transparent non-toxic liquid (patented), either an alcohol base or aqueous salt solutions containing chlorides, fluorides or phosphates, are typically used because of their high light transmittance properties. Both ends are sealed with short silica fused windows.

Figure 2.18: Liquid light guides

The liquid light guides are ideal for UV-VIS applications attributed primarily to two factors; they have a large acceptance cone i.e., a large diameter allows for higher light throughput, but more significantly, there are no packing fraction losses. Unlike glass fibre optic bundles, they are actually composed of liquid and therefore do not suffer from packaging fraction losses-spaces between fibres that can cause reduced coupling efficiency, illustrated in Fig. 2.19. Their overall transmission is therefore higher than that of glass fibre bundles. Furthermore, repeated handling of liquid light guides does not result in the breakage typical of glass bundles, which can effectively reduce efficiency over time.

Overall, liquid light guides can offer many advantages over bundles of fibre optic:

- Higher transmission in the UV, down to 300 nm
- Higher transmittance in the NIR
- Higher overall transmission than glass bundles
- No packing fraction loss or breakages
- More uniform light throughput
- Larger acceptance angles
- Significantly less expensive compared to fibre bundles

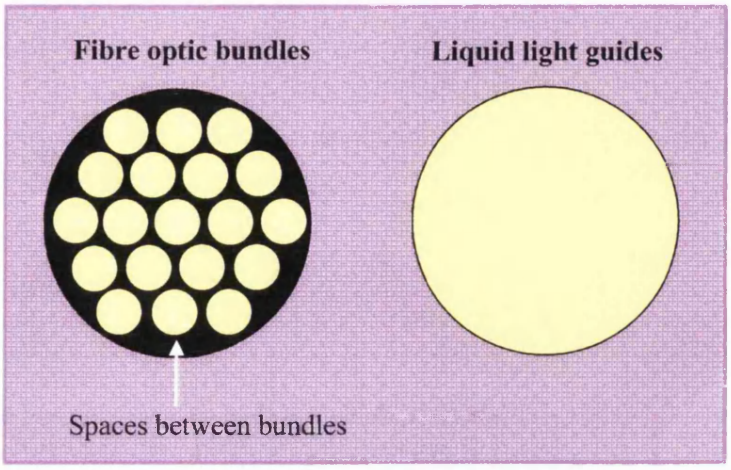

Figure 2.19: Comparison of packing fraction of fibre bundles and liquid light guides

It is estimated that in fibre optic light guides about 30% of the light transmission is lost as a result of the spaces between the bundles with 6% loss per foot. Liquid light guides, inevitably, obviate these losses and therefore exhibit excellent light transmission.

2.2.1.4 Polka-Dot Beamsplitter

Polka-dot beamsplitters consists of an optical ultraviolet grade fused silica substrate, with a vacuum deposited aluminium coating. The coating is applied in such a manner that 50% of the beamsplitter is coated, while the other 50% remains uncoated. It is this 50:50 split between the coated and uncoated area that gives a constant reflection-to-transmission ratio and the surface area of the beamsplitter a perforated or "polka-dot" appearance, depicted in Figure 2.20.

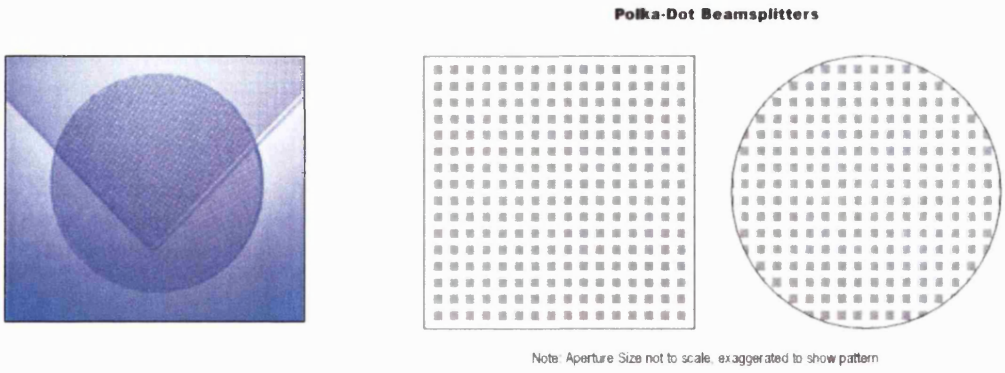

Figure 2.20: Polka-dot beamsplitters

When light is projected at the beamsplitter, the beam is split as the light rays that encounter the uncoated surface are transmitted through with very little energy loss whilst the rays that impact on the aluminium coating are reflected. This effectively splits evenly the input beam: 50% of the incident light is reflected by the coated area and 50% is transmitted through the glass (uncoated area).

A polka dot beamspliter (38mm^2 diameter, 1.5 mm thickness) was placed at a 45^o angle into a specially constructed unit (described later) so that the beam reflected at a 90^o angle directly into the liquid light guide. Since this versatile beamsplitter is not angle sensitive, it is ideal for splitting energy from a radiant light source with no significant divergence from diffraction.

2.2.1.5 First Surface Mirrors

Figure 2.21: First surface mirrors

First surface mirrors (Fig. 2.21), also referred to front surface mirrors, are coated with enhanced aluminium that provides > 90% image reflection in the visible region. A reflection of 95% can be achieved depending on the wavelength of light used. A rectangular shaped mirror (38mm^2 diameter, 3.2 mm thickness) was the ideal choice and positioned behind the polka-dot beamsplitter since they are extremely useful in applications where the mirror is mounted at 45° to produce a 90° bend in light path.

2.2.1.6 Plano-convex lens

Two plano-convex lenses (PCX) were used to form part of the focussing assembly attached on to the lower end of the beam splitter. Each lens was placed directly between its respective shutter and liquid light guide; one on the sample side and the other on the reference side. The lenses (25.4 mm diameter, 5.84 mm centre thickness) are UV Grade manufactured using synthetic fused silica and provide excellent transmission characteristics. A broadband anti-reflection coated PCX lens was chosen for optimised throughput in the ultraviolet spectrum.

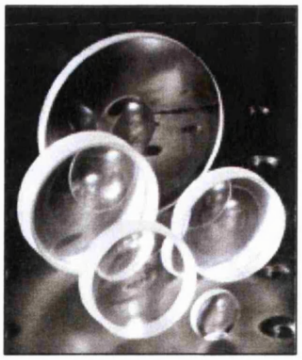

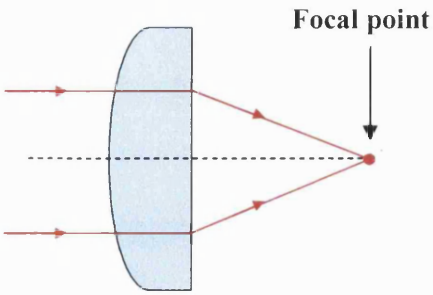

Figure 2.22: Plano-convex lens

2.2.1.7 Plano-concave lens

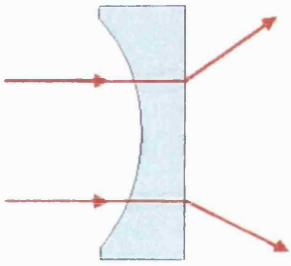

Figure 2.23: Plano-Concave Lens

A plano-concave lens (PCV) was placed between the lamp and the polka-dot beamsplitter to re-direct the rays and collimate the light. The PCV lens (25.4 mm diameter, 2 mm centre thickness) has one flat and one inward curved side which helps collimate the light into to the beam splitter.

2.2.2 Instrument Development

Using the optical components, as those described above in section 2.2.1, a novel irradiation apparatus was constructed. Figure 2.24 depicts the complete optical assembly.

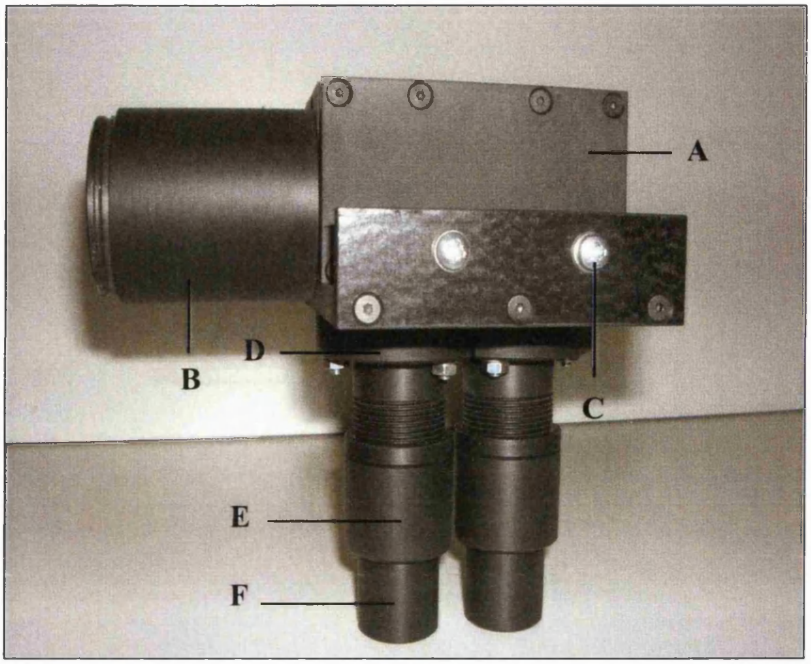

Figure 2.24: The optical assembly; A: optical beam splitter - *contains a set of mirrors; polka-dot and first surface*; B: connector to IR filter / cooling system; C: shutters; D: focussing lens; E: adjustable focussing assembly; F: light guide connectors

The optical beam splitter assembly contains two mirrors; a polka-dot beamsplitter and first surface mirror (Figure 2.25). The shutters beneath each mirror can be used to control the amount of light input into the ampoules by manual adjustment of the screw fixture (Figures 2.26 and 2.27). The screws can be tightened or loosened accordingly to minimise or maximise light exposure so that the shutters can be set at different levels i.e., open, middle, or closed (part C). (It is important to note, however, that because of the nature of the design it was not possible to close the shutters entirely and what is referred to as the "closed position" is intended to refer to the maximum level that the screws, controlling the shutters, could be adjusted to limit the light throughput. In effect, approx. ¼ of the shutters still remained opened in the "closed position"). The PCX lenses are situated directly beneath the shutters (part D). The light focus and spread can be altered by adjusting the rings at the lower end of the assembly. This ultimately alters the total distance between the end of the optic tip and the base of the ampoule and, consequently, changing the light focus and footprint (part E).

All these features are designed in such as way so to allow the light entering each ampoule to be more equally matched. Further photographic images of the light box and its components are shown in Figures 2.25 – 2.27.

Figure 2.25: Open view of light box; A: polka-dot mirror; B: first surface mirror

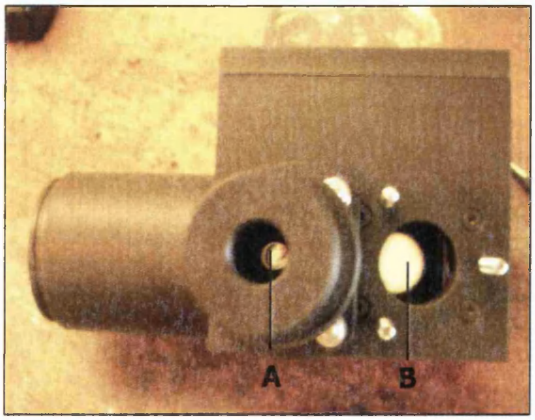

Figure 2.26: Upside down view of light box; A: light guide insert; B: open shutter

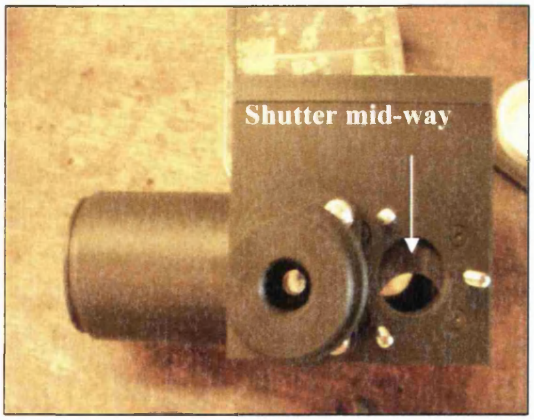

Figure 2.27: Upside down view of light box showing shutter half-closed

The light guides attach on to the end of the beam splitter assembly and are inserted through the re-designed metal column (similar to that described earlier in section 2.1.3). The column was re-made to fit the dimensions of the new light guide. Figure 2.28 shows the final construction of the column through which the liquid light guide is inserted.

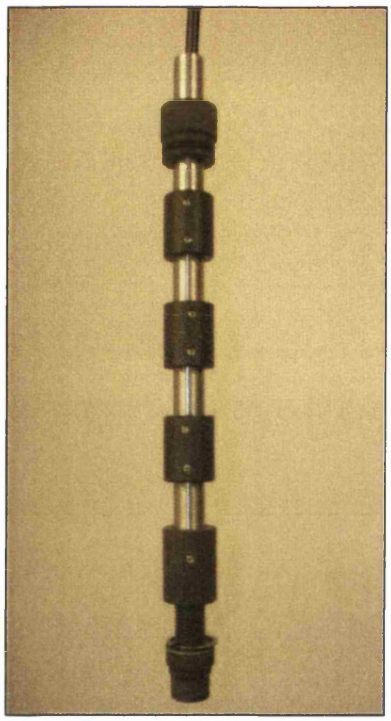

Figure 2.28: Liquid-light guide contained in specially constructed column insert

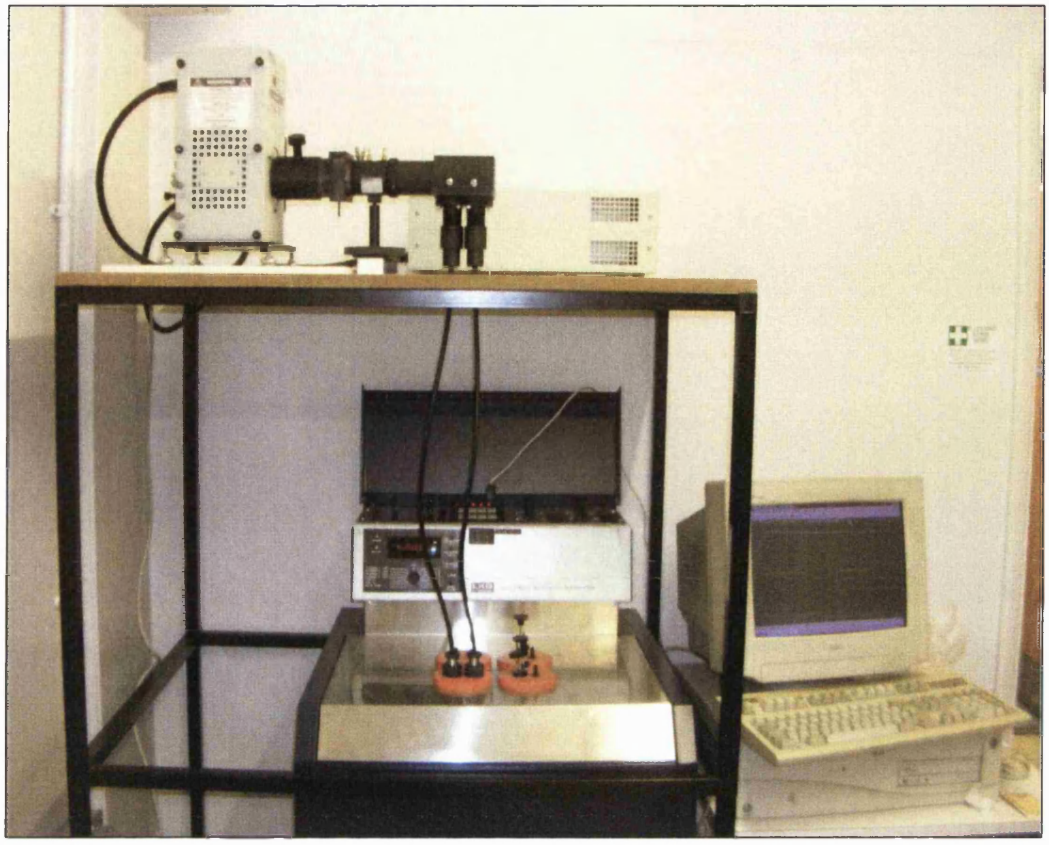

Figure 2.29: The re-designed photocalorimeter (Mark II)

With the overall construction of the photocalorimeter complete, a metal frame network was built around the TAM to support the light apparatus and provide instrument stability. This enabled the light box and components to be mounted in a fixed position relative to the TAM. The final design is pictured in Figure 2.29 and a schematic of the irradiation apparatus built is illustrated in Figure 2.30.[6]

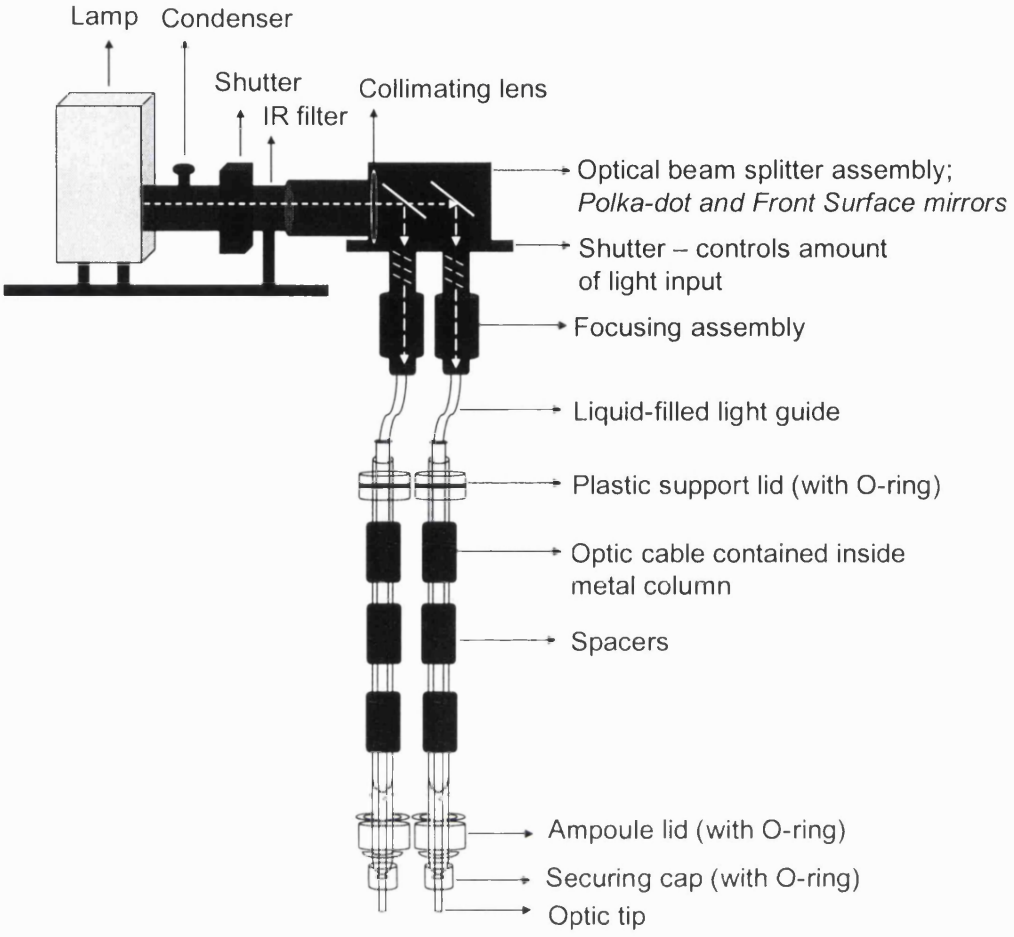

Figure 2.30: Schematic of the re-designed photocalorimeter (Mark II)

2.2.3 Investigating baseline stability with the Mark II Photocalorimeter

The earlier design modifications showed that the instrument was capable of producing a zero signal with no light input. Therefore, a similar response was expected with the new system. The method used has already been described (Section 2.1.1) with the exception of lowering the ampoules using hand-wound lab jacks. Since the lab jacks became superfluous to this design, a metal support bar with clips (specially made at The School of Pharmacy, London) was readily attachable and de-attachable to the sample and reference insertion columns (Figure 2.31). This served two functions; one as a stopper to situate the ampoules in the equilibrium position, and secondly, to keep the columns at

a fixed distance apart to ensure simultaneous lowering into the measuring position in order to minimise the occurrence of large thermal shocks. The latter is achieved by attaching the clips on the top end of the column. The cables were lagged with polyethylene pipe lagging for insulation against external environmental influences.

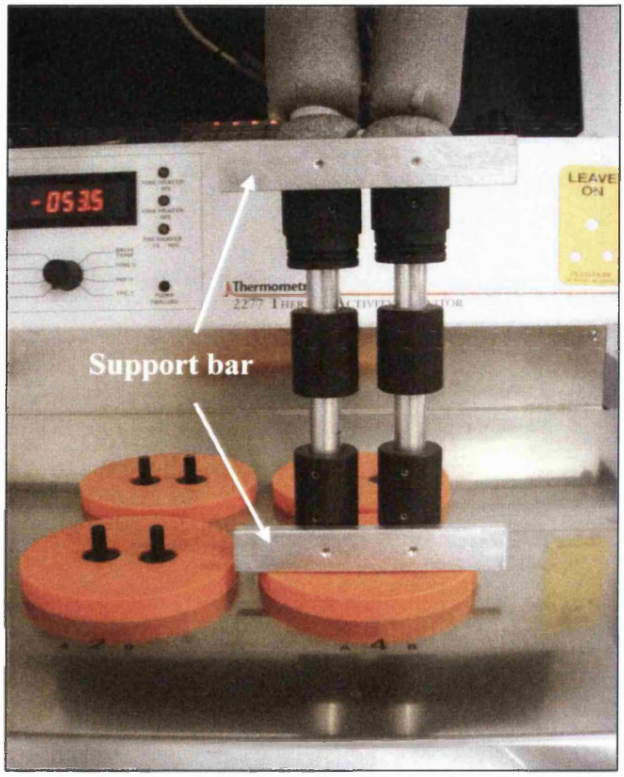

Figure 2.31: Metal support bars used to aid support during column lowering

The baseline stability of five measurements was taken (Figure 2.32).

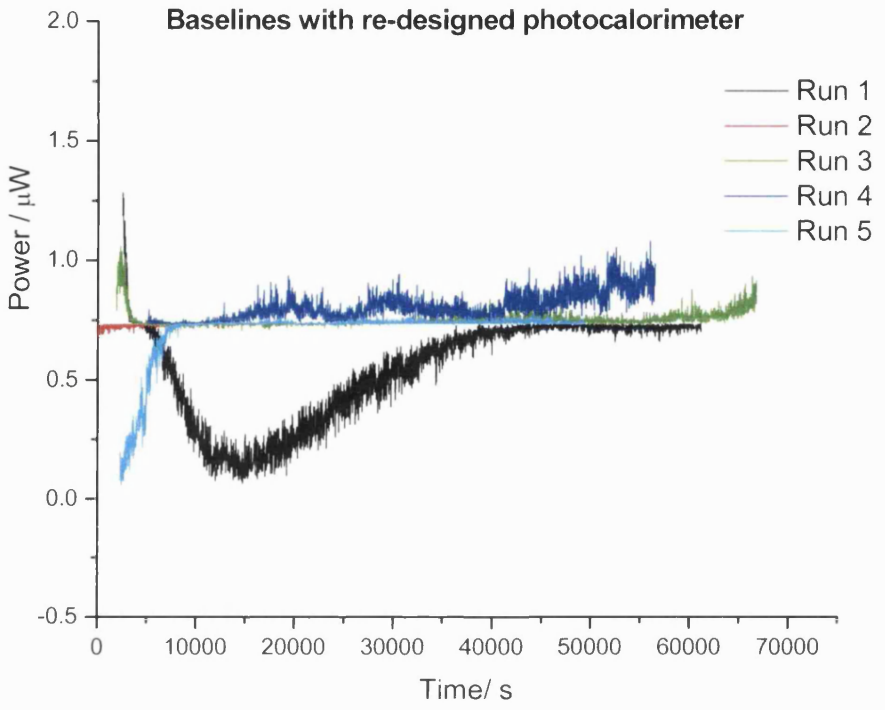

Figure 2.32: TAM output without light input using Mark II

Using empty calorimetric ampoules, an average offset signal of **0.73 ± 0.02 µW** was determined for the five measurements taken (Fig 2.32), therefore, satisfying the baseline noise and stability limits of ± 2 µW as specified by manufacturers.[3]

2.2.3.1 The effect of light

With the instrument responding satisfactorily without the addition of light, the next, and most important, step was to assess the response of the TAM when light was introduced. The basic operative method has been described previously in section 2.1.2. In addition, the intensity reaching the calorimetric ampoules was adjusted using the shutters on the optical assembly to control the apertures until a stable zero baseline was attained. The light was then switched off and on three times for repeatability.

Figure 2.33 is an illustrative example of the outcome obtained upon making these adjustments.

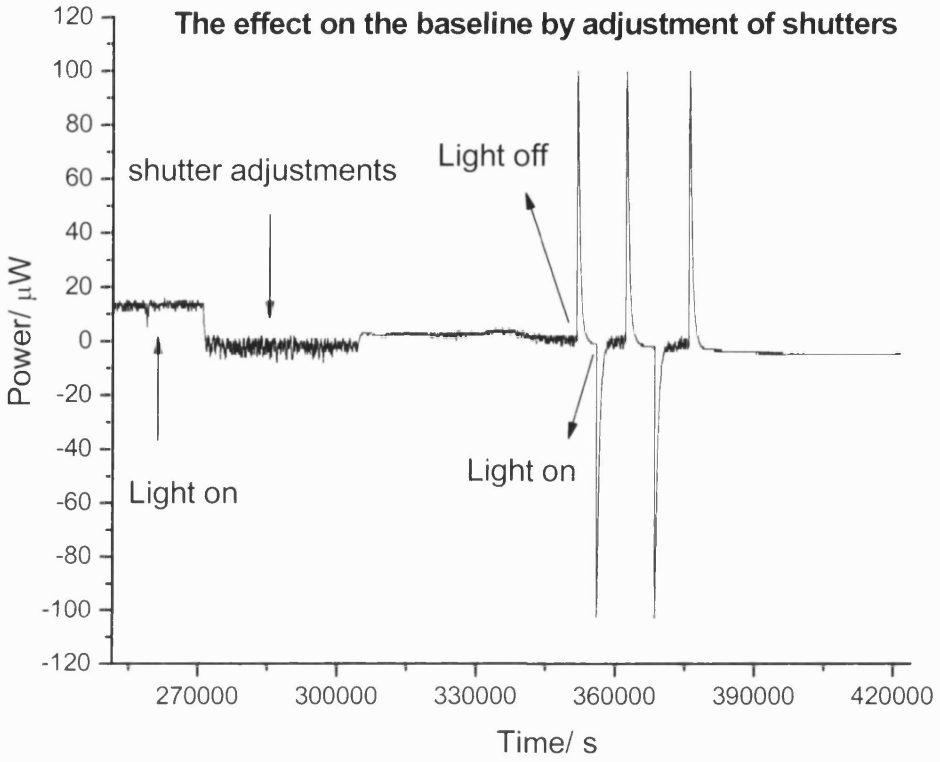

Figure 2.33: The effect on the baseline by adjustment of shuttering assembly to control light input and response to baseline with light off post adjustment

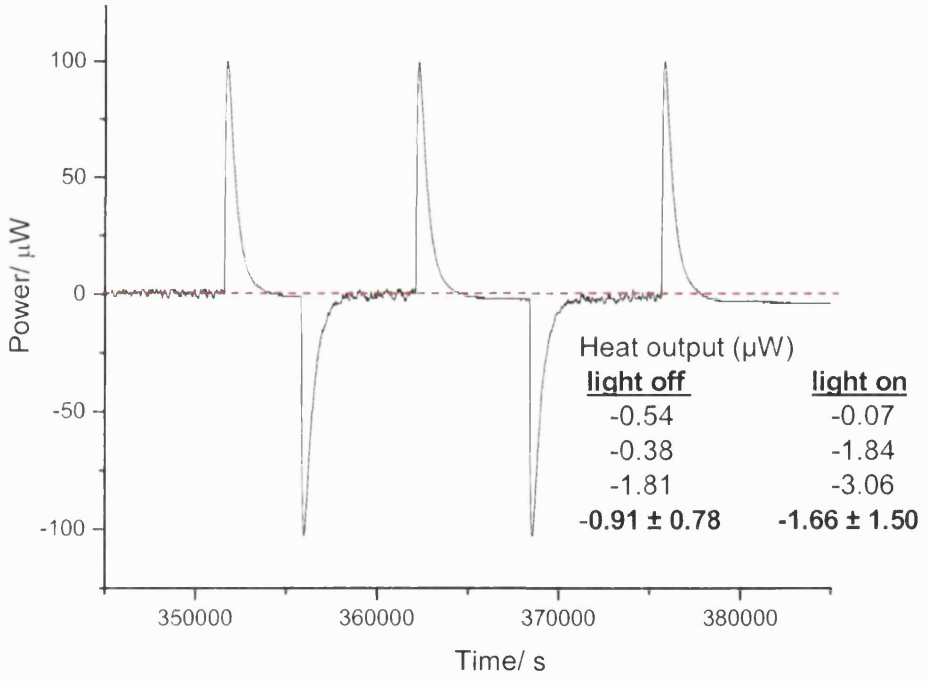

Figure 2.34: Magnified plot of Figure 2.33 showing baselines with and without light input post adjustment. ***The red line represents a zero heat output***

Initial trials showed a remarkable improvement to the baseline with the light on as depicted in Figures 2.32 and 2.33. These also showed excellent repeatability upon switching the light on and off after the shutters were initially set to exhibit a zero power signal. In this case, an average signal of **0.07 ± 0.06 μW** was obtained with the light off and **-0.04 ± 0.11 μW** with the light on. These values are almost equal, evident of an overall net signal of zero, and compare favourably with the manufacturers stated baseline noise of **± 2 μW** for a 20 mL ampoule capacity.

Being able to attain a zero baseline with the light on and off marked a significant step in the project. With the fundamentals of the design in place, the next step was then to quantify the light being delivered to sample. This is known as Chemical Actinometry and is further explained in Chapter 3 which details the measurements performed on an ICH listed actinometer, 2-nitrobenzaldehyde (2NB).

2.2.4 Problems associated with xenon arc lamps

Over the course of the project, it was noted that there was a significant decline in the lamp performance over a short period of time making it difficult to obtain consistent experimental measurements.

Although xenon arc lamps are superb at mimicking solar spectral irradiance, there are a number of issues associated with them:

- Short lamp life – because of the extreme conditions inside the bulb, Xe lamps typically have a lifetimes ranging from 200 to ~2000 h (or 1 to 12 weeks of continuous operation). The 300 W Xe lamp used with the Mark II photocalorimeter served a lifespan of ~900 h (~5 weeks of continuous operation).

- The lamps require power consumption of several hundred watts to obtain sufficient intensities. Smallest bulbs available are usually 50 or 75 W types and the largest are usually 500 W.

- Only a fraction of the consumed power is emitted as light, while a large portion is converted to heat, which must be dissipated. This usually requires the need for expensive water cooling systems.

- The arc within the bulb requires alignment each time upon striking. This can alter the geometry, and hence transmission, of the light path to some degree.

- Their ignition requires high voltages (~ 30 kV). This is a potential shock hazard and can cause strong electromagnetic interferences with other electronic equipment.

- Because of the high pressure inside the bulb (~ 8 to 10 bar), xenon lamps pose a threat of explosion if not handled properly.

All these factors combined can cause irregularity in the amount of light delivered and the intensity can vary across measurements. The changes in the light output can be measured through actual photon flux measurements using a spectroradiometer. This is known as Physical Actinometry (explained further in Chapter 3) where it was possible to obtain spectral intensity and real time flux measurements.

The aging of the lamp will cause deterioration in intensity levels, and evidently will impact heavily on the power output on the TAM. Several light on/off tests, using empty ampoules, were performed to assess the level of deterioration after the lamp had surpassed its recommended life span of 900 h. The shutters were initially pre-defined to give a zero baseline on the TAM. The light was then switched on and off to assess if the baseline signal gave a repeatable signal at zero. An example of the variability in the TAM output is shown in Figure 2.35. In this example, the signal gradually drifts from ~40 μW in the first instance to ~18 μW in the latter showing approx. 50% signal decline over an irradiation period of about 5 hours. In the case of drug photodegradation, such instability will significantly impact on the TAM output resulting to misleading data interpretation.

Repeating the light on/off tests followed no set pattern and the outputs were arbitrary. Figure 2.36 is representative of the discrepancy associated in the power signal with light input. The lamp power in all cases was set to 240 W.

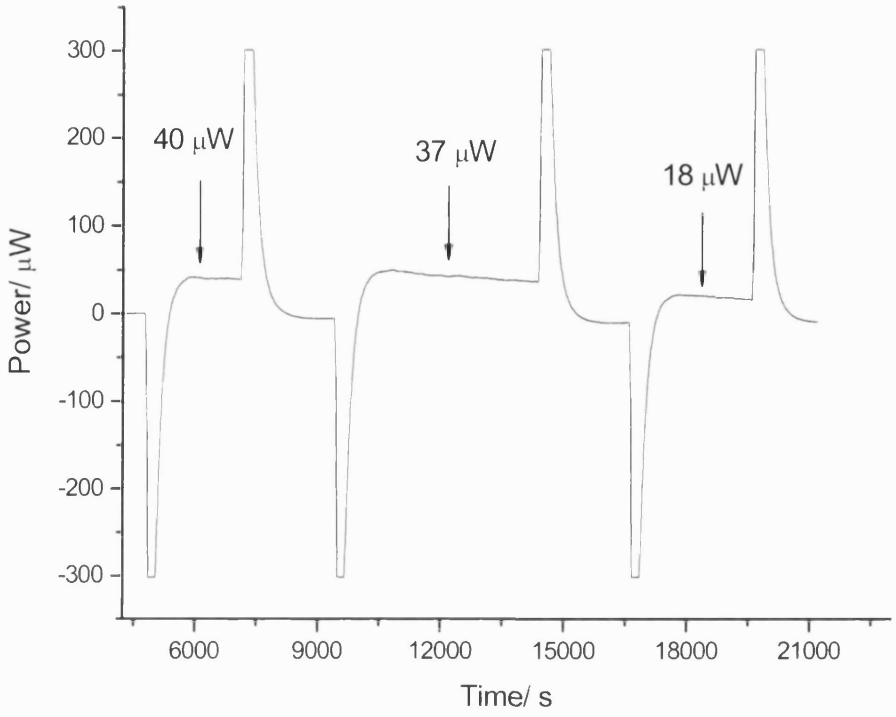

Figure 2.35: Light on/off tests showing a gradual decline in heat output caused by deterioration in lamp performance

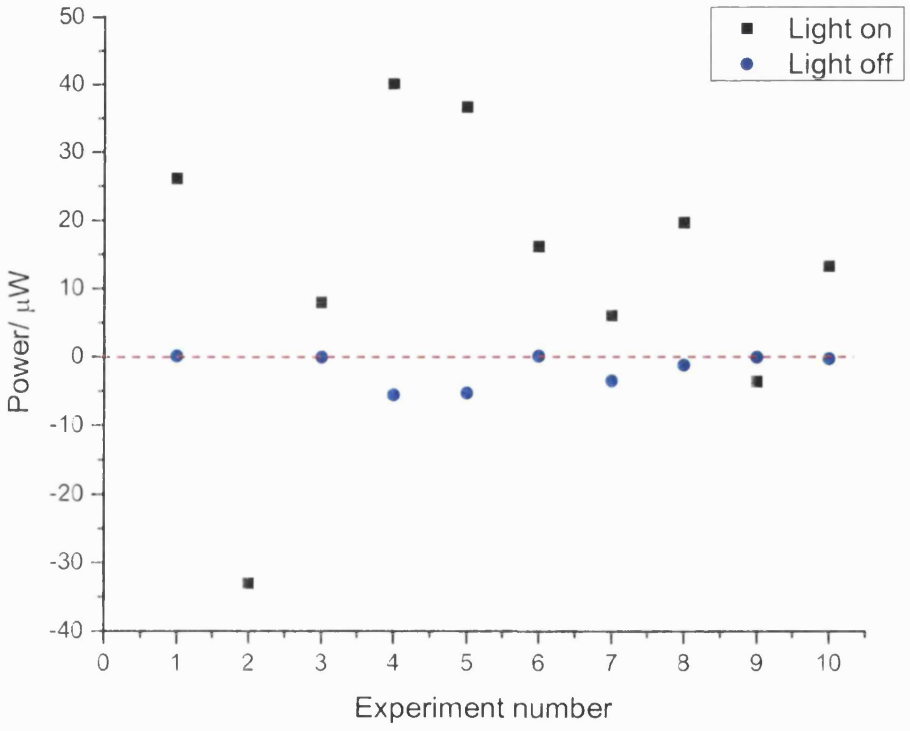

Figure 2.36: A scatter plot to show the variation in power with the light on/off

The dotted line represents an ideal zero-baseline (Figure 2.36). The scattered points show the deflection in power, with the light off and on, from a zero baseline. A random variation in the calorimetric signal is clearly observed when light is introduced into the photocalorimeter. In contrast, the signal with the light off is very encouraging. The data is scattered within close proximity to the zero-baseline and exhibits a baseline stability of ±5 μW. An average baseline deflection signal of **-1.71 ± 2.37 μW** was determined. The disparity in the data with the light on is large with a deflection maximum of 40 μW and minimum of -33 μW, giving an average of **12.97 ±21.07 μW**. Variations of this magnitude made it extremely difficult to correlate data with drug samples (Chapter 3).

If it can be assumed that the source of intensity is constant then it is quite possible to make a rapid assessment and measurement for the rate of photodecomposition particularly in the case of a rapid reaction. Unfortunately, this is not the case for Xe lamps and is highlighted by the outcomes presented in Figure 2.36. Inconsistencies in light intensity will impact on the calorimetric output making it difficult, or worse, impossible, to conduct an accurate evaluation on the photostability of samples. For these reasons, an alternative light source was investigated in order to try and overcome these obstacles.

2.3 The Light-Emitting Diode Photocalorimeter (Mark III)

A number of issues associated with the light output from a Xe lamp were highlighted in section 2.2.4 because of which an alternative light source was sought after. The use of Light-Emitting Diodes (LED) may represent an alternative light source for photocalorimetric applications. Based on literature published to date, it is the first time that LEDs have been used in-conjunction with an Isothermal Microcalorimeter (TAM).

LEDs are becoming increasingly more efficient as designs improve and have received considerable acceptance for its wide use in a range of applications as LED technologies advance. They are ubiquitous in modern society – readily available in any electronic store – from being indicators (stereo, microwave ovens, automobile dashboards), numeric displays (clock radios, digital watches), to telecommunications for short range optical signal transmission (TV, DVD etc, remote controls). LEDs have also found

application in; criminology (counterfeit money checking), the environmental and medical industries e.g. phototherapy for treatment of acne[7] and spectroscopic analysis.[8]

The LED is basic in operation (Figure 2.37). It typically comprises a semiconductor device for emitting light and has a positive and negative terminal (P-N junction). When a current is applied electrons flows into the junction from the p-side, or anode, to the n-side, or cathode causing the electrons to release energy in the form of photons. It is the composition and condition of the semiconducting material that determines the colour of the light the LED produces. For example, inorganic materials such as Gallium Nitride/Indium Gallium Nitride (GaN/InGaN) are typically used to produce near UV, blue/green LEDs whereas materials such as Aluminium nitride/ Aluminium Gallium nitride (AlN/AlGaN) can be used to produce near to far UV LEDs (down to 210 nm). The entire unit is totally embedded in a solid epoxy resin which provides a hard case to protect the LED semiconductor. This solid-state device thus controls current without heated filaments and is therefore a very reliable source of radiation.

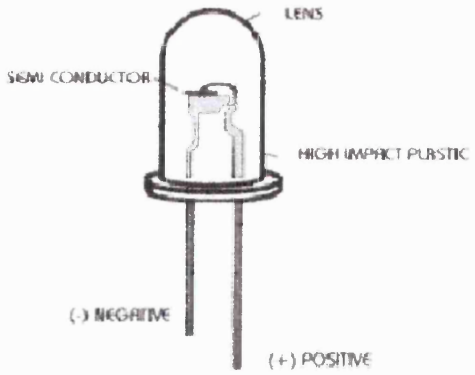

Figure 2.37: Basic construction of an LED

LEDs can offer great potential for a number of reasons which could represent a highly advantageous alternative to Xe lamps. The advantages are that LEDs;

- have an extremely long life span. Typically lifetimes upwards of 100,000 to 50,000 h have been reported when operated at their rated power and 5000 h for shorter wavelength LEDs generally below 380 nm. This is some 100 times greater than a 300 W Xe lamp.

- emit in a narrow-spectrum. LEDs typically emit over a 10 nm bandwidth giving monochromatic lighting ability. Using selected wavelengths, an array of LEDs comprised of different wavelengths can collectively be arranged to create a specific spectrum of desired wavelengths across the UV-VIS region.

- are low-self heating. This obviates the need for a circulating cooling system as required for Xe lamps which can be very costly.
- can be switched on and off very quickly and hence light up very quickly.
- do not suffer with problems associated with arc imaging/alignment and collimation of the light each time prior to the light being switched on.
- can achieve full brightness in a few microseconds whereas Xe lamp requires a warm period of at least 1 hour prior to sample exposure.
- are widely available in different intensities, shapes and sizes. A single LED is relatively small is size and requires low power consumption thus maintenance costs are negligible.
- are inexpensive compared with the cost of a Xe arc lamp. LEDs can cost as little as a few pounds (GBP), in contrast to the several hundreds of pounds for a Xe arc lamp!

The advantages given above make LEDs a superb choice as a radiation source for application in photocalorimetry. A prototype design was thus set-up and a schematic of the design is represented in Figure 2.38.

The LED photocalorimeter (Mark III) uses an array of standard (5 mm round) LEDs in-conjunction with liquid light guides to deliver light in to the sample and reference ampoules. The light is emitted from two separate irradiation LED sources. This means that the light beam is no longer split from the same light source as with the earlier design (Mark II). The amount of light in each side can, therefore, be controlled independently with its respective LED array. A simple schematic of the instrument design is shown below (Figure 2.38).

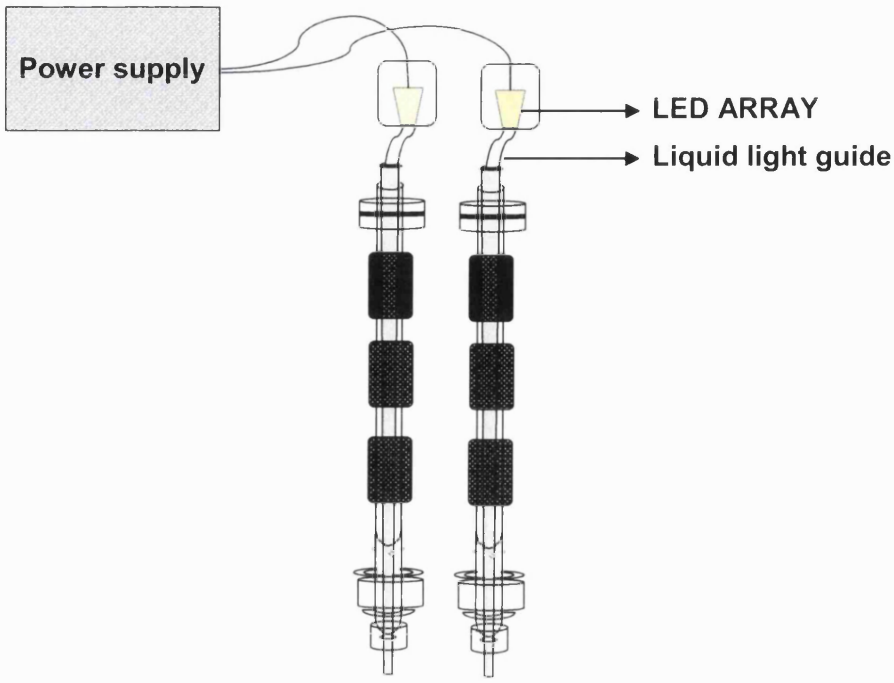

Figure 2.38: Schematic of LED photocalorimeter – Mark III

This very simple design set-up allows the light intensity to be controlled in the sample and reference sides, in a similar manner to that of the Mark II, but here a simple power supply with two output controls was used to generate a constant current to the LEDs. Each LED is wired separately with an in-line resistor to a control knob on the power supply. The voltage on each side can be controlled independently; the voltage on the sample side was set to a desired current and the voltage on the reference side then is adjusted to obtain a zero calorimetric signal with the light on. This feature essentially replaces the optical beam splitter where the shutters were used as a means to control the light input.

2.3.1 Response of using a single LED on TAM output

Prior to the set-up described above, preliminary tests using a 350 millcandela (mcd) (peak wavelength 400 nm) (purchased from RS components) LED were performed to determine proof-of-concept and assess whether the LEDs could emit enough light power to cause photodegradation of the sample without saturating the TAM amplifiers. Initially a single LED was directly fed through the metal column (which usually holds the liquid light guide) and into a specially made ampoule lid. The LED was thus situated

directly on top of the sample inside the TAM channel. The data showed that the light emitted was far too intense at 20 V due to the short distance between the LED and sample. The voltage on the reference side was reduced until a power signal was obtained within a detection limit of 3000 μW set on the TAM amplifiers. This was found to be around 5 V indicating that saturation of the amplifiers occurred above 5 V. However, at 5 V degradation of photochemical materials may be insufficient, or far too slow to attain quantifiable data, and also leaves little leeway to adjust the voltage on the reference side. The LEDs were, therefore, situated outside the TAM channel and connected to the liquid light guides to direct light into the ampoules. This increased the distance between the light source and sample and hence reduced the light intensity to the ampoule. In order to compensate for the loss in intensity, Ultra-bright high intensity UV LEDs were purchased from RS components© (Part No: 454 – 4403).

The Mark III photocalorimeter was thus initially set up using extreme Ultra-bright super UV LEDs (5 mm round) emitting a luminous intensity of 10,000 mcd. These were purchased from Ultraleds© Ltd and covered a narrow spectrum in the UV region (380 – 410 nm).

The TAM was electrically calibrated at 300 μW. The light was switched on after a zero baseline with the light off was attained. The current on the sample and reference sides were set to 10 V until a constant signal was observed. The reference side only was then adjusted in order to obtain a zero signal with the light on.

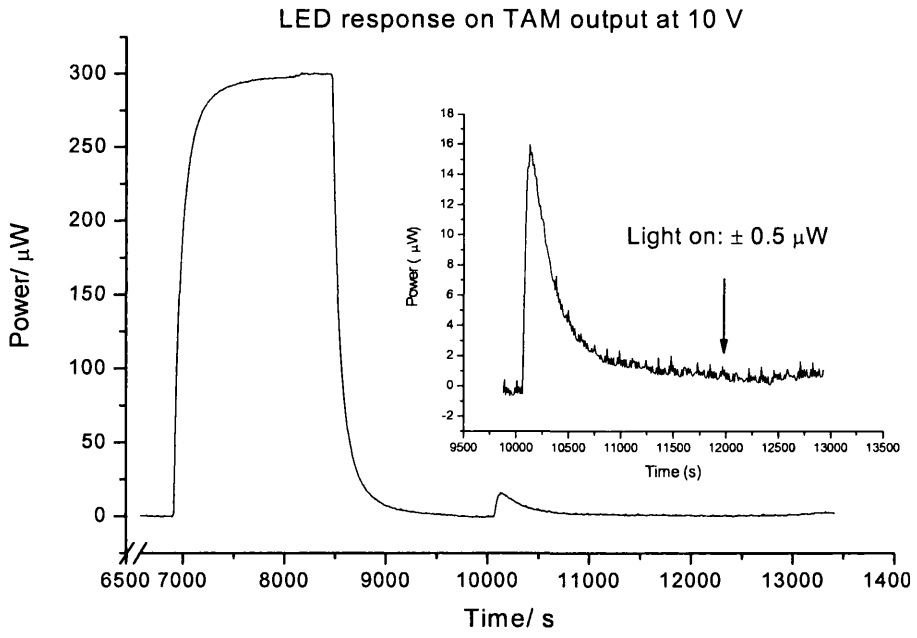

Figure 2.39: Photocalorimetric response to light input from single LED. Inset figure showing close up of baseline after light is switched on.

Figure 2.39 shows a very encouraging response from the LED on the TAM output. This light test was conducted on empty ampoules to assess the stability of the light. The baseline stability with the LEDs was very encouraging with a stable signal being exhibited ca 0.5 h after switching the light on. Several light tests performed gave an average signal of **0.4 ± 1.1 µW** with the light on. The use of the dial controls on the power supply made it possible to adjust finely the amount of light reaching the ampoules to achieve a zero baseline.

Using this set-up, the light delivered was quantified using 2-nitrobenzaldeyde (2NB) solution as a chemical actinometer (further discussed in the Chapter 3). In order to assess if the system was responding accordingly, the photolysis of 2NB was tested at 3 different voltages; 10 V, 15 V and 20 V, to evaluate if there was a direct correlation of increasing voltage to the power output of the photodegradation of 2NB. These results are discussed in Chapter 3.

2.3.2 LED Array

LEDs emit over a very narrow bandwidth (~ 10 nm) due to their small and simple structure, and hence it is not possible, presently, to simulate the solar spectrum from a single LED unlike Xe lamps. Each LED, however, presents monochromatic lighting ability and thus by careful selection of wavelengths, it is possible to create a custom array of wavelengths in the UV-VIS. In this system it was possible to cover a wavelength range from 350 – 700 nm in the UV-VIS using a selection of LEDs.

The following LEDs (standard 5mm round with UV epoxy resin) were purchased from Roithner LaserTechnik GmbH, (Vienna, Austria);[9]

Table 2.3: LEDs peak wavelengths and part numbers

Peak Wavelength of LED (nm)	Part Number
395	RSL-UV395
380	RSL-UV380
370	NS370L-5RLO
360	RLT360-1.0-15
350	RLT350-0.3-15
White (400 – 700)	5W4HCA-P

The LEDs were situated and secured in a metal holder, made from Aluminium (Figure 2.40). It was only possible to arrange for five LEDs to be fully operational at the same time due to the nature of the design. This was because each LED was positioned at a 15° angle in order to achieve maximum throughput. Increasing the angle to 30° made it possible to accommodate for a sixth LED, this, however, minimised the light contact between the LED and light guide which resulted in limited throughput of light. For this reason the LEDs were set at an angle of 15°.

The following five LEDs were chosen to comprise an array; 360, 370, 380, 395, 400 – 700 nm (white), giving an overall coverage of 360 – 700 nm (full array) in the near UV-VIS range. The sample and reference sides comprised the same set of LEDs and were positioned in their respective holders. The output from the LED peaking at 350 nm was far too little to quantify using a spectroradiometer (see Chapter 3) and therefore it was disregarded from the set-up. Generally, near UV emitters at wavelengths around 375 – 395 nm are cheap and common at relative high intensities. Shorter wavelength diodes

(below 370 nm), however, tend to have limited power outputs and are thus commercially scarce. At present, LEDs below 350 nm are not commercially available as standard 5 mm bulbs due to their limited power output. With the technology fast advancing, LEDs in the far UV are becoming more commercially available down to 247 nm[9,10] and are known as UVTOPS®. These LEDs were not considered for application in this system because, not only are they substantially more expensive than standard LEDs, they are much larger in size and hence are not suitable for this particular design structure. Note the major source of the damaging effects of sunlight stem primarily from the ultraviolet portion of the spectrum between 290 and 400 nm (UVB and UVA). The different ultraviolet wavelengths penetrate the skin to different depths and can have different biologic consequences.

Using the system in place, it is possible to study causative wavelengths, by illuminating a LED at a specific wavelength, as well as full spectrum (360 – 700 nm). In order to alternate between individual LEDs for monochromatic lighting, a circuit switch board was constructed allowing each LED to be switched on, or off, in turn as required (Figure 2.41).

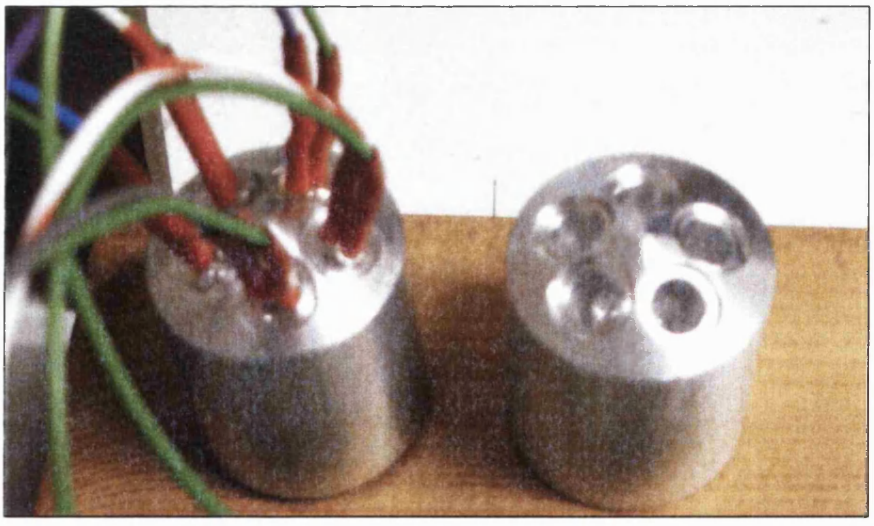

Figure 2.40: LED assembled in specially made adapters

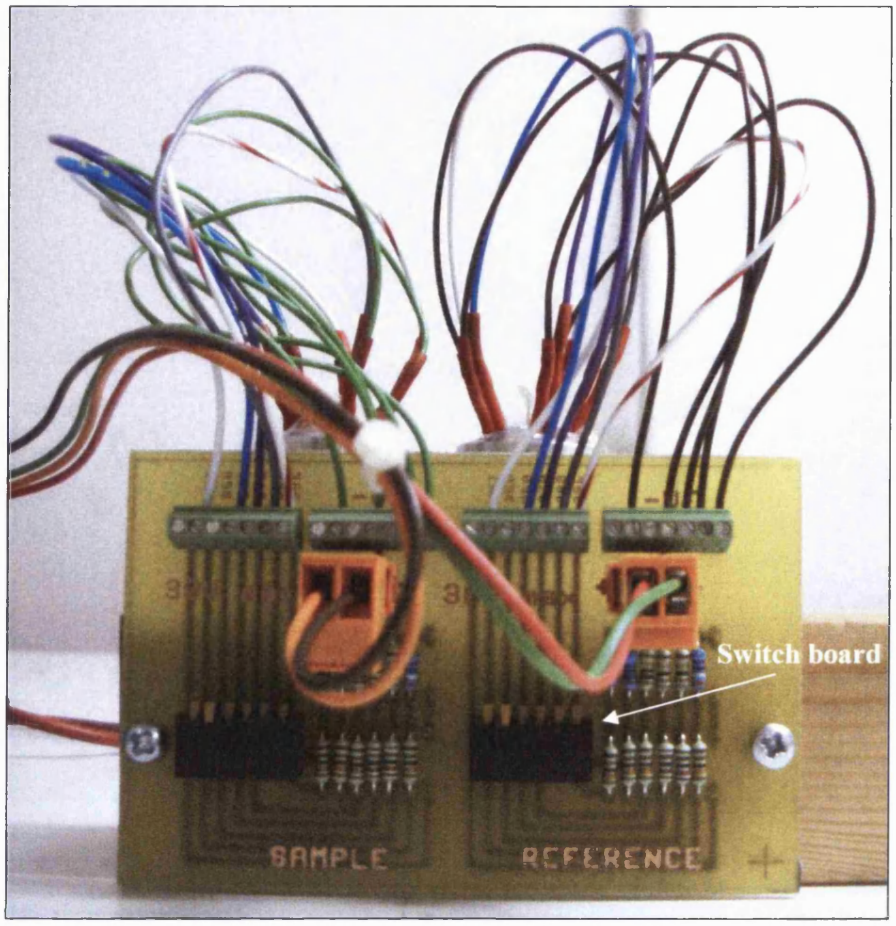

Figure 2.41: LED Array with circuit board

A basic diagram of the above circuit board is shown Figure 2.42. A circuit diagram of the switch board is presented in Figure 2.43 and represents the current flow direction in illuminating the LEDs. Each LED was wired with an in-line resistor built into the circuit board to limit the current in the LED to a safe value. The resistance of each LED was determined by Ohm's law (Equation 2.1) in accordance to its individual rated operating power.

$$R_S = \frac{V_S - V_F}{I_F} \qquad \text{Eqn. 2.1}$$

where;

R_S is the Resistance (Ω or Ohms)

V_S is the Power Supply Max (V)

V_F is the Forward Voltage of LED (V)

I_F (typ) is the Forward Current of LED (A)

A 380 nm LED, for example, has a rated operating power of **3.4 V @ 20 mA** typical i.e. V_F = 3.4 V and I_F (typ) = 20 mA. The maximum operating current allowed on the power supply max is 30 V. The resistance required is therefore 1330 Ohms (Ω).

$$R_S\ (\Omega) = \frac{30\ (V) - 3.4\ (V)}{2 \times 10^{-2}\ (A)} = 1330\ \Omega$$

The calculated resistance for each of LED used is shown below (Fig 2.42).

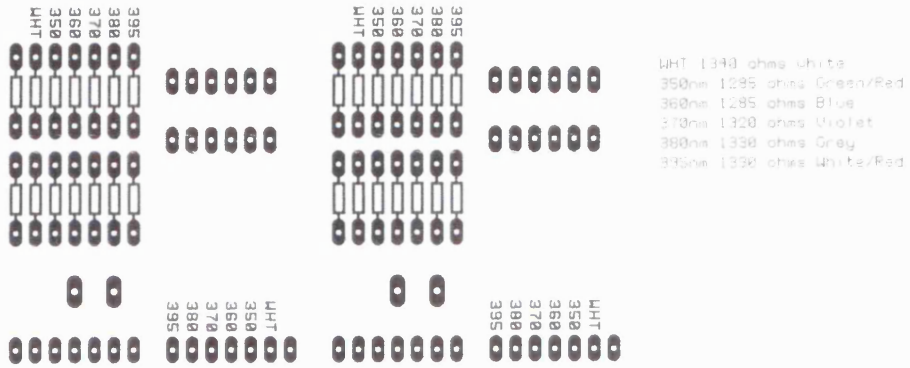

Figure 2.42: Basic diagram showing the information etched onto the LED circuit board and calculated resistance values for each LED

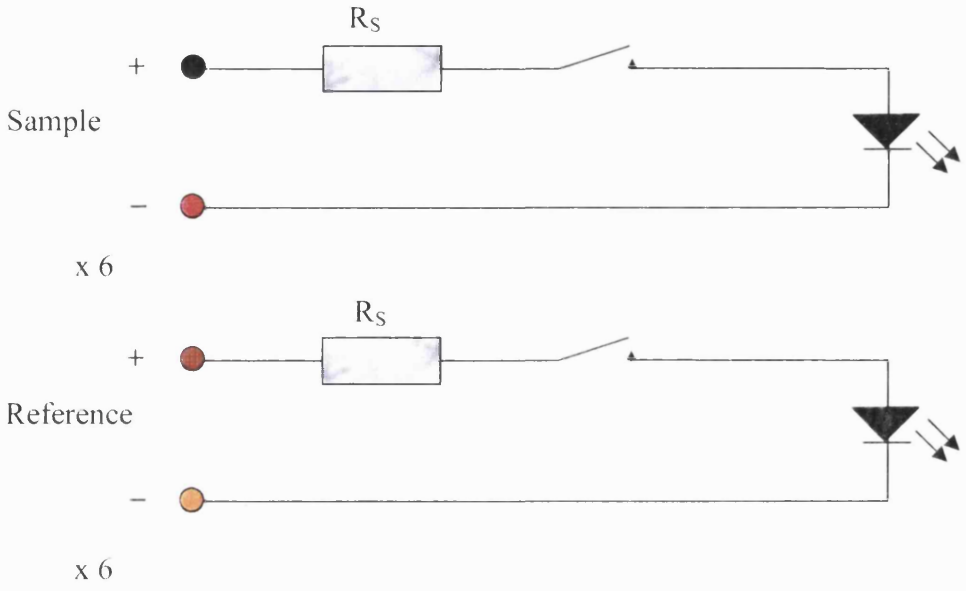

Figure 2.43: Circuit diagram of LED switch board

The final design of the LED photocalorimeter is presented in Figure 2.44.

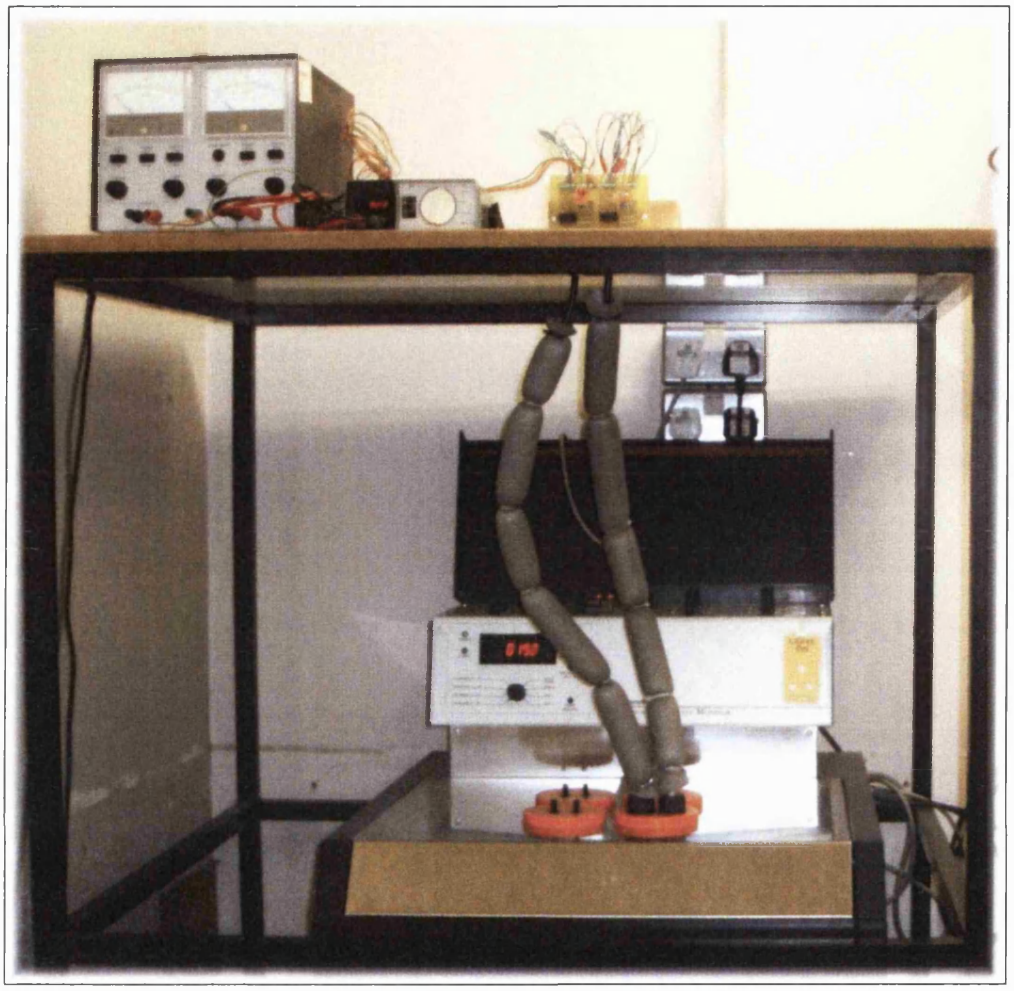

Figure 2.44: Final LED Photocalorimeter (Mark III)

Having arrived at the final instrumental setup, consideration to the experimental method was given. The standard method of loading and lowering ampoules into the isothermal microcalorimeter has been followed previously and described in section 2.1.1. This method is commonly used where standard 3 mL ampoules are employed. However, the development of a new photocalorimeter has brought the opportunity to investigate the best method of lowering 20 mL ampoules into the TAM. The ampoules (20 mL stainless steel, Thermometric Ltd) and were filled with 4 mL distilled water. Five different methods of lowering the ampoules into the TAM were investigated; the best method is governed by the one that most quickly recovers from thermal shock to allow measurement of thermal activity to commence once a stable baseline signal is achieved.

The five methods tested were as follows;

- **Method 1** – ampoules lowered straight down into measuring position and data recording started immediately.
- **Method 2** – ampoules lowered straight down into measuring position for 30 minutes and then data recording started.
- **Method 3** – ampoules lowered into equilibrium position for 30 minutes, then lowered into measuring position for 30 minutes and then data recording started.
- **Method 4** – ampoules lowered into equilibrium for 30 minutes, then lowered into measuring position and data recording started immediately.
- **Method 5** – ampoules lowered straight down into measuring position for 1 hour and then data recording started.

A comparison of the TAM outputs obtained using each method is plotted in Figure 2.45.

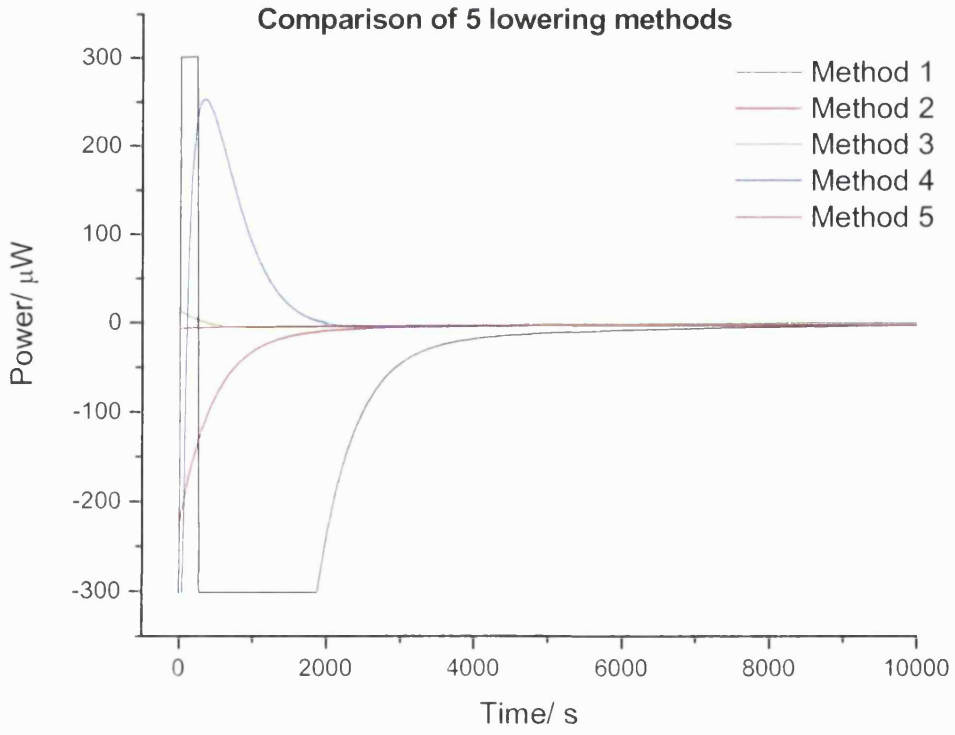

Figure 2.45: A plot to show a comparison of 5 different ampoule lowering methods

Figure 2.45 clearly shows the effect different lowering methods have on the calorimetric output. The degree of thermal shock varies significantly and generally it is the case that the longer the ampoules are held in the measuring position the less of an impact there is of a thermal shock. As expected, Method 1 demonstrated the worst thermal effects with a baseline stabilising some 2.5 h after the experiment had began. Positioning the ampoules in equilibrium or keeping the ampoules in the measuring position for at least 1 hour showed to reduce thermal effects significantly and exhibit a stable output. The outputs using Methods 3 and 5 were most promising. The thermal effects using Method 3 is very short lived (approx 10 minutes) before the baseline reaches plateau. In particular, Method 5 gave the most stable signal and exhibited no thermal effects. Therefore this method was adopted throughout all the experimental work reported herein, unless otherwise stated.

As with the previous design, it was important to assess the baseline stability with the light off and on. An average baseline of **-0.45 ± 0.93 μW** was achieved with this system.

The baseline stability with the light on was assessed using the power supply to control the amount of the light input. The current was set typically to a predefined setting e.g. 15 V whilst the current on the reference side was then compensated for until a zero baseline signal on the TAM was obtained. Figure 2.46 shows the stepwise manner in which the voltage on the reference side can be adjusted to achieve a zero baseline. A digital volt meter was connected to the reference side of the power supply to measure accurately the current (unlike the earlier design (Mark II), which had no way to quantify the level of adjustment using the shutters). The current on the sample and reference side was accurately set to 15 V using the digital voltage reader. The voltage on the reference side was then gradually adjusted in a stepwise manner of 0.5, 1 and 2 V to assess if the response was proportional to the TAM output.

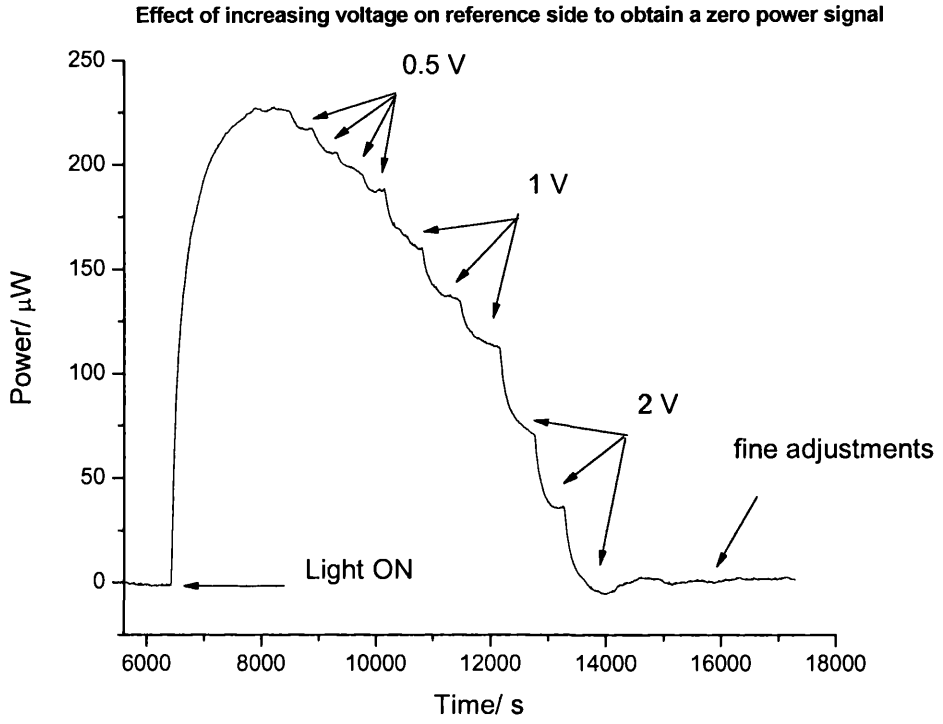

Figure 2.46: LED light response on TAM output

The signal immediately increased and settled to give an exothermic signal of ~ +225 µW. This showed that the intensity of light was greater in the sample side compared to the reference. The voltage on the reference side was therefore gradually increased until the signal reached a zero power signal. The difference in the power signals obtained upon increasing the voltage is shown in Table 2.4. The plateau time after switching on the light was approx. 30 minutes. Following a gradual decline in voltage (0.5, 1 and 2 V), the signal settled to plateau after approx. 7 minutes. The signal decline is proportional as the voltage is increased. This demonstrates the system is working well.

Table 2.4: Voltage – Power Data of the LED photocalorimeter

Voltage change on reference side (V)	Average difference in power (µW)
0.5	9.8 ± 1.7
1	25 ± 2.6
2	39 ± 3.6

Several light on/off tests were performed to assess the system error of the baseline when the light is switched on. The measurements were conducted in the same manner as that described above. Five measurements were taken in each case. The baseline reproducibility for the five measurements taken with the light off gave an average signal of **1.18 ± 0.82 μW** (with solvent ethanol/water mixture). The baseline deflection with the light on was **2.37 ± 1.02 μW**. Any power signal generated outside these limits is attributed to the photoreactivity of the sample during irradiation.

With the development of the instrument complete, the next stage was to establish methods of validation and quantification of the light delivery during photodegradation of a sample. The methods employed were that of Physical and Chemical actinometry. A spectroradiometer was used to characterise the performance of the LEDs and establish the intensity of light emitted from the LEDs at each wavelength and as an array (360 – 700 nm). This work is explained in Chapter 3. This method of calibration, however, gives no information on the level of exposure during irradiation of a sample, and hence, an in-situ validation of instrumental parameters is preferable to an external calibration. Thus, the suitability of a number of chemical actinometers (solution phase and solid-state systems) was assessed in order to validate the performance of the photocalorimeter. Chapter 3 details the Chemical Actinometry work undertaken in order to achieve this using the photodegradation of 2-nitrobenzaldehyde as a model solution phase system.

2.4 Summary

The design and development of a novel easy-to-use and versatile photocalorimeter has been successfully implemented. Two prototype designs were successfully developed; both demonstrating much potential in application for photostability testing. The original photocalorimeter, developed by Morris,[1] whilst useful for providing proof-of-concept data was not ideal because it proved impossible to obtain a zero power signal with and without irradiating the sample cell, rendering quantitative analysis of data challenging.

Fundamental instrumental changes were therefore implemented. The instrument was re-designed using a beam splitter and liquid-filled light guides to direct light into the calorimetric cells from a high intensity Xe arc lamp. Using a number of shuttering and focusing adjustments it became possible to improve the baseline signal and average baselines of **0.73 ± 0.02 µW (cf. to 74.1 ± 8.1 µW with the original design) and -1.66 ± 1.50 µW (cf. 217 ± 5.8 µW with the original design)** with the light off and on, respectively, were attained. However, the challenges associated in obtaining consistent quantitative data became apparent during photodegradation studies. This is primarily because Xe lamps are notorious for their short life expectancy ensuing in a deterioration in the performance of the light intensity. Necessarily, an alternative light source was investigated. Light-Emitting Diodes (LED) were chosen as a feasible alternative primarily because they offer extremely long lifetimes. The monochromatic lighting ability of LEDs allows potential to study causative wavelength ranges of photosensitive samples. A selection of LEDs were used to design an array achieving coverage over 360 – 700 nm in the UV-VIS regions. A constant current input is used to balance the delivery of light in the sample and reference calorimetric cells using a variable DC power supply in order to obtain a zero power signal on the TAM. With this system, the average baseline offsets obtained were **1.18 ± 0.82 µW** and **2.37 ± 1.02 µW** with the light off and on, respectively.

Overall, LEDs have demonstrated much potential in application to the successful development of a robust and rapid photocalorimeter for the assessment of photostability.

2.5 References

1 Morris, A.C. (2004) Ph.D Thesis. University of Greenwich, Kent, UK.

2 Oriel Light Sources Catalogue (2004).

3 Technical Specification, Thermometric AB, Note 22016.

4 Perfusion Shaft Operating Instructions, Thermometric AB.

5 Universal arc lamp housing manual 66901-M, Spectra Physics Ltd.

6 Dhuna, M., Beezer, A.E., Morris, A.C., Gaisford, S., O'Neill, A.A.M., Hadgraft, J., Connor, J.A., Clapham, D., Frost, J. (2007) Development of an Isothermal Heat-Conduction Photocalorimeter. *Rev Sci Instrum* 78 (doi:10.1063/1.2670220), 025105

7 Lee, S.Y., You, C.E., Park, M.Y. (2006) Blue and red light combination LED phototherapy for acne vulgaris in patients with skin phototype IV. *Lasers Surg Med* 139, 180-188

8 Kern, C., Trick, S., Rippel, B., Platt, U. (2006) Applicability of light-emitting diodes as light sources for active differential optical absorption spectroscopy measurements. *Applied Optics* 45, 2077-2088

9 Roithner LaserTechnik GmbH, http://www.roithner-laser.com

10 Sensor Electronic Technology, Inc., http://www.s-et.com

- Chapter Three -

Actinometry

3. Introduction

In succession to the development of the two prototype photocalorimeters (Mark II and III), described in Chapter 2, the subsequent step was then to develop a suitable method to allow measurement of the radiant energy delivered to the sample during a photochemical process – the study of which is known as Actinometry. Since each photocalorimeter was built with a different light source; one with a xenon (Xe) arc lamp (Mark II) and the other with LEDs (Mark III), it was necessary to conduct actinometry work for each system. The suitability of the photodegradation of 2-nitrobenzaldehyde as a chemical test and reference reaction was studied in order to validate the performance of the instruments. Although the instrument is capable of monitoring solid-state systems, there are limited numbers of solid-state test reference materials reported in the literature[1] (a result of the complexities involved in dealing with quantification). It is important firstly to understand simple systems to test proof-of-concept. Necessarily, the actinometry work detailed herein is considered for simple solution phase systems only.

Prior to the construction of the LED photocalorimeter, initial actinometry development work was carried out using the Xe lamp photocalorimeter. As the project progressed, problems using the Xe lamp became evident through inconsistencies in the data obtained and thus subsequent work was pursued solely with the LED photocalorimeter. As mentioned in Chapter 2, prior to the development of the LED array system, to test proof-of concept, a single high intensity UV LED was used to conduct preliminary actinometry work. Thereafter, the array system was used throughout. This chapter therefore follows the actinometry work undertaken using three systems; xenon arc lamp (Mark II), Single LED and Array of LEDs (Mark III) and highlights the problems encountered in using a high intensity xenon arc light source.

3.1 Actinometry

Actinometry provides a way by which quantification of intensity, that is, the number of photons in a beam, can be determined. It is vital to quantify the efficacy of photodegradative processes that may take place in order to evaluate the photostability of drugs and validate the performance of the instrument. This essentially allows a means to

standardise photostability testing within different laboratories. An actinometer can be a chemical system or a physical device which determines the number of photons in a beam integrally or per unit time. Typically, an intensity measurement of a light source by means of physical actinometry is achieved using instruments such as a spectroradiometer, radiometer, luxmeter, etc, which transform the energy of incident photons into measurable quantities. Although physical instrumentation can be very convenient, their need for frequent recalibration is a hindrance to their widespread application to quantification of intensity. The devices can also be very expensive. More importantly, they provide no information of the number of photons actually absorbed by a sample during a photochemical process. For these reasons, an in-situ validation of instrumental parameters is preferable to external calibration. Thus, chemical test reactions (or chemical actinometer systems) provide a suitable alternative because a photochemical reaction of known characteristics (e.g. quantum yield) is monitored when subjected to the same irradiation conditions as the test sample. This allows the determination of absolute intensity, that is, the number of photons actually absorbed by the sample, rather than the incident total.

Having a suitable chemical test and reference reaction in place is vital to ensure that the instrument is operating properly and is functioning correctly. By maintaining regular checks on the performance of the instrument, data from different laboratories or different instruments can be compared and validated for regulatory purposes. Further benefits include; traceability of experimental data conducted on the same instrument, training of new operators on instrument use and analysis of experimental data, and trouble-shooting the causes of poor/imprecise instrument performance. There are a number of requirements a suitable test reaction should fulfil; it should be robust, simple to perform, require commonly available materials which are relatively easy to handle and prepare and it should be applicable across a range of instrumentation. There are many suitable test reactions suggested in the literature for validating different types of commercially available calorimeters.[1-6] Such test and reference reactions have defined values for their kinetic and thermodynamic parameters, which allow assessments to be made of the calorimeter's performance. For example, the imidazole catalysed hydrolysis of triacetin is the adopted standard test method for quantitative chemical validation of isothermal microcalorimeters as recommended by International Union of Pure and Applied Chemistry (IUPAC)[2] since the reaction parameters have been well established.[3]

These data can be used to ensure the performance of a particular type of calorimeter falls within specifications or to allow comparison of the performance of different instrument designs. Similarly, for the validation of the photocalorimeter, there are a number of test reactions discussed in literature and the IUPAC recommended test reaction is the photoreduction of potassium ferrioxalate.[1] However, the system is not without its limitations and thus an alternative test reaction is investigated here; the photodegradation of 2-nitrobenzaldehyde (2NB).

Whilst chemical actinometers are extremely useful for providing an in-situ validation of the photocalorimeter, the technique provides no information on spectral intensities of the light source itself. Therefore, spectroradiometers can be used in combination with chemical methods to provide useful information about the spectral irradiance of a light source across a range of wavelengths, and when coupled with latest computer software packages, the instrument can be used to perform a number of additional functions such as real-time recording of irradiance data calculated in radiant flux (or photon flux) per unit area (W/m^2).

Chemical Actinometry (chemical photodegradation) and spectroradiometry (instrumental approach) were the two principal actinometric techniques considered for use with both the Xe lamp and LED photocalorimeters in order to allow a quantitative measure of the radiant energy reaching a given surface area (sample in the case of a chemical actinometer, or a photomultiplier tube in the case of a spectroradiometer). This measurement is known as the photon flux (F_0) or "light dose" and is expressed in units of watts per square meter (W/m^2).

The photodegradation of 2-nitrobenzaldehyde (2NB) was studied as a potential chemical test and reference reaction for photocalorimetry and used to determine quantitatively the photon flux of a 300 W Xe lamp and LEDs (single and array systems). Thereafter, photon flux measurements were taken by spectroradiometry. The photon flux data obtained from the two actinometric techniques were then directly compared for the two light sources.

3.2 Chemical Actinometry

A chemical actinometer is useful as it can mimic the experimental situation of the sample of interest i.e., the same illumination conditions are used. In particular, it gives a response over the full range of wavelengths to which the test sample is exposed therefore allowing the measurement of the absolute number of photons absorbed in a sample. The data obtained from the degradation of a chemical actinometer and its correlation to irradiance within the defined wavelength range can then be used to determine the photon flux (W/m^2). Generally, a chemical actinometer has well defined photodegradation characteristics including a well established quantum yield (ϕ) which is constant across a wide range of wavelengths. ϕ is defined as a ratio of the number of molecules consumed during photodegradation over the number of photons absorbed per unit volume per unit time;

$$\phi = \frac{\text{number of drug molecules reacted}}{\text{number of photons absorbed}}$$

This provides a true constant describing the rate or efficacy of a photoreaction. The rate at which a reaction takes place is related to the rate at which the photons absorb and thus it is possible to translate data obtained from the rate constant and quantum yield to determine the photon flux to which the actinometer (and samples) is exposed.

Typically, most chemical actinometers are in the form of solutions, but there are a number of chemical actinometers available that are applicable to all types of photoprocesses. These have been summarised in a technical report for the International Union of Pure and Applied Chemistry Commission on Photochemistry (IUPAC).[1] There is no ideal standard actinometric system in place at present as it is technically demanding and complicated to relate the photon absorption rate to a reaction rate that can be applicable to all experimental settings.

Many methods and general principles of chemical actinometry have been discussed in the literature.[1,7-15] The currently approved chemical actinometer recommended by the International Committee of Harmonisation (ICH) QIB guidelines[16] is quinine hydrochloride dehydrate[17] (referred to quinine hereafter). Although simple in preparation, it has several limitations and in recent years its integrity as a chemical actinometer has been questioned; in addition to being wavelength dependent, it has been

shown to be sensitive to temperature, pH, and dissolved oxygen content[18-21]. Moreover, the major drawback is that the quantum yield for quinine photodecomposition has not been determined.[19,22] For these reasons, the suitability of a quinine actinometer for use in this work was disregarded. The ICH guidelines permit the use of other actinometric systems.

The photodecomposition of Potassium Ferrioxalate has been widely used for many years[10,15,23-31] and is an IUPAC recommended chemical actinometer for photocalorimetry[1]. However, a major drawback is that the photoreaction is very rapid in relation to most drug photodecomposition processes when used with a wide range of wavelengths. The actinometer is reported to react sufficiently in 5 or 10 minutes, yet it can take several hours of exposure before a suitable change of a drug sample is detected. This creates a problem in cases where an output from a photon source is non-uniform such as that with xenon arc lamps which can vary as much as 20% over a period of 5 or 6 hours.[32] Another drawback is that the procedure for sample preparation is technically cumbersome and the actinometric solution is difficult to handle. This observation was also supported by Morris[33] who studied the photodegradation of potassium ferrioxalate as a chemical test and reference reaction for the original photocalorimeter (Mark I) mentioned in Chapter 2. The actinometer was found to be sensitive to dissolved oxygen and required an inert atmosphere for solution preparation and storage. This limits the usefulness of potassium ferrioxalate as a chemical actinometer and it was felt that this system was, therefore, not robust enough to be useful as a general test and reference reaction. For these reasons, the potassium ferrioxalate actinometer was not investigated. Hence, the suitability of the photodegradation of 2-nitrobenzaldehyde (2NB) as an alternative chemical actinometer for solution-phase systems was studied. 2NB has been suggested as a chemical actinometer for photostability testing as it is convenient and easy to handle/prepare.[34] Moreover, the 2NB system was also considered a better suited alternative to that of the IUPAC recommended ferrioxalate actinometer for photocalorimetry by Morris.[33]

3.2.1 The potential of 2-nitrobenzaldehyde as a Chemical Actinometer

The photodecomposition of 2-nitrobenzaldehyde (2NB) in solution was studied as a potential chemical test and reference reaction for the validation of the photocalorimeters. This was investigated with both the Mark II and Mark III photocalorimetric systems.

The use of 2NB as a chemical actinometer has been studied for several years. Its photochemistry was first described in the 1900s by Ciamician and Silber.[35] The photoreaction of 2NB (Figure 3.1) proceeds via an intramolecular rearrangement involving transfer of an $-NO_2$ oxygen atom to the aldehyde functionality yielding the 2-nitrosobenzoic acid (2NBA) product.

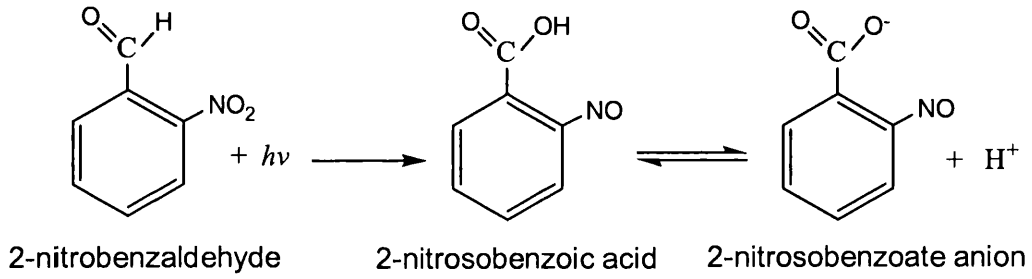

Figure 3.1: The photoreaction of 2-nitrobenzaldehye

In the early 1920's, Bowen established a quantum yield of 0.5 for the photolysis of 2NB in solid, solution and gaseous phases. This means that for a quantum yield of 0.5, every 1 mole of photons (or einstein) will cause 0.5 moles of 2NB to undergo conversion to a photoproduct. Since then the quantum yield of 0.5 in a range of 300 – 410 nm in the UV region has been confirmed by several others.[36,37] In 1965, the use of 2NB as a convenient actinometer was proposed by Pitts[38] for atmospheric pollution studies and it was also found that the quantum yield for conversion is wavelength and temperature independent. In recent years, Allen et al[34] extended the work of Pitts [38]in adaptation for photostability testing. It allowed the 2NB actinometer to perform a pass/fail assessment for photostability of a predetermined UV dose based on a simple visual colour change of the actinometric solution.

The use of 2NB as a chemical actinometer has some unique advantages, which makes it an interesting candidate for photocalorimetry;

- The actinometer has potential for use in solid, solution and colloid dispersion systems.
- Absorbs strongly in the UV region (300 – 410 nm).
- A quantum yield of 0.5 is well established in solid, liquid or vapour phase and is wavelength and temperature independent.
- The sample preparation and experimentation is relatively simple and straightforward.
- The photoreaction is known to follow zero-order kinetic behaviour.

3.2.2 Actinometric Concepts and Considerations

In order to relate the quantum efficacy of the actinometer to that of the number of photons actually absorbed by a sample, information regarding the intensity and the rate of the photoreaction are paramount. With knowledge of the quantum yield and reaction order, the irradiance (I_o) and photon flux (F_o) parameters of the light source can readily be determined. The reaction order and kinetic parameters, namely, the rate constant and reaction enthalpy, of a photolytic reaction can be obtained from the calorimetric output.

3.2.2.1 Relationship to Calorimetric Data

The photodegradation of 2NB is considered to follow zero-order kinetics.[34,38] Thus, this should give a constant deflection from zero in the photocalorimeter. The basic calorimetric equation for zero-order reactions relates the rate constant (k), reaction enthalpy (ΔH) and calorimetric output as;

$$\Phi = k\Delta HV \qquad \text{Eqn 3.1}$$

where; Φ is the calorimetric output (W)

k is the rate constant (mol dm^{-3} s^{-1})

ΔH is the reaction enthalpy (J mol^{-1})

V is the volume of the actinometer solution (dm^3)

In order to relate the irradiance and, subsequently, the photon flux of the light source to the calorimetric output, there is a stipulation that either the rate constant or reaction enthalpy be known. However, neither of these parameters is well established in the literature. This puts a constraint on the system and requires the need for an ancillary method of investigation for the determination of either k or ΔH. There is insufficient information available in the literature to make an accurate calculation of the bond enthalpies associated in solution phase systems during the photolysis of 2NB. Therefore an auxiliary method for determining a value for k was sought. Since the photodecomposition of 2NB results in the formation of an acidic product, 2NBA, it is possible to derive a value for k with the knowledge of the number of moles of product formation and the irradiation time. This can be obtained by monitoring the changes in pH as the photoproduct, 2-nitrosobenzoic acid, builds up as the actinometer solution is irradiated or a simple titration with a basic solution (e.g. NaOH) can be performed to determine the number of moles of acid [H^+] formed. These measurements were taken for the two light sources used; Xe arc lamp and an array of LEDs (pH measurements were taken for the LED light source only).

Once a value for k has been established, the irradiance and photon flux can be readily determined following the procedure outlined[11] in section 3.2.2.2. All experimental procedures are detailed in section 3.2.3.

3.2.2.2 Determination of Irradiance

Using equation 3.2, the irradiance (I_0) can be calculated.

$$I_o = \frac{k}{\phi} \qquad \text{Eqn. 3.2}$$

where; I_0 is the irradiance delivered to the sample (einstein dm^{-3} s^{-1})

k is the rate constant for the photodegradation (mol dm^{-3} s^{-1})

ϕ is the quantum yield

3.2.2.3 Determination of Photon Flux

The photon flux (F_0) can be determined using the following formula;

$$F_o = \frac{I_o V N_A E_\lambda}{A} \qquad \text{Eqn. 3.3}$$

where; F_0 is the irradiance delivered to the sample (W m^{-2})

I_0 is the irradiance delivered to the sample (einstein dm^{-3} s^{-1})

V is the volume of the actinometer solution (dm^3)

A is the cross-sectional area of exposed actinometric solution (m^2)

N_A is Avogadro's number 6.02 x 10^{23} (mol^{-1})

E_λ is the energy of a photon of wavelength λ (J $photon^{-1}$)

The cross-sectional area (A) that the solution is exposed to can be found from;

$$A = \pi r^2 \qquad \text{Eqn. 3.4}$$

where; r is the radius of the ampoule (m)

The dimensions of a 20 mL calorimetric ampoule (Fig. 3.2) were measured accurately using a micrometer in order to calculate the cross-sectional area of the base (Fig. 3.3).

Fig. 3.2: 20 mL stainless steel calorimetric ampoule

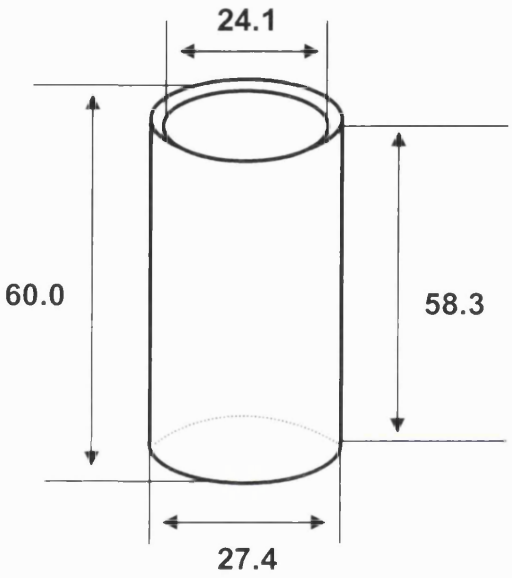

Fig. 3.3: Dimensions (mm) of a 20 mL calorimetric ampoule

All dimensions are given in mm units; Inner diameter: 24.1, Outer diameter: 27.4, Depth: 58.3, Height: 60.0.

∴ Area (A) of ampoule base (in unit of m^2) is: $\pi 0.01205^2 = 4.56 \times 10^{-4}$ m^2

∴ Cross-sectional area of ampoule base used was 4.56×10^{-4} m^2.

The distance between the tip of the liquid light guide and the base of the ampoule was measured at 24.3 mm (Fig. 3.4).

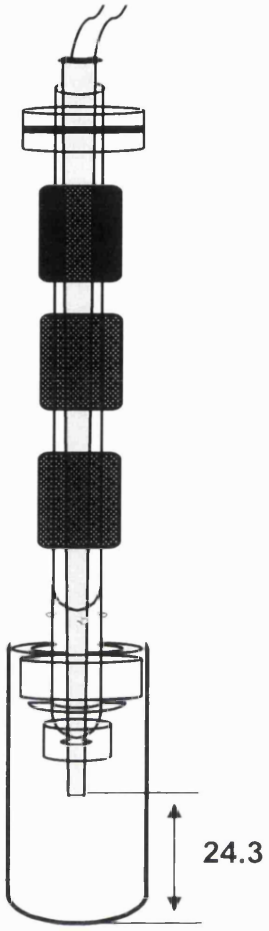

Figure 3.4: Distance (in mm) of optic tip from ampoule base

3.2.2.4 Determination of Photon Energy

The photon energy can then be calculated using Planck's law (Eqn. 3.5).

$$E_\lambda = h\nu = \frac{hc}{\lambda} \qquad \text{Eqn. 3.5}$$

where; h is Planck's constant (6.63×10^{-34} Js photon^{-1})

c is the speed of light (2.99×10^{8} ms^{-1})

λ is the weighted-average wavelength to which the actinometer solution is exposed (m)

The wavelength range of interest is between 290 – 400 nm therefore the 2NB actinometer solution should absorb all the photons between these ranges converting the 2NB to 2NBA with equivalent efficiency. However, when a polychromatic light source, such as that of a Xe arc lamp is used, it emits a different number of photons over the period of irradiation at each wavelength. The number of photons that are released over a specific bandwidth (e.g. 380 – 382 nm) will impact on the total energy flux in the 290 – 400 nm range i.e. the release of a relatively large number of photons at shorter wavelengths may have higher energy photons compared to fewer photons at longer wavelengths. It is, therefore, necessary to estimate a weighted-average photon energy incident upon and absorbed by the actinometer solution. This estimation is required in all cases where a polychromatic light source is used for photostability testing.

Typically, the weighted-average wavelength can be determined by examination of the energy distribution (spectroradiometric data) which is available either from manufacturers of the light source for the specific lamp used, or by in-house measurement using spectroradiometry (discussed later section 3.3). The spectroradiometric data are used to calculate the weighted-average wavelength for that specific light source. These data were obtained using a spectroradiometer for the two light sources; Xe arc lamp and LED. The energies expressed in units of W/m^2 were obtained over a narrow bandwidth in the wavelength range of interest i.e. 290 – 400 nm for the Xe lamp, 370 – 400 nm for the single LED system, and 350 – 400 nm for the array of LEDs used. If the wavelength range for the Xe lamp is taken as an example, the weighted-average wavelength was determined by the product of the wavelengths and irradiance over each bandwidth summed over the wavelength range of 290 – 400 nm and divided by the irradiance over each bandwidth summed over 290 – 400 nm. This can be expressed using the following formula;

$$\frac{\sum_{290nm}^{400nm} (\lambda \text{ nm}) \text{ (irradiance } Wm^{-2})}{\sum_{290nm}^{400nm} \text{irradiance } Wm^{-2}} \qquad \text{Eqn. 3.6}$$

The weighted-average values obtained using the Xe lamp and LED light source were determined in this manner and are given in section 3.3. These data were then used to

calculate a weighted-average photon energy value using Planck's law as already described (Eqn. 3.5).

3.2.3 Determination of rate constant (*k*) using ancillary methods

3.2.3.1 Photochemical Titration Analysis of 2NB

One of the methods used to determine a zero-order rate constant for the photodegradation of 2NB was to measure the formation of the photoproduct as a function of irradiation time using titration analysis. The photochemical reaction results in a conversion of the aldehyde functionality into an acid. Knowledge of the irradiation time, over which this photolytic process occurs, can be used to calculate readily the acid formation by means of titration of the actinometer solution with a basic solution (NaOH). The endpoint of the reaction can then be determined using an acid-base indicator (phenolphthalein) so that a visible colour change (from yellow to pink) could be detected. These measurements were performed with only the Mark II photocalorimeter i.e. Xe lamp source.

Materials and Methods

2-Nitrobenzaldehyde (2NB, >98%) and Phenolphthalein indicator was purchased from Sigma Aldrich UK. Sodium Hydroxide (GPR) was purchased from BDH Laboratory Supplies Ltd, UK. Ethanol (99.7-100%) was purchased from Hayman Ltd, UK. Deionised water was used throughout. All materials were used as received.

2NB Actinometer Solution Preparation

The actinometer solution was prepared using 0.1 M 2NB. 1.5112 g of 2NB was weighed and crushed using a pestle and mortar to aid dissolution of the sample. The solid was dissolved using 1:1 ethanol/de-ionised water solvent mixture and stirred for approx. 30 minutes using a magnetic stirrer until the solid had completely dissolved. The solution was then made up to volume (100 mL).

Reference Photocalorimetric Experiment

It was necessary to perform a reference experiment to blank the instrument before sample measurements were taken. This was required in order to obtain an overall net zero power signal when the light was switched on.

This was achieved by placing 1:1 ethanol/de-ionised water solvent mixture (4 mL) in both the sample and reference ampoules (20 mL stainless steel) prior to the sample measurement. The ampoules were lowered into the TAM (described in Chapter 2) and the Xe lamp was set to 240 W and switched on for at least one hour before irradiating the solutions. The photocalorimeter's optical arrangement using the shutters was set so as to obtain a zero power output with the light on. The light on/off repeatability was assessed in at least duplicate. The light was then switched off. Assuming that the experimental set up remains unchanged throughout the measurements on the sample tested, it would be the case that the net signal is zero and therefore any change is as a result of the photodegradation of the actinometer solution.

Sample Experiment – Titration Method

Exactly 4 mL of the actinometric solution was pipetted into a 20 mL stainless steel calorimetric ampoule. The Xe arc lamp (240 W) was switched on for at least one hour. The actinometer solution was then irradiated for a known period of time. The irradiated sample was then transferred to a pyrex glass flask and approximately 30 μL 0.1% w/v phenolphthalein indicator was added after the sample had been irradiated. The indicator solution was prepared using 1:1 ethanol/de-ionised water. The actinometer solution was titrated with 0.03 M NaOH using a 10 μL pipette until an endpoint (visible colour change from yellow to pink) was reached. This photochemical titration method was repeated for samples that were irradiated every 10 minutes up to 1 hour total exposure time. A reference titration was performed with un-irradiated freshly prepared 2NB solution representing $t = 0$. The volume of NaOH used to reach the endpoint was used to determine the number of moles of acid formed upon photolysis and plotted against irradiation time. Consequently, a value of the rate constant in mol dm^{-3} s^{-1} can be obtained by determining the gradient of the plot.

3.2.3.2 pH measurements

Another method used to determine a rate constant of the 2NB photolytic reaction was by means of pH measurements. The changes in pH were followed as the actinometer solution was irradiated and used to determine the number of moles of acid formed [H^+] as a function of irradiation time. These measurements were performed for both the Mark II and Mark III photocalorimeters i.e. light sources; Xe lamp and array of LEDs, respectively.

Materials and Methods

2-Nitrobenzaldehyde (>98%) and ethylenediamine tetraacetic acid (EDTA) were purchased from Sigma Aldrich UK. Ethanol (99.7 – 100%) was purchased from Hayman Ltd, UK. Deionised water was used throughout. All materials were used as received.

Reference Photocalorimetric Experiment

The actinometer solution (0.1 M 2NB) was prepared and a blank experiment was performed. The method for the solution preparation and reference experiment method for the Xe lamp photocalorimeter have already been described above in section 3.2.3.1).

The reference experiment using the LED photocalorimeter was performed in a similar manner to that of the Xe lamp photocalorimeter. The calorimetric ampoules were loaded with 1:1 ethanol/de-ionised water solvent mixture (4 mL) prior to the sample measurement. The method of lowering ampoules into the TAM has already been described (Chapter 2). The voltage supplied to the sample and reference sides was set to a desired voltage (e.g. 15 V). The full array of LEDs (covering a wavelength range of 360 – 700 nm) was switched on and the voltage on the reference side was then adjusted until a zero calorimetric signal was obtained. Following the blank (reference) experiment, the sample ampoule was replaced with the actinometer solution (the methods of which are given below for the Xe arc lamp and LED photocalorimeters).

Sample Experiment

The pH measurements were recorded with a Hamilton pH glass electrode; electrochemical sensor (sensitive to 0.01 unit), which was connected to a Hanna pH microcomputer HI9024. Buffer solutions at pH 4 and 8 were used to calibrate the pH meter. A 4 mL aliquot of the actinometer solution was pipetted into in a 20 mL stainless steel calorimetric ampoule. The 2NB solution was then irradiated for a known period of time and the pH was measured. The same sample solution was re-attached to the liquid light guide for further UV exposure and the pH was determined again. This process was repeated several times taking pH readings at every 10 min irradiation intervals for a total exposure time of 3 hours. The rate constant was determined by following the changes in pH as the amount of photoproduct, 2NBA, built up as a function of irradiation time.

All titration and pH experiments were conducted in at least in triplicate. For each new experiment a fresh aliquot of 2NB solution was taken from the stock solution. The ampoule was washed with deionised water and ethanol and dried after each experiment. The sample solution was maintained at a constant temperature of 310 K by placing the ampoule in a steel heat block.

All actinometry experiments were performed under dark conditions i.e. red light and all solutions were contained in amber glassware that was foil wrapped.

Method for Photocalorimetric measurements

The method for the preparation of 2NB solution and the procedure for the reference experiment using the Xe lamp photocalorimeter have already been described in section 3.2.3.1.

The procedure for the reference experiment using the LED photocalorimeter has already been described in section 3.2.3.2.

Sample Photocalorimetric Experiment

Following the reference experiment to obtain a zero baseline with the light off and on using a solvent system, the ampoule on the sample side was replaced with exactly 4 mL of the 2NB actinometric solution (0.1 M). The reference ampoule remained containing the 1:1 ethanol/de-ionised water solvent mixture.

All measurements were made in at least triplicate. All data were analysed using Origin™.

NB. All standard deviations reported throughout were calculated using *xσn-1* function with a 68% confidence limit.

The following section is divided in two; the first section gives an account of the data obtained using the Xe lamp photocalorimeter and then subsequently an account is given of use of the LED photocalorimeter with the main objective to determine a value for a zero-order rate constant for the photolysis of 2NB.

3.2.4 Results and Discussions using Xe lamp (Mark II Photocalorimeter)

3.2.4.1 Evaluation of *k* by Photochemical Titration Analysis

The data presented in Tables 3.1 describes the colour changes observed during a photochemical titration of 2NB after 10 minutes of irradiation. The yellow colour at the start is due to the presence of the aldehyde functionality of 2NB. As the solution was irradiated over a known period of time, the colour change typically followed;

Yellow ⟶ Orange ⟶ Pale Orange/Pink ⟶ Pink ⟶ Dark Pink/Purple

The endpoint of the titration as indicated by Phenolphthalein was determined by a distinct visual colour change from yellow to pink. The volumes of NaOH required to reach this endpoint at each irradiation period (10 – 60 minutes) were used to determine the number of moles of acid formed. Each data point is given as an average of 3 measurements alongside a standard deviation. The experiment was repeated in this manner for repeatability. The data from both experiments conducted are represented as Run 1 and Run 2, respectively, as shown in Table 3.2 and Figure 3.1.

Table 3.1: Typical colour change of 2NB during photochemical titration

Irradiation time 10 minutes at 240 W

Volume of NaOH (mL)	pH	Colour
0.00	8.0	pale yellow
0.04	8.1	pale orange
0.09	8.8	pale pink
0.12	9.5	pink
0.17	9.9	dark pink

Table 3.2: Amount of product formed with time

Irradiation time (s)	Run 1		Run 2	
	Product formed $[H^+]$ mol dm^{-3}	± Standard Deviation	Product formed $[H^+]$ mol dm^{-3}	±Standard Deviation
0	7.75×10^{-4}	1.15×10^{-4}	1.20×10^{-3}	7.50×10^{-5}
600	9.00×10^{-3}	1.50×10^{-4}	1.43×10^{-3}	1.50×10^{-4}
1200	1.05×10^{-3}	7.75×10^{-5}	1.55×10^{-3}	1.15×10^{-4}
1800	1.20×10^{-3}	1.33×10^{-4}	1.73×10^{-3}	7.50×10^{-5}
2400	1.38×10^{-3}	1.57×10^{-4}	1.90×10^{-3}	4.33×10^{-5}
3000	1.43×10^{-3}	1.33×10^{-4}	1.95×10^{-3}	1.30×10^{-4}
3600	1.53×10^{-3}	4.62×10^{-5}	2.10×10^{-3}	1.98×10^{-4}

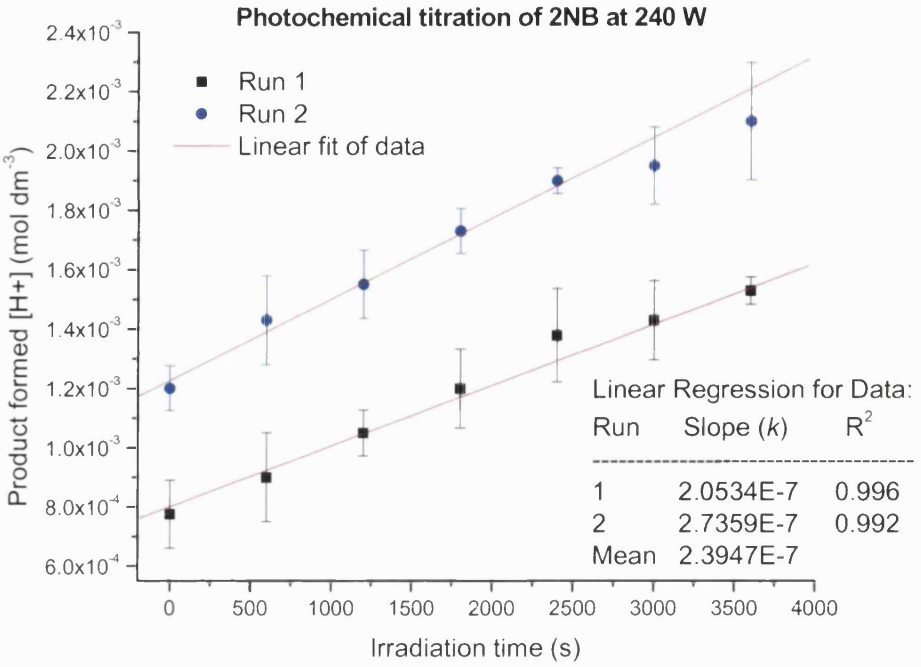

Fig 3.5: Photochemical titration of 2-nitrobenzaldehyde to 2-nitrosobenzoic acid. (Note *n* = *3* for each data point).

A linear increase in the amount of acid formed was exhibited as a function of irradiation time (Fig. 3.5) for both experiments conducted. The slope from the plot gave a rate constant of **2.05 x 10^{-7} mol dm^{-3} s^{-1} (± 1.75 x 10^{-8} mol dm^{-3} s^{-1})** and **2.74 x 10^{-7} mol dm^{-3} s^{-1} (± 5.00 x 10^{-9} mol dm^{-3} s^{-1})** for Run 1 and Run 2, respectively. This gives an average *k* value of **2.39 x 10^{-7} mol dm^{-3} s^{-1} (± 4.88 x 10^{-8} mol dm^{-3} s^{-1})**. These values are in the same order of magnitude as the data obtained in previous work by Morris[33] (cf. 1.4 x 10^{-7} mol dm^{-3} s^{-1}) and agree favourably.

Although the two measurements taken show 2NB to photodegrade at the same rate, it was noticed that the amount of product formed in Run 2 was ca. 1.5 times greater than that of Run 1. The difference in the measurements was probably a result of the fall in the initial pH of the solution that was used for Run 2. The measurements conducted for Run 1 were done using freshly prepared 2NB solution with an initial pH value of 8. The second measurement conducted approx. 4 days after the actinometric solution had been prepared and its initial pH value was 6. This indicated that there may be an issue with the stability of the 2NB solution the longer it is left after preparation and suggests that the actinometric solution may be sensitive to non-photochemical processes such as

oxidation. A significant change in pH can have significant impact on the photostability of the solution and required further investigation.

Furthermore, this approach is somewhat tedious and problematic because the change in colour occurred very rapidly with the addition of very small quantities of base (as shown above in Table 3.1). Typically <0.3 mL of base was a sufficient amount to reach the reaction endpoint, for which reason, 10 μL of base was added at a time to ensure accuracy. Moreover, it should be noted that making a colour change observation under subdued light i.e. dark room using red light, can be subjective and makes it difficult to define accurately the true end point. Attempts to detect the endpoint under normal room lighting within the laboratory to get a better visual of the colour change to pink proved more difficult because the reaction solution changed colour very rapidly; reverting the colour from pink, back to orange and/or yellow. This suggests that the reaction was unstable and undergoing a combined effect of both 2NB photolysis and the photodegradation of phenolphthalein.

In order to avoid such errors, and to investigate further the change in the solution pH as observed with the photochemical titration data, another approach to determine a rate constant was sought; the changes in the solution pH were monitored as the photoreaction proceeded.

3.2.4.2 Evaluation of *k* by pH measurements

The changes in pH were followed every 10 minutes over an irradiation period of three hours. The number of moles of acid $[H^+]$ formed in a 4 mL sample solution was then readily calculated using the pH formula; $pH = -\log [H^+]$.

The data obtained are represented in Table 3.3 and Figure 3.6.

Over the course of the experiments, it was found that the response obtained from the pH data was unexpected. It can be seen that over an initial period of ca. 100 min there was very little change in the amount of product formed. After this period, there was a sharp linear increase with time. In terms of the changes in pH; freshly prepared 2NB solution gave an initial pH of 8 before gradually declining to pH 6 during the initial 100 min of

exposure. As the sample was irradiated further, the rate of change in pH became rapid over which time the pH declined from 6 to 4, consistent with the formation of 2-nitrosobenzoic acid. The initial "lag phase" observed implies that an additional event may be occurring prior to photodegradation into 2-nitrosobenzoic acid and, because of the considerable curvature, it was not possible to determine a rate constant for the reaction.

Suspecting that an oxidation process was responsible, based on observations from pH and acid-base titration measurements, the experiment was repeated with the addition of a small quantity of ethylenediamine tetraacetic acid (EDTA). In the event of an oxidation process, EDTA can be used as a chelating agent to remove any free metal ions and so to prevent them catalysing oxidative processes. The metal ions may have unavoidably been introduced into the solution as contaminants present in the deionised water used and on the glassware.

The 2NB solution was prepared in the same manner as that described in section 3.2.3.1, but in addition, approximately 50 mg of EDTA was added to the actinometric solution. The pH measurements were conducted in the same manner over an irradiation period of 3 hours.

The data obtained in the presence and absence of EDTA is tabulated in Table 3.3 and shown in Figure 3.6 for comparison.

Table 3.3: pH changes of 2NB in the presence and absence of EDTA at 240 W

Irradiation time (min)	Photolysis of 2NB		Photolysis of 2NB and EDTA	
	Product formed $[H^+]$ mol dm^{-3}	± Standard Deviation	Product formed $[H^+]$ mol dm^{-3}	± Standard Deviation
0	2.04×10^{-6}	3.79×10^{-7}	7.91×10^{-4}	3.19×10^{-5}
10	2.68×10^{-6}	1.08×10^{-7}	9.48×10^{-4}	1.19×10^{-4}
20	3.23×10^{-6}	3.33×10^{-7}	1.06×10^{-3}	1.93×10^{-4}
30	3.99×10^{-6}	5.90×10^{-7}	1.18×10^{-3}	1.51×10^{-4}
40	5.40×10^{-6}	1.25×10^{-6}	1.27×10^{-3}	1.74×10^{-4}
50	6.82×10^{-6}	9.34×10^{-6}	1.36×10^{-3}	1.42×10^{-4}
60	8.93×10^{-6}	1.81×10^{-6}	1.49×10^{-3}	1.03×10^{-4}
70	1.28×10^{-5}	2.51×10^{-6}	1.58×10^{-3}	1.23×10^{-4}
80	2.14×10^{-5}	5.66×10^{-6}	1.69×10^{-3}	1.02×10^{-4}
90	6.06×10^{-5}	2.65×10^{-5}	1.91×10^{-3}	1.11×10^{-4}
100	2.02×10^{-4}	1.18×10^{-4}	2.02×10^{-3}	1.16×10^{-4}
110	4.65×10^{-4}	2.10×10^{-4}	2.20×10^{-3}	1.04×10^{-4}
120	8.83×10^{-4}	3.62×10^{-4}	2.41×10^{-3}	8.51×10^{-5}
130	1.44×10^{-3}	4.75×10^{-4}	2.56×10^{-3}	1.18×10^{-4}
140	2.06×10^{-3}	6.31×10^{-4}	2.74×10^{-3}	1.08×10^{-4}
150	2.78×10^{-3}	7.13×10^{-4}	2.94×10^{-3}	6.76×10^{-5}
160	3.61×10^{-3}	9.35×10^{-4}	3.15×10^{-3}	7.25×10^{-5}
170	4.50×10^{-3}	8.97×10^{-4}	3.32×10^{-3}	4.43×10^{-5}
180	5.34×10^{-3}	1.34×10^{-3}	3.61×10^{-3}	8.32×10^{-5}

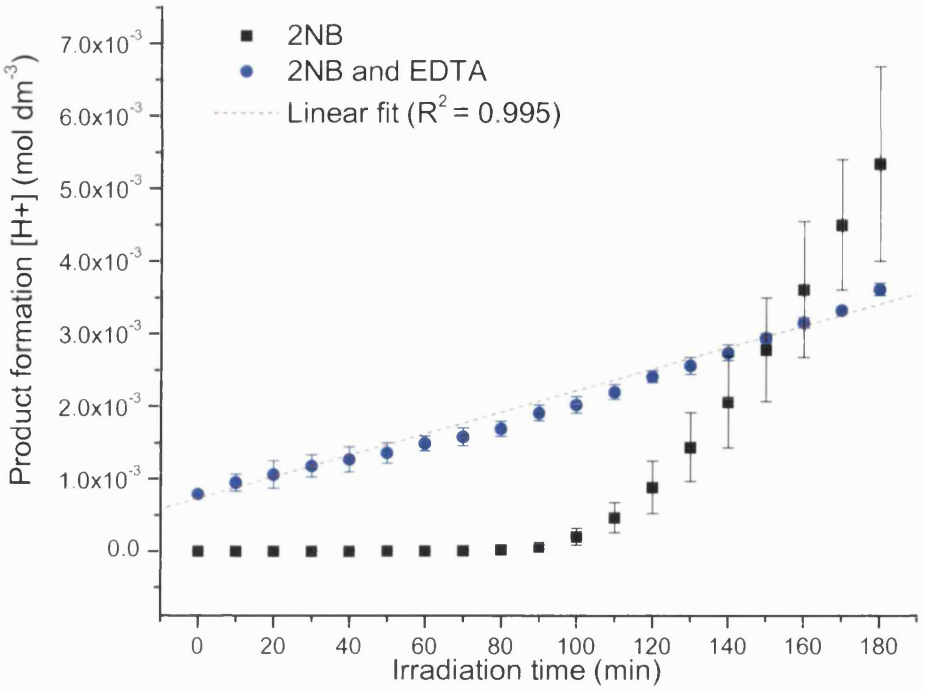

Figure 3.6: Changes in pH during the photolysis of 2-nitrobenzaldehyde in the presence and absence of EDTA at 240 W

It is clearly evident by comparison of the concentration of product formed versus time profile with and without the addition of EDTA (Fig. 3.6) that 2NB is undergoing an oxidation event in addition to photodegradation. When EDTA is added to the solution, the initial "lag phase" prior to photodegradation disappears, although there is still some curvature in the data and a small break point still appears at ca. 100 min. Thereafter the concentration of 2NBA increases linearly with increasing exposure time over a period of 3 hours (R^2 = 0.995). A rate constant of **2.47 x 10^{-7} mol dm^{-3} s^{-1} ± 8.08 x 10^{-9} mol dm^{-3} s^{-1}** (standard deviation derived taken from triplicate measurements) was derived from the slope of the plot containing EDTA in solution, and this corresponds well with the rate constants obtained using the photochemical titration method and with the data obtained by Morris.[33]

Clearly, there appears to be a problem with the stability of the 2NB solution which can limit its usefulness as a chemical actinometer. To address this issue further, the actinometric solution was prepared under various conditions. The solutions were prepared in the same manner as that described in 3.1.3.1, except that it was attempted to

create an oxygen-free environment by degassing the solution under vacuum and maintaining an inert atmosphere with a steady flow of N_2 gas over the sample as the pH measurements were taken. The solution was degassed under vacuum for ca. 5 minutes as longer degassing times may result in loss of solvent by evaporation. Solutions were also prepared with and without degassing under vacuum for comparison. In order to avoid adding EDTA into the solution, all the glassware used was rinsed with a solution of EDTA (0.1 M) to remove the presence of metal ions. Figure 3.7 shows a comparison of the data obtained using these conditions.

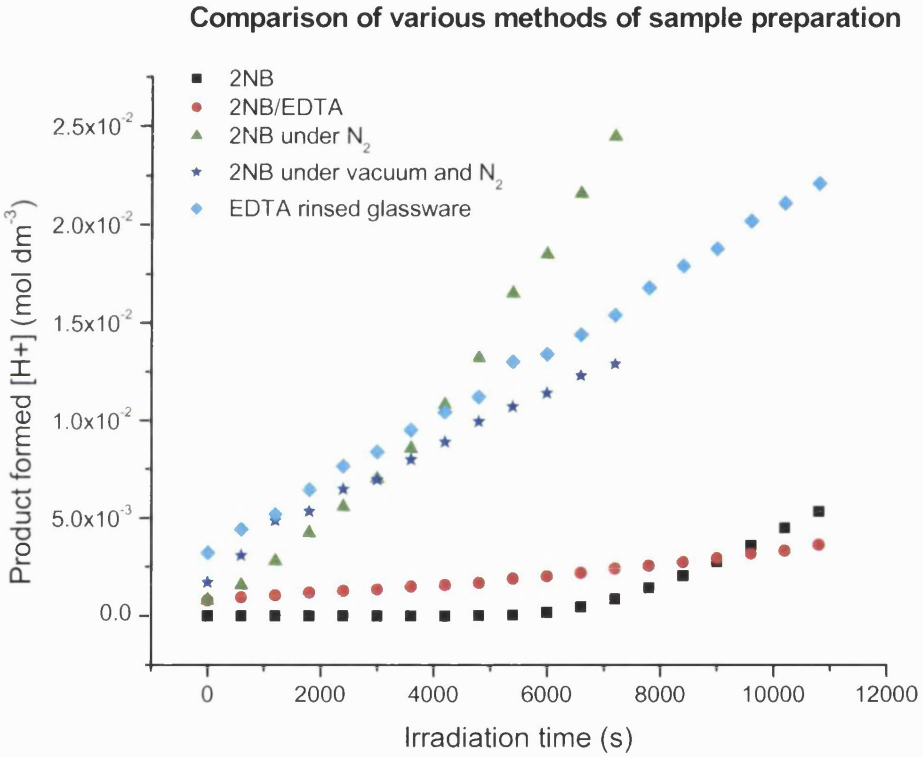

Fig. 3.7: Comparison of the changes in pH using different methods of 2NB solution preparation at 240 W

In general, changing the conditions of solution preparation changed the rate of photolysis considerably. The data showed that the initial lag phase was no longer present in solution suggesting 2NB is sensitive to its method of preparation. Moreover, the continuous flow of N_2 (g) caused a turbid and viscous solution to form as the sample precipitated out of solution and it was noted that the solution became more acidic upon irradiation. This was observed after approx. 30 min of irradiation.

The data indicate that the photodegradation of 2NB may not follow a simple reaction scheme as that shown in Fig. 3.1, which considers the photorearrangement of 2NB into 2NBA as an irreversible process with no side-reactions occurring. However, several investigators in recent years have suggested otherwise and different types of reaction processes have been proposed.[39-41] Using analytical techniques such as Electron Spin Resonance (ESR)[40] and Femtosecond Vibrational Spectrosopy[41] it has been postulated that the formation of mixed radicals, during the photochemical process, result in parallel or secondary reactions occuring simultaneously with the photoisomerisation of 2NB into 2NBA. The extent to which the reactions occur is governed by the type of light source, experimental design and set-up, conditions of sample preparation, intensity of light, etc, and so all these factors will influence the rate and extent of any photodegradation process. Usually, there are two stages involved in a photochemical reaction. These are; a primary reaction that occurs as a direct consequence of photon absorption, and thus involves the excited state of molecules; the primary reaction will then often be followed by secondary (thermal) reactions occurring from intermediate products produced by primary processes (radicals, radical ions, etc). Such intermediates can eventually react through 'dark' reactions to form final, stable products. The light intensity will influence the extent to which the photodegradation occurs i.e., at a high intensity level, secondary reactions may readily occur, but this may not necessarily be the case at low intensity levels as it would take longer for the reaction to reach a secondary stage and thus this will not be detected during the observed irradiation period. Since an exhaustive study of the photodegradation of 2NB was not the main objective of this project, further work was not conducted. However, it is simply noted that there appears to be complexity in the photochemical reaction of 2NB and shows sensitivity to non-photochemical processes which can limit its use as a chemical actinometer particularly for use with high intensity xenon arc light sources. For its purpose of use in this work, it is important to note that care must be taken during preparation/handling and use of 2NB.

The next stage was then to study the response of the photolysis of 2NB in the photocalorimeter.

3.2.4.3 Photocalorimetry of 2NB using Xe lamp

The photodegradation of 2NB is known to follow zero-order kinetics, thus, in the calorimeter typically a zero-order output will yield a constant deflection i.e. a horizontal line parallel to zero. Isothermal Microcalorimetric techniques are non-discriminating and hence follow the progress of a reaction by recording the time-dependent heat output for *all* reactions that occur. Therefore, if an additional event, other than photodegradation, is occurring then this would clearly impact on the measured response in the photocalorimeter.

Figure 3.8 is typical of the response obtained from the photocalorimeter as 2NB (freshly prepared sample) was irradiated. It can be seen that the photocalorimeter is sensitive to photodegradation of 2NB and that the magnitude of the signal is much greater than the baseline response. Ideally, a zero-order response was expected, but it can be seen clearly that was not observed and a distinct initial non-zero order like behaviour was extended for ca. 5 hours following the start of irradiation (circled in red in Fig. 3.4). Thereafter the calorimetric data settled to a zero-order deflection.

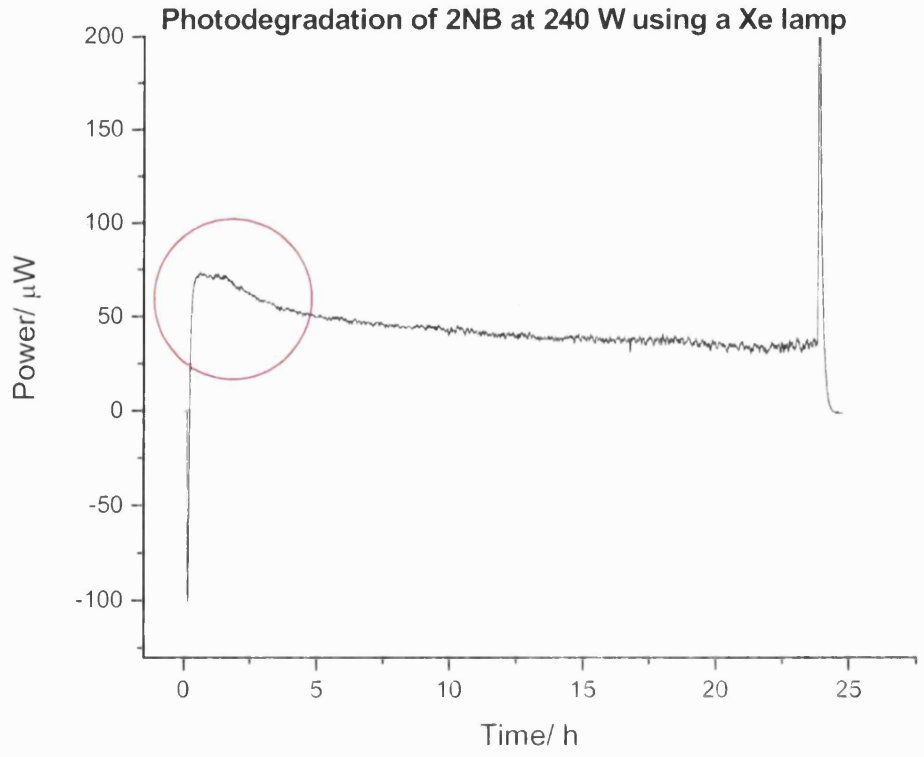

Figure 3.8: Power-time data for the photodegradation of 2NB at 240 W

These data suggest that an oxidation event is the likely cause for the non-zero-order region observed in the calorimeter. This discrepancy is also consistent with the pH data obtained and suggests that an oxidation event was the most likely cause of the pseudo-zero-order kinetic behaviour observed in the TAM.[42]

The calorimetric experiment was repeated with the inclusion of EDTA to see if it produced a notably different response, as noted in the pH data. Figure 3.8 shows a comparison of the data obtained for the photodegradation of 2NB in the presence and absence of EDTA. The data represented in red in Figure 3.9 are typical of the response obtained from the photocalorimeter when EDTA was added to the actinometric solution.

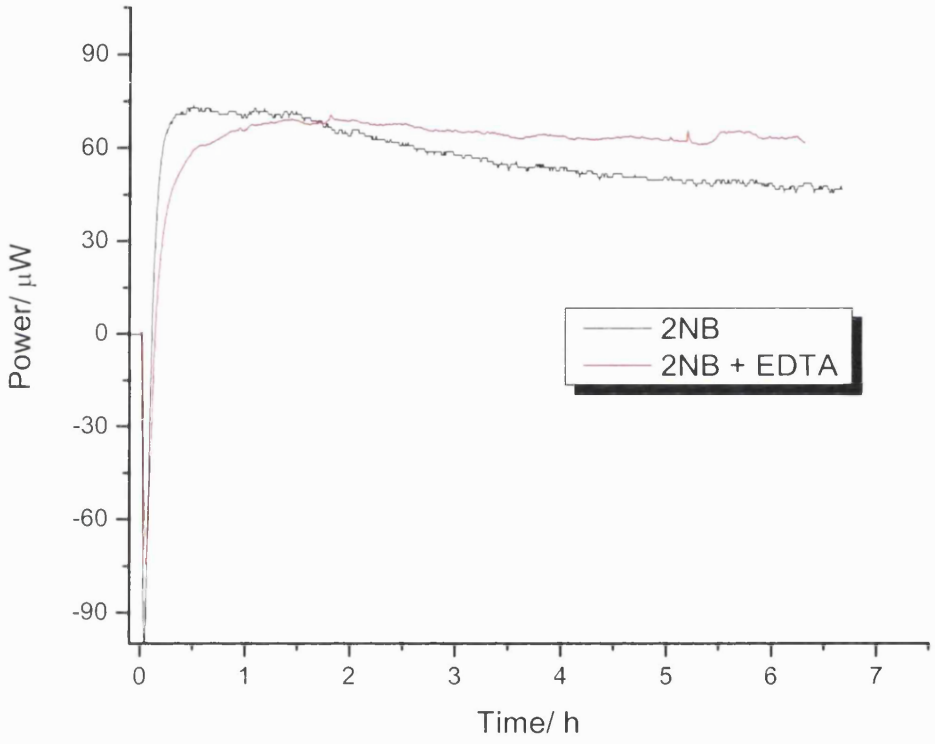

Figure 3.9: Comparison of power-time data for the photodegradation of 2NB (showing non-zero-order behaviour) and the photodegradation of 2NB with the addition of EDTA

Clearly, the presence of EDTA in solution has made a significant impact on the calorimetric output. The reaction shows a steady deflection from zero in the calorimeter and does not display an initial non-zero-order region that had been observed previously in the absence of EDTA (Fig. 3.8) indicating the oxidation process was inhibited. These data are consistent with the pH data obtained with the disappearance of the "lag phase"

(observed with 2NB alone) when EDTA was added to the solution. The signal with EDTA settled to give a stable deflection of ca. 67 μW, although there is a slow drift in the signal to ca. 63 μW after about 4 hrs of irradiation (Fig. 3.9). This is also consistent with the small variation noted in the pH measurements containing EDTA. Repeat measurements (Fig. 3.10) showed a similar response, although, Run 3 in particular showed a larger drift than those for the first two experiments suggesting the reaction may still not be truly zero order. There are a number of factors that could cause the signal to drift such as complexity in the reaction mechanism, random noise caused by small thermal fluctuations within solutions, long-term changes in the baseline as a result of environmental temperature changes, and uncertainties in the variation of the photon energies produced from the polychromatic photon source (xenon arc). It is estimated that the output from xenon arc lamps can fluctuate as much as 20% over a period of 5 or 6 hours.[32] These factors, therefore, can profoundly affect the output of a sensitive TAM and can introduce limits to the reproducibility of the measurements.

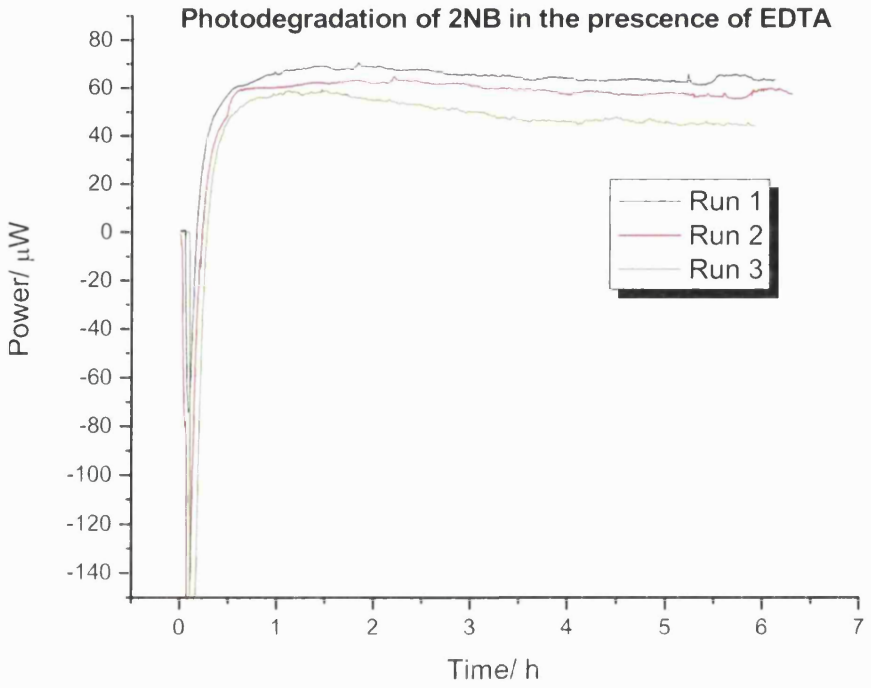

Figure 3.10: Power-time data for the photodegradation of 2NB in the presence of EDTA

Generally, the data have demonstrated that 2NB has sensitivity to non-photochemical processes. With the inclusion of EDTA, the initial oxidation process exhibited within the first 5 hours of irradiation appears to be inhibited, although there does still appear to be some sensitivity shown towards either non-photochemical processes and/or factors related to instrumental performance (such as those mentioned above). Under such circumstances it became difficult to quantify accurately the "light dose" delivered to the sample. Because of the oxidation event, it was not possible to determine the photon flux for the photolysis of 2NB alone, but using the 2NB and EDTA data above (Fig. 3.10), the photon flux can be estimated. These results are given in section 3.4 where the photon flux data for all the light sources used are compared.

Furthermore, as mentioned in Chapter 2 (section 2.2.4), over the course of the measurements, there was a gradual decline in the performance of the lamp which made it difficult to obtain reproducible experimental measurements (Fig. 2.34 and further explained in section 3.3.1.2). This then led on to the development of an alternative system where the use of Light-Emitting Diodes was investigated as an alternative photon source.

3.2.5 Results and Discussion using LED Mark III Photocalorimeter

Much of the initial actinometry work, prior to the construction of the custom-made array of LEDs used in the final set-up, was conducted using a single Ultra-bright UV LED (10,000 mcd). This was done in order to test proof-of-concept i.e., to assess if the intensity of light generated from a LED was sufficient enough to produce a detectable power signal during a photochemical reaction. As the instrumental development work progressed, the single LED was replaced with an array and subsequently actinometry work was repeated using the LED array system. The set-up of both these systems has already been detailed in Chapter 2.

This section details the chemical actinometry work undertaken using, firstly, the single LED system and subsequently the LED array photocalorimeter. The photodegradation of 2NB was followed for both the systems where a "light dose" delivered to the sample was determined across 370 – 410 nm and 350 – 700 nm using the single LED system and LED array system, respectively.

3.2.5.1 Preliminary Tests - Application of a single LED system

In order to quantify the photon flux between using the single LED system, the same principles and sequence of steps were followed as already described above (section 3.2.2). The first step was to determine a rate constant for the photodegradation of 2NB, then by applying it to the calorimetric output the irradiance and photon flux can be readily determined.

The photon flux was determined using the photodegradation of 2NB at 3 different voltages; 10 V, 15 V, and 20 V. The rate constants were obtained by following the pH changes at each input voltage. The process was then monitored in the photocalorimeter and it was hoped that there would be a direct correlation between increasing voltage and the power output of the photodegradation of 2NB.

The methods followed have already been described (section 3.2.3).

3.2.5.1.1 Evaluation of *k* by pH measurements

Figure 3.11 shows pH-time profiles for the photodegradation of 2NB at 10, 15 and 20 V. A linear relationship between the amount of product formed and the irradiation time is observed. It can be seen that in this system, a lag phase is not observed in the first 100 min of irradiation as in the case with the Xe lamp photocalorimeter. Xe lamps are extremely powerful, far more intense than LEDs and, hence, it is thought that at such intensity it may be the case that additional reactions (to photodegradation) are occurring. There is already some evidence in the literature of multiple (parallel or simultaneous) reactions occurring as a result of mixed radicals. It may be the case that the Xe lamp is producing intensity that is far in excess of that required to form 2NBA alone and as a result initiating further reactions. It may be the case that the reaction may not proceed this far with a single LED as the light intensity is far less. This may be why a lag phase is observed within the first 100 min of exposure using a Xe lamp and not with the LED system.

Table 3.4: The amount of product formed using a single LED

Irradiation time (min)	Amount of product formed [H^+] (mol dm^3)		
	10 V	**15 V**	**20 V**
10	3.76×10^{-3}	4.76×10^{-3}	5.22×10^{-3}
20	5.43×10^{-3}	6.48×10^{-3}	7.21×10^{-3}
30	5.95×10^{-3}	8.15×10^{-3}	8.67×10^{-3}
40	6.48×10^{-3}	9.88×10^{-3}	1.04×10^{-2}
50	6.48×10^{-3}	1.10×10^{-2}	1.14×10^{-2}
60	7.10×10^{-3}	1.22×10^{-2}	1.41×10^{-2}
70	7.73×10^{-3}	1.30×10^{-2}	1.47×10^{-2}
80	8.47×10^{-3}	1.45×10^{-2}	1.61×10^{-2}
90	9.15×10^{-3}	1.58×10^{-2}	1.65×10^{-2}
100	9.98×10^{-3}	1.69×10^{-2}	1.77×10^{-2}
110	1.08×10^{-2}	1.80×10^{-2}	2.03×10^{-2}
120	1.12×10^{-2}	1.93×10^{-2}	2.13×10^{-2}
130	1.18×10^{-2}	2.08×10^{-2}	2.18×10^{-2}
140	1.22×10^{-2}	2.08×10^{-2}	2.28×10^{-2}
150	1.26×10^{-2}	2.18×10^{-2}	2.33×10^{-2}
160	1.29×10^{-2}	2.30×10^{-2}	2.50×10^{-2}
170	1.32×10^{-2}	2.41×10^{-2}	2.50×10^{-2}
180	1.35×10^{-2}	2.50×10^{-2}	2.62×10^{-2}

The slope of the plots determined the following rate constants; **9.2×10^{-7}, 2.1×10^{-6}, and 2.2×10^{-6} mol dm^3 s^{-1} at 10, 15, and 20 V, respectively** (Fig. 3.11). As expected, the rate of reaction is faster as the voltage input is increased.

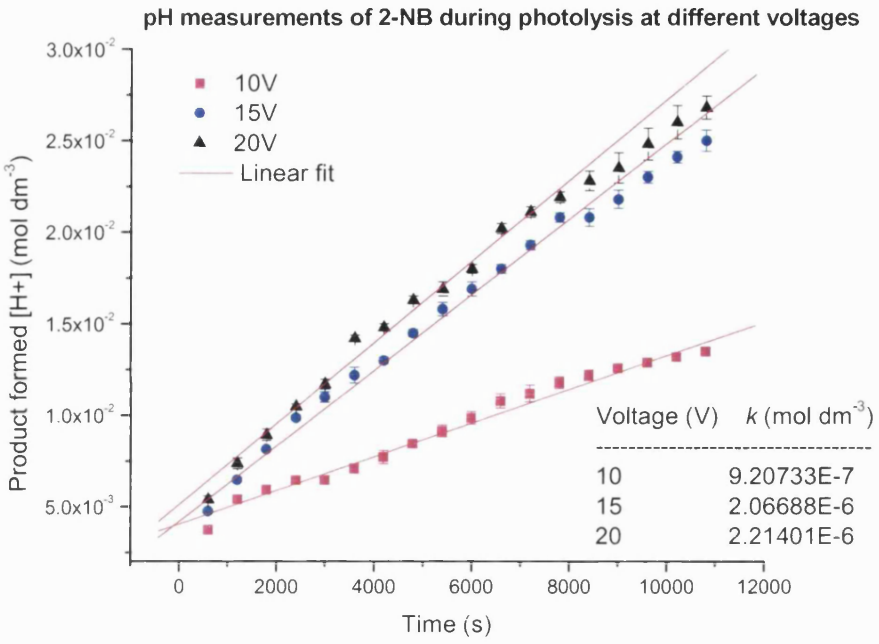

Figure 3.11: Comparison of pH-time profiles at different voltage inputs

3.2.5.1.2 Photocalorimetry of 2NB using a single LED light source

Typical power *vs* time traces obtained for the photodegradation of 2NB at 10, 15, and 20 V are represented in Figure 3.12 – 3.14.

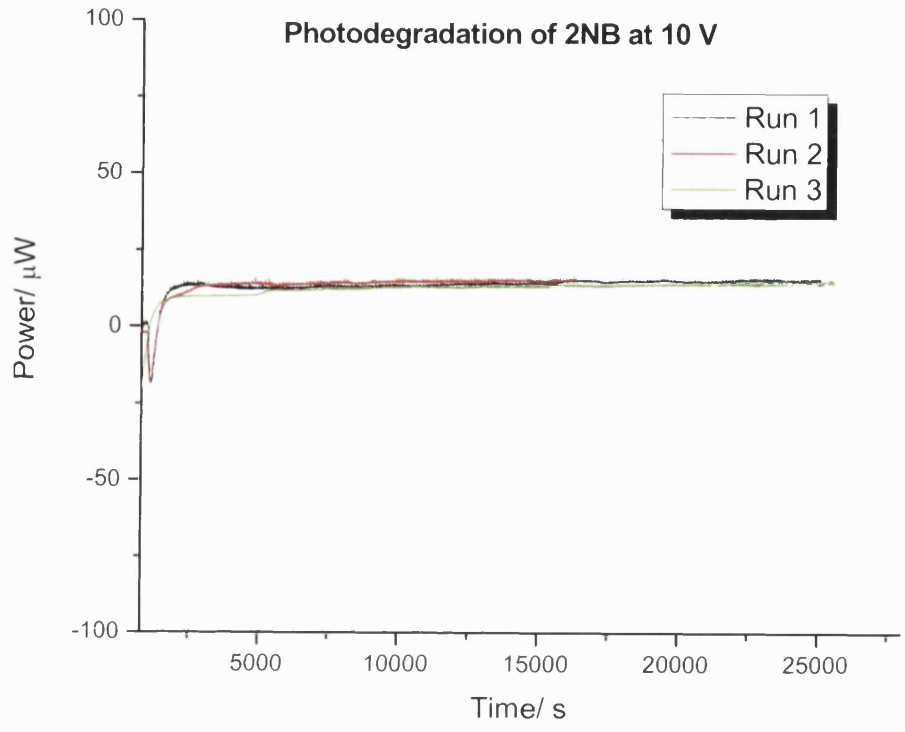

Figure 3.12: Power-time plots of 2NB photolysis at 10 V

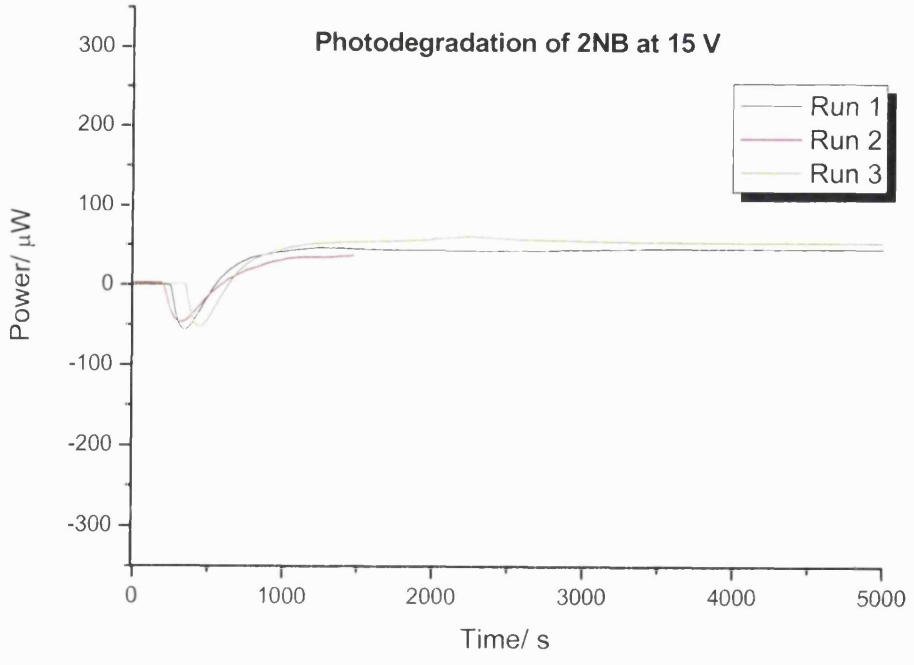

Figure 3.13: Power-time plots of 2NB photolysis at 15 V

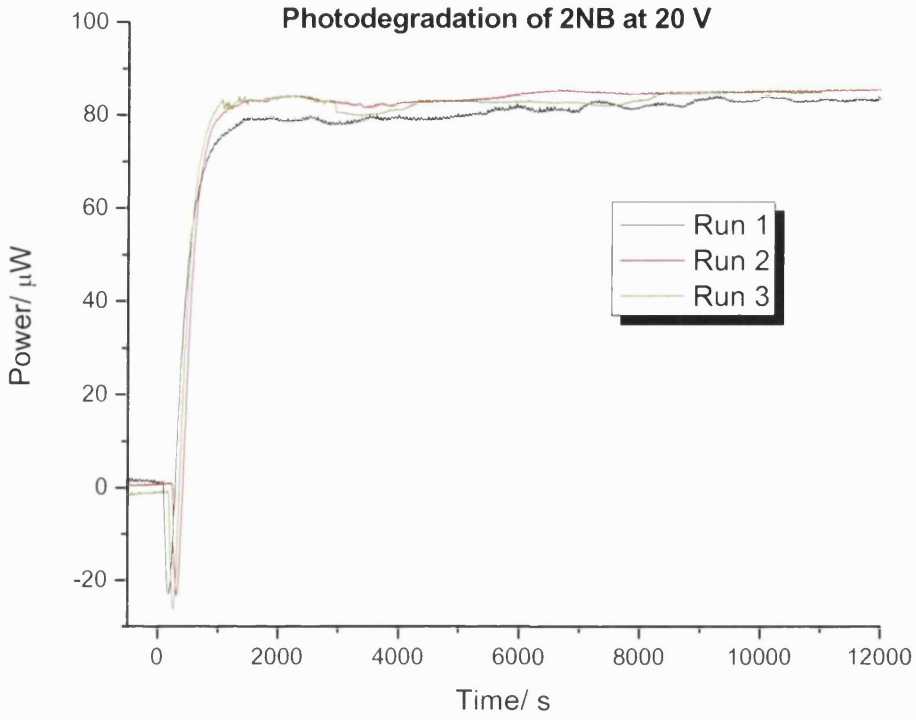

Figure 3.14: Power-time plots of 2NB photolysis at 20 V

The power outputs obtained for all measurements are summarised in Table 3.5.

Table 3.5: Power output and rate constants obtained at different voltages

Voltage (V)	Power Output (µW)				
	1	2	3	Mean ± SD	%RSD
10	12.5	12.1	12.0	12.2 ± 0.3	2.5
15	45.0	47.7	48.0	46.9 ± 1.6	3.4
20	86.0	85.8	84.5	85.5 ± 0.8	0.9

Figure 3.15 shows an overall comparison of the power-time curves at the 3 voltages studied.

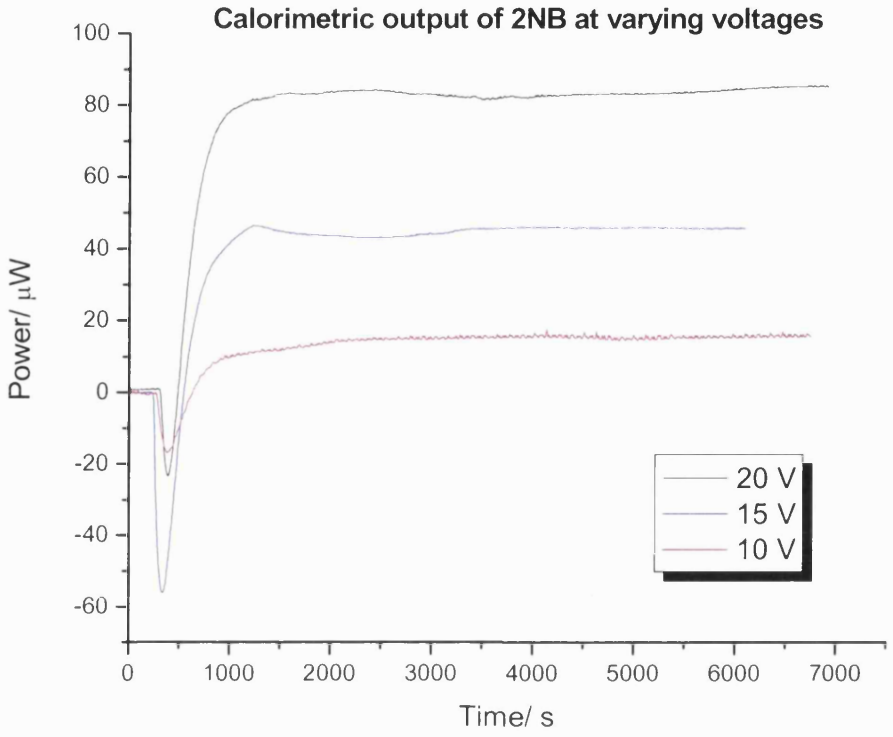

Figure 3.15: Comparison of power-time curves at 10, 15 and 20 V during 2NB photolysis

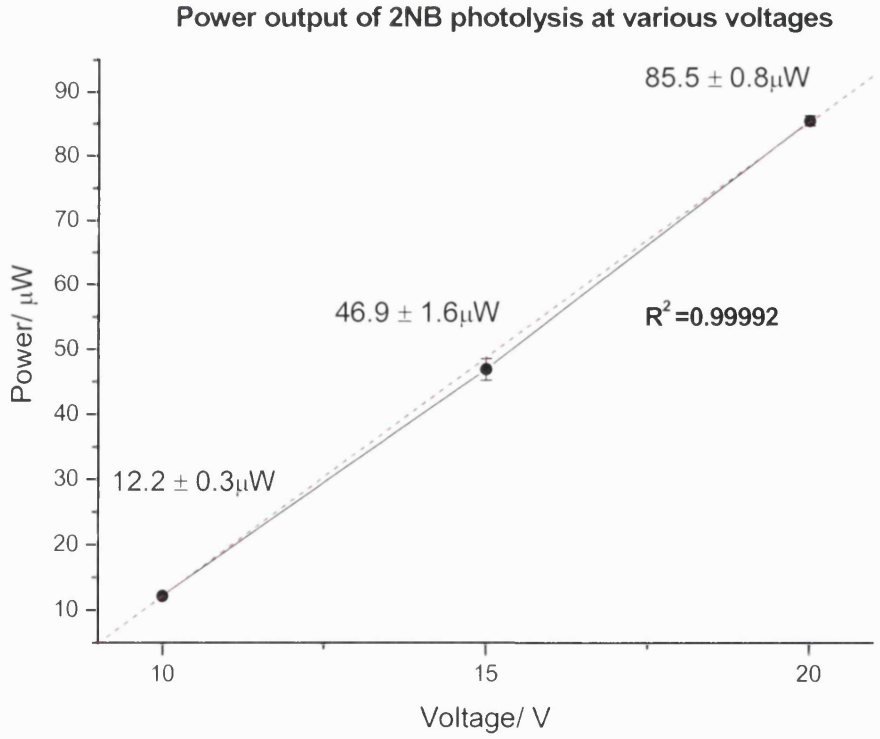

Figure 3.16: Effect of increasing LED voltage on power output of TAM

The data obtained are extremely encouraging. The first thing to note is that the outputs show a constant deflection from zero in the calorimeter, evidence for zero-order kinetics. Secondly, the voltage inputted to the system is directly proportional to the power output of the TAM. The higher the voltage, the larger the number of moles that react within the actinometer solution, and hence, the greater the power output in the TAM. The relationship between the power output and voltage input is represented in Figure 3.16 where measurements performed at 10 V, 15 V, and 20 V showed that the heat output from the photolysis of 2NB increased in proportion to the increase in voltage supplied to the light source.

Generally, it can be seen that heat output is constant over the period of irradiation using the LEDs and the photoreaction does not exhibit the difficulties that were experienced with the xenon arc lamp. The intensity of the Xe arc lamp is very powerful compared to the LEDs and it may be likely that the pseudo-zero order behaviour observed with 2NB using the xenon lamp was caused as a result of additional reactions occurring in the solution. Moreover, another possible reason for this non-zero order behaviour could be overheating of the sample caused by the high heat output generated by xenon arc lamps, and this also may lead to thermal decomposition processes that will complicate the issue.

The above initial tests demonstrate that the system responds as hoped and, more importantly, shows that LEDs have much potential in application to pharmaceutical photostability testing.

3.2.5.1.3 Determination of ΔH and application to obtain k – single LED

Given the values of k from the pH data and outputs (Φ) from the calorimeter, the enthalpy of reaction (ΔH) can be determined using the zero-order calorimetric equation:

$$\Phi = k\Delta HV \qquad \text{(Eqn. 3.1)}$$

Taking the measured response of the first experiment at each voltage only, ΔH was calculated by a simple re-arrangement of Equation 3.1:

$$\Delta H = \frac{\Phi}{kV} \qquad \text{Eqn. 3.1.1}$$

The calculated values of ΔH are given in Table 3.6. It can be seen from the data, that the values for ΔH at 10, 15 and 20 V are not constant. According to Hess' law, the ΔH of a reaction should remain constant regardless of the reaction mechanism by which the chemical reaction occurs providing the products remain the same and the initial and final concentration remains constant. If these conditions are met then ΔH of the process should remain constant as a function of voltage input. This is not the case, as observed from the data obtained. The value of ΔH increases in succession to the increase of voltage supplied to the LEDs i.e., the values of ΔH at 10, 15 and 20 V were determined as 3533, 5625, and 9773 J/mol. This indicates that the different reactions are occurring during the photodegradation of 2NB and further suggests that there is complexity within the photochemical process as already observed when using the Xe arc lamp. This also supports claims of complexity within the reaction as highlighted by others.[40,41] This limits the use of 2NB as a chemical actinometer for application in photocalorimetry since complexity in a reaction renders data analysis challenging.

The value of ΔH in each case was kept constant at a given voltage and applied to calculate a value of k for all subsequent 2NB experiments conducted where it is assumed there is no prior knowledge of the rate constant. Re-arranging Equation 3.1 to yield k gives;

$$k = \frac{\Phi}{\Delta HV} \qquad \text{Eqn. 3.1.2}$$

The calculated values for k are summarised for each measurement in Table 3.7.

Table 3.6: Thermo-kinetic parameters obtained from 2NB photolysis

Voltage (V)	Φ (W)	ΔH (J mol^{-1})	V (dm^3)	k (mol dm^{-3} s^{-1})*
10	13 x 10^{-6}	3533	0.004	9.2 x 10^{-7}
15	45 x 10^{-6}	5625	0.004	2.1 x 10^{-6}
20	86 x 10^{-6}	9773	0.004	2.2 x 10^{-6}

**** All values of k in Table 3.6 were obtained from slope of pH-time profiles***

Table 3.7: Calculated rate constants with applied ΔH

Experiment	k (mol dm^{-3} s^{-1})		
	10 V	**15 V**	**20 V**
1	9.2×10^{-7}	2.0×10^{-6}	2.2×10^{-6}
2	8.5×10^{-7}	2.1×10^{-6}	2.2×10^{-6}
3	8.5×10^{-7}	2.1×10^{-6}	2.2×10^{-6}
Mean	$\mathbf{8.7 \times 10^{-7}}$	$\mathbf{2.1 \times 10^{-6}}$	$\mathbf{2.2 \times 10^{-6}}$
± SD	$\mathbf{4.0 \times 10^{-8}}$	$\mathbf{5.8 \times 10^{-8}}$	**0**
% RSD	**4.6**	**2.8**	**0**

3.2.5.1.4 Determination of irradiance and photon flux – single LED

Applying these values of k to Equations 3.2 and 3.3, the irradiance and photon flux can be readily determined. The values obtained were calculated using Mathcad©.

The weighted-average photon energy incident upon the actinometer solution was determined using Equation 3.5. In order to determine the weighted-average wavelength of light, Equation 3.6 was modified to cover a wavelength range of 370 – 400 nm (Eqn. 3.6.1). The corresponding irradiance data used to calculate this was obtained using a spectroradiometer (further explained in section 3.3). These data are shown in Table 3.8 below.

Table 3.8: Irradiance data for a single UV LED across 370 – 400 nm

Wavelength (nm)	Intensity ($\mu W/cm^2$)	Wavelength (nm)	Intensity ($\mu W/cm^2$)
370.12	0.39	385.40	9.04
370.71	0.45	385.99	10.54
371.30	0.48	386.58	12.28
371.88	0.50	387.17	14.45
372.47	0.54	387.75	16.61
373.06	0.58	388.34	19.30
373.65	0.63	388.93	21.96
374.24	0.67	389.52	25.08
374.83	0.73	390.10	29.07
375.41	0.82	390.69	33.04
376.00	0.93	391.28	37.50
376.59	1.04	391.86	41.41
377.18	1.19	392.45	46.00
377.77	1.36	393.04	51.61
378.35	1.54	393.63	55.94
378.94	1.75	394.21	60.39
379.53	1.99	394.80	63.43
380.12	2.32	395.39	65.11
380.70	2.75	395.97	67.07
381.29	3.19	396.56	68.21
381.88	3.74	397.15	66.87
382.47	4.28	397.73	66.04
383.05	5.01	398.32	64.90
383.64	5.80	398.91	62.41
384.23	6.71	399.49	58.46
384.82	7.77	400.08	53.30

By applying the spectroradiometric data from Table 3.8 to Equation 3.6.1, the weighted-average value for photon wavelength obtained across 370 – 400 nm was determined as **394nm.**

$$\frac{\sum_{370\ nm}^{400\ nm} (\lambda\ nm)\ (\text{irradiance } Wm^{-2})}{\sum_{370\ nm}^{400\ nm} \text{irradiance } Wm^{-2}} \qquad \text{(Eqn. 3.6.1)}$$

The energy of the 394 nm photon is then readily computed by, firstly, expressing the 394 nm weighted-average wavelength in meters;

$$394 \text{ nm} \left(\frac{1 \text{ m}}{1 \text{ x } 10^{9} \text{ nm}} \right) = 3.94 \text{ x } 10^{-7} \text{ m}$$

Then, applying the data to Eqn. 3.5, gives an average photon energy of **5.03 x 10^{-19} J.**

$$E = \frac{hc}{\lambda} = \frac{\left(6.63 \text{ x } 10^{-34} \text{ Js}^{-1}\right)\left(2.99 \text{ x } 10^{8} \text{ ms}^{-1}\right)}{3.94 \text{ x } 10^{-7} \text{ m}} = 5.03 \text{ x } 10^{-19} \text{ J}$$

Therefore, on average a photon delivers 5.03 x 10^{-19} J of energy to the actinometric solution where it is assumed that all photons in the range of 370 – 400 nm convert 2NB to 2NBA with equivalent efficiency.

The Irradiance (I_o) and Photon Flux (F_o) data as determined by Mathcad© are outlined in the worksheets printed below and all data is summarised in Table 3.9.

Irradiance and Photon Flux Calculations of a single UV LED

The following steps were used to calculate the irradiance and photon flux at 10, 15, and 20 V across 370 - 400 nm

Step 1: All parameters required are entered into Mathcad as follows;

Values of *k* obatined at 10, 15 and 20 V will be known as ; k1, k2 and k3, respectively.

10 V $k1a := 9.2 \cdot 10^{-7}$ $k1b := 8.5 \cdot 10^{-7}$ $k1c := 8.5 \cdot 10^{-7}$

15 V $k2a := 2.0 \cdot 10^{-6}$ $k2b := 2.1 \cdot 10^{-6}$ $k2c := 2.1 \cdot 10^{-6}$

20 V $k3a := 2.2 \cdot 10^{-6}$ $k3b := 2.2 \cdot 10^{-6}$ $k3c := 2.2 \cdot 10^{-6}$

Quantum yield of 2-nitrobenzaldehyde will be known as Q.

$$Q := 0.5$$

Step 2: The irradiance (i) for each experiment is calculated by [Equation 3.2];

10 V $i1a := \frac{k1a}{Q}$ $i1b := \frac{k1b}{Q}$ $i1c := \frac{k1c}{Q}$

$$\frac{k1a}{Q} = 1.84 \times 10^{-6} \qquad \frac{k1b}{Q} = 1.7 \times 10^{-6} \qquad \frac{k1c}{Q} = 1.7 \times 10^{-6}$$

$$\frac{\left(\frac{k1a + k1b + k1c}{3}\right)}{0.5} = 1.747 \times 10^{-6}$$

15 V $i2a := \frac{k2a}{Q}$ $i2b := \frac{k2b}{Q}$ $i2c := \frac{k2c}{Q}$

$$\frac{k2a}{Q} = 4 \times 10^{-6} \qquad \frac{k2b}{Q} = 4.2 \times 10^{-6} \qquad \frac{k2c}{Q} = 4.2 \times 10^{-6}$$

$$\frac{\left(\frac{k2a + k2b + k2c}{3}\right)}{0.5} = 4.133 \times 10^{-6}$$

20 V $i3a := \frac{k3a}{Q}$ $i3b := \frac{k3b}{Q}$ $i3c := \frac{k3c}{Q}$

$$\frac{k3a}{Q} = 4.4 \times 10^{-6} \qquad \frac{k3b}{Q} = 4.4 \times 10^{-6} \qquad \frac{k3c}{Q} = 4.4 \times 10^{-6}$$

$$\frac{\left(\frac{k3a + k3b + k3c}{3}\right)}{0.5} = 4.4 \times 10^{-6}$$

Step 3: The energy of the photon (e) can be described by Planck's constant (h), the speed of light (c) and the weighted-average photon wavelength (l) [Equation 3.5];

$h := 6.63 \cdot 10^{-34}$ $c := 2.99 \cdot 10^{8}$ $l := 3.94 \cdot 10^{-7}$

$e := \frac{(h \cdot c)}{l}$ $\boxed{e := 5.03 \cdot 10^{-19}}$

Step 4: Finally, the determination the Photon Flux (f) of each experiment requires the following parameters;

Irradiance (i), Weighted-average photon energy (e), Volume of actinometric solution (v), Avogadro's number (n), cross-sectional area of ampolue base (a) [Equation 3.3];

$v := 0.004$ $n := 6.02 \cdot 10^{23}$ $a := 4.56 \cdot 10^{-4}$

10 V $\frac{i1a \cdot e \cdot v \cdot n}{a} = 4.887$ $\frac{i1b \cdot e \cdot v \cdot n}{a} = 4.516$ $\frac{i1c \cdot e \cdot v \cdot n}{a} = 4.516$

$f1a := 4.89$ $f1b := 4.52$ $f1c := 4.52$

$\boxed{\frac{f1a + f1b + f1c}{3} = 4.643}$

15 V $\frac{i2a \cdot e \cdot v \cdot n}{a} = 10.625$ $\frac{i2b \cdot e \cdot v \cdot n}{a} = 11.156$ $\frac{i2c \cdot e \cdot v \cdot n}{a} = 11.156$

$f2a := 10.63$ $f2b := 11.16$ $f2c := 11.16$

$\boxed{\frac{f2a + f2b + f2c}{3} = 10.983}$

20 V $\frac{i3a \cdot e \cdot v \cdot n}{a} = 11.687$ $\frac{i3b \cdot e \cdot v \cdot n}{a} = 11.687$ $\frac{i3c \cdot e \cdot v \cdot n}{a} = 11.687$

$f3a := 11.69$ $f3b := 11.69$ $f3c := 11.69$

$\boxed{\frac{f3a + f3b + f3c}{3} = 11.69}$

In summary, the irradiance (i) and photon flux (f) values calculated at each voltage are;

10 V	$i1 := 1.75 \cdot 10^{-6}$	$f1 := 4.64$
15 V	$i2 := 4.13 \cdot 10^{-6}$	$f2 := 10.98$
20 V	$i3 := 4.40 \cdot 10^{-6}$	$f3 := 11.69$

Table 3.9: Summary of Irradiance and Photon Flux data at each voltage

Experiment	10 V		15 V		20 V	
	I_0 (einstein dm^{-3} s^{-1})	F_0 (W/m^2)	I_0 (einstein dm^{-3} s^{-1})	F_0 (W/m^2)	I_0 (einstein dm^{-3} s^{-1})	F_0 (W/m^2)
1	1.84×10^{-6}	4.89	4.00×10^{-6}	10.63	4.40×10^{-6}	11.69
2	1.70×10^{-6}	4.52	4.20×10^{-6}	11.16	4.40×10^{-6}	11.69
3	1.70×10^{-6}	4.52	4.20×10^{-6}	11.16	4.40×10^{-6}	11.69
Mean	$\mathbf{1.75 \times 10^{-6}}$	**4.64**	$\mathbf{4.13 \times 10^{-6}}$	**10.98**	$\mathbf{4.40 \times 10^{-6}}$	**11.69**
± SD	$\mathbf{8.08 \times 10^{-8}}$	**0.21**	$\mathbf{5.8 \times 10^{-8}}$	**0.31**	**0**	**0**
% RSD	**4.6**	**4.6**	**2.8**	**2.8**	**0**	**0**

In general, the initial calorimetric response of the photodegradation of 2NB using an LED light source were promising and formed the basis of the development of an array system in order to assess photostability over a wider wavelength range. The many advantages, particularly the long life span, offered by LEDs appear to have had a profound effect on the reproducibility and the stability of the outputs thus allowing successful quantification of irradiance and photon flux.

Having established the values of irradiance and photon flux via chemical actinometry, the next stage was to compare the data with an alternative technique – Spectroradiometry (discussed further in sections 3.3 and 3.4).

3.2.5.2 Application of LED Array System

Having successfully applied a LED (single system) as a light source to test for photostability, the next step was to repeat the work using the LED array photocalorimeter. Here, the "light dose" using the 2NB actinometer solution was assessed across a wider wavelength range (350 – 700 nm) in the UV/VIS regions. The following work was performed only at 15 V because of time constraints.

The same procedure as that already described for the single LED system (section 3.2.5.1) was followed i.e., a rate constant (following the changes in pH for the

photodegradation 2NB) was established, then applied to the calorimetric output to determine the irradiance and photon flux.

3.2.5.2.1 Evaluation of *k* by pH measurements – LED Array

Table 3.10 below shows the data obtained for the LED array system by following the changes in the pH as the 2NB solution was irradiated.

Table 3.10: The amount of product formed using the array LED system at 15 V

Irradiation time (min)	Amount of product formed [H^+] (mol dm^3)				
	1	2	3	Mean	SD
10	1.81×10^{-3}	2.08×10^{-3}	2.08×10^{-3}	**1.99×10^{-3}**	**1.55×10^{-4}**
20	2.62×10^{-3}	3.01×10^{-3}	2.74×10^{-3}	**2.79×10^{-3}**	**1.98×10^{-4}**
30	3.01×10^{-3}	3.87×10^{-3}	3.15×10^{-3}	**3.34×10^{-3}**	**4.65×10^{-4}**
40	3.37×10^{-3}	4.15×10^{-3}	3.87×10^{-2}	**3.80×10^{-3}**	**3.94×10^{-4}**
50	4.25×10^{-3}	4.87×10^{-3}	4.25×10^{-3}	**4.46×10^{-3}**	**3.63×10^{-4}**
60	4.66×10^{-3}	5.22×10^{-3}	4.87×10^{-3}	**4.92×10^{-3}**	**2.86×10^{-4}**
70	5.47×10^{-3}	6.28×10^{-3}	5.60×10^{-3}	**5.78×10^{-3}**	**4.36×10^{-4}**
80	5.86×10^{-3}	6.73×10^{-3}	6.14×10^{-3}	**6.24×10^{-3}**	**4.44×10^{-4}**
90	6.58×10^{-3}	7.21×10^{-3}	6.43×10^{-3}	**6.74×10^{-3}**	**4.16×10^{-4}**
100	7.55×10^{-3}	8.47×10^{-3}	7.55×10^{-3}	**7.86×10^{-3}**	**5.32×10^{-4}**
110	8.28×10^{-3}	8.87×10^{-3}	7.91×10^{-3}	**8.35×10^{-3}**	**4.86×10^{-4}**
120	8.87×10^{-3}	9.50×10^{-3}	8.67×10^{-3}	**9.22×10^{-3}**	**3.22×10^{-4}**
130	9.29×10^{-3}	9.95×10^{-2}	9.29×10^{-3}	**9.73×10^{-3}**	**3.84×10^{-4}**
140	9.73×10^{-3}	1.04×10^{-2}	9.73×10^{-3}	**1.02×10^{-2}**	**4.02×10^{-4}**
150	1.02×10^{-2}	1.07×10^{-2}	1.07×10^{-2}	**1.07×10^{-2}**	**4.91×10^{-4}**
160	1.07×10^{-2}	1.12×10^{-2}	1.09×10^{-2}	**1.11×10^{-2}**	**3.88×10^{-4}**
170	1.14×10^{-2}	1.14×10^{-2}	1.17×10^{-2}	**1.16×10^{-2}**	**3.11×10^{-4}**
180	1.20×10^{-2}	1.25×10^{-3}	1.20×10^{-2}	**1.22×10^{-2}**	**2.82×10^{-4}**

The slope of the mean plot determined the rate constant as **$1.04 \times 10^{-6} \pm 3.56 \times 10^{-9}$ mol dm^{-3} s^{-1}** (Fig. 3.17). The value for *k* is in good agreement and within the same order of magnitude with the rate constant obtained for the single LED system at 15 V (cf. **$2.10 \times 10^{-6} \pm 5.80 \times 10^{-8}$ mol dm^{-3} s^{-1}**).

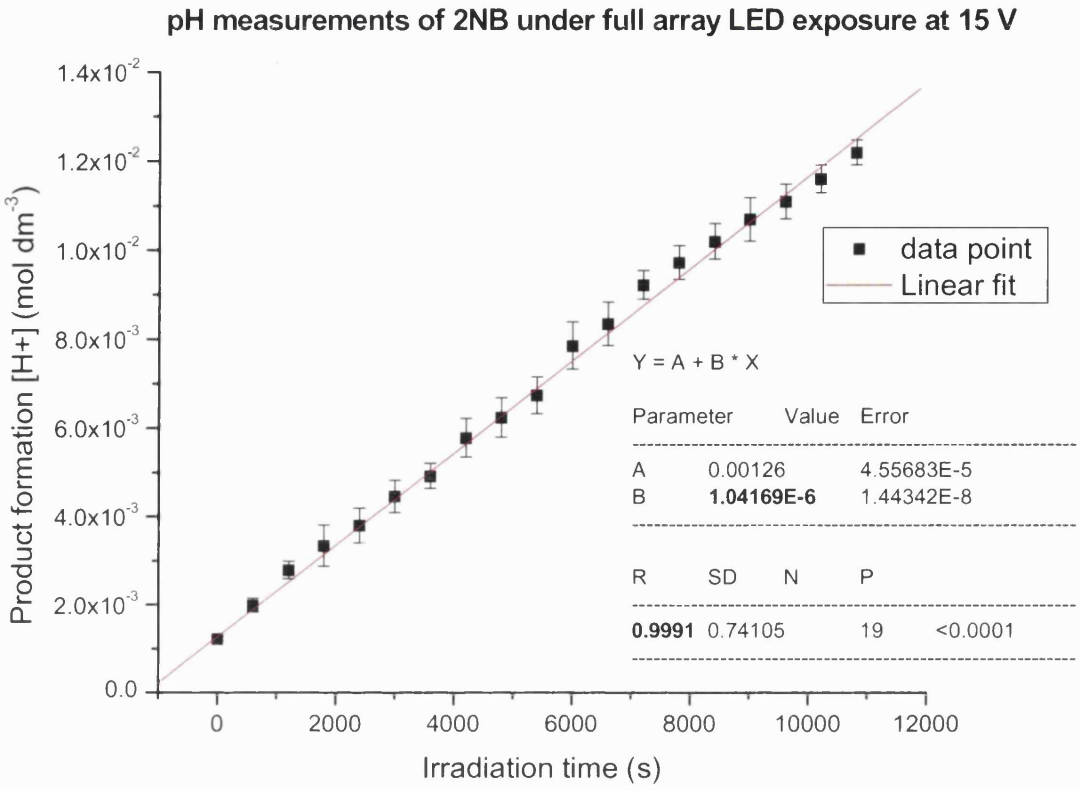

Figure 3.17: pH-time profile using LED array system

3.2.5.2.2 Photocalorimetry of 2NB using LED array system

The photodegradation of 2NB was monitored using the LED array photocalorimeter. Figure 3.18 is typical of the response observed over of period of about 5 hours of irradiation. During this period, a constant deflection from zero in the microcalorimeter is observed therefore showing the actinometer to follow zero-order kinetics. At an input of 15 V, the output response of the TAM is ca. 21.5 μW. This value was deduced from an average of data points over the irradiation period. The signal is very steady with only small fluctuations (± 1 μW).

In order to assess the repeatability of the signal under irradiation, the light was switched on and off a number of times for a defined period of 30 min each time. Since the photodegradation of 2NB follows zero order kinetics, the heat output should remain constant over the time period for which the sample is exposed to light and unchanged at the time intervals during the light on and off process. By performing a series of light

on/off tests in this manner, the total heat, Φ, given out by the reaction over the irradiation period can be calculated by integrating the area under the calorimetric curve from the start of irradiation (t_{on}) to the end of measurement (t_{end}). The measurable time frame of irradiation is defined as $t_{on} - t_{off} = t_{irr}$ i.e. the duration from where the light is switched on (t_{on}) to when it is switched off (t_{off}). The calorimetric data can be used to determine the heat output (Q in Joules) and total heat flow (Φ in Watts) during the photodegradation of 2NB.

Figure 3.19 is typical of the response obtained during a light on/off test of 2NB and illustrates the time points taken from which the Q and Φ can be calculated. Integrating the area under the curve from t_{on} to t_{end} gives the value for Q in Joules. Dividing Q by the irradiation period, t_{irr} (in seconds) determines the value for Φ in Js^{-1} (or Watts) for the photoreaction.

Integrating the cumulative area;

$$t_{on} - t_{end} = Q$$

Defining irradiation period;

$$t_{on} - t_{off} = t_{irr}$$

Therefore, the total heat flow is determined by;

$$\Phi = \frac{Q}{t_{irr}}$$

From the calorimetric outputs represented in Figures 3.20 – 3.22, the total heat flow was calculated by following the procedure given above. Three experiments were carried out and each measurement shows the response obtained as the sample was repeatedly (in triplicate) exposed/not exposed to irradiation for a period of approx. 30 min. The heat flow for each light on/off test was determined using the above calculation method. The deflection of the power output was also measured by taking an average of the data points after the signal had settled and compared to that of the calculated output. The data for each experiment are summarised in Tables 3.11 – 3.14 where the heat flow using the calculated method and an average of the data points from the calorimetric plot are defined as Φ calc and Φ average, respectively.

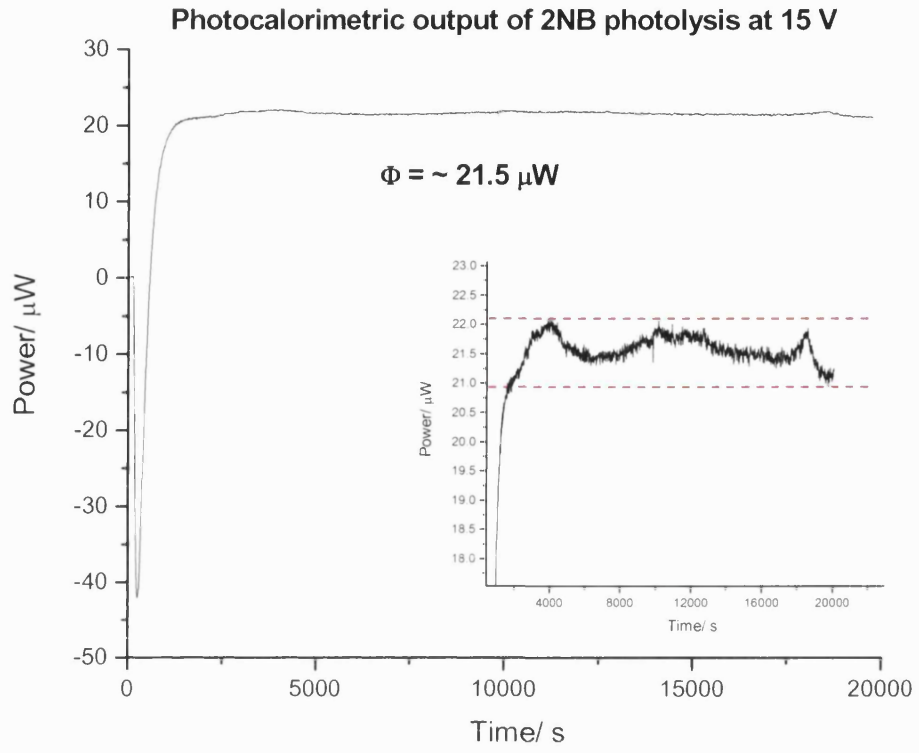

Figure 3.18: Zero order response of 2NB photodegradation at 15 V

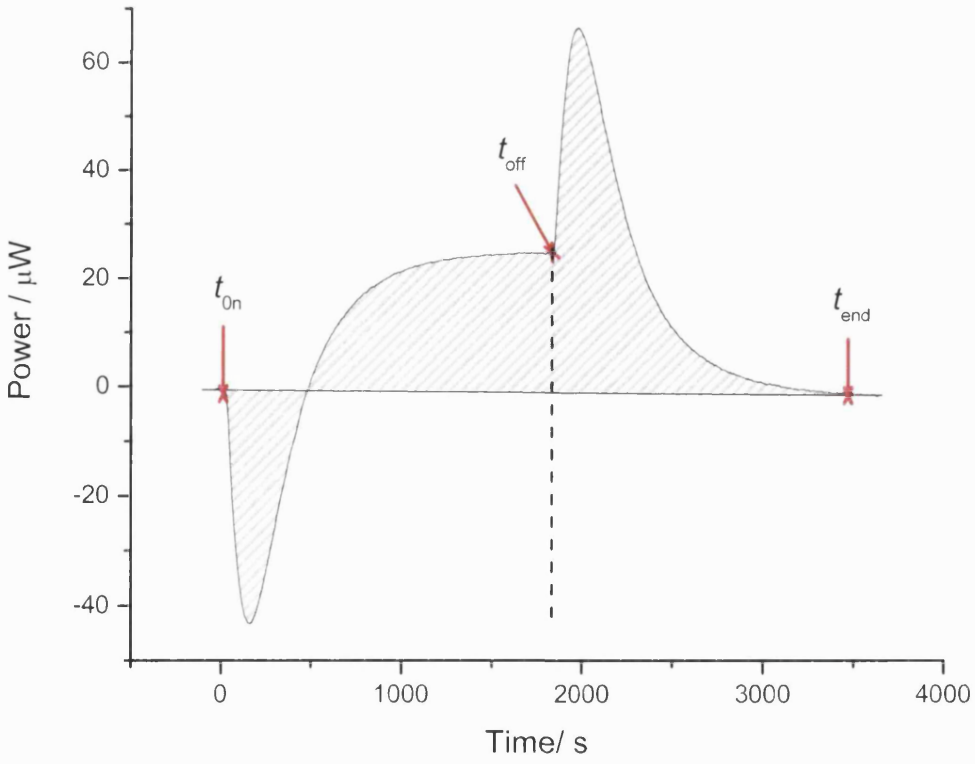

Figure 3.19: Example of a typical photocalorimetric output of 2NB during a light on/off test. ***The shaded region represents the integrated area under the calorimetric curve used to calculate the total heat flow (Φ). T_{on}=light on, t_{off} = light off, t_{end} = end of measurement.***

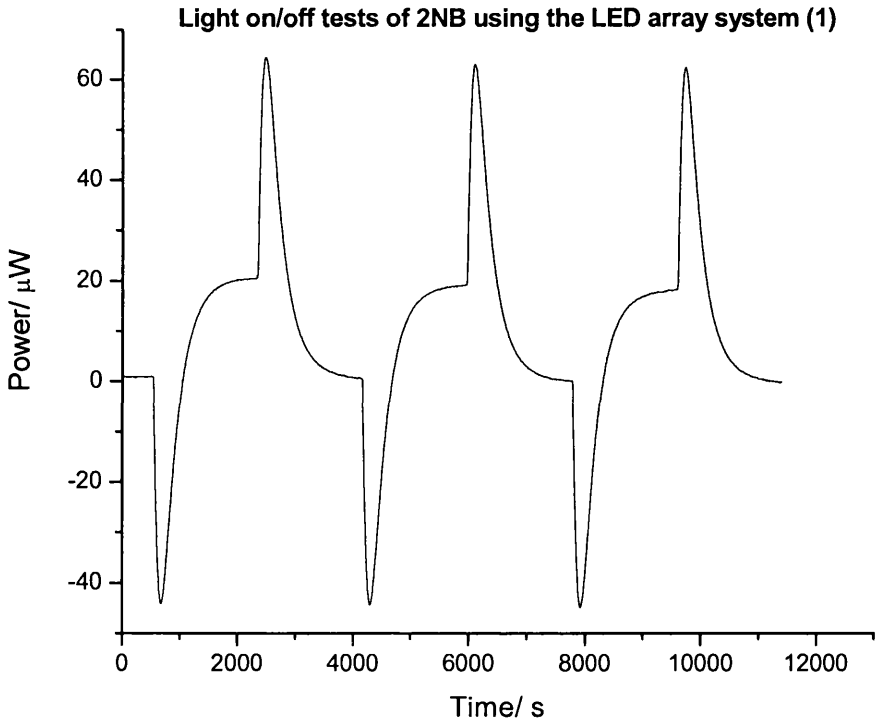

Figure 3.20: LED array photocalorimetric output of 2NB at 15 V (1)

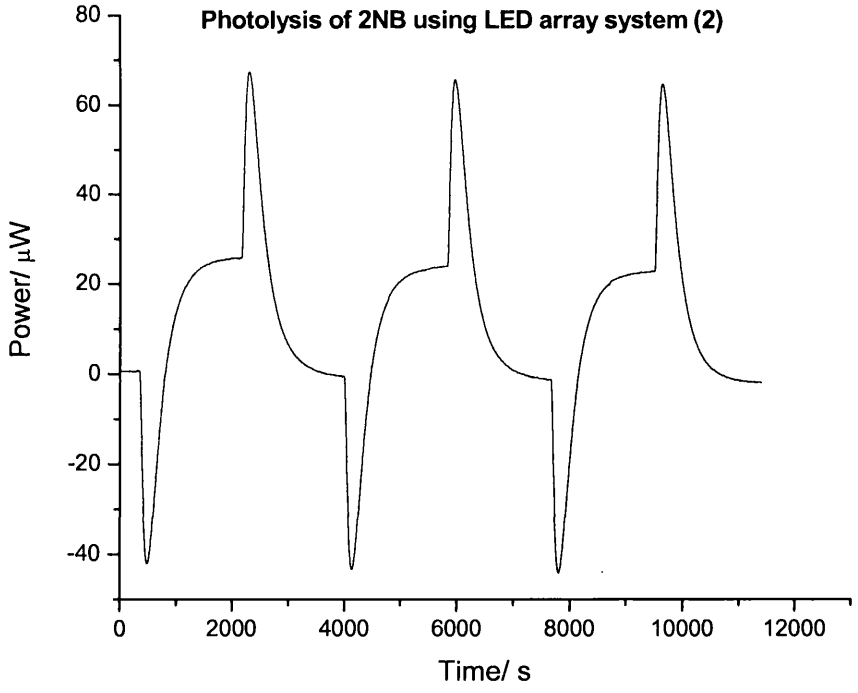

Figure 3.21: LED array photocalorimetric output of 2NB at 15 V (2)

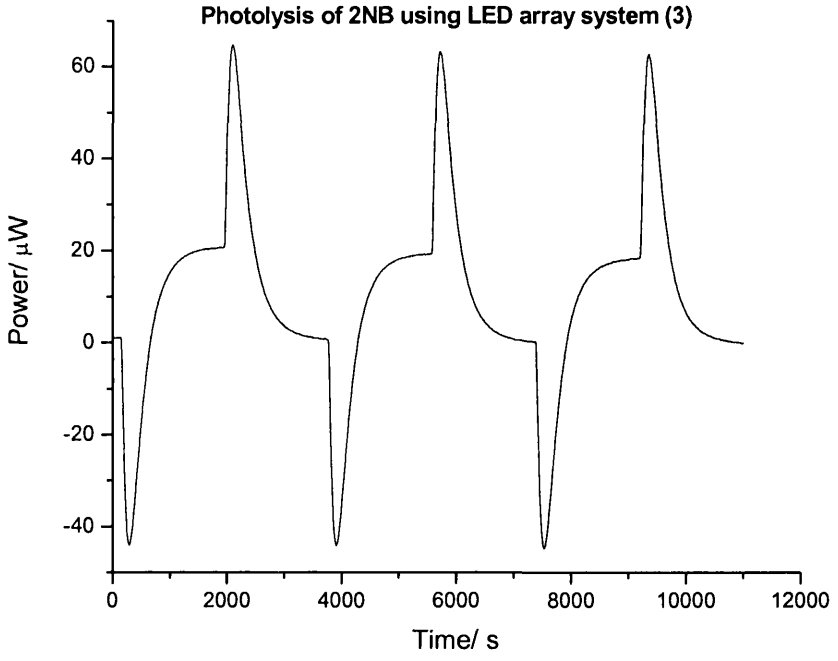

Figure 3.22: LED Array photocalorimetric output of 2NB at 15 V (3)

Table 3.11: Light on/off data for Experiment 1

Light test	t_{irr} (s)	Q (μJ)	Φ calc (μW)	Φ average (μW)
1	1800	38324.42	21.29	20.48
2	1820	34926.22	19.19	19.09
3	1820	32771.15	18.01	18.28
Mean		**35340.60**	**19.50**	**19.28**
SD		**2799.73**	**1.66**	**1.11**
% RSD		**7.9**	**8.52**	**5.77**

Table 3.12: Light on/off data for Experiment 2

Light test	t_{irr} (s)	Q (μJ)	Φ calc (μW)	Φ average (μW)
1	1810	46744.87	25.83	25.80
2	1820	41602.26	22.86	23.93
3	1840	37794.25	20.54	22.67
Mean		**42047.13**	**23.08**	**24.13**
SD		**4491.86**	**2.65**	**1.57**
% RSD		**10.68**	**11.49**	**6.53**

Table 3.13: Light on/off data for Experiment 3

Light test	t_{irr} (s)	Q (μJ)	Φ calc (μW)	Φ average (μW)
1	1800	38829.08	21.57	20.57
2	1820	35505.91	19.51	19.33
3	1820	33318.65	18.31	18.43
Mean		**35884.55**	**19.80**	**19.44**
SD		**2774.66**	**1.65**	**1.07**
% RSD		**7.73**	**8.33**	**5.53**

Table 3.14: Overall power outputs determined during 2NB photolysis using the calculated and average of deflection methods

Experiment	Φ calc (μW)	Φ average (μW)
1	**19.50**	**19.28**
2	**23.08**	**24.13**
3	**19.80**	**18.65**

The power-time data of 2NB photodegradation show the calorimetric output to be reproducible as the sample is irradiated at 30 min intervals and the deflection is constant over the duration of irradiation (as expected in a zero-order reaction). The calorimetric power output using the calculated method is consistent with the output obtained using an average of the deflection. The error associated with the calculation method (7.7% error) is marginally larger than that determined by taking an average of the deflections (5.5% error). The calculation method is seen as a more accurate way to determine the power output since it accounts for the total heat given out by the reaction over the entire irradiation period in contrast to taking an average of a small portion of the deflection after the signal had settled down and the expected flat line ensued (approx. 1500 seconds after the light had been switched on). The subsequent "light dose" calculations were thus made using the calculated power outputs. Following the same procedure as described earlier, the irradiance and photon flux was calculated using the above calorimetric data.

3.2.5.2.3 Determination of ΔH and application to obtain k – LED Array

Applying the value of k (1.04 x 10^{-6} mol dm^{-3} s^{-1}) determined from the pH data (Fig. 3.17) and the power output (Φ calc for Experiment 1) into Eqn. 3.11, the value of ΔH was calculated as **4687.5 J mol^{-1}.** This value was then kept constant and applied to calculate k for subsequent 2NB measurements using Eqn. 3.12.

The calculated values for k are summarised for each measurement in Table 3.15.

Table 3.15: Thermo-kinetic parameters of 2NB photolysis at 15 V with LED array system

Experiment	Φ (W)	ΔH (J mol^{-1})	V (dm^3)	k (mol dm^{-3} s^{-1})
1	19.5 x 10^{-6}	4687.5	0.004	1.04 x 10^{-6}
2	23.1 x 10^{-6}	4687.5	0.004	1.23 x 10^{-6}
3	19.8 x 10^{-6}	4687.5	0.004	1.06.x 10^{-6}

Calculated values of k after applying ΔH

As mentioned in section 3.2.5.1.3, the value of ΔH should, in principle, remain constant providing the reaction taking place is the same. The ΔH for the array LED system determined above differs from those obtained earlier with the single LED system. This again shows that the reaction process is not the same throughout the irradiation period and multiple reactions may be occurring putting a constraint on the usefulness of 2NB as a chemical actinometer.

3.2.5.2.4 Determination of irradiance and photon flux – LED Array system

Using the same equations as those applied previously in the single LED system, the irradiance (I_o) and photon flux (F_o) was calculated using Mathcad©.

The weighted-average wavelength of light was calculated in the UV region (350 – 400 nm) by using the irradiance data obtained by spectroradiometry (in section 3.3) and applied to Equation 3.6.1. The weighted-average wavelength of **387 nm** was

determined. Applying Equation 3.5, the average photon energy of **4.54 x 10^{-19} J** was calculated where it is assumed that all photons in the range 350 – 400 nm convert 2NB to 2NBA with equivalent efficiency.

The values for I_o and F_o as determined by Mathcad© are outlined in the worksheets printed below and all data is summarised in Table 3.16.

Irradiance and Photon Flux Calculations using LED Array

The following steps were used to calculate the irradiance and photon flux of the 2N actinometer at 15 V across 350 - 400 nm

Step 1: All parameters required are entered into Mathcadas follows;

Values of *k* obtained for Experiments 1, 2 and 3 will be known as k1, k2 and k3, respectively.

$k1 := 1.04 \cdot 10^{-6}$ $k2 := 1.23 \cdot 10^{-6}$ $k3 := 1.06 \cdot 10^{-6}$

Quantum yield of 2-nitrobenzaldehyde will be known as Q.

$Q := 0.5$

Step 2: The irradiance (i) for each experiment is calculated by; (Equation 3.2);

$i1 := \frac{k1}{Q}$ $i2 := \frac{k2}{Q}$ $i3 := \frac{k3}{Q}$

$\frac{k1}{Q} = 2.08 \times 10^{-6}$ $\frac{k2}{Q} = 2.46 \times 10^{-6}$ $\frac{k3}{Q} = 2.12 \times 10^{-6}$

$$\frac{\frac{k1+k2+k3}{3}}{0.5} = 2.22 \times 10^{-6}$$

$i1 := \frac{k1}{Q}$ $i2 := \frac{k2}{Q}$ $i3 := \frac{k3}{Q}$

Step 3: The energy of the photon (e) can be described by Planck's constant (h), th speed of light (c) and the weighted-average photon wavelength (l) [Equation 3.5];

$h := 6.63 \cdot 10^{-34}$ $c := 2.99 \cdot 10^{8}$ $l := 3.87 \cdot 10^{-7}$

$e := \frac{(h \cdot c)}{l}$ $e := 5.12 \cdot 10^{-19}$

Step 4: Finally, the determination for the Photon Flux (f) of each experiment require the following parameters;

Irradiance (i), Weighted-average photon energy (e), Volume of actinometric solution (v), Avogadro's number (n), cross-sectional area of ampolue base (a) [Equation 3.3

$v := 0.004$ $n := 6.02 \cdot 10^{23}$ $a := 4.54 \cdot 10^{-4}$

$\frac{i1 \cdot e \cdot v \cdot n}{a} = 5.009$ $\frac{i2 \cdot e \cdot v \cdot n}{a} = 5.924$ $\frac{i3 \cdot e \cdot v \cdot n}{a} = 5.105$

$f1 := 5.01$ $f2 := 5.92$ $f3 := 5.11$

$$\frac{f1 + f2 + f3}{3} = 5.347$$

In summary, the irradiance (i) and photon flux (f) values calculated using the LED array photocalorimeter at 15 V were;

$i := 2.22 \cdot 10^{-6}$ $f := 5.35$

Table 3.16: Summary of Irradiance and Photon Flux data using LED Array

Experiment	I_0 (einstein dm^{-3} s^{-1})	F_0 (W/m^2)
1	2.08×10^{-6}	5.01
2	2.46×10^{-6}	5.92
3	2.12×10^{-6}	5.11
Mean	**2.22×10^{-6}**	**5.35**
± SD	**2.09×10^{-7}**	**0.50**
% RSD	**9.4**	**9.3**

The 2NB actinometer has been successfully applied to determine the radiant intensity using the LED array photocalorimeter. The next step was then to determine the photon flux value in real-time using spectroradiometry (section 3.3) and to see how they compare.

3.3 Spectroradiometry

Spectroradiometry is a technique for measuring the Spectral Power Distribution (SPD) or spectral irradiance per unit area per unit wavelength of a light source. This is a relative measurement showing the shape of the spectrum and the spectral irradiance provides an absolute measurement showing the shape and power. Spectroradiometers are commercially available instruments that are capable of precise measurement of absolute spectral intensities providing the instrument is accurately calibrated. The instrumentation is capable of performing a number of additional functions simultaneously such as real-time recording of irradiance data, calculated in radiant flux per unit area ($\mu W/cm^2$, or, as preferred by photochemists, W/m^2), lumens, lux, etc.

Following the work on chemical actinometry, spectral irradiance measurements were conducted for the light sources; Xe lamp and LEDs (Single UV LED and LED Array) to evaluate the irradiance and photon flux delivered from the Mark II and III photocalorimeters, respectively.

The instrument used for all the measurements was an AvaSpec-2048 fibre optic spectrometer purchased from Avantes Ltd (Figure 3.23). The device is simple in construction and generally consists of optics, monochromator, and detector. The spectrometer was calibrated prior to use and then measurements were taken for the two light sources used. The methodology for this is given below.

Figure 3.23: Avantes AvaSpec© 2048 fibre optic spectroradiometer

Methods

The spectral irradiance and the photon flux were measured through the ends of the sample and reference liquid light guide using an Avantes AvaSpec-2048 fibre optic spectrometer (spectrometer serial number: 0309004S1). One end of the fibre optic was connected directly into the spectrometer and the other to the source of measurement i.e. to the end of light guide or calibration light source. Using the dedicated software (Avasoft© 6.0), the instrument was first calibrated. This was achieved using a calibration lamp (DH-2000 Mikropack UV-VIS-NIR light source) prior to performing measurements.

The calibration procedure used is described below.[43]

Protocol for lamp calibration

For absolute spectral intensity measurements it is important that the instrument is calibrated or certified to ensure accuracy. The following calibration was performed using a calibrated light source; DH-2000 Mikropack.

Note: the DH-2000 Mikropack is a calibrated light source for use in the UV/VIS/NIR spectral range (205–1095 nm).

1. One end of a fibre optic was connected to the spectroradiometer input port and the other to the calibration lamp source.

2. The absolute irradiance application on the AvaSoft 6.0 programme was started and "Perform Intensity Calibration" was selected.

3. Parameters such as channel to be calibrated, calibration lamp file and diameter of the fibre optic used were entered appropriately.

4. The DH-2000 Mikropack reference light source was switched on for 15 minutes to warm up and the fibre tip was inserted directly in the light source.

5. The option to "Start Intensity Calibration" was then selected.

6. The integration time was adjusted so that the maximum count over the wavelength range was about 15000 counts.

7. The smoothing parameters were adjusted to optimise smoothing for the fibre diameter used.

8. The calibration lamp was turned off. A dark reference was saved.

9. The calibration was saved ("Save Intensity Calibration"). The calibration was saved with the extension *fbr since the calibration was performed with a bare fibre optic.

10. The irradiance mode was selected. The system was then ready to take measurements.

The same intensity calibration was loaded prior to measurements. A dark spectrum was saved before switching to irradiance mode.

Parameters used during measurements

Avasoft© parameters for intensity measurements were set as follows;

Integration time: 2 ms

Average no. of scans: 3

Number of pixels used for smoothing: 6

Note: Using a long integration time, the detector was exposed to too much light during a single scan, which meant it was not possible for a signal to be detected. A shorter integration time was chosen to minimise the signal for detection such that a maximum count over the wavelength range was around 15000 counts.

Experimental measurements

Measurements were taken from the sample and reference light guides. The method for measuring the SPD (absolute irradiance) and photon flux using the spectrometer was relatively straightforward;

1. An end of the light guide was connected directly to an end of the fibre optic of the spectrometer. The cables were held together during measurements by a specially constructed attachment punched with holes to fit both ends of the cables securely.

2. In the case of the Xe lamp set to a defined power setting (240 W), a warm up period of 1 hour was allowed before taking measurements. A warm up period of this length was not necessary with the LED system as LEDs are capable of achieving full brightness within a few milliseconds.

3. The light was exposed to the spectroradiometer. The SPD was measured and photon flux readings were taken over a period of approx. 1 hour before the light was switched off.

All data were imported as an ASCII file into Origin™.

The set-up of the photocalorimeters remained unchanged from previous actinometry experiments (described in section 3.2.3). These parameters remained the same throughout the following experiments, unless stated otherwise.

3.3.1 Measurements from Xe lamp source

3.3.1.1 Spectral Power Distribution (SPD)

The light distribution from the sample and reference cables was very encouraging because, firstly, it can be seen that there was a relatively large spectral output in the UV and Visible regions: characteristic of Xe lamps. Secondly, the output spectra between the sample and reference SPD were very well matched, as shown by the overlays of the SPD measurements (Fig. 3.24).

The integrated areas under each spectrum (determined from Fig. 3.19) were:

Sample: 12391.2 $\mu W/cm^2/nm$ **Reference:** 11782.1 $\mu W/cm^2/nm$

There is a similarity of 95% in the distribution between the sample and reference sides. This indicates the split of the light via the beam splitter is proportional through each cable.

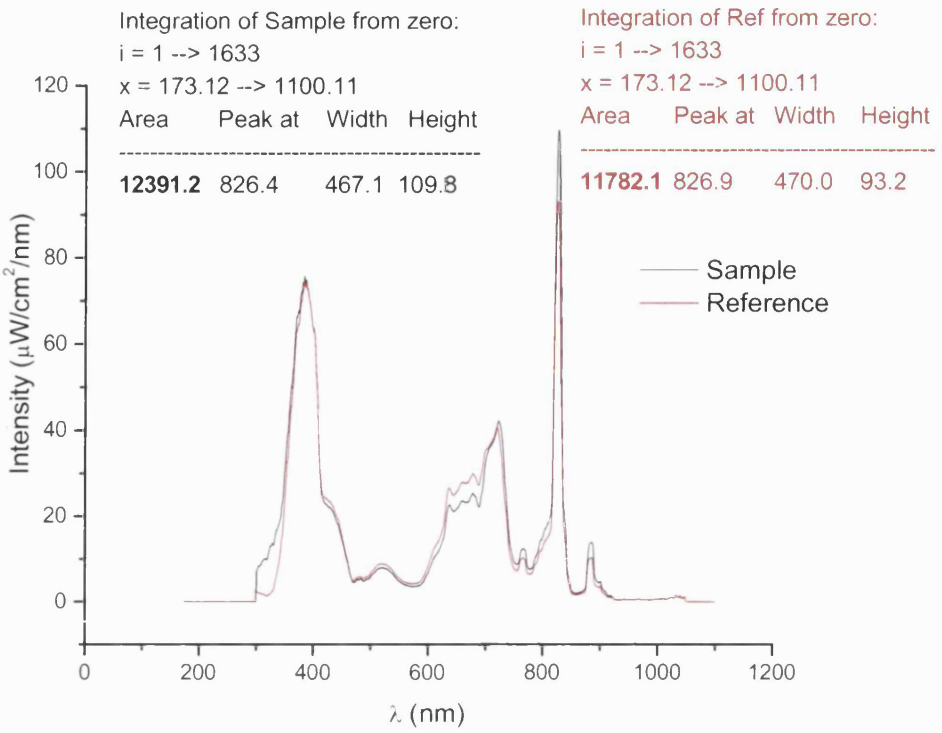

Figure 3.24: Comparison of Spectral Power Distribution of Xe lamp (240 W) through the sample and reference light guides

3.3.1.2 Photon Flux measurements

The photon flux in real-time was measured through the sample side. The measurements were taken after the shutters on the beam splitter were adjusted so that a zero baseline signal was attained on the TAM. This setting will be known as the pre-defined level. It is using this set-up that all chemical actinometry work (on the Mark II) was conducted i.e., the sample was irradiated. Thus, under the same set-up conditions, in principle, it is possible to evaluate and compare the flux data obtained by the spectroradiometer with that obtained through chemical actinometry. Measurements were also taken by adjusting the position of the shutters on the beam splitter so as to give an idea of the absolute maximum and absolute minimum radiant power that the system was capable of producing. Altering the position of the shutter will impact on the extent of flux output. Thus, the flux was evaluated at different shutter positions and the output from the sample side was recorded with the shutter set in the following positions; 1) Open, 2) Mid-way, 3) Pre-defined level (so that a zero baseline signal on TAM was achieved prior to sample analysis), and 4) Closed. Note, as mentioned in Chapter 2, the "closed

position" is referred to the maximum level that the screws controlling the shutters could be adjusted to reduce the light throughput and not the shutters themselves. Hence, only limiting the light entry into the system and not blocking it out completely.

The data were recorded from the sample side at 240 W power output over a period of about 1 hour. Figure 3.25 depicts a comparison of the flux outputs obtained at the different shutter positions.

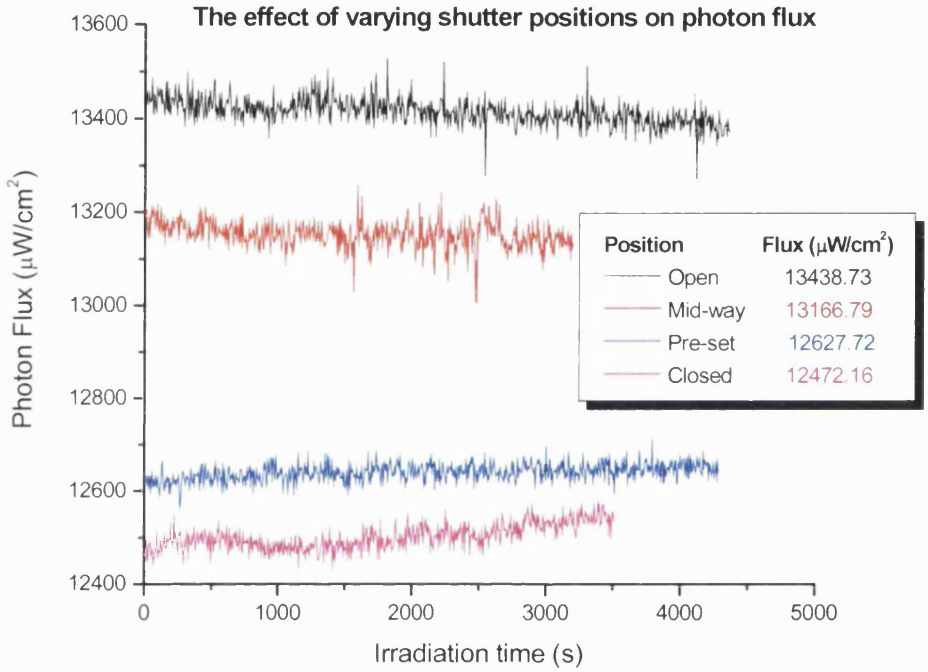

Figure 3.25: Comparison of the change in Photon Flux of a Xe light source (240 W) with different shutter positions

A stable flux output is exhibited during measurements from which an average output value was obtained over the irradiation period. The corresponding values obtained from the outputs shown in Fig. 3.25 are tabulated below. The values, given in $\mu W/cm^2$, can easily be converted to W/m^2 as tabulated in Table 3.17.

Table 3.17: Photon flux at different shutter positions

Shutter position	Photon flux (W/m^2)
Open	134.4
Mid-way	131.7
Pre-defined	124.3
Closed	124.7

The pre-defined level is the setting that was used to irradiate samples and according to the outputs a value of **126.3 W/m^2** is detected by the spectrometer which signifies the amount of radiant power delivered to a sample during a photolytic reaction. The tabulated data show there is very little difference in flux outputs at the different shutter positions; at its maximum it is 134.4 W/m^2 and 124.7 W/m^2 at its minimum (about 7% difference) in the radiant power when the shutters are opened or closed, respectively. The flux outputs show that there is a substantial amount of radiant power delivered from the end of the light guide to the spectrometer.

As mentioned earlier, the primary reason for the development of the LED photocalorimeter was because over the course of the project irregularities in the flux output from the Xe arc lamp were observed, which made it impossible to obtain a stable output on the TAM. It was noted that this was experienced after ~900 h of lamp usage, surpassing the recommended life span of the lamp. Figure 3.26 is typical of the unstable output observed over a period of 24 hours. Evidently, such an irregular output will impact directly on the calorimetric output when the light is switched on, as illustrated in Figure 3.27, which follows a similar pattern as that of the flux output.

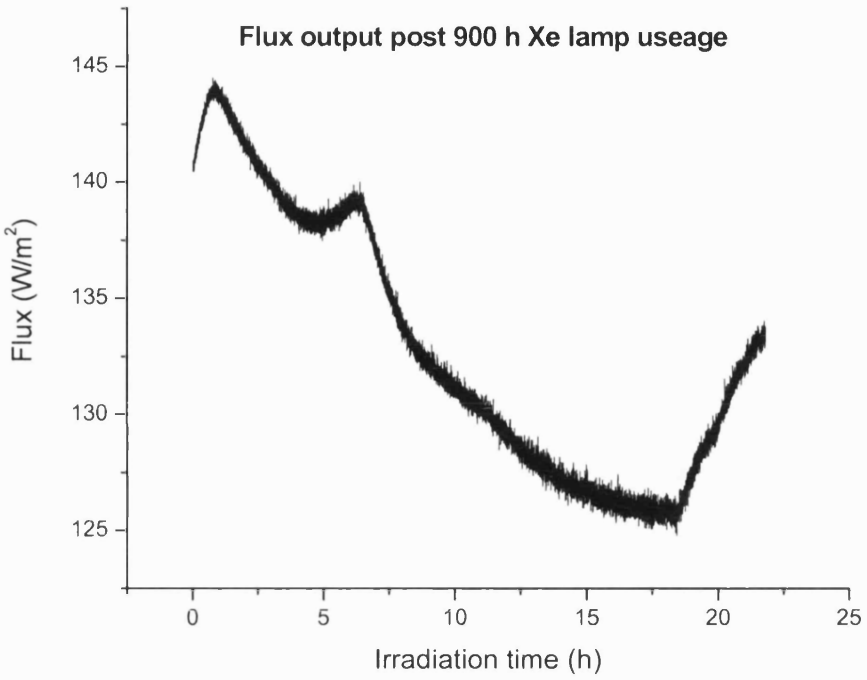

Figure 3.26: Unstable flux output obtained during irradiation by spectroradimetry

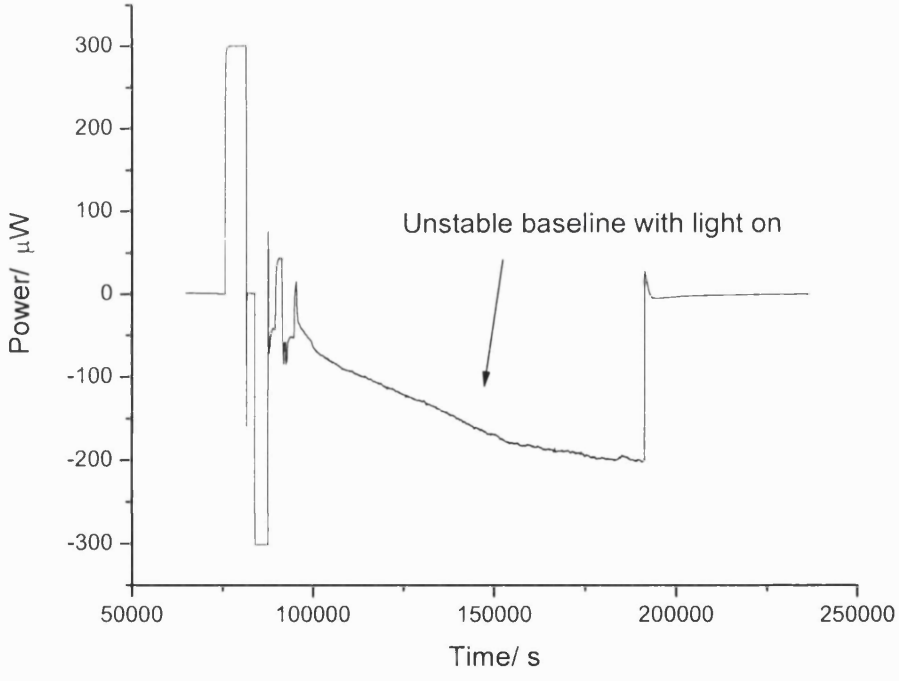

Figure 3.27: Unstable TAM output during irradiation

Because of their short life span, the performance of xenon arc lamps degrade rapidly making it difficult to perform studies over a long experimental period using the same photon source. This drawback means that a lamp requires frequent replacement, which can be a potential cause of error for long term experimental measurements such that only a relatively small number of samples can be irradiated using the same bulb. This can make it difficult to correlate and validate photostability data using different bulbs because of the inherent differences in intensities that exist from lamp to lamp, i.e., each new bulb has its own unique properties and the irradiance of which could be potentially very different. For this reason, LEDs were investigated as an alternative light source primarily for their longevity.

3.3.2 Measurements from LED Single light source

3.3.2.1 Spectral Power Distribution

Figure 3.28 represents the Spectral Power Distribution (SPD) from a single Ultrabright UV LED that was used in preliminary studies for chemical actinometry, and emits a wavelength maximum of 390 nm. A neighbouring peak is also exhibited at 430 nm characteristic of violet light in the visible region.

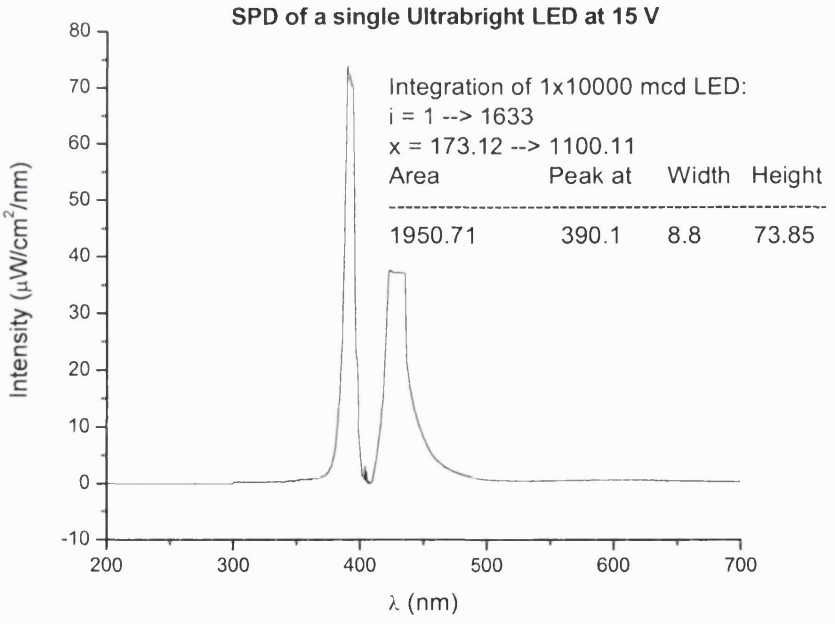

Figure 3.28: SPD of LED single light source through the sample light guide

3.3.2.2 Photon flux

The real-time photon flux measurement taken with the spectroradiometer at 10, 15 and 20 V is shown in Figure 3.24. The plots are extremely encouraging and show stable light outputs from the LED over an irradiation period of about 1.5 hrs. Following a linear fitting through each data set, the flux values derived were; **9.41, 21.38, and 24.16 W/m^2 at 10, 15 and 20 V, respectively.**

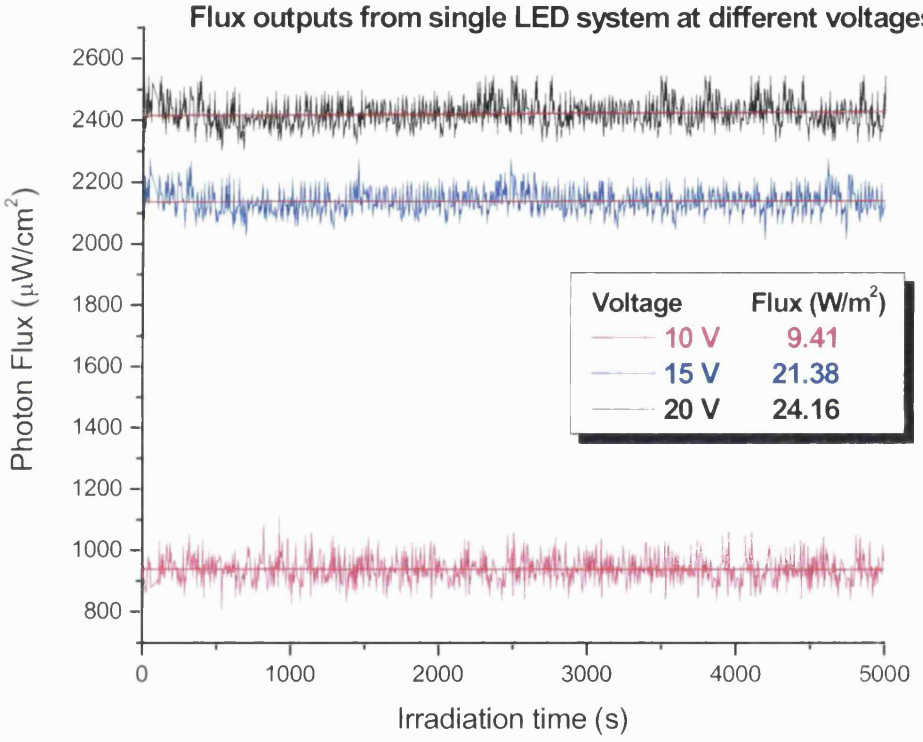

Figure 3.29: Comparison of the change in photon flux from a single LED light source with varying voltages. ***Red line is representative of linear regression fitting.***

The flux data is about 50% greater than that obtained by chemical actinometry showing a 2:1 ratio between values determined by the spectroradiometer and chemical actinometer, respectively. Further discussion on the comparison of the two techniques is given in section 3.4.

3.3.3 Measurements from LED Array

3.3.3.1 Spectral Power Distribution

As mentioned previously, the array of LEDs is comprised of a set of 5 individual LEDs. Each LED is unique to a specific wavelength range. With the voltage output set to 15 V, the peak wavelengths and variation in the radiant power delivered from each individual LED can be seen in the emitted light spectrums shown in Figure 3.30. The overall spectral transmission with all the LEDs switched on (LED array) shows good coverage across 350 – 700 nm in the UV-VIS, as anticipated (Figure 3.31). The overlays of sample and reference outputs are well matched indicating the throughputs are proportional.

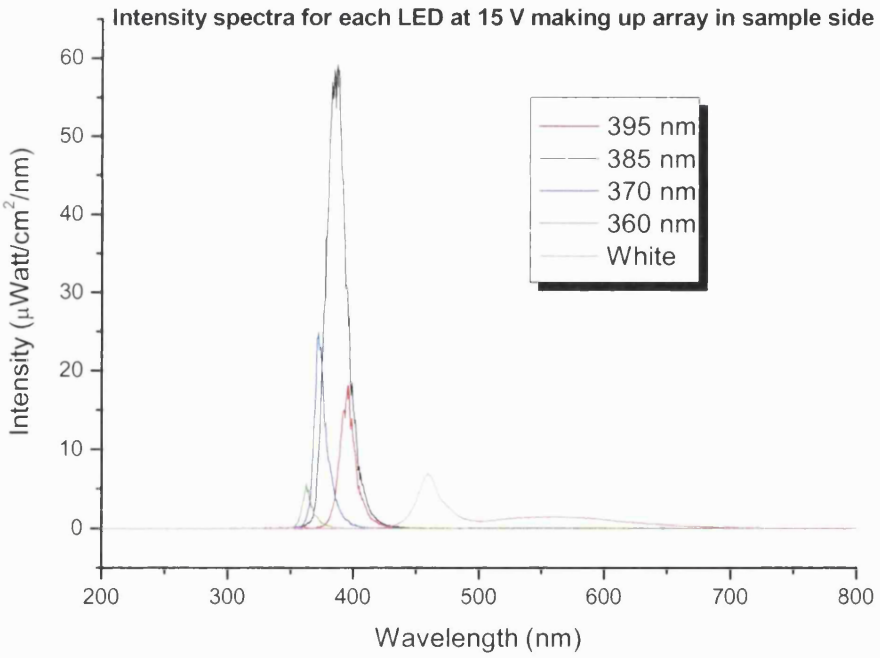

Figure 3.30: Spectral Power Distribution of 5 LEDs used to comprise array. Throughput measured via light guide in sample side at 15 V

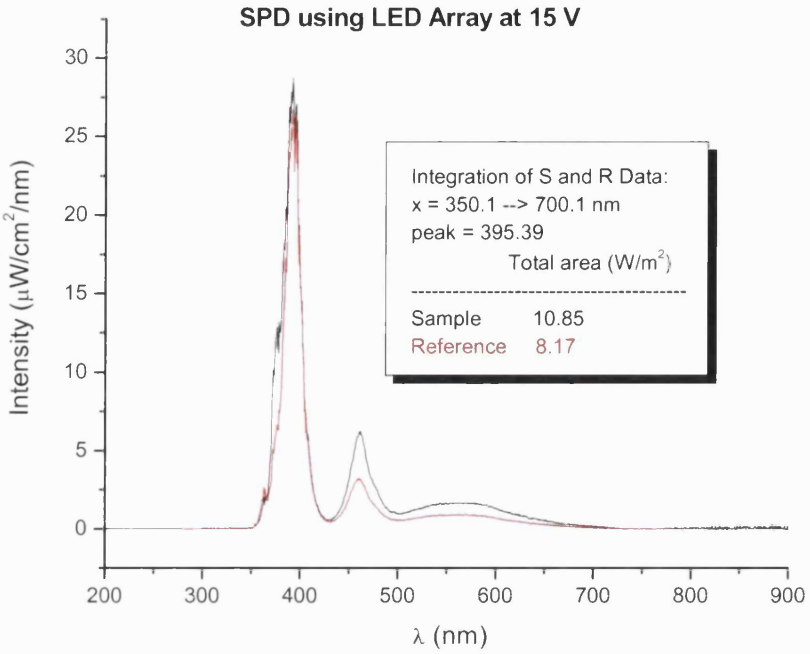

Figure 3.31: SPD through sample and reference light guides with the LED array

The radiant power of each LED is different at each wavelength used. The maximum power emission was exhibited at a peak wavelength of 385 nm. Limited light output was observed at a peak wavelength of 360 nm. Figure 3.32 shows the difference in the light intensities from each LED where the data shown is representative of the integrated area under each peak. Ideally, the summation of the intensities from each individual LED should correspond with the total intensity delivered from the array of LEDs i.e., full spectrum (350 – 700 nm). However, it can be seen from Figure 3.31 that at full spectrum the total intensity (10.85 W/m^2) is some 30% lower than the expected intensity of 15.65 W/m^2 (calculated as the sum of intensities from individual LEDs). It is difficult to explain fully why these transmission losses occur; possible reasons may be due to small changes in the geometry of set-up during measurements. Although the instrument was well-secured, it is inevitable that small changes in the position or orientation of the optic cable and light guide will arise each time the instrument is handled.

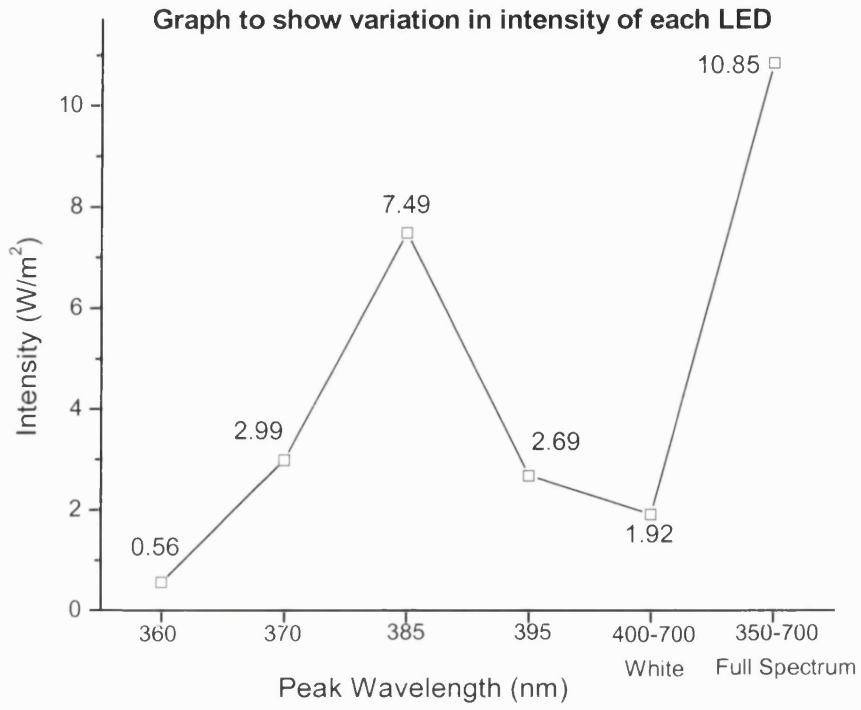

Figure 3.32: Graph showing variation in intensity of the LEDs

3.3.3.2 Photon Flux

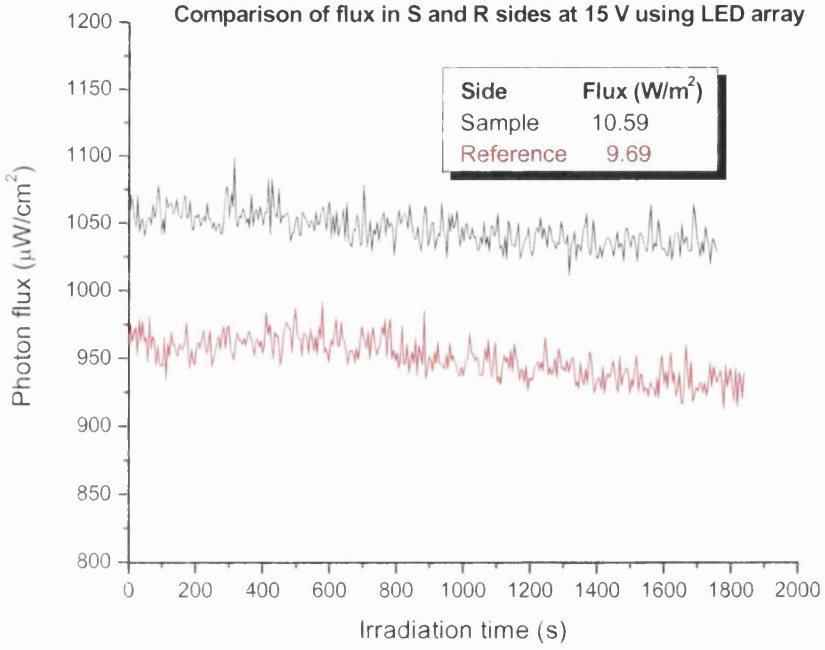

Figure 3.33: Photon flux from a LED array through sample and reference light guides

The data from the integrated area compare well with the real-time flux measurements (Figure 3.33), and show that, on average, the amount of light delivered through the sample side was **10.6 W/m^2 and 9.7 W/m^2** through the reference side.

The voltage of the LED array was increased successively to assess the response of the flux. Figure 3.34 shows the progressive step-wise increase in flux as the voltage was increased. The flux output is proportional to the increase in voltage showing a linear relationship. This demonstrates that the system is responding very well.

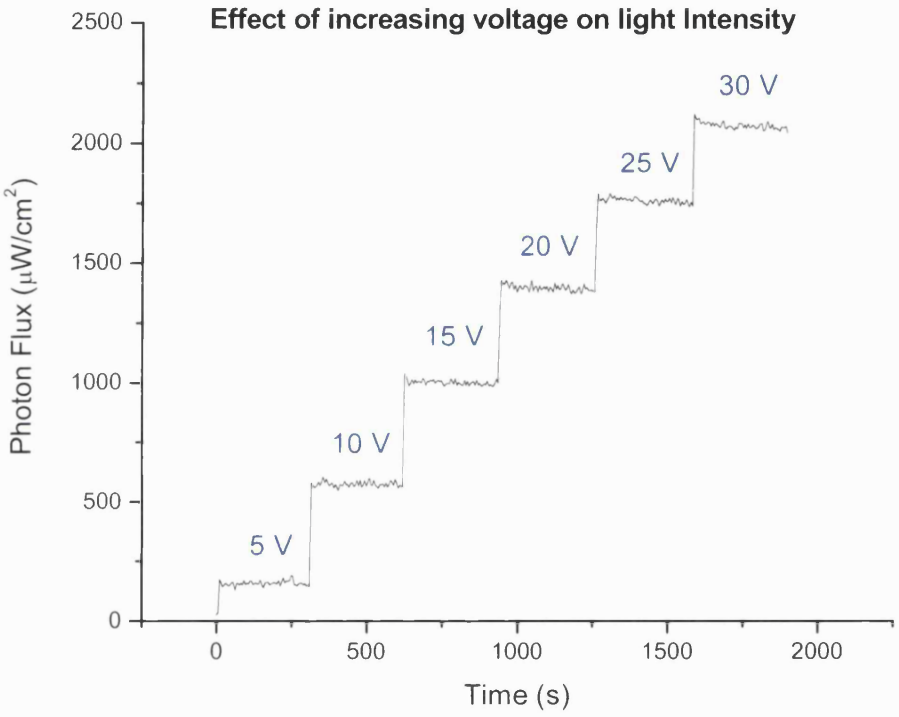

Figure 3.34: Photon flux of LED array as voltage is increased

Table 3.18: Values of photon flux at different voltages

Voltage (V)	Photon flux (W/m^2)
5	1.5
10	5.8
15	10.4
20	14.6
25	18.9
30	21.8

3.4 Comparison of actinometric methods

Two different actinometeric techniques; chemical actinometry and spectroradiometry, have been used to quantify the amount of light exposure for two types of lamp sources; Xe arc lamp and LEDs (single and array system). Having studied the two techniques with two different light sources, it was possible to determine successfully the photon flux for each system. Although because of the additional oxidation event that was observed the during the chemical actinometry work, it was not possible to determine the photon flux for the photolysis of 2NB alone. The flux value, however, can be estimated for the 2NB/EDTA photoreaction since the oxidation process was inhibited. Following the same calculation outline as that already described for the LED systems above (section 3.2.1.3), the flux values for the Xe arc lamp for the 2NB/EDTA data (Fig. 3.9) was determined. The 2NB/EDTA data shown in Fig. 3.10 showed that generally the power signal settled to a constant deflection after approx. 1 hour of irradiation. The Φ signal for each measurement were as follows; 67, 62 and 57 μw for Runs 1, 2, and 3 respectively, giving an average of **62 μW ± 5 μW**. Applying the value of k obtained from the pH data with 2NB/EDTA (2.47×10^{-7} mol dm^{-3} s^{-1}) into Eqn. 3.11, the value for ΔH was calculated as **62753 J mol^{-1}**. This value, again, differs from those determined by the LED single and array photocalorimeters. Moreover, it is also not in agreement with the value of ΔH determined by Morris[33] (cf. 202464 J mol^{-1}) using the Mark I photocalorimeter showing the photoreaction exhibits complexity. The irradiance and photon flux values were determined, and the calculation are outlined in the Mathcad© worksheets below.

Irradiance and Photon Flux calculations using xenon arc lamp

The following steps were used to calculate the irradiance and photon flux for the photodegradation of 2NB containing EDTA at 240 W across 290 - 400 nm

Step 1: All parameters required are entered into Mathcad as follows;

The rate constant determined through pH measurements will be known as k.

$$k := 2.47 \cdot 10^{-7}$$

Quantum yield of 2-nitrobenzaldehyde will be known as Q.

$$Q := 0.5$$

Step 2: The irradiance (i) for each experiment is calculated by; (Equation 3.2);

$$\frac{k}{Q} = 4.94 \times 10^{-7} \qquad i := 4.94 \cdot 10^{-7}$$

Step 3: The energy of the photon (e) can be described by Planck's constant (h), the speed of light (c) and the weighted-average photon wavelength (l) [Equation 3.5];

$$h := 6.63 \cdot 10^{-34} \qquad c := 2.99 \cdot 10^{8} \qquad l := 3.52 \cdot 10^{-7}$$

$$e := \frac{(h \cdot c)}{l} \qquad e := 5.63 \cdot 10^{-19}$$

Step 4: Finally, the determination for the Photon Flux (f) of each experiment requires the following parameters;

Irradiance (i), Weighted-average photon energy (e), Volume of actinometric solution (v), Avogadro's number (n), cross-sectional area of ampolue base (a) [Equation 3.3];

$$v := 0.004 \qquad n := 6.02 \cdot 10^{23} \qquad a := 4.56 \cdot 10^{-4}$$

$$\frac{i \cdot e \cdot v \cdot n}{a} = 1.469 \qquad f := 1.47$$

Overall, the values for I_0 and F_0 as determined by Mathcad© were; **4.94 x 10^{-7} einstein dm^{-3} s^{-1} and 1.47 W/m^2**, respectively.

The values established for the photon flux using the two methods of quantification are tabulated for comparison in Table 3.19.

Table 3.19: Comparison of Photon Flux values using chemical actinometry and spectroradiometry

		Mean Photon Flux (W/m^2)	
Light source		**2NB**	**Spectroradiometry**
Xe arc lamp	240 W	1.5*	126.3
Single LED	10 V	4.6	9.4
Single LED	15 V	11.0	21.4
Single LED	20 V	11.7	24.2
Array LEDs	15 V	5.4	10.6

**Data calculated from 2NB/EDTA measurements*

The data show that generally the spectroradiometric photon flux values are almost twice that of the chemical actinometric values (Xe arc lamp measurements excepted). The 2:1 ratio between the spectroradiometric and chemical actinometric values, respectively, can most probably be explained by the differences in the footprint and geometry of the light that exist between the two techniques. In carrying out the spectroradiometric measurements, one end of the liquid-light guide was attached directly, and securely, onto the end of the fibre optic cable of the spectrometer. The light was thus shone directly into the spectroradiometer. In contrast, for the chemical actinometric measurements, there was a distance of at least 24.3 mm between end of the light guide and the base of the ampoule (Figure 3.4). The inverse relationship between light distance and light intensity essentially means that the footprint and geography of the light shone into the spectroradiometer is different from that of the calorimetric experiments leading to different levels of light intensity between experiments using the two techniques. Thus, care must be taken not treat the data from the spectroradiometer as the "correct value" because of the differences that exist between the two experimental set-ups. These are influenced by a number of factors such as the length of the light guide, the age of the bulb, the footprint of the light irradiating the sample, and

the distance between the optic tip of the light guide and the sample. All these factors can introduce changes in the photon flux outputs. Furthermore, a difference of 50% in the photon values using these two techniques also correlates well with previous actinometry work reported by Morris[33] using the Mark I photocalorimeter and the values from a 240 W powered Xe arc lamp were determined as **1.1 W/m^2** and **2.4 W/m^2** by chemical actinometry (2NB photolysis) and spectroradiometry, respectively. Needless to say, these values cannot be directly correlated with those obtained using the Mark II photocalorimeter (Xe arc lamp) reported here because the experimental set-up was completely different. The Mark II instrument had a far greater throughput of light intensity than the Mark I, as expected, because of the replacement of the fibre optic cables (Mark I) with liquid-light guides. These greatly improved the light transmission (~ 80%) and also using a beam splitter instead of a trifurcated cable meant that there was a greater portion of light split down two light cables (not three branches as with Mark I photocalorimeter). Consequently, a value of **126.3 W/m^2** – ~50% greater light output than that found with the Mark I – was attained through spectroradiometry using Mark II photocalorimeter.

The spectroradiometric value using the Xe arc lamp was found to be much greater (~ 84 times) than that obtained using the chemical method. The difference in the flux values was found to be inconsistent and is difficult to explain fully. The calculated photon flux value for the Xe arc lamp may inevitably be embedded with some errors because the calculations were made for a zero-order reaction, and as noted earlier, the data showed that the 2NB photoreaction may still not be truly zero-order. Other sources of error include instrumental factors such as lamp aging, lamp output variances, fluctuations in thermal and photon energies. Furthermore, it was observed that the footprint of light using the Xe lamp was non-uniform in spread across the base of the ampoule during the chemical actinometry work conducted. Note this was far less obvious whilst operating the LEDs since the light intensity was far less intense. A photographic image shown in Figure 3.35 was taken using a 20 mL glass ampoule to obtain a visual of the coverage on the cross-sectional area for the Mark II photocalorimeter.

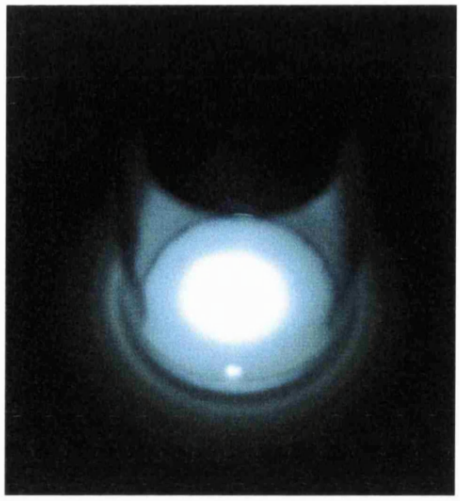

Figure 3.35: Coverage of light across the base of a glass ampoule from a Xe light source

The image clearly shows that the intensity of light exposure is not uniform across the ampoule base. A fraction of the area in the centre of ampoule is exposed to a higher intensity of light with a diffuse surrounding. The illuminated area was measured on a white sheet of paper by removing the glass ampoule, whilst the optic cable was held at the fixed distance (same distance in an experiment) using a clamp. The diameter of the illuminated coverage was 10 mm (Figure 3.36). This shows that 42% of the ampoule base is illuminated intensely with a coverage area of 7.85×10^{-5} m^2. Although, not a major problem for homogeneous samples the non-uniform coverage poses more of an issue for heterogeneous samples (solids). This will lead to some inaccuracies in calculation of the photon intensity. A diffuser was later tested to achieve a uniform coverage, but because of lamp degradation it was not possible to obtain consistent outputs.

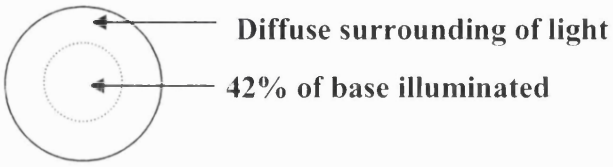

Figure 3.36: Representation of light exposure across ampoule base taken shown in photographic image taken from Figure 3.35

3.5 Summary

Quantification of a photon source is important in the evaluation of photostability of drug substances and drug products. Actinometry offers a way of quantifying intensity, that is, the number of photons in a beam, by means of chemical or physical systems. Chemical actinometers are a preferred choice to external calibrations because they provide an in-situ validation of the instrument and information of the number of photons actually absorbed by a sample during a photochemical process. For reliability and validity of experimental data, a suitable chemical actinometer, ideally, needs to be one that is robust, has a simple reaction mechanism, and exhibits low-sensitivity to non-photochemical processes. The photodegradation of 2-nitrobenzaldehyde (2NB), an ICH listed actinometer, was studied as a potential chemical test and reference reaction for validation of performance of the Xe arc lamp and LED (single and array) photocalorimeters.

It has been demonstrated in this chapter that of the two light sources used it proved difficult to obtain consistent photochemical data from the Xe arc lamp. Data obtained from the pH and photocalorimetric measurements showed non-zero order behaviour for the photodegradation of 2NB using the powerful Xe arc lamp. This suggested that 2NB is likely to be sensitive to non-photochemical processes. With the inclusion of a small amount of EDTA it was possible to inhibit the additional reaction that occurred suggesting an oxidation process was a likely cause of the non-zero order behaviour that was observed, although there was still some evidence of pseudo-zero-order behaviour even in the presence of EDTA. This is indicative of complexity within the reaction and it is the first time that complexity for the photodegradation of 2NB has been detected calorimetrically, although complexity has been highlighted by several others in the literature.[39-41] The data obtained are, however, in discordance with those obtained by Morris[33] using the Mark I photocalorimeter. This is not surprising because with the new experimental design and set-up (Mark II), the light intensity was essentially twice that compared with the earlier model.

The non-zero behaviour observed calorimetrically was more prominent using the Xe arc lamp than the LED systems because the intensity of LEDs is far less than that generated by the Xe arc lamp. The magnitude of the radiant intensity from the xenon lamp is some 12 times greater than that of the LED array as determined by the spectroradiometric

values. The radiant intensity produced by the LEDs is, however, sufficient to cause the photodegradation of 2NB and to produce a detectable calorimetric signal. The high intensity can potentially cause additional secondary or thermal decomposition processes to occur. Since the calorimeter measures *all* thermal processes, discriminating between the types of reactions that may occur is very complicated. Furthermore, the disadvantages associated in combining a powerful xenon arc lamp with the sensitivity of an isothermal microcalorimeter outweigh those of applying LEDs to the instrument. Namely, the short lamp life, variable output, and high heat output generated from xenon arc lamps, all hinder the performance of the instrument leading to erroneous photostability data.

The applicability of LEDs as a light source for photocalorimetric measurements has shown much potential and the results are extremely encouraging. It has been demonstrated that it is possible to quantify successfully the photon flux of the single and array LEDs system using both chemical actinometry and spectroradiometry. With both systems, the 2NB actinometer followed zero-order kinetics (represented by a constant calorimetric deflection), subsequently leading to the derivation of reaction parameters such as k, ΔH, I_0 and F_0. The single LED system showed excellent correlation between the voltage input and calorimetric output (Φ); the signal increased linearly in proportion to the three voltages tested; 10, 15 and 20 V. All data showed very good stability and repeatability (<5% error). Similar results were obtained for the LED array system tested at 15 V (<10% error).

The complexity observed with 2NB using the xenon arc lamp and LED system evident through the variation in the value of ΔH obtained, which should, in principle, remain constant regardless of the reaction mechanism providing the products remain the same and the initial and final concentration remains constant. The values of ΔH were found not to be constant suggesting that the photoreaction of 2NB is complex with more than one reaction occurring and because of which the resultant irradiance and photon flux data determined may be erroneous. Thus, it has been shown that 2NB is sensitive to non-photochemical processes and the reaction is complex which limits the usefulness of 2NB as a suitable chemical test and reference reaction for photocalorimetry and validation of instrument performance.

It should be kept in mind that the photon fluxes values obtained from chemical actinometry and spectroradiometry typically showed a difference of 1:2, respectively. Although, spectroradiometry is very useful for information of spectral intensities, chemical actinometers remain the preferred method of choice because they provide in-situ validation.

Overall, it is apparent from the data obtained that the applicability of LEDs as a light source in photocalorimetry is promising for the assessment of photostability testing.

3.6 References

1 Kuhn, H.J., Braslavsky, S.E., and Schmidt, R. (2004) Chemical Actinometry. *Pure Appl.Chem* 76, 2105-2146

2 Wadso, I., Goldberg, R. N. (2001) Standards in isothermal microcalorimetry (IUPAC technical report). *Pure.Appl.Chem* 73, 1625-1639

3 Beezer, A., Hills, A.K., O'Neill, M.A.A., Morris, A.C., Kierstan, K.T.E., Deal, R.M., Waters, L.J., Hadgraft, J., Mitchell, J.C., Connor, J.A., Orchard, J.E., Willson, R.J., Hofelich, T.C., Beaudin, J., Wolf, G., Baitalow, F., Gaisford, S., Lane, R.A., Buckton, G., Phipps, M.A., Winneke, R.A., Schmitt, E.A., Hansen, L.D., O'Sullivan, D., and Parmar, M.K. (2001) The imidazole catalysed hydrolysis of triacetin: an inter- and intra-laboratory development of a test reaction for isothermal heat conduction microcalorimeters used for determination of both thermodynamic and kinetic parameters. *Therm.Acta* 380, 13-17

4 O'Neill, M.A.A., Beezer, A.E., Labetoulle, C., Nicolaides, L., Mitchell, J.C., Orchard, J.A., Connor, J.A.,Kemp, R.B., Olomolaiye, D. (2003) The base catalysed hydrolysis of methyl paraben: a test reaction for flow microcalorimeters used for the determination of both kinetic and thermodynamic parameters. *Therm.Acta* 399, 63-71

5 Ramos, R., Gaisford, S., Buckton, G., Royall, P.G., Yff, B.S.S., O'Neill, M. (2005) A comparison of chemical reference materials for solution calorimeters. *Int.J.Pharm.* 299, 73-83

6 O'Neill, M.A.A., Gaisford, S., Beezer, A.E., Skaria, C.V., Sears, P. (2006) A comparison of the performance of calorimeters. Application of a test and reference recation. *J.Therm.Anal.Cal.* 84, 301-206

7 Kuhn, H.J., Braslavsky, S.E., and Schmidt, R. (1989) Chemical Actinometry. *Pure Appl.Chem* 61, 187-210

8 Piechocki, J.T. (1998) Principles of chemical actinometry. In *Drugs photochemistry and photostability* (Albini, A., and Fasani, E., ed.), The Royal Society of Chemisty

9 Piechocki, J.T., Wolters, R.J. (1993) Use of actinometry in photolysis stability studies. *Pharm.Tech* 17, 46-52

10 Gauglitz, G., and Hubig, S.M. (2007) Chemical Actinometry. In *Pharmaceutical photostability and stabilization technology* (Vol. 163) (Piechocki, J.T., and Thoma, K., ed.), Informa Healthcare

11 Willet, K., and Hites, R. A. (2000) Chemical actinometry: Using o-Nitrobenzaldehyde to measure lighht intensity in photochemical experiments. *J.Chem.Edu.* 77, 900-902

12 Theweleit, E., and Kunze, W. (1987) Methods and applications of photocalorimetry. *Kunststoffe* 77, 23-25

13 Teixeira, C. (1999) *Photocalorimetry: Methods and Applications in Energetics of Stable Molecules and Reactive Intermediates., M. E. Minas da Piedade, Ed. 105-136*

14 Thatcher, S., Mansfield, R.K., Miller, R.B., Davis, C.W., and Baertschi, S.W. (2001) "Pharmaceutical photostability" A technical guide and practical interpretation of the ICH guideline and its application to pharmaceutical stability - Part II. *Pharm.Tech* 25, 58-64

15 Rabek, J.F. (1982) Experimental methods in photochemistry and photophysics. Part 2. John Wiley and Sons

16 ICHQ1B. (1997) Photostability Testing of New Active Substances and Medicinal Products. *EMEA*, CPMP/ICH/2791/2795

17 Drew, H. (1998) Quinine photochemistry: A proposed chmical actinometer system to monitor UV-A exposure in photostability studies of pharmaceutical drug substances and products. *Pharm.Forum* 24, 6334-6346

18 Christensen, K.L., Christensen, J.,Frokjaer S., Langballe, P.,and Hansen, L. (2000) Influence of temperature and storage time after light exposure on the quinine monohydrochloride chemical actinometric system. *Eur.J.Pharm.Sci* 9, 317-321

19 Tonnesen, H.H., and Karlsen, J. (1995) Photochemical degradation of components in drug formulations. III. A discussion of experimental conditions. *Pharmeuropa* 7, 137-141

20 Sequeira, F., and Vozone, C. (2000) Photostability studies of drug substances and products. Practical implications of the ICH guideline. *Pharm.Tech* 24 (8), 30-35

21 Baertschi, S.W. (1997) Commentary on the quinine actinometry system described by the ICH draft guidelines on photostability testing on new drug substances and products. *Drug Stab.* 1, 193-195

22 Moore, D.E. (1996) Standardization of photodegradation studies and kinetic treatment of photochemical reactions. In *Photostability of drug and drug formulations* (Tonnesen, H.H., ed.), Taylor and Francis

23 Adamson, A.W., Vogler, A., Kunkely, H., and Wachter, R. (1978) Photocalorimetry. Enthalpies of photolysis of *trans*-azobeneze, ferrioxalate and cobaltioxalate ions, chromium hexacarbonyl, and dirhenium decarbonyl. *J Am Chem Soc.* 100, 1298-1300

24 Almmand, A.J., and Webb, W.W. (1929) The photolysis of potassium ferrioxalate solutions. Part I. experimental. *J. Chem. Soc*, 1518-1531

25 Almmand, A.J., and Webb, W.W. (1929) The photolysis of potassium ferrioxalate solutions. Part II. discussion. *J. Chem. Soc.*, 1531-1537

26 Cooper, G.D., and DeGraff, B.A. (1971) On the photochemistry of the ferrioxalate system. *J.Phys.Chem* 75, 2897-2902

27 Fernandez, E., Figuera, J.M. and Tobar, A. (1979) Use of potassium ferrioxalate actinometer below 254 nm. *J.Photochem* 11, 69-71

28 Hatchard, C.G., and Parker, C.A. (1956) A new sensitive chemical actinometer II. Potassium ferrioxalate as a standard chemical actinometer. *Proc. R. Soc. London, Ser.* 235, 518-536

29 Nicodem, D.E., and Aquilera, O.M.V. (1983) Standardization of the potassium ferrioxalate actinometer over the temperature range 5-80 °C. *J.Photochem* 21, 189-193

30 Parker, C.A. (1953) A new sensitive chemical actinometer I. Some trials with potassium ferrioxalate. *Proc. R. Soc. London, Ser.* 220, 104-116

31 Parker, C.A. (1954) Induced Autoxidation of oxalate in relation to the photolysis of potassium ferrioxalate. *Trans. Faraday Soc.* 50, 1213-1221

32 Oriel Light Sources Catalogue (2004).

33 Morris, A.C. (2004) Ph.D Thesis. University of Greenwich, Kent, UK.

34 Allen, J.M., Allen, S.K., and Baertschi, S.W. (2000) 2-Nitrobenzaldehyde: a convenient UV-A and UV-B chemical actinometer for drug photostability testing. *J.Pharm.Biomed.Anal* 24, 167-178

35 Ciamician, G., and Silber, P. (1901) *Chem.Ber.* 34, 2040-2046

36 Pitts, J.N., Wan, J.K.S., and Schuk, E.A. (1963) Photochemical studies in an alkali halide matrix I. An σ-Nitrobenzaldehyde actinometer and its application to a kinetic study of the photoreduction of Benzophenone by Benzhydrol in a pressed potassium bromide disk. 86, 3606-3610

37 Leighton, P.A., Lucy, F.A. *J. Chem. Phys.* 2, 756-761

38 Pitts, J.N., Vernon, J.M., and Wan, J.K.S. (1965) A rapid actinometer for photochemical air pollution studies. *Int. J. Air Wat. Pollu.* 9, 595-600

39 Trench, A.J., and Coppens, P. (1963) Free radicals formed from o-substituted nitro compounds. *J.Phys.Chem* 67, 1378

40 Chen, D., Zhou, J., Tian, Q. (1996) Mechanisms and structures of free radicals in the photoreaction processes of o-substituted nitrobenzaldehydes. *Journal of Photochemistry and Photobiology A: Chemistry* 98, 21-26

41 Laimgruber, S., Schreier, W.J., Shrader, T., Koller, F., Zinth, W., and Gilch, P. (2005) The photochemistry of *o*–Nitrobenzaldehyde as seen by Femtosecond Vibrational Spectroscopy. *Angew.Chem.Int Ed.* 44, 7901-7904

42 Dhuna, M., Beezer, A.E., Morris, A.C., Gaisford, S., O'Neill, A.A.M., Hadgraft, J., Connor, J.A., Clapham, D., Frost, J. (2007) Development of an Isothermal Heat-Conduction Photocalorimeter. *Rev Sci Instrum* 78 (doi:10.1063/1.2670220), 025105

43 Avasoft for Avaspec (2003) Spectroradiaometer operator manual.

- Chapter Four -

Chemometric approach to complexity

4. Introduction

Many pharmaceutical formulations (tablets, creams, lotions, etc) are complex multi-component systems. Often it is likely that their stability is dependent on the degradation kinetics of several independently degrading components and not just on the behaviour of the active pharmaceutical ingredient alone. Moreover, the degradation reaction mechanisms in such multi-component systems are numerous, and include parallel, consecutive and/or a combination of such processes. Very often it is the case that the complexities in these systems are difficult to analyse using conventional analytical techniques.

The principles of Isothermal Calorimetry (IC) and the analysis of calorimetric data for simple systems were introduced in Chapter 1. Chapters 2 and 3 subsequently demonstrated how the technique can be extended to monitor photodegradative processes, and to determine quantitatively the radiant flux delivered to a sample in a simple photochemical process. Dealing with complex behaviours poses a far greater problem, even more so for photosensitive reactions, because the combined effects of heat and radiation adds to the complexity. Although photocalorimetry shows promise for the study of complex reaction systems, the interpretation and correlation of data can be especially problematic.[1] Even when non-photochemical processes are studied, the interpretation of complexity in isothermal calorimetric data is not straightforward, since the calorimeter measures *all* thermal processes that occur, without discriminating between individual processes. The observed power signal is therefore a summation of the powers arising from each individual event that occurs (which can be physical as well chemical change).

The challenge, however, lies in deconvoluting the observed power signal into its individual component parts to help identify the degradation kinetic behaviour for each individual process. A number of methods for quantitative analysis of complexity, both in solution[2-4] and solid states[5] have been described. However, for complex reactions, these approaches require prior knowledge of the reaction mechanism.

One alternative approach to the problem of complexity in multivariate data sets is the application of chemometric analysis. It is the purpose of this chapter to analyse the

potential application of chemometric analysis for interpretation of complex isothermal calorimetric data focusing specifically on consecutive reaction schemes.

4.1 Chemometric analysis

Chemometric analysis is the application of mathematical or statistical methods to extract information from multivariate chemical data. It involves the application of techniques such as principal component analysis (PCA) to deconvolute the overall process into the constituent individual processes. The PCA approach allows a way of identifying patterns in data and expressing the data in such a way as to highlight their similarities and differences. The patterns are searched from a matrix of data containing at least three different variables and offer the significant advantage of being model-free. Hence, PCA is recognised as a powerful tool for analysing complex data.

The use of chemometrics has been well established for spectroscopic analysis[6-8] and many commercially software packages are available (for example, DiKnow Ltd, U.K. and Infometrix Inc, U.S.A.). The data outputted from the chemometric software is, thus, in the form of intensity (arbitrary units) versus time. Chemometric analysis has also been well established for the interpretation of non-isothermal (scanning) calorimetric data, where it is the changes in temperature during the experiment that gives rise to complexity in the data.[9,10] However, at present, with little information available in literature, there is no chemometric package written specifically for the analysis of IC data, hence limiting the use of IC as a quantitative tool. The main focus of this chapter is to address this knowledge gap by adapting chemometric analysis to the analysis of complex IC data sets so to enable IC to fulfil its true potential as a quantitative tool.

4.1.1 Chemometric approach to isothermal calorimetric data

IC provides no direct molecular information about the reactions that occur, and so there is a need to find a matrix that can yield the number of processes and the reaction order. In order to test the appropriateness of the analysis, there is the requirement that all the reaction orders of each process are integral. Subsequent analysis can then be performed

to recover kinetic and thermodynamic parameters once the number and reaction orders of individual processes are known.

In terms of pattern analysis, since the overall power signal is a summation of the individual processes, each component will have a unique maximum over the time course of experiment at a set temperature. This suggests that the data could potentially be analysed by a multivariate method provided a suitable matrix can be generated. The successful application of chemometric analysis to spectroscopic systems is primarily because the technique generates large quantities of data (intensity) as a function of other variables such as wavenumber, pH, temperature, time, etc. Conventionally, a matrix of data consists of at least three variables to facilitate pattern searching or multivariate type analysis. This type of data matrix has x, y and z properties which describes the information as row, column and intensity, respectively. IC output data, however, consist of only two variables, that is, power and time (at a fixed temperature). There is, thus, a need to introduce a third variable component from the system. Selecting a third component is a little more problematic with available calorimetric instruments and it is uncertain as to what form this third variable should take. One option is to record a large number of replicate runs of the same experiment. These replicate runs will naturally encompass some small differences between measurements i.e., variations in sample mass will introduce some small changes.[11] In effect, each run will vary from the other in the total power output making it suitable as a third variable and possibly permit successful chemometric analysis. In terms of the data matrix for the calorimetric measurements, the variables in the power-time data results in t time points and P powers. The third variable (intensity) provides S sets of data for the replicate runs of the same sample. A simple schematic representation of the data format suitable for deconvolution using these three variables is illustrated in Figure 4.1.[11]

In order to construct a suitable trivariate data matrix, M, which can be subjected to chemometric analysis for deconvolution, would require at least $2n + 2$ repeat runs (i.e., $S = 2n + 2$) to allow analysis, where n is the number of species that evolve in a reaction process. [11]

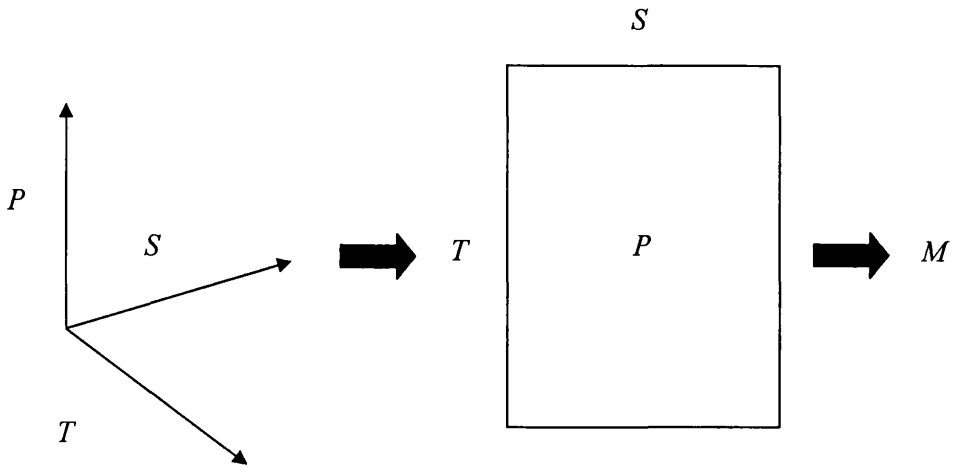

Figure 4.1: Representation of a schematic data format suitable for deconvolution.
***Abbreviations; P* is power; *S* is sample mass, *T* is time, and *M* is matrix**

The successful application of chemometric analysis will result in the deconvolution of calorimetric data to allow determination of the number of reaction steps, which contribute to the overall mechanism. Each reaction step will exhibit an individual pattern of the processes occurring in the system, i.e. there is a unique maximum for each process that occurs. This can aid identification of products and intermediates as well as the time at which the maximum concentration of each species is present. Therefore, each individual step should conform to a single-step kinetic equation making it possible, in principle, to analyse the kinetic and thermodynamic behaviour for each step. This should allow derivation of reaction parameters such as rate constant, reaction order, enthalpy of reaction, etc. It should be noted that the deconvoluted data that are returned from the chemometric analysis are in the form of intensity (cf. power) versus time. Since the relationship between intensity and power is not clear, it is not possible to deduce accurate thermodynamic information directly from the deconvoluted data. However, it is possible to derive kinetic information via analysis such as iteration[2] since the shape of the data (rate of change) is not affected.

4.2 Data Simulation

The data presented in this chapter is that of simulated data, which was created using a suitable mathematical worksheet (MathCad©). MathCad© can be used to simulate the calorimetric output that would be expected from a hypothetical reaction. Simulated data are ideal because they are free from any imperfections that might be expected in real data, such as noise from baseline instability, random thermal/electrical errors, and other artefacts that may be present in real data. Moreover, the reaction mechanism and reaction parameters are known unequivocally.

The data simulated were selected for a three-step consecutive irreversible reaction system, where the initial substances and intermediate products can react in **one** direction only (Figure 4.2). It is assumed that each step in the consecutive reaction follows first-order kinetics and appropriate values for the reaction parameters were selected for first-order rate constants, k_1, k_2 and k_3, and reaction enthalpies, ΔH_1, ΔH_2 and ΔH_3, respectively. Note: *D* is representative of the end product.

$$A \xrightarrow[\Delta H_1]{k_1} B \xrightarrow[\Delta H_2]{k_2} C \xrightarrow[\Delta H_3]{k_3} D$$

Figure 4.2: Three step consecutive reaction scheme, where each step is first-order, with enthalpies of ΔH_1, ΔH_2, and ΔH_3, respectively.

Calorimetric equations that describe three-step, first order, consecutive order reaction schemes are well established.[12] The concentration ([ ]) of any compound reacted at time *t* can be expressed in the following rate equations described below;

$$\frac{d[A]}{dt} = -k_1[A] \qquad \text{Eqn. 4.1}$$

$$\frac{d[B]}{dt} = k_1[A] - k_2[B] \qquad \text{Eqn. 4.2}$$

$$\frac{d[C]}{dt} = k_2[B] - k_3[C] \qquad \text{Eqn. 4.3}$$

$$\frac{d[D]}{dt} = k_3[C] \qquad \text{Eqn. 4.4}$$

Integration of Equations 4.1 gives;

$$[A] = A_0 e^{-k_1 t} \qquad \text{Eqn. 4.5}$$

where; A_0 is the initial quantity of the reactant (mol).

The reaction A→B thus follows;

$$\frac{d[A]}{dt} = -k_1 A_0 e^{-k_1 t} \qquad \text{Eqn. 4.6}$$

Substitution of the value $[A_0]$ (Eqn. 4.5) into Equation 4.2 yields;

$$\frac{d[B]}{dt} = k_1 A_0 e^{-k_1 t} - k_2[B] \qquad \text{Eqn. 4.7}$$

Equation 4.7 can then be integrated using an integrating factor, if $B_0 = 0$, to give;

$$[B] = \frac{A_0 k_1}{k_2 - k_1}(e^{-k_1 t} - e^{-k_2 t}) \qquad \text{Eqn. 4.8}$$

Substitution of Equation 4.8 into Equation 4.3 yields;

$$\frac{d[C]}{dt} = k_2\left[\frac{A_0 k_1}{k_2 - k_1}(e^{-k_1 t} - e^{-k_2 t})\right] - k_3[C] \qquad \text{Eqn. 4.9}$$

Equation 4.9 can be integrated using the integrating factor $e^{-k_3 t}$ to give;

$$[C]=\left(\frac{k_2^2k_1A_0e^{-k_2t}}{-k_1k_2-k_3k_2+k_2^2+k_3k_1}\right)+\left(\frac{k_2k_1^2A_0e^{-k_1t}}{-k_1k_2+k_3k_2-k_3k_1+k_1^2}\right)$$
$$-\left(\frac{k_2k_1A_0e^{-k_3t}}{-k_1k_2-k_3k_2+k_2^2+k_3k_1}\right)-\left(\frac{k_2k_1A_0e^{-k_3t}}{-k_1k_2+k_3k_2-k_3k_1+k_1^2}\right) \quad \text{Eqn. 4.10}$$

The sum of the reactant concentrations must equal A_0 (if B, C and D are not present initially) and it follows that;

$$[D]=A_0-[A]-[B]-[C] \quad \text{Eqn. 4.11}$$

Thus gives Equation 4.12;

$$[D]=A_0-\left(A_0e^{-k_1t}\right)-\frac{A_0k_1}{k_2-k_1}(e^{-k_1t}-e^{-k_2t})$$
$$-\left(\frac{k_2^2k_1A_0e^{-k_2t}}{-k_1k_2-k_3k_2+k_2^2+k_3k_1}\right)-\left(\frac{k_2k_1^2A_0e^{-k_1t}}{-k_1k_2+k_3k_2-k_3k_1+k_1^2}\right) \quad \text{Eqn. 4.12}$$
$$+\left(\frac{k_2k_1A_0e^{-k_3t}}{-k_1k_2-k_3k_2+k_2^2+k_3k_1}\right)+\left(\frac{k_2k_1A_0e^{-k_3t}}{-k_1k_2+k_3k_2-k_3k_1+k_1^2}\right)$$

Differentiation of Equation 4.12 gives;

$$\frac{d[D]}{dt}=A_0k_1e^{-k_1t}-\frac{A_0k_1}{(k_2-k_1)}(-k_1e^{-k_1t}-k_2e^{-k_2t})$$
$$+\left(\frac{k_2^2k_1A_0e^{-k_2t}}{-k_1k_2-k_3k_2+k_2^2+k_3k_1}\right)+\left(\frac{k_2k_1^2A_0e^{-k_1t}}{-k_1k_2+k_3k_2-k_3k_1+k_1^2}\right) \quad \text{Eqn. 4.13}$$
$$-\left(\frac{k_2k_1A_0k_3e^{-k_3t}}{-k_1k_2-k_3k_2+k_2^2+k_3k_1}\right)-\left(\frac{k_2k_1A_0k_3e^{-k_3t}}{-k_1k_2+k_3k_2-k_3k_1+k_1^2}\right)$$

In terms of calorimetric data, the power associated with each reaction step (based on the equations above) is given in Equations 4.14 to 4.17. These equations can be used to simulate power-time data for each reaction step, i.e., A to B, B to C, and C to D, where;

P (or $dq/dt \equiv \Phi$, where q is the heat output to time t) is the power from the calorimetric output (J/s), and A_0 is the initial quantity of the reactant (mol).

$$P_{A\rightarrow B} = \Delta H_1 k_1 A_0 e^{-k_1 t} \qquad \text{Eqn. 4.14}$$

$$P_{B\rightarrow C} = \Delta H_2 k_1 k_2 A_0 \frac{e^{-k_1 t} + e^{-k_2 t}}{k_2 - k_1} \qquad \text{Eqn. 4.15}$$

$$P_{C\rightarrow D} = \Delta H_3 \left[A_0 k_1 k_2 k_3 \left(\frac{e^{-k_1 t}}{(k_2 - k_1)(k_3 - k_1)} + \frac{e^{-k_2 t}}{(k_1 - k_2)(k_3 - k_2)} + \frac{e^{-k_3 t}}{(k_1 - k_3)(k_2 - k_3)} \right) \right] \qquad \text{Eqn. 4.16}$$

A summation of the power-time data for each reaction step would then give the simulated power-time output that would be observed calorimetrically. This can be obtained by combining Equations 4.14 to 4.16 to give Equation 4.17, where P_{obs} is the observed (or overall) power-time data for a consecutive, three-step, first-order reaction scheme.

$$P_{obs} = \Delta H_1 k_1 A_0 e^{-k_1 t} + \Delta H_2 k_1 k_2 A_0 \frac{e^{-k_1 t} + e^{-k_2 t}}{k_2 - k_1} + \Delta H_3 \left[A_0 k_1 k_2 k_3 \left(\frac{e^{-k_1 t}}{(k_2 - k_1)(k_3 - k_1)} + \frac{e^{-k_2 t}}{(k_1 - k_2)(k_3 - k_2)} + \frac{e^{-k_3 t}}{(k_1 - k_3)(k_2 - k_3)} \right) \right] \qquad \text{Eqn. 4.17}$$

The above equations were then used to fit calorimetric power-time data for a three-step consecutive reaction, assuming all the steps follow first-order kinetics.

All simulated data presented herein were constructed using the MathCad© programme. The data constructed were then imported into a suitable analysis programme, Origin pro 7.0 (Microcal Software Inc), and treated as if they were derived from a real calorimetric experiment.

As mentioned earlier, the data matrix requires at least three variables for successful chemometric analysis. Raw calorimetric data offer only two variables; power and time, the third parameter was thus generated. This was achieved by varying experimental parameters, such as the value of the initial quantity of the reactant (A_0) and reaction enthalpy for the replicated runs. Such variations will naturally be present in real calorimetric data as random errors (electrical, thermal, etc) within the system. The simulated data therefore took form of random errors as a third variable.

The individual power-time data of each component, comprising the three-step consecutive reaction, were simulated in MathCad© using Equations 4.14 to 4.16 and the overall power-time data were simulated using Equation 4.17. The parameters used to generate the data for the three components ($A \rightarrow B, B \rightarrow C,$ and $C \rightarrow D$) were chosen as follows; k values were 9 x 10^{-5} s^{-1}, 2 x 10^{-4} s^{-1}, and 5 x 10^{-6} s^{-1}, respectively. The values for ΔH were 1 x 10^4 J mol^{-1}, 8 x 10^4 J mol^{-1}, and 9 x 10^4 J mol^{-1}, respectively. Note, for the simulation of the eight overall calorimetric outputs, a random variation of ±2% in the values of ΔH was entered. The values of A_0 ranged from 7.5 x 10^{-5} to 9 x 10^{-5} moles. The equations and parameters used to construct the simulated data are represented in the MathCad© worksheet given in Figure 4.3. The resultant outputs (individual and overall) are depicted in Figure 4.4.

The simulation of a three-step A to B to C to D consecutive reaction scheme:

$A := 7.5 \cdot 10^{-5}$ $k1 := 9 \cdot 10^{-5}$ $k2 := 2 \cdot 10^{-4}$ $k3 := 5 \cdot 10^{-6}$

$t := 0, 10 .. 100000$ $H1 := 1.0 \cdot 10^{4}$ $H2 := 8.0 \cdot 10^{4}$ $H3 := 9.0 \cdot 10^{4}$

The reaction for A to B (step 1) can be described by;

$$a(t) := A \cdot H1 \cdot k1 \cdot e^{-k1 \cdot t}$$

The reaction for B to C (step 2) can be described by;

$$b(t) := A \cdot k1 \cdot k2 \cdot H2 \cdot \frac{e^{-k1 \cdot t} - e^{-k2 \cdot t}}{k2 - k1}$$

The reaction for C to D (step 3) can be described by;

$$c(t) := H3 \cdot \left[A \cdot k1 \cdot k2 \cdot k3 \cdot \left[\frac{e^{-k1 \cdot t}}{(k2 - k1) \cdot (k3 - k1)} + \frac{e^{-k2 \cdot t}}{(k1 - k2) \cdot (k3 - k2)} + \frac{e^{-k3 \cdot t}}{(k1 - k3) \cdot (k2 - k3)} \right] \right]$$

Figure 4.3: The simulation of a three-step consecutive first order *A→B→C→D*, reaction scheme.

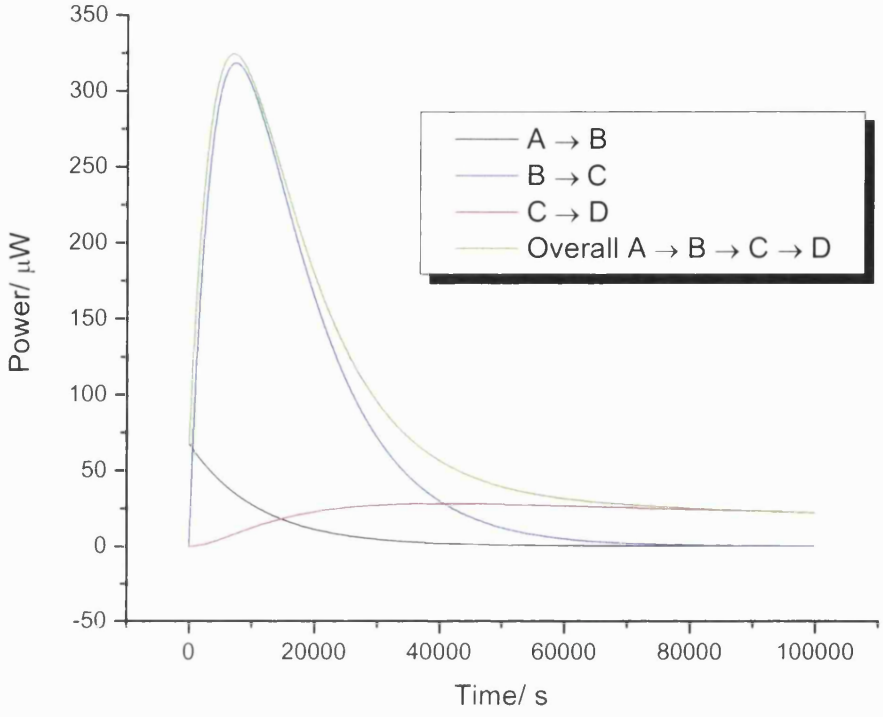

Figure 4.4: Simulated power-time outputs for each component step comprising the overall three-step reaction. ***Constructed from simulated data shown in Figure 4.3***

As noted earlier, to construct a suitable trivariate data matrix would require at least $2n$ + 2 replicated runs. A three-step consecutive reaction would thus acquire a minimum of eight data sets to enable successful PCA analysis. The final data matrix hence comprised of eight simulated calorimetric outputs, which showed the "overall" calorimetric output as a summation of the individual reaction steps. Thus, no information on the mechanism was provided prior to analysis. Each output was simulated by varying (arbitrary) the initial concentrations of A_0 with overlaid noise, as stated above. Figure 4.5 represents the set of overall simulated calorimetric data that was entered into the chemometric software for PCA analysis.

The InSight software package (coded in Matlab software) was used to perform the PCA analysis in order to determine the number of reaction steps (or principal components) comprising the overall calorimetric signal.

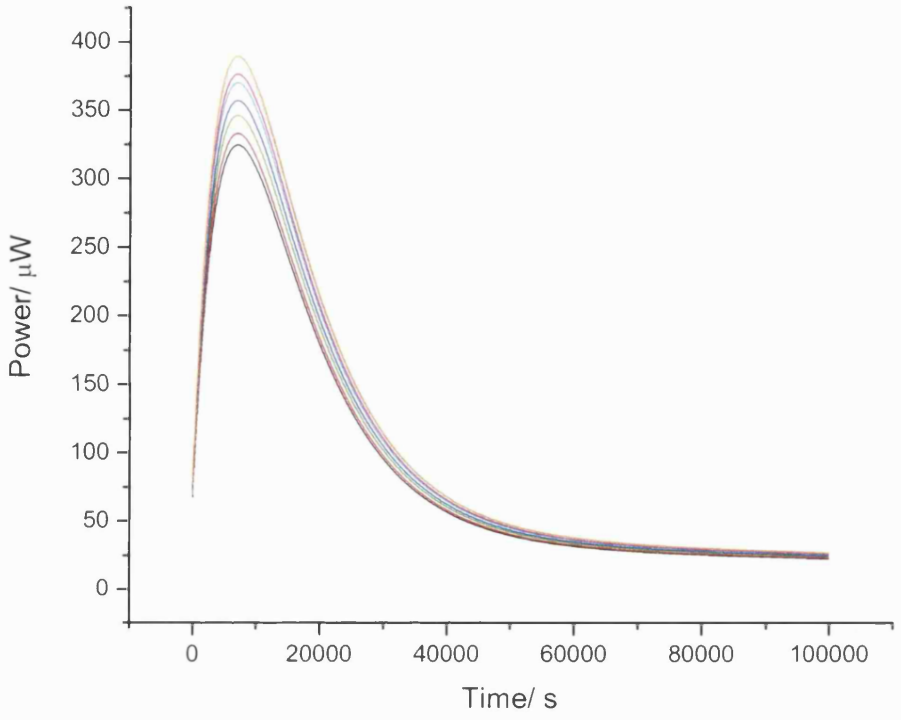

Figure 4.5: Set of simulated data entered into chemometrics software for PCA analysis[13]

4.3 Results and Discussion

PCA analysis allows for the deconvolution of a process into its individual components. The simulated power-time data that were used to create a suitable matrix were that for a three-step reaction system. Hence, successful PCA analysis should, in principle, result in the detection of same number of components as the model used to generate the data i.e. three principal components, noting that the number of principal components determined did not require prior knowledge of reaction mechanism.

The type of PCA analysis performed to analyse the deconvoluted data matrix was that of factor analysis.[11] Factor analysis uses various forms of mathematical scrutiny to determine if the data have any real chemical or physical meaning following the deconvolution into its principal components (or abstract factors). This form of analysis was used for deconvolution based on the assumption that the power signal at the time *t* is a linear sum of all the species present at that moment, and that the signal is proportional to the sample mass in the calorimeter.[11]

Following PCA analysis on the raw power data, the outputs showed, distinctly, the presence of three different patterns. The outputs of the deconvoluted data are represented in Figure 4.6. The outputs of the three factors 1, 2, and 3 correspond favorably to the three-step reaction processes of $A \rightarrow B$, $B \rightarrow C$, and $C \rightarrow D$, respectively. These outputs are extremely encouraging and demonstrate the ability of PCA analysis to successfully return the "correct" number of principal components.

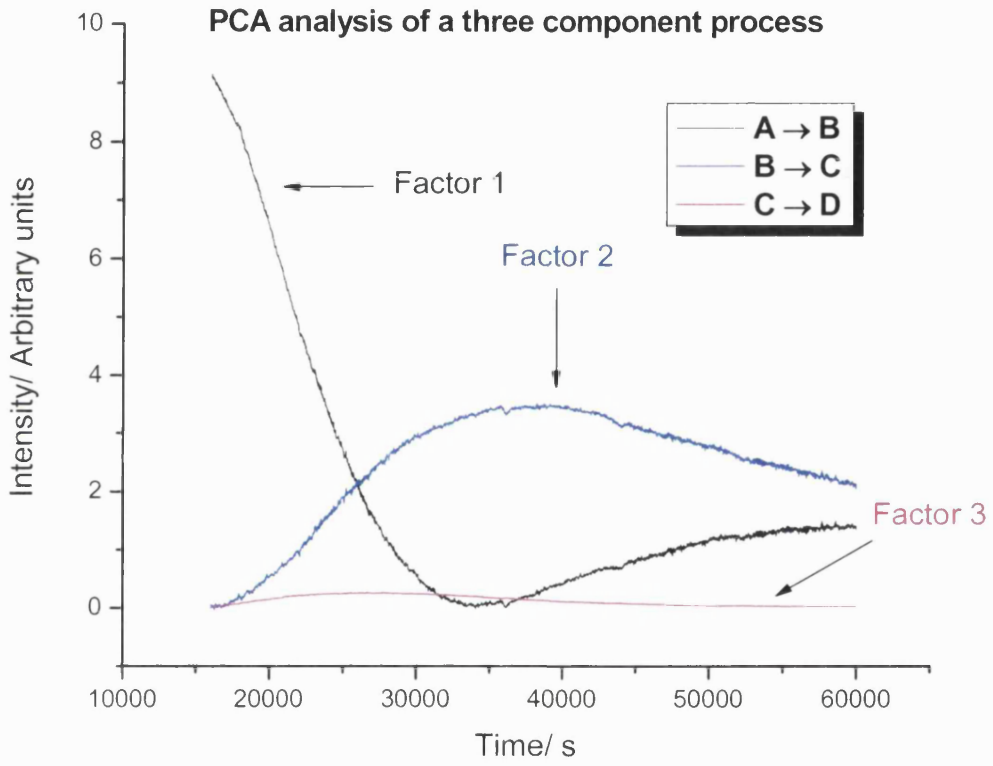

Figure 4.6: Deconvoluted outputs from chemometric analysis showing the presence of three principal components. Factors 1, 2, 3 correspond to reaction steps; $A \rightarrow B$, $B \rightarrow C$, and $C \rightarrow D$, respectively in a three-step consecutive reaction

Upon determining the three principal components in the process, it is necessary to check that each reaction process that occurred from PCA analysis conformed to an integral kinetic order. This examines the appropriateness of the output. Fitting the deconvoluted data to its corresponding single-step kinetic equation via iterative procedures[2,14,15] should return parameters for the individual reaction such as reaction order. Therefore it

is possible to check if the individual processes are of integral order. It was found that the returned values from the fittings using deconvoluted data were not integral. This is not surprising since outputs from real calorimetric data are embedded with random errors as mentioned earlier. This, in effect, will introduce some uncertainty into the returned order values. Moreover, the deconvoluted data were a composite response of eight repeat data sets, which is likely to introduce further errors to the analysis.

In general, it has been demonstrated, from the simulated data above, that chemometric analysis shows much potential in the treatment of complex IC data to determine the number of reaction processes in complex reaction schemes. Whilst the analysis was successful for simulated IC data, the challenge is in the PCA analysis of real-systems and the determination of reaction parameters thereafter. This has recently been successfully demonstrated for a two-step consecutive, first-order, reaction process for the degradation of potassium hydroxylamine disulfonate in solution.[16] PCA analysis was used to deconvolute successfully the IC data showing the presence of two principal components (two step reaction) which corresponded to the hydrolysis of the disulfonate to hydroxylamine monosulfonate and then into hydroxylamine by a two-step consecutive reaction. The data were subjected to kinetic modelling using an iterative procedure, before and after deconvolution in order to compare kinetic and thermodynamic information obtained for the individual steps. Although the rate constant was successfully obtained for the two-step process, the challenge is in obtaining thermodynamic information such as ΔH. Since the chemometric software was written specifically for spectroscopic analysis, there is a lack of knowledge of the relation between power and intensity and hence it is difficult to determine accurately values for ΔH for real systems using iterative procedures. This knowledge gap is addressed in section 4.3.2, where theoretical consideration using two approaches is given for the determination of reaction enthalpies in a two-step, first-order, consecutive reaction, which, in principle, can be applied to real systems. Note: The theoretical approach is not limited to two-step reaction schemes, and can be extended to multi-step reaction processes using the same principles.

Having deconvoluted the three-step reaction (shown above), the next step was then to establish whether it was possible to determine quantitatively reaction parameters, k, and reaction enthalpy, ΔH from the chemometric outputs.

One approach that was considered for analysis was based on analysing fractional extents of the reaction obtained from the chemometric outputs to determine reaction parameters such as rate constant, k, and reaction enthalpy, ΔH. The deconvoluted data from PCA analysis does not have a defined y-axis (as shown in Fig. 4.6). Since the software used was designed specifically for spectroscopic analysis, the y-axis is plotted as an arbitrary intensity (a result of the fact that no calibration curve is used for a deconvolution process). If analysis based on fractions of the reaction is considered, this will normalise the y-axis data. Determining a value for k should then be relatively straightforward since they are time dependent (and the x-axis, time, is unaffected by the deconvolution process). This, however, is not the case for the determination of ΔH since its value is power dependent.

A mathematical approach which can determine both parameters (k and ΔH) was thus considered for a three-step, first-order, consecutive reaction scheme (shown above in Fig. 4.2). Note: extension to multi-step schemes can be readily achieved using the same principles.

4.3.1 Determination of k following deconvolution

4.3.1.1 Calculation of k_1

Determining a value of k_1 for the first principal component (A) is relatively straightforward. A plot of ln(intensity) versus time for a reaction following first-order kinetics should be linear, and the slope of the plot gives the rate constant (Fig. 4.7).

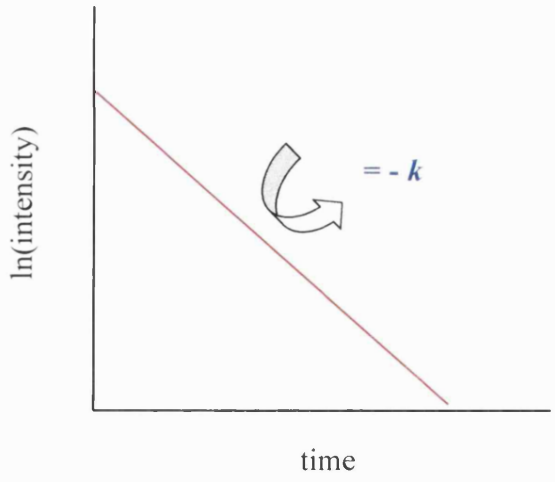

Figure 4.7: Representation of an ln(intensity) *vs* time plot for a first-order reaction

In some instances an alternative would be to plot ln(power) versus time i.e., from the observed calorimetric signal. During the initial first few hours of data, the reaction $A \rightarrow B$ may predominate. Therefore taking the slope of the (ln)power-time data over the first few hours could allow determination of k_1.

The value of k_1 was determined by plotting ln(intensity) vs time for the deconvoluted data of Factor 1. A ln(intensity) plot of Factor 1, shown in Figure 4.8, yielded a straight line over the first few hours of the reaction showing it to follow first-order kinetics. The slope of the straight line was taken from the first hour's data set and a first-order rate constant of **8.93×10^{-5} s^{-1}** was determined. This agrees favourably with the rate constant used to simulate the power-time data for the three-step consecutive reaction (ca. 9×10^{-5} s^{-1}).

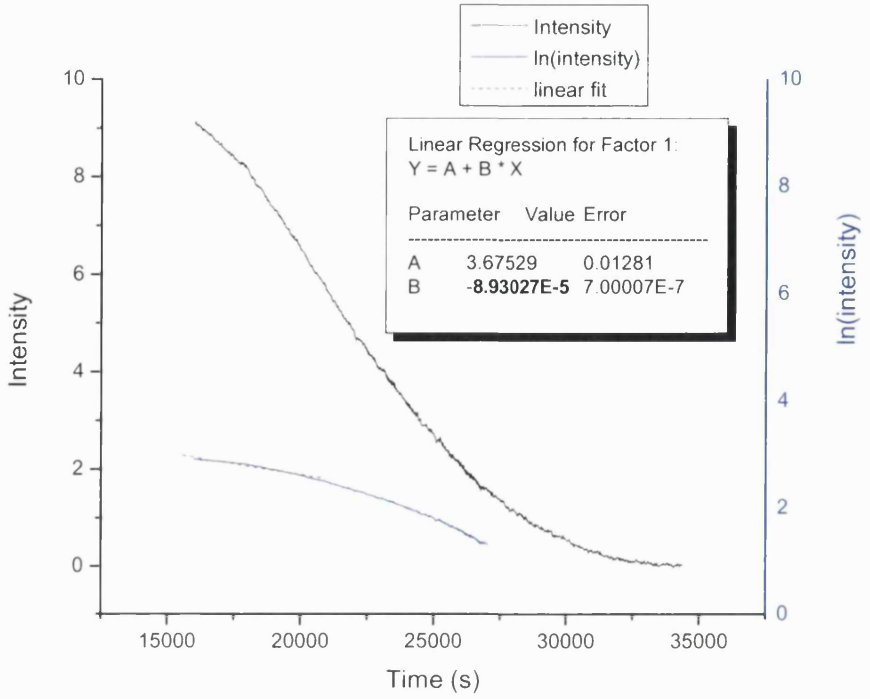

Figure 4.8: Intensity-time and ln(intensity)-time plots of deconvoluted data for Factor 1 representing step 1 ($A \rightarrow B$) in a three-step consecutive reaction. Intensity data are shown in black (—). The ln(intensity) of the deconvoluted data are represented in blue (—) and the corresponding value of k_1 was determined by application of linear regression (---)

4.3.1.2 Calculation of k_2

For a two-step consecutive, first-order, reaction ($A \rightarrow B \rightarrow C$) there is only one intermediate compound, B. It is thus possible to calculate the value for k_2 by analysing any fractional area of the reaction using the following equations (Equations 4.18 – 4.20). The concentration of product C ($[C]$) as a function of time follows;

$$[C] = A_0\left[1 + \frac{1}{k_1 - k_2}\left(k_2 e^{-k_1 t} - k_1 e^{-k_2 t}\right)\right] \qquad \text{Eqn. 4.18}$$

Consider the two-step reaction to have reached half-way i.e., when 50% of the reaction has occurred (assuming that all of A will degrade to C), it follows;

$$[C] = \frac{A_0}{2} \qquad \text{Eqn. 4.19}$$

If the fraction of the reaction (F) is taken at the time at which 50% of the reaction has occurred (t_{50}), then Equation 4.20 follows;

$$F = 0.5 = 1 + \frac{1}{k_1 - k_2}\left[\left(k_2 e^{-k_1 t_{50}} - k_1 e^{-k_2 t_{50}}\right)\right] \qquad \text{Eqn. 4.20}$$

It should be noted that this method is valid for *any* fraction of the reaction providing the reaction has progressed to completion during the experimental time frame. The value for k_2 can then be calculated by iteration since k_1 is now known.

In order to determine a value of k_2 using the above equations, data were simulated using MatchCad© for a two-step consecutive, first-order, reaction. The same data as those used to generate the three-step process (Fig. 4.3) were used, except that in this case the third step was not required. The data were imported into Origin and the value of t_{50} was determined for the second step by taking the time at which the fraction of the reaction was 50%. The data are represented in Figure 4.9 and shows that the time of t_{50} determined was **13090 s**.

The value of 13090 s was applied as the t_{50} to Equation 4.20 and returned a corresponding value of 0.5, as shown in Figure 4.10. This is in accordance with analysing 50% of the reaction. As mentioned before, the fraction of reaction analysed is not limited to 50% as illustrated in Figure 4.10 where fractions at 25% and 75%, for example, were taken after accurately determining the corresponding value of t_{25} and t_{75}, respectively.

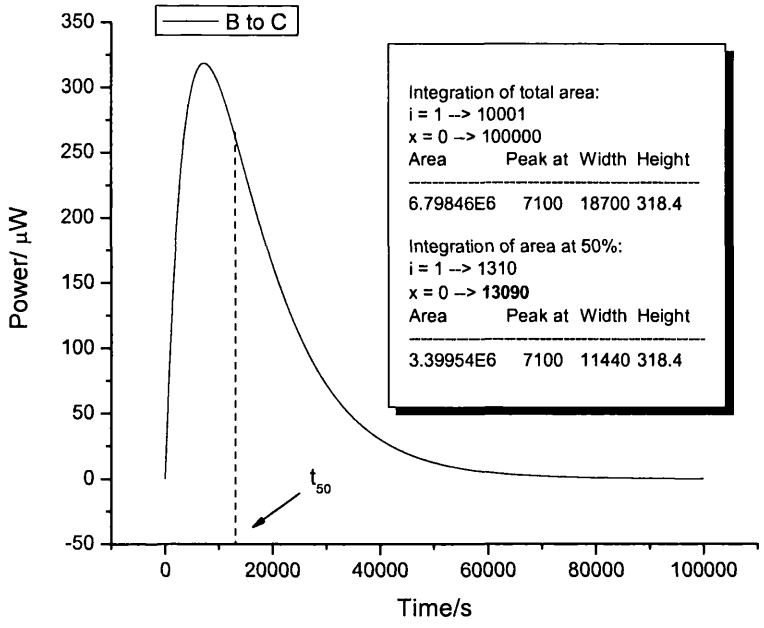

Figure 4.9: Simulated data for Step 2 ($B \rightarrow C$) representing determination of t_{50} at 13090 s when 50% of the reaction has occurred

Calculation of k_2 for step 2 (B to C) in a two-step consecutive process

$A := 7.5 \cdot 10^{-5}$ $k1 := 9 \cdot 10^{-5}$ $k2 := 2 \cdot 10^{-4}$

$H1 := 1.0 \cdot 10^{4}$ $H2 := 8.0 \cdot 10^{4}$

$t := 0, 10 .. 100000$ $t50 := 13090$ $t25 := 7360$ $t75 := 21560$

The fraction of the reaction at t_{50} then follows Equation 4.20;

$$1 + \frac{1}{k1 - k2}\left(k2 \cdot e^{-k1 \cdot t50} - k1 \cdot e^{-k2 \cdot t50}\right) = 0.5$$

Similarly, the fraction of the reaction at t_{25} follows;

$$1 + \frac{1}{k1 - k2}\left(k2 \cdot e^{-k1 \cdot t25} - k1 \cdot e^{-k2 \cdot t25}\right) = 0.25$$

And at t_{75} follows;

$$1 + \frac{1}{k1 - k2}\left(k2 \cdot e^{-k1 \cdot t75} - k1 \cdot e^{-k2 \cdot t75}\right) = 0.75$$

k_2 can then be determined at 50% (for example) using the equation below;

$k2 := 0.000001, 0.000002 .. 0.01$

$$f(k) := \frac{1}{k - k1} \cdot \left(k \cdot e^{-k1 \cdot t50} - k1 \cdot e^{-k \cdot t50}\right)$$

Figure 4.10: Simulated data for Step 2 ($B \rightarrow C$) representing determination of reaction time at various fractions of reaction

If there are more than two consecutive steps, then the rate constant for the final step of the reaction can be obtained in the same manner as above. An alternative method to determine k_2 for a reaction of more than two-steps in the reaction process is to determine the maximum yield of each intermediate product and this is determined from the t_{max}. In

terms of the calorimetric output, this corresponds to the peak power output in the power-time curve. The kinetic expression for this follows;

$$\frac{k_1 e^{-k_1 t_{max}}}{k_2 - k_1} + \frac{k_2 e^{-k_2 t_{max}}}{k_1 - k_2} = 0 \qquad \text{Eqn. 4.21}$$

The value of k can then be easily determined by iteration.

Calculation of k_2 for step 2 (*B* to *C*) in a two-step consecutive process

$A := 7.5 \cdot 10^{-5}$ $\quad k1 := 9 \cdot 10^{-5}$ $\quad k2 := 2 \cdot 10^{-4}$

$H1 := 1.0 \cdot 10^{4}$ $\quad H2 := 8.0 \cdot 10^{4}$

$t := 0, 10 .. 100000$ $\quad tmax := 7100$

Application o f t_{max} follows Equation 4.21;

$$\frac{k1 \cdot e^{-k1 \cdot tmax}}{k2 - k1} + \frac{k2 \cdot e^{-k2 \cdot tmax}}{k1 - k2} = -7.627 \times 10^{-3}$$

Figure 4.11: Simulated data for calculation of k_2 in a three-step consecutive reaction using t_{max} of intermediate step

The value of k_3 in a three-step consecutive reaction may then be obtained by analysing fractional areas using the same principles as those described above (Equation 4.20).

4.3.2 Determination of ΔH following deconvolution

As mentioned earlier, the lack of knowledge of the relation between power and intensity is a hindrance to the determination of reaction enthalpies. Below, a theoretical account

is given which considers two approaches for the determination of ΔH for a two-step, first-order, consecutive reaction.

Once the rate constants are determined, the reaction enthalpies can be readily determined in one of two ways[11,13]; (1) taking two points from the power-time data or (2) taking two points from the heat-time data (i.e. integrated power-time data). Both methods can be applied to simulated data; the power-time method is simpler, but is more subject to random noise error. Thus it is likely that, in practice, the heat-time method will be more robust because it averages data over the chosen time periods selected, hence minimising random errors.

4.3.2.1 Calculation of ΔH using power-time data

In a two-step consecutive, first-order reaction the power output for the reaction is given by the summation of Equations 4.14 and 4.15;

$$\frac{dq}{dt} = k_1 \Delta H_1 A_0 e^{-k_1 t} + k_1 k_2 \Delta H_2 A_0 \frac{e^{-k_1 t} - e^{-k_2 t}}{k_2 - k_1} \qquad \text{Eqn. 4.22}$$

From the power-time data generated using Equation 4.22, two power outputs (P_1 and P_2) can then be selected at two respective time points (t_1 and t_2). This gives;

$$P_1 = k_1 \Delta H_1 A_0 e^{-k_1 t_1} + k_1 k_2 \Delta H_2 A_0 \frac{e^{-k_1 t_1} - e^{-k_2 t_1}}{k_2 - k_1} \qquad \text{Eqn. 4.23}$$

$$P_2 = k_1 \Delta H_1 A_0 e^{-k_1 t_2} + k_1 k_2 \Delta H_2 A_0 \frac{e^{-k_1 t_2} - e^{-k_2 t_2}}{k_2 - k_1} \qquad \text{Eqn. 4.24}$$

Equation 4.23 can be re-written to make ΔH_1 the subject;

$$\Delta H_1 = \frac{P_1(k_2 - k_1) - k_1 k_2 \Delta H_2 A_0 \left(e^{-k_1 t_1} - e^{-k_2 t_1}\right)}{k_1 A_0 (k_2 - k_1) e^{-k_1 t_1}} \qquad \text{Eqn. 4.25}$$

Substitution of Equation 4.25 into 4.24 and rearranging for ΔH_2 as the subject gives;

$$\Delta H_2 = \frac{(k_2 - k_1)\left(P_1 e^{-k_1 t_2} - P_2 e^{-k_1 t_1}\right)}{k_1 k_2 A_0 \left(e^{-k_1 t_1 - k_2 t_2} - e^{-k_1 t_2 - k_2 t_1}\right)} \qquad \text{Eqn. 4.26}$$

Equation 4.26 can then be used to calculate the value of ΔH_2. When the value of ΔH_2 is known then ΔH_1 can be calculated. If $t_1 = 0$ then P_1 becomes equal to the initial power output of the reaction. Thus Equation 4.26 is reduced to;

$$\Delta H_2 = \frac{(k_2 - k_1)\left(P_1 e^{-k_1 t_2} - P_2\right)}{k_1 k_2 A_0 \left(e^{-k_2 t_2} - e^{-k_1 t_2}\right)} \qquad \text{Eqn 4.27}$$

4.3.2.2 Calculation of ΔH using heat-time data

By taking two points along the calorimetric signal (t_1 and t_2) the corresponding heat outputs (q_1 and q_2) can then determined. The heat values for q_1 and q_2 can be obtained by selecting the area under the curve between the two points, t_1 and t_2, respectively, using the approach given below. Equation 4.22 can be integrated between t_i and t_1 and t_i and t_2 (where t_i is a chosen initial time, which does not have to be zero) and yields Equations 4.28 and 4.29.

$$q_1 = A_0 \Delta H_1 \left(k_1 e^{-t_i k_1} - k_2 e^{-t_i k_1} + k_2 e^{-t_i k_1} - k_1 e^{-t_i k_1}\right) + A_0 \Delta H_2 \frac{\left(k_1 e^{-t_i k_2} - k_1 e^{-t_i k_2} + k_2 e^{-t_i k_1} - k_2 e^{-t_i k_1}\right)}{(k_2 - k_1)} \qquad \text{Eqn 4.28}$$

$$q_2 = A_0\Delta H_1\left(k_1e^{-t_2k_1} - k_2e^{-t_2k_1} + k_2e^{-t_1k_1} - k_1e^{-t_1k_1}\right) + A_0\Delta H_2\frac{\left(k_1e^{-t_2k_2} - k_1e^{-t_1k_2} + k_2e^{-t_1k_1} - k_2e^{-t_2k_1}\right)}{\left(k_2 - k_1\right)} \quad \text{Eqn 4.29}$$

If Eqn. 4.28 is re-written to make ΔH_1 the subject;

$$\Delta H_1 = \frac{\left[\frac{q_1\left(k_2 - k_1\right)}{A_0} - \Delta H_2k_2e^{-t_1k_1} + \Delta H_2k_1e^{-t_1k_2} + \Delta H_2k_2e^{-t_1k_1} - \Delta H_2k_1 - e^{-t_1k_2}\right]}{\left(-k_2e^{-t_1k_1} + k_1e^{-t_1k_1} + k_2e^{-t_1k_1} - k_1e^{-t_1k_1}\right)} \quad \text{Eqn. 4.30}$$

Eqn. 4.30 can then be substituted into Eqn. 4.29 and re-arranged for ΔH_2 to give;

$$\Delta H_2 = -q_2\left[\left(-e^{-t_1k_1} - e^{-t_1k_1}\right)\left(k_2 - k_1\right)\right] \frac{-q_1\left[\left(\left(k_2 - k_1\right)e^{-2t_1k_1}\right) + \left(\left(k_1 - k_2\right)e^{-(t_1+t_2)k_1}\right)\right]}{A_0\left(k_2\alpha + k_1\beta\right)} \quad \text{Eqn. 4.31}$$

where α and β represent;

$$\alpha = e^{-t_2k_1} - e^{-k_1(2t_1+t_2)} - e^{-t_1k_1} + e^{-3t_1k_1} \quad \text{Eqn. 4.32}$$

$$\beta = e^{-t_1k_1-t_1k_2-t_1k_1} + e^{-t_1k_2-t_1k_1-t_2k_1} + e^{-2t_1k_1-t_2k_2} - e^{-t_2k_2-t_1k_1-t_1k_1} - e^{-t_1k_2-2t_1k_1} - e^{-t_1k_1-t_1k_2-t_2k_1} \quad \text{Eqn. 4.33}$$

Therefore, Equation 4.31 can be used to calculate the value for ΔH_2. ΔH_2 is then known, ΔH_1 can be determined using Equation 4.22.

If the reaction was initiated at time zero (i.e. where $t_i = t_0$) then Equation 4.31 reduces to;

$$\Delta H_2 = \frac{-q_2\left[\left(-e^{-t_1k_1} - 1\right)\left(k_2 - k_1\right)\right] - q_1\left[\left(k_2 - k_1\right) + \left(k_1 - k_2\right)e^{-t_2k_1}\right]}{A_0k_1\left(e^{-t_1k_1} + e^{-t_1k_2-t_2k_1} + e^{-t_2k_2} - e^{-t_2k_2-t_1k_1} - e^{-t_1k_2} - e^{-t_2k_1}\right)} \quad \text{Eqn. 4.34}$$

It should be noted that in most calorimetric experiments there is a delay between the initiation time of the reaction and data recording because it takes some time (ca. 30 – 40 min) to reach thermal equilibrium after the ampoules have been lowered into the calorimeter. In the case of long term reactions the data lost is negligible and for short term reactions extrapolation of data to the initiation time is possible.[17,18] Generally, in either case, Equations 4.27 and 4.34 can be used to determine a value for ΔH_2.

4.4 Summary

Extracting quantitative reaction parameters from complex isothermal calorimetric data can be a difficult task primarily because the calorimeter measures *all* thermal processes (both to physical and chemical changes) that occur in a reaction. The challenge is therefore to deconvolute the observed calorimetric signal into its individual component parts and allow the determination of quantitative reaction parameters for each reaction step. The application of chemometric analysis offers a model-free approach to the problem of complexity in isothermal calorimetric data; i.e., no prior knowledge of the reaction mechanism is required.

In this chapter, it has been shown that the use of chemometric analysis, using principal component analysis (PCA), has much potential in the interpretation of complex isothermal calorimetric data. The deconvolution of a three-step, first-order, consecutive reaction was successfully demonstrated using this model-free approach. Successful deconvolution of the process resulted in the production of three distinct patterns of reaction that contributed towards the overall process. PCA analysis of the data matrix successfully returned the correct number of principal components corresponding favourably with the three-step reaction process. Using simulated data it was possible to construct successfully a suitable trivariate data matrix where two of the required variables consisted of power and time, which were obtained from raw calorimetric data. The third variable in the matrix was generated by running a number of replicate runs of the same experiments where each replicate run had a small variation in the number of moles of compound and, hence, the total power output. Using appropriate kinetic models, it was possible to determine reaction parameters such as rate constants for the individual steps contributing the overall process. However, the determination of reaction enthalpies is more difficult because the relation between the recovered intensity (chemometric output) and the power components of the calorimetric data (TAM output) requires further understanding. The theoretical approach considers one of two ways in which the reaction enthalpies in multi-component systems can be determined, which, in principle, can be applied to real systems.

The application of chemometric analysis to isothermal calorimetric data is relatively new and the need to generate a third variable (to create a suitable matrix) with a large number of replicate runs can be challenging in cases where a new drug compound is in

limited quantity. Nevertheless, the use of chemometrics is an extremely useful tool because the distinction of the contributing factors to the overall calorimetric signal reduces the burden on any further kinetic/thermodynamic analysis of the data by allowing an appropriate kinetic model to be employed in an iterative analysis.

4.5 References

1 Glass, B.D., Novak, C. S., and Brown, M.E. (2004) The thermal and photostability of solid pharmaceuticals. *J.Therm.Anal.Cal.* 77, 1013-1036

2 Willson, R., Beezer, A., Mitchell., J.C., and Watson, L. (1995) Determination of thermodynamic and kinetic parameters from isothermal heat conduction microcalorimetry: applications to long-term reaction studies. *J.Phys.Chem* 99, 7108-7113

3 O'Neill, M.A.A. (2005) Recent Developments for the Analysis of Data Obtained from Isothermal Calorimetry. *Curr.Pharm.Biotechnol.* 6, 205-214

4 Skaria, C.V., Gaisford, S., O'Neill, M.A.A., Buckton, G., Beezer, A.E. (2005) Stability assessment of pharmaceuticals by isothermal calorimetry: two component systems. *Int.J.Pharm.* 292, 127-135

5 O'Neill, M.A.A., Beezer, A.E., Morris, A.C., Urakami, K., Willson, R.J., Connor, J. (2003) Solid-state reactions from isothermal heat conduction microcalorimetry: Theoretical approach and evaluation via simulated data. *J.Therm.Anal.Cal.* 73, 709-714

6 Dias, M., Hadgraft, J., Raghavan, S.L., Tetteh, J. (2003) The effect of solvent on permeant diffusion through membranes studied using ATR-FTIR and chemometric data analysis. *J.Pharm.Sci* 93, 186-196

7 Geladi, P. (2003) Chemometrics in spectroscopy. Part 1. Classical chemometrics. *Spectrochimica Acta* 58 (Part B), 767–778

8 Geladia, P., Sethson, B., Nystrom, J., Lillhonga, T., Lestander, T., Burger, J. (2004) Chemometrics in spectroscopy. Part 2. Examples. *Spectrochimica Acta* 59 (Part B), 1347– 1357

9 Brown, M.E., Maciejewski, M., Vyazovkin, S., Nomen. R., Sempere, J., Burnham., A., Opfermann, J., Strey, R., Anderson, H.L., Kemmler, A., Keuleers, R., Janssens, J., Desseyn, H.O., Chao-Rui Li., Tangi, B. T., Roduit, B., Malek, J., Mitsuhashi, T. (2000) Computational aspects of kinetic analysis Part A: The ICTAC kinetics project-data, methods and results. *Therm.Acta* 355, 125-143

10 Galwey, A.K. (2003) Perennial problems and promising prospects in the kinetic analysis of nonisothermal rate data. *Therm.Acta* 407, 93-103

11 Gaisford, S., and O'Neill, M.A.A. (2007) *Pharmaceutical Isothermal Calorimetry*, Informa Healthcare

12 Gaisford, S. (1997) Ph.D Thesis. University of Kent, UK

13 O'Neill, M.A.A., Beezer, A.E., Tetteh, J., Gaisford, S., Dhuna, M. (2007) Application of Chemometric Analysis to Complexity in Isothermal Calorimetric Data. *J. Phys. Chem. B*

14 Willson, R.J. (1995) Ph.D Thesis. University of Kent, UK.

15 Willson, R., Beezer, A., Hills, A.K., and Mitchell., J.C. (1999) The imidazole catalysed hydrolysis of triacetin: a medium term chemical calibrant for isothermal microcalorimeters. *Therm.Acta* 325, 125-132

16 Skaria, C.V. (2007) Ph.D Thesis. The School of Pharmacy, University of London, UK.

17 Beezer, A., Morris, A.C., O'Neill, M.A.A., Willson, R.J., Hills, A.K., Mitchell, J.C., and Connor, J.A. (2001) Direct determination of equilibrium thermodynamic and kinetic parameters from isothermal heat conduction microcalorimetry. *J.Phys.Chem B* 105, 1212-1215

18 O'Neill, M.A.A. (2002) Ph.D Thesis. University of Greenwich, UK

- Chapter Five -

Applications

5. Introduction

Following on from the development of the photocalorimetric systems (described in Chapter 2) and having established a suitable method for actinometry allowing quantitative measurements of photon flux and irradiance (described in Chapter 3), the next step was to apply the instrument to known photosensitive materials.

Chapter 2 detailed the development of two prototype photocalorimetric systems; one design consisted of a 300 W Xe arc lamp and the latter used solid-state LED lighting. Because of the design problems inherent in using a Xe arc lamp, the data (shown in Chapters 2 and 3) showed conclusively that the design did not produce satisfactory data. As a result, the experimental measurements presented in this chapter, therefore, were conducted using solely the LED photocalorimeter.

One of the objectives for developing the LED photocalorimeter was that it allowed the opportunity to create a 'custom' light spectrum by selecting a range of LEDs that were specific to a particular wavelength. Since each LED emits over a very narrow wavelength range and the fact that a number of LEDs are arranged in an array mean that the photocalorimeter can be used to determine the causative wavelength of degradation of a sample, because it is possible selectively to switch on each LED individually.

This chapter describes the application of the novel LED photocalorimeter for photostability testing of a well known photosensitive drug, nifedipine. The main objectives are;

- to study the photosensitivity of nifedipine in solution phase and the response of the photocalorimetric output
- to determine the photostability of nifedipine across the UV–VIS range using full spectrum lightening (limited to 350 – 700 nm)
- to determine a causative wavelength range(s) of nifedipine photodegradation

5.1 Application of photocalorimetry to the photodegradation of nifedipine

Nifedipine (dimethyl 1,4-dihydro-2,6-dimethyl 1-4-(2-nitrophenyl) pyridine-3,5-dicarboxylate, $C_{17}H_{18}N_2O_6$) is a well-known photoliable substance. It has been used commonly as a calcium channel blocker, which is useful in hypertension therapy.[1] It has also been used as a vasodilator to regulate blood pressure,[1,2] prevention of myocardial ischemia,[3] and for the prevention of post-partum preeclampsia-eclampsia (pregnancy induced hypertension).[4,5] Other uses include treatment of high altitude pulmonary oedema,[6] atherosclerosis,[7] and cocaine-addiction.[8]

The photodegradation of nifedipine has been widely studied in solutions[9-12] and solid state.[12-18] Nifedipine has also found use as a test drug for photostability testing in the development of new photon sources for irradiation lamps.[19] Moreover, various strategies to protect nifedipine from light have also been studied intensively.[20-23]

Nifedipine is highly photosensitive and decomposes into two major products, nitro-and nitroso-derivatives under UV light, in the solution phase.[11] The photoproducts are represented in Figure 5.1. In the solid-state up to four decomposition products have been reported when exposed to UV light.[13] In addition to the two major products, the third and fourth photoproducts are minor. The third photoproduct has been identified as an azoxybenzene, whilst the fourth has been observed in trace amounts and yet remains unidentified.[13] The most thermodynamically stable form is the nitro-derivative, 4-(2-nitrophenyl)-2,6-dimethyl-3,5-dimethoxycarbonylpyridine, which corresponds to a dehydrogenated form of nifedipine (Product I). The nitroso-derivative, 4-(2-nitrosophenyl)-2,6-dimethyl-3,5-dimethoxycarbonylpyridine, and the azoxy-derivative, 2,2′-bis-(2,6-dimethyl-3,5-dimethoxycarbonylpyridine-4-yl)azoxybenzene (Products II and III, respectively) are metastable. The photoreactivity of nifedipine is a result of the co-presence of the hydrogen abstracting group and an easily asbtractable benzylic hydrogen. Upon exposure to sunlight, the nitro group is reduced to a nitroso group while the ring oxidises. However, under exposure to UV light, the nitroso group is reoxidised to reform the nitro group. The kinetics of nifedipine photodegradation are strongly dependent on light intensity, and wavelength distribution of the used radiation source.

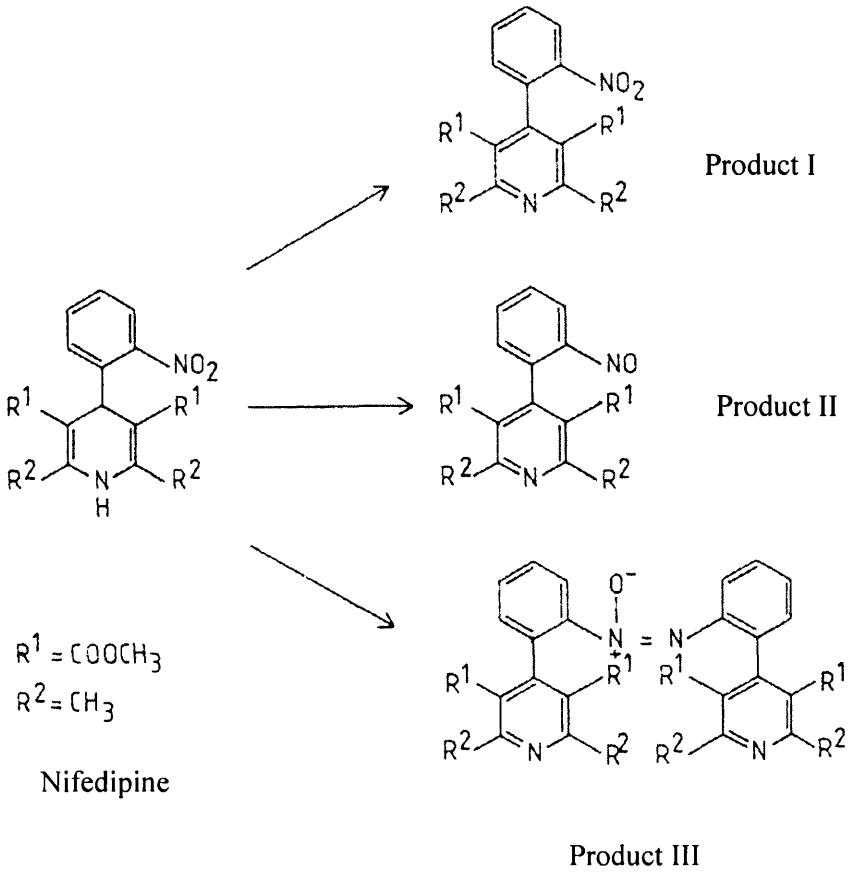

Figure 5.1: The chemical structures of nifedipine and photoproducts. Product I, nitro-derivative; Product II, nitroso-derivative; Product III, azoxy-derivative. (*Figure adapted from reference source*[13])

5.1.1 Materials and Methods

Nifedipine (>98%) was purchased from Sigma-Aldrich, UK. Ethanol (>99.7-100%) was purchased from Hayman Ltd, UK. All materials were used as received.

Nifedipine solutions (1 % w/v) were prepared for measurement. Nifedipine powder (500 mg) was dissolved using ethanol and stirred using a magnetic stirrer (approx. 30 min) until the solid had completely dissolved. The solution was then made up to volume (50 mL) in a volumetric flask with ethanol. All solutions were prepared fresh prior to

measurement light under a red light in a dark room. Amber glass volumetric flasks were used throughout and were wrapped in aluminium foil to protect from stray light.

All photocalorimetric measurements were performed using the LED photocalorimeter at 37°C. Prior to sample measurements, a reference experiment was conducted for each LED used in order to achieve an overall net zero power signal on the TAM when the light was switched on at a chosen wavelength. This was achieved by pipetting 4 mL of ethanol in both the sample and reference calorimetric ampoules (20 mL stainless steel). The ampoules method of lowering into the TAM following the lowering method described in Chapter 2 (Section 2.3.2). The voltage supplied to the sample and reference sides was preset to 15 V. The light was then switched on and the voltage on the reference side was adjusted until a zero calorimetric signal (±2 μW) was obtained. Following the reference experiment, the sample ampoule was replaced with nifedipine solution (4 mL) and the photodegradation of nifedipine was monitored. Using this procedure, the photodegradation of nifedipine in solution was monitored at 15 V under full spectrum (350 – 700 nm) coverage i.e. switching on all the LEDs comprising the array, and using monochromatic wavelength, i.e. 360 nm, 370 nm, 380 nm, 395 nm, and 400 – 700 nm. Each LED at a chosen wavelength was blanked with the reference solution individually before sample measurements at the same wavelength commenced. All measurements were taken in triplicate thus the standard deviations are given as n=3.

Photon flux values were recorded step-wise for each LED measurement using an Avantes spectrometer (already described in Chapter 3, Section 3.2). Each LED was switched on successively (15 V) and the photon flux was recorded in real-time.

5.2 Results and Discussion

5.2.1 Photodegradation of nifedipine under full spectrum light

Figure 5.2 is typical of the calorimetric output obtained for the photodegradation of nifedipine under full spectrum light i.e. covering a wavelength range of 350 – 700 nm. From the observed calorimetric outputs the magnitude of the signal is far greater than the baseline response of the reference experiment, which contained the solvent (ethanol)

system. This indicates the photocalorimeter is sensitive to the photodegradation of nifedipine.

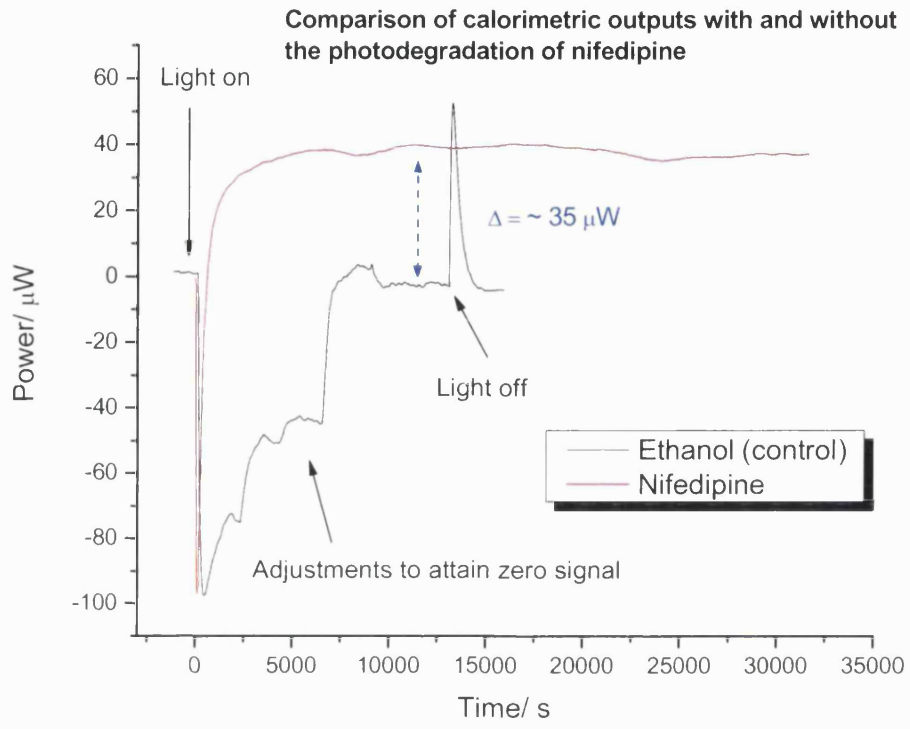

Figure 5.2: Comparison of the calorimetric outputs for the photodegradation of nifedipine in solution and Ethanol to show the photocalorimeter is sensitive to nifedipine photolysis

Figure 5.3 shows a comparison of three measurements taken for the photodegradation of nifedipine at 15 V and the power data from the outputs are summarised in Table 5.1. The power outputs stated were taken as an average for the duration of irradiation after approx. 4000 s once the signal reached plateau. According to the literature the photodegradation of nifedipine in a solution phase system initially follows zero-order kinetics and later, when the reaction proceeds to more than 50%, the kinetics behave in a pseudo-first order like behaviour.[10,11] The zero-order like behaviour is consistent with the observed calorimetric output obtained for the photodegradation of nifedipine, which shows a constant deflection of the signal from zero over ca. 9 hours observation period.

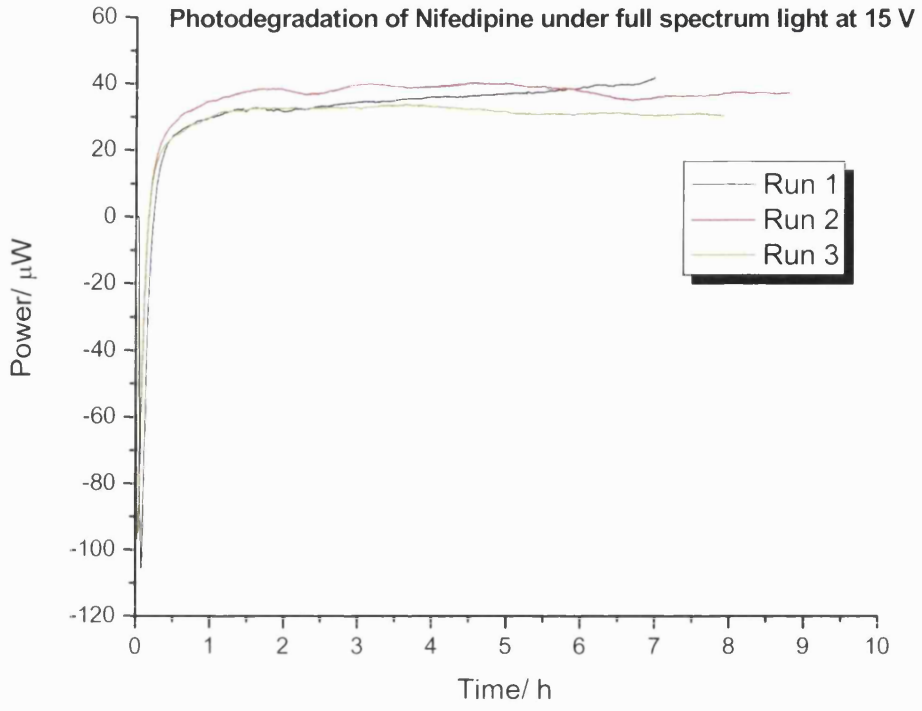

Figure 5.3: Power-time data for the photodegradation of nifedipine in solution at 15 V under full spectrum light

Table 5.1: Power data of nifedipine photolysis at 15 V under full spectrum

Run	Power signal (µW)
1	35.72
2	37.96
3	33.65
Mean	35.78
± SD	2.15
% RSD (error)	6 %

The calorimetric response of nifedipine showed a constant deflection over the irradiation period thus following zero-order like kinetic behaviour. However, any predictions about the reaction enthalpy, rate constant and duration of the photoreaction to completion are impossible to predict, without ancillary methods, because of the lack of knowledge of the changes in concentration. Further experiments are therefore

required in this area to establish such reaction parameters before the photocalorimeter can be used to produce reliable quantitative data. Thus, it is simply noted here that the preliminary tests performed shows that the photocalorimeter is working satisfactorily and is capable of monitoring the photosensitivity of nifedipine.

5.2.2 Photodegradation of nifedipine under monochromatic light

Following the photodegradation of nifedipine under full spectrum light, the application of the individual LEDs that comprise the array was tested to observe the photodegradation of nifedipine under specific wavelengths.

Figure 5.4 to 5.8 show the calorimetric outputs for the photoreactivity of nifedipine at peak wavelengths of 360, 370, 380, 395 and 400 – 700 nm (white LED), respectively. Figure 5.9 shows a comparison of the power outputs obtained under specific and full array lighting. All the power data from the outputs are summarised in Table 5.2 where the values given are an average (after approx. 4000 s as the signal reached plateau) of the three measurements.

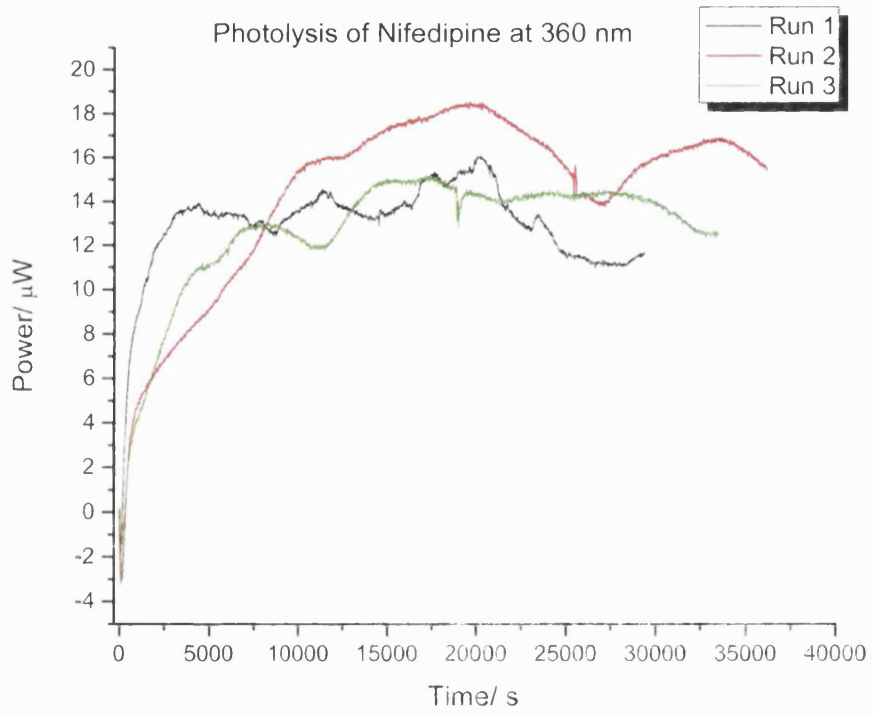

Figure 5.4: Power-time data for the photodegradation of nifedipine in solution at 360 nm

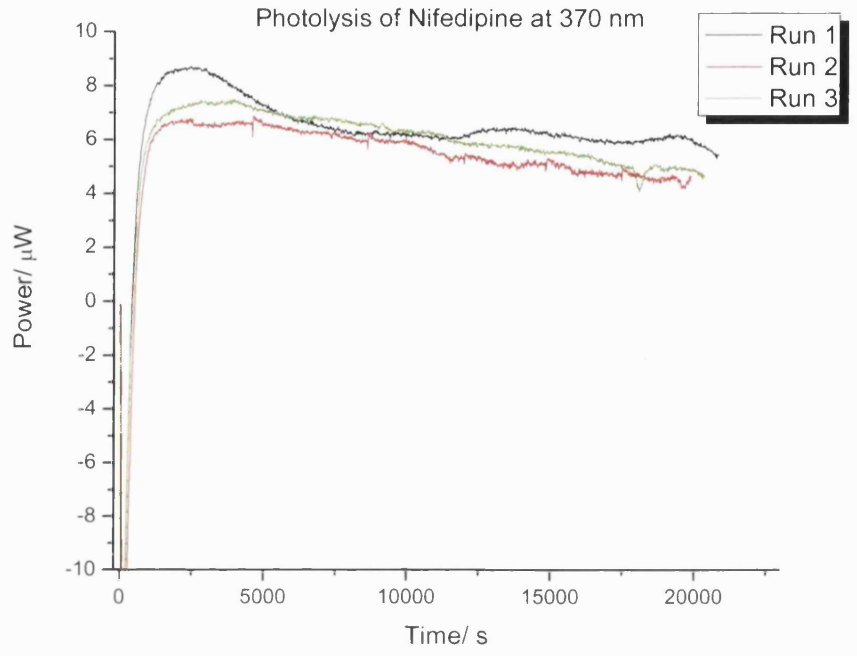

Figure 5.5: Power-time data for the photodegradation of nifedipine in solution at 370 nm

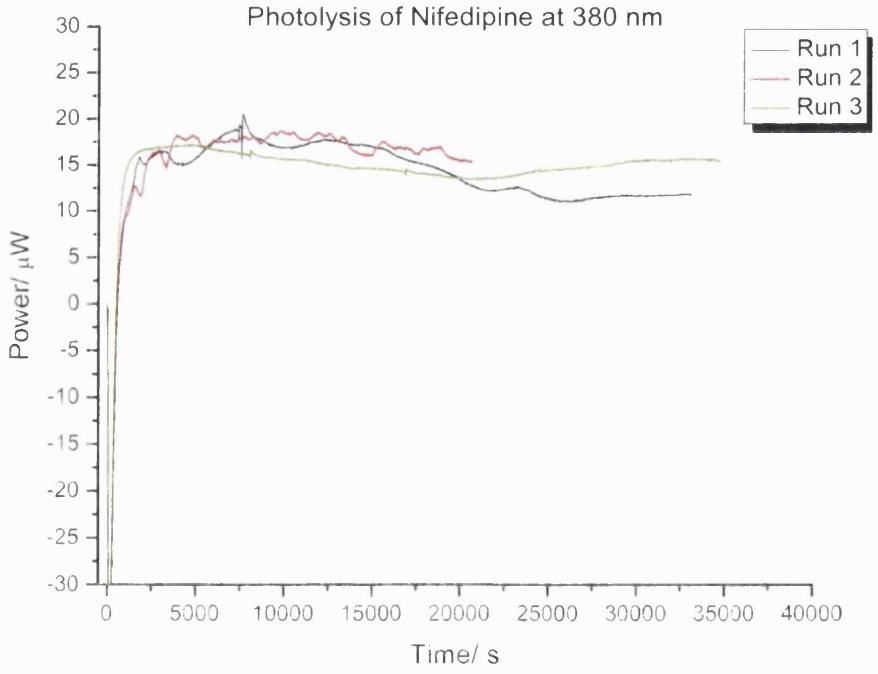

Figure 5.6: Power-time data for the photodegradation of nifedipine in solution at 380 nm

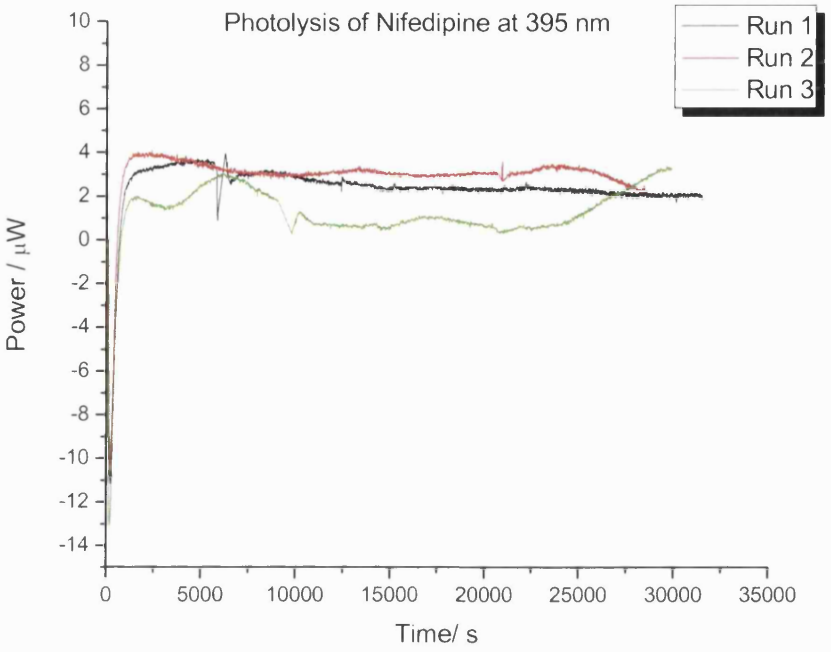

Figure 5.7: Power-time data for the photodegradation of nifedipine in solution at 390 nm

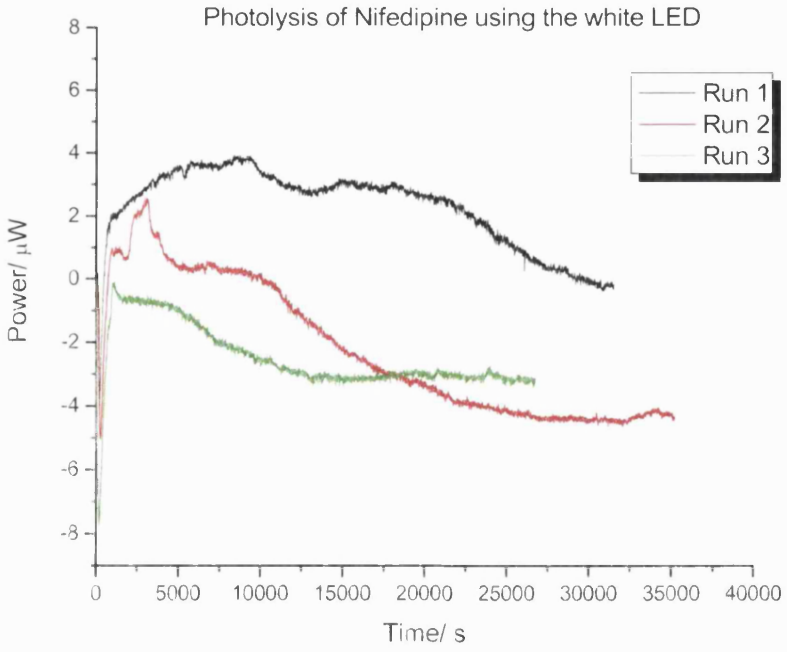

Figure 5.8: Power-time data for the photodegradation of nifedipine in solution using a white LED (400 – 700nm)

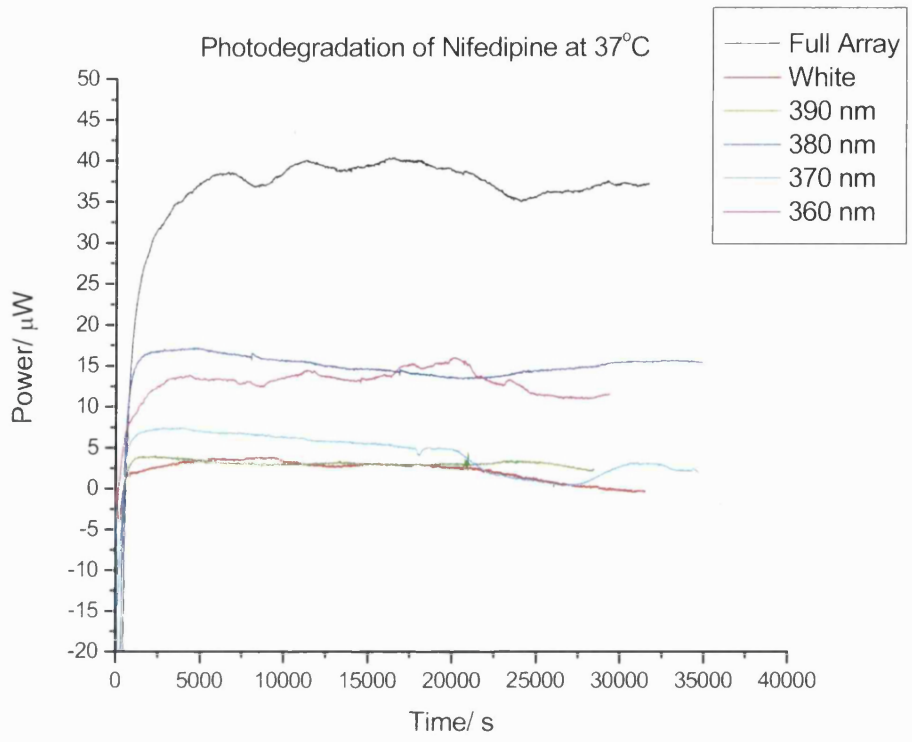

Figure 5.9: A comparison of power-time data for the photodegradation of nifedipine in solution under full spectrum lighting and varying wavelength

Table 5.2: Power data of nifedipine photolysis at 15 V under full spectrum and monochromatic lighting (n=3)

Wavelength (nm)	Power (µW)	± SD	%RSD
360	13.21	1.6	12.1
370	7.58	0.4	5.3
380	17.97	0.1	0.6
395	3.13	0.6	5.1
400-700 (white)	1.67	2.0	119.8
Full Array	35.78	2.2	6.0

The data obtained are very encouraging and show the wavelength of light significantly affects the degradation of nifedipine. The response of the power output from each wavelength tested varied showing clearly that the extent of photodegradation of nifedipine is dependent on the wavelength used. It is important to note that, however,

that the intensity of each LED is different from each other (shown below) and therefore the observed power output is not only a result of nifedipine photodegradation but is also governed by the amount of radiant energy that is delivered to the sample during irradiation. Different levels of radiant energy will impact on the calorimetric output. Since the radiant energy differs in each LED it is not possible to directly compare the extent of the power outputs that occurred during the photoreaction at each of the wavelengths tested.

It can be seen from the power-time profiles that the nifedipine photoreaction is best described as pseudo-zero-order kinetics under full spectrum lighting using the LED array and using specific wavelengths. However, it should be kept in mind that many variables such as external temperature surrounding the light guides and LED assembly, fluctuations inherent in photon delivery from LEDs, lamp life deterioration, changes in instrument geometry between sampling, sample mass variation, etc, can collectively contribute to instabilities in the calorimetric power signal during measurements, which consequently can markedly affect the kinetics of the reaction.

The maximum photodegradation of nifedipine was found at 380 nm and 360 nm, followed by degradation at 370 nm. The least photosensitivity to nifedipine and most variability in the calorimetric response were found in a wavelength range of 400 – 700 nm using the white LED. This is consistent with previous work[11,12] where studies have shown that the photodegradation of nifedipine does not appear to be caused by any specific wavelength in the visible range (typically 400 – 700 nm). This is in agreement with the power signals obtained which show minimal deflection from the baseline and range within ± 4 μW. Since the magnitude of the signal is very small and unstable, it is difficult to discriminate whether the signal is attributed to photosensitivity of reaction, variability in factors such as baseline noise (typically ± 2 μW), flux fluctuation, etc,. Consequently, any photosensitivity of nifedipine in the visible range is not obvious from these data.

The extent of the calorimetric response to nifedipine photodegradation is not only dependent on the wavelength used, but also on the intensity of the LED. As mentioned in Chapter 3, each of the LEDs comprising the array differs in intensity. The real-time measurements recorded with the spectroradiometer show the flux distribution of each

LED comprising the array is represented in Figure 5.10. The data of the corresponding intensity and LEDs are summarised in Table 5.2.

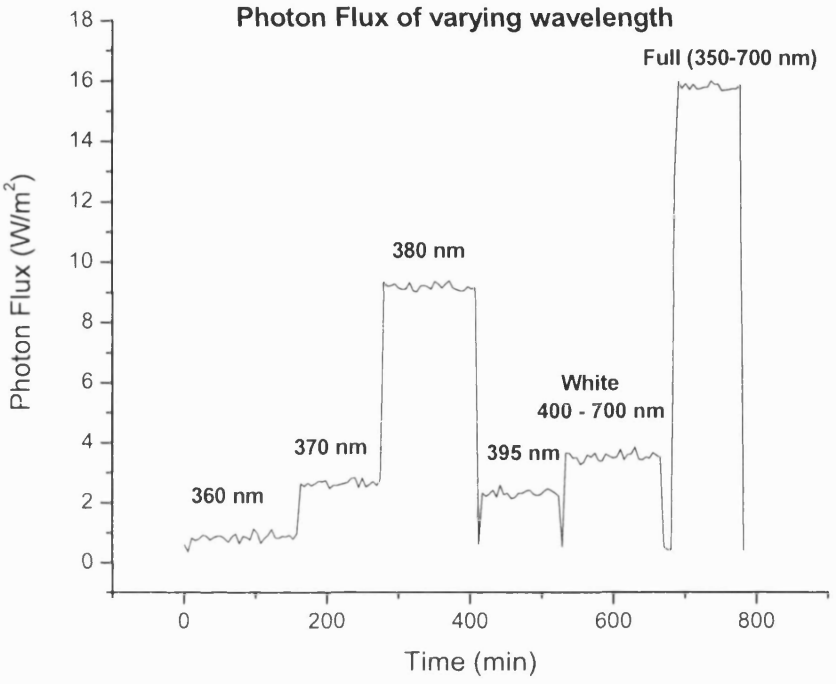

Figure 5.10: Photon flux of LEDs at varying wavelengths at 15 V

Table 5.3: Photon flux values at different wavelengths and a percentage comparison of the flux and power outputs

λ (nm)	Photon flux (W/m^2)	% Flux output	% Power output	Flux :Power ratio
360	0.71	4.21	36.92	1:9
370	2.47	14.64	21.19	1:1
380	9.28	55.01	50.22	1:1
395	1.95	11.56	8.75	1:1
White (400 – 700)	2.94	17.43	4.67	1:1
Full Array (350-700)	16.87	100.00	100.00	1:1

The flux value using the array of LEDs (16.78 W/m^2) is relatively well matched to the sum of the flux values of the individual LEDs i.e., 360 nm to white (cf. 17.35 W/m^2).

Using the flux values above, the power data from the photodegradation of nifedipine where compared as represented in Figure 5.11 below.

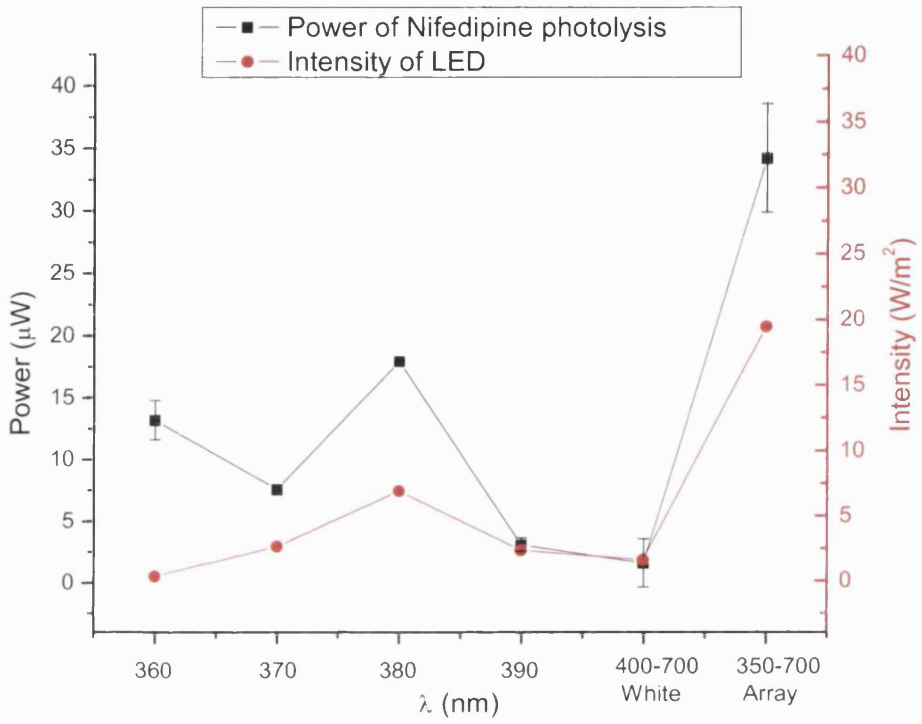

Figure 5.11: Comparison of power and intensity data obtained for the photolysis of nifedipine from each LED

Figure 5.11 generally show that the greater the intensity of the LED, the greater the power output during the photolysis of nifedipine, except that at 360 nm and 370 nm this is not the case. Although there is limited output intensity with the 360 nm LED, the calorimetric response produced is more significant than that generated at 370 nm, which has an output intensity ~3.5 times greater than the 360 nm LED. Moreover, the largest calorimetric output was that at 380 nm comprising of ca. 50% of the observed output (full array). However, it can be seen from the data presented in Table 5.3 that the response of the signal is largely predominated by the amount of light intensity generated from the LED (ca. 55% of the total flux output) and not from the photodegradation of nifedipine. Consequently, the ratio between the light intensity and power output is 1:1 suggesting that at a wavelength of 380 nm the photodegradation of nifedipine is not

notably different from that at 370 nm and above. In contrast, it is only at the wavelength of 360 nm that the photodegradation of nifedipine is more prominent where the observed power output is ~8 times greater than that of its light intensity (ratio of 1:8).

This suggests nifedipine has is particularly sensitive at a wavelength of ca. 360 nm. These data are very encouraging and agree favourably with previous studies[11,18,24] which have shown nifedipine to have maximum absorbance peak at 360 nm. In addition, the literature also reports an absorption peak at 237 nm,[11,24] but because of the nature of the instrument design it was not possible to study wavelengths below 350 nm. This can be a hindrance in a screening process for any photolabile drug which could potentially degrade below 350 nm. Thus, the focus of future work in this area therefore requires further engineering improvements to incorporate such wavelengths.

One way of dealing with the different levels of intensity can be to compensate for it with the voltage supplied to the LEDs. The adjustment of the voltage input to the each LED can be independently controlled until a desired intensity level is attained. This can be readily monitored on the spectroradiometer. Further engineering work is currently underway at The School of Pharmacy, University of London, in order to address this issue where an automated power supply is being constructed which can electronically balance the power outputs and intensity of each LED.

5.3 Summary

The LED photocalorimeter has shown much potential to monitor the photostability of nifedipine. Preliminary tests have shown that the instrument is working satisfactorily and has demonstrated much potential for the determination of nifedipine photodegradation under full spectrum and specific wavelengths of light for screening of causative wavelengths.

Having monitored the photodegradation of nifedipine at specific wavelengths; 360 nm, 370 nm, 380 nm, 395 nm and a wavelength range in the visible region (400 – 700 nm), the data showed that nifedipine photodegradation was most prominent at 360 nm. This was most noticeable since at limited intensity output, the magnitude of the calorimetric response using the 360 nm LED was much greater than those at 370 nm and above. As a result, the magnitude of the observed power output was 8 times greater than that of its light intensity. Since the intensity levels differ in each LED it was not possible directly to compare the extent of the power outputs that occurred during the photoreaction at each of the wavelengths tested. An automated power supply is, however, currently under development which can adjust the LED intensity to reach a desirable level.

In general, the data showed that nifedipine is not sensitive to photodecomposition at wavelengths above 370 nm, particularly in the visible region (between 400 – 700 nm) where no obvious photosensitivity was detected by the photocalorimeter. These data support the findings for causative wavelength studies as those reported in literature[11,12,18,24] and thus is a good indication that the instrument is working appropriately.

Although the initial trials using LEDs as a light source for the photodegradation of nifedipine are promising, the real challenge would, however, lie in deriving quantitative thermodynamic and kinetic parameters for the photoreaction in solution-phase and solid-state systems. Further work in this area is required with the need to use ancillary methods for the derivation of reaction parameters such as the rate constant. There is also a need for further instrumental development to allow for the investigation of causative wavelengths below 350 nm.

It should be anticipated that all degradation reactions are complex. This is also evident from the power-time profiles obtained from the nifedipine photodegradation using

specific wavelengths where pseudo-zero order like behaviour was observed. An interesting and useful tool for data analysis of nifedipine that can be used for future applications is based on the chemometric approach (as discussed in Chapter 4). Although not fully established yet, the chemometric approach is able to deconvolute complex reaction data.

Overall, the results show that the photocalorimeter is capable of detecting and responding accordingly to a selection of wavelengths providing a rapid method of screening nifedipine for causative wavelength in the range of 350 – 700 nm in real-time.

5.4 References

1 Yamagishi, S., and Nakamura, K. (2007) Revival of nifedipine, a dihydropyridine-based calcium blocker. *Medical Hypotheses* 68, 565-567

2 Lubsen, J., Voko, Z., Poole-Wilsond, P.A., Kirwan B., and Brouwer, S. (2007) Blood pressure reduction in stable angina by nifedipine was related to stroke and heart failure reduction but not to coronary interventions. *Journal of Clinical Epidemiology* 60, 720-726

3 Seitelberger, R., Zwolfer, W., Huber, S., Schwarzacher, S., Binder, T.M., Peschl, F., Spatt, J., Holzinger, C., Podesser B., and Buxbaum, P.,. (1991) Nifedipine reduces the incidence of myocardial infarction and transient ischemia in patients undergoing coronary bypass grafting. *Circulation* 83, 460-468

4 Sambrooka, A.M., Small, R.C. (2008) The treatment of hypertension in pregnancy. *Anaesthesia and Intensive Care Medicine* 9, 128-131

5 Podymow, T., and August, P. (2007) Hypertension in Pregnancy. *Advances in Chronic Kidney Disease* 14, 178-190

6 Maggiorini, M. (2006) High altitude-induced pulmonary oedema. *Cardiovascular Research* 72, 41-50

7 Yamagishi, S., and Nakamura, K. (2007) Prevention of diabetic vascular calcification by nifedipine, a dihydropyridine-based calcium channel blocker. *Medical Hypotheses* 68, 1096-1098

8 Calcagnetti, D.J., Keck, J., Quatrella, L.A., and Schechter, M.A. (1995) Blockade of cocaine-induced conditioned place preference: Relevance to cocaine abuse therapeutics. *Life Sciences* 56, 475-483

9 Matsuura, I., Imaizumi, M., and Sugiyama, M. (1990) Method of kinetic analysis of photodegradation: Nifedipine in solutions. *Chem.Pharm.Bull* 38, 1692-1696

10 Shamsipur, M., Bahram, H., Akhond, K.J., Ramin, M. (2003) A study of the photo-degradation kinetics of nifedipine by multivariate curve resolution analysis. *J.Pharm.Biomed.Anal* 31, 1013-1019

11 Majeed, I.A., Murray, W.J., Newton, D.W., Othman, S, and Al-turak, W.A. (1987) Spectrophotometric study of the photodecomposition kinetics of nifedipine. *J.Pharm.Pharmacol* 39, 1044-1046

12 Lehto, V.P., Salonen, J., and Laine, E. (1999) Real time detection of photoreactivity in pharmaceutical solids and solutions with isothermal microcalorimetry. *Pharm.Research* 16, 368 - 373

13 Matsuda, Y., Teraoka, R., and Sugimoto, I. (1989) Comparative evaluation of photostability of solid-state nifedipine under ordinary and intensive light irradiation conditions. *Int.J.Pharm.* 54, 211-221

14 Lehto, V.P., Salonen, J. and Laine, E. (1999) A microcalorimetric study on the role of moisture in photolysis of nifedipine powder. *J.Therm.Anal.Cal.* 56, 1305-1310

15 Marciniec, B., and Rychcik, W. (1994) Kinetic analysis of nifedipine photodegradation in the solid state. *Pharmazie* 49, 894-897

16 Vippagunta, S.R., Maul, K.A., Tallavajhala, S., and Grant, D.J.W. (2002) Solid-state characterisation of nifedipine solid dispersions. *Int.J.Pharm.* 236, 111-123

17 Aman, W., and Thoma, K. (2002) The influence of formulation and manufacturing process on the photostability of tablets. *Int.J.Pharm.* 243, 33-41

18 Morris, A.C. (2004) Ph.D Thesis. University of Greenwich, Kent, UK.

19 Matsudo, M., Machida, Y., Furuichi, H., Nakama, K. and Takeda, Y. (1996) Suitability of photon sources for photostability testing of pharmaceutical products. *Drug stab.* 1, 179-187

20 Thoma, K., and Klimek, R. (1991) Photostabilization of drugs in dosage forms without protection from packaging materials. *Int.J.Pharm.* 67, 169-175

21 Tonnesen, H.H. (1991) Photochemical degradation of components in drug formulations. I. An approach to the standardization of degradation studies. *Pharmazie* 46, 263-265

22 Tonnesen, H.H. (2001) Formulation and stability testing of photolabile drugs. *Int.J.Pharm.* 225, 1-14

23 Béchard, S.R., Quaraishi, O., and Kwong, E. (1992) Film coating: effect of titanium dioxide concentration and film thickness on the photostability of nifedipine. *Int.J.Pharm.* 87, 133-139

24 Tronchin, M., Callegarin, F., Elisei, F., Mazzucato, U., Reddi, E., Jori, G. (1998) A comparison between the photochemical and photosensitising properties of different drugs. In *Drugs: Photochemistry and Photostability* (Albini, A., and Fasani, E., ed.), The Royal Society of Chemistry

- Chapter Six -

Summary and Future Work

6. Summary and Future Work

It has been shown through the work presented in this thesis that photocalorimetry is a useful and versatile tool, which offers much potential for the routine screening of APIs in the assessment of photostability. The overall outcome is extremely encouraging in that a photocalorimeter was successfully developed, which can be used to derive thermo-kinetic information for a system during a photochemical process.

The development of a novel photocalorimeter, which utilises an array of light-emitting diodes (LEDs), has been demonstrated in Chapter 2. This was built through a series of iterative prototype designs in order to achieve the final design. It was shown that although the original photocalorimeter (developed as part of a former PhD project which utilised a xenon arc light source) was useful for providing proof-of-concept data, it was not ideal because it proved impossible to obtain a zero power signal with and without irradiating the sample cell, rendering quantitative analysis of data challenging. Subsequent re-development of the instrument was extremely encouraging and resulted in reducing the baseline signal with the light off and on. The unique shuttering and focussing assemblies featured on the optical beam splitter allowed the light to be adjusted, whilst the power output was being monitored on the TAM, until a zero power signal was obtained. However, over the course of the project, it was shown that the challenges associated in obtaining consistent quantitative data using a xenon arc lamp became apparent, primarily because of the rapid deterioration in performance of the light source. The use of LEDs as an alternative showed greater applicability as a light source for the photocalorimeter. Selecting a number of LEDs made it possible to construct an array of wavelengths in the UV-VIS range. The system was designed so that LEDs could be used all together (full spectrum) or independently within a wavelength range of 360 – 700 nm; the latter allowing the study of causative wavelength (s) by illumination of a LED at a specific wavelength. The baseline signal can be adjusted, in a similar manner to the earlier design, by balancing the voltage input, and hence light intensity, on the power supply so that a zero calorimetric power output can be obtained.

One of the issues associated with the LED photocalorimeter is that each LED within the array exhibits a different level of intensity (as highlighted in Chapters 3 and 5). This

was captured in the spectroradiometric data. Different LED intensities make it difficult to assess if the measured calorimetric response is a result of the photodegradation of the sample that takes place or from the associated radiant energy of the LED, which will also impact on the calorimetric output. One way to deal with this is to establish a level of intensity that is proportional between the LEDs by controlling independently the voltage supplied to each LED until a desired intensity level is attained. Further instrumental developments are currently under development in order to address this issue as part of the future work required in this area. An automated electronic-balancing power supply which enables the autobalance of the power signals in the sample and reference sides is currently under development as an accessory to the photocalorimeter at The School of Pharmacy, University of London. The autobalance power supply allows an electronic balance of the sample and reference power outputs so that a zero calorimetric signal can be obtained. This is achieved by increasing or decreasing the voltage supplied to the reference LED whilst the sample LED is at a fixed voltage in order to compensate for the difference in intensities, and hence power output, that exist between the two sides. A schematic of the autobalance power supply is give below in Figure 6.1 along with the workings of the system.

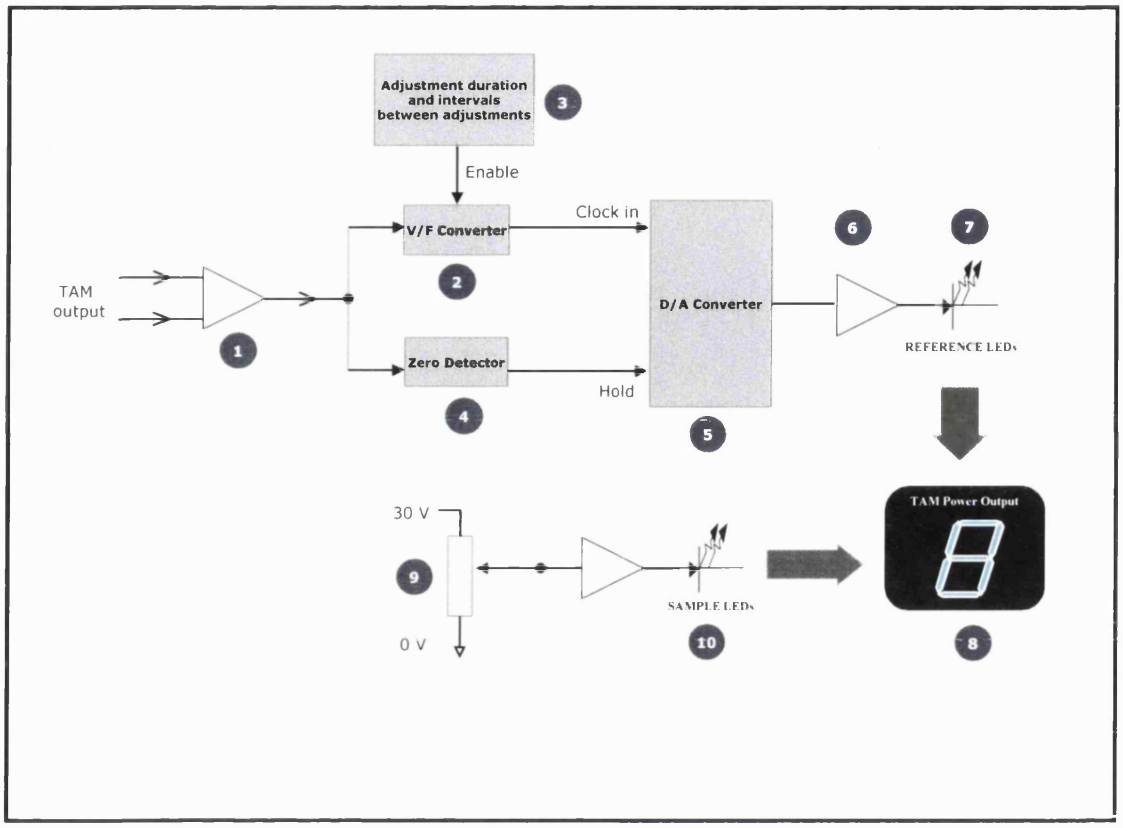

Figure 6.1: A schematic to show a circuit of the Autobalance Power Supply

1. **Differential Amplifier** – Differential operational amplifier amplifies the analogue output signal from the TAM. This signal being the out of balance or zero error signal.

2. **Voltage/Frequency converter** – The amplified zero error voltage is converted to a train of TTL (transistor-transistor logic) pulses, the frequency of which is proportional to the amplitude of the amplified zero error.

3. **Adjustment duration and the interval between adjustments** – The duration of each adjustment and the interval between each of these adjustments is defined, e.g., the system can be set to make an adjustment every 5 min for 20 ms.

4. **Zero Detector** – The zero crossing detector detects when the TAM power signal has reached zero, i.e. no zero error. Once the zero value has been detected a

signal will be sent to the D/A which halts any further change in the D/A's output voltage and therefore any further change to the voltage applied to the Reference LEDs.

5. **Digital/Analogue converter** – converts the digital count into an analogue output voltage (set between 0-5 V max).

6. **Power amplifier** – amplifies power delivered to reference LEDs.

7. **Reference LEDs** – delivers light into the reference side of the photocalorimeter (TAM).

8. **Power output displayed on TAM** – the net power signal (zero) is detected on the calorimeter after the autobalance.

9. **Sample Voltage Input** – manually set and kept constant (between 0 – 30 V max) throughout the irradiation period.

10. **Sample LEDs** – delivers light into the sample side of the photocalorimeter (TAM).

Clock in - This is an input pin to the D/A converter. The D/A can count up to 128 pulses and for every clock pulse entered. Its output will increment by 1/128 of the value set as its maximum output voltage, for example, if the maximum output is entered as 5 volts and 64 pulses, the output voltage of the D/A will be 2.5 volts. Therefore the output voltage is directly proportional to the number of pulses entered into the **clock in** input pin and the pulses will continue to be added to the previous count until the D/A is instructed to **hold.** When the D/A is instructed to **hold,** the number of pulses counted cannot be added to and the D/A output is locked. Thus when there is an output from the **zero detection** circuit indicating that the TAM output is balanced, the D/A is instructed to **hold** and its output voltage is locked.

Enable - This is an input to the V/F converter. Its role is to allow (enable) the V/F converter to pass the pulses on to the **clock in** input of the D/A. It acts like a switch which permits the pulses generated by the V/F Converter to pass to the D/A **clock in.** The pulses will be added to the count in the D/A only for the duration and at intervals that are set in "box 3" represented in Figure 6.1.

Note: The schematic represents the essence of the system and one or two interconnections are left out for simplicity.

From the actinometry work presented in Chapter 3, the photodegradation of 2-nitrobenzaldehyde (2NB) – an ICH listed chemical actinometer – was the candidate of choice as a chemical test and reference reaction for the validation of the photocalorimeter as it offered some unique advantages and is considered to follow zero-order kinetic behaviour. The data presented in Chapter 3 showed the reaction to follow non-zero-order behaviour and showed evidence towards sensitivity of non-photochemical processes suggesting the reaction is complex. This observation was more prominent with irradiation of a powerful xenon arc light source than with the LED light source. Since the magnitude of intensity produced by the xenon arc lamp is far greater than that generated by the LEDs, there is the possibility for the occurrence of additional secondary or thermal decomposition processes. The reaction therefore requires further investigation in the future. A number of problems were also highlighted using the xenon arc lamp, namely short lamp life and variable output, which made it difficult to obtain consistent data. In contrast, the application of LEDs as a light source demonstrated much potential for the assessment of photostability and using suitable equations it was possible to derive reaction parameter such as rate constant (k), reaction enthalpy (ΔH), Irradiance (I_0) and Photon Flux (F_0) for 2NB. The complexity observed with 2NB using the xenon arc lamp and LED system were evident through the variation in the value of ΔH obtained, which should, in principle, remain constant regardless of the reaction mechanism providing the products remain the same and the initial and final concentration remains constant. Thus, the sensitivity to non-photochemical processes of 2NB and its complexity limits the usefulness of 2NB as a suitable chemical test and reference reaction for photocalorimetry and validation of instrument performance. Other potential chemical actinometric systems must therefore be sought for the photocalorimeter.

Dealing with the interpretation of complex isothermal calorimetric data without the prior knowledge of a reaction mechanism was successfully demonstrated in Chapter 4 by the application of chemometric analysis using principal component analysis (PCA). Using simulated data for a three-step, first-order, consecutive reaction, PCA successfully returned the correct number of principal components for a three-step

reaction process. It has been shown that it is possible to construct successfully a suitable trivariate data matrix where two variables can be obtained from raw calorimetric data; power and time, and the third can be generated by running a number of replicate runs of the same experiments where each replicate run had a small variation in the number of moles of compound and, hence, the total power output. The use of chemometrics has been shown to be a useful tool in the interpretation of complex calorimetric data and one which reduces the burden on further kinetic/thermodynamic analysis of the data. The real challenge, however, is to be able to convey the theoretical approach (considered in Chapter 4) to a real-system for the derivation of reaction parameters. One system that could be an interesting candidate for use as part of future work in this area is that of nifedipine (described in Chapter 5), principally because the reaction is complex in nature and comprises at least three products.

The application of photocalorimetry to test the photostability of nifedipine was very encouraging and showed the LEDs were able to successfully detect photodegradation under full spectrum and specific wavelength lighting as shown in Chapter 5. Working through the series of specific wavelengths showed that nifedipine photodegradation was at its maximum at 360 nm giving a good indication that the instrument was working appropriately. Initial trials using LEDs as a light source for the photodegradation of nifedipine were very promising. Further work in this area is required using ancillary methods for the derivation of reaction parameters which subsequently can be applied to those in photocalorimetry. Further instrumental improvement would also be required if studies below 350 nm are to be performed. Overall, the ability for the photocalorimeter to be able to select specific wavelengths has provided a way for the rapid screening for causative wavelength of nifedipine in real-time.

Appendix

The work reported in this thesis has been published in the following journals:

Dhuna, M., Beezer, A.E., Morris, A.C., Gaisford, S., O'Neill, M.A.A., Hadgraft, J., Connor, J.A., Clapham, D., Frost, J. (2007) Development of an Isothermal Heat-Conduction Photocalorimeter. *Rev Sci Instrum* 78 (doi:10.1063/1.2670220), 025105

O'Neill, M.A.A., Beezer, A.E., Tetteh, J., Gaisford, S., **Dhuna, M.** (2007) Application of Chemometric Analysis to Complexity in Isothermal Calorimetric Data. *J. Phys. Chem. B* 111, 8145-8149

Development of an isothermal heat-conduction photocalorimeter

Meena Dhuna and Anthony E. Beezer
The School of Pharmacy, University of London, 29-39 Brunswick Square, London WC1N 1AX, United Kingdom

Andrew C. Morris
Medway Sciences, University of Greenwich, Medway Campus, Chatham Maritime, Kent ME4 4TB, United Kingdom

Simon Gaisford,[a] Michael A. A. O'Neill,[b] and Jonathan Hadgraft
The School of Pharmacy, University of London, 29-39 Brunswick Square, London WC1N 1AX, United Kingdom

Joseph A. Connor
Medway Sciences, University of Greenwich, Medway Campus, Chatham Maritime, Kent ME4 4TB, United Kingdom

David Clapham
GlaxoSmithKline, New Frontiers Science Park, Harlow, Essex CM19 5AW, United Kingdom

John Frost
The School of Pharmacy, University of London, 29-39 Brunswick Square, London WC1N 1AX, United Kingdom

(Received 31 December 2006; accepted 21 January 2007; published online 22 February 2007)

Assessing photostability (particularly of pharmaceuticals) is of growing importance, but hampered by a lack of reliable, rapid experimental testing protocols and instrumentation. In particular, most approaches require irradiation of the sample separately from the analytical measurement, which increases both experimental complexity and the number of assumptions that must be made when calculating stability. One technique that may obviate this is photocalorimetry, principally because the reporter of change (heat) is measured directly as a sample is irradiated. Although not a new idea, the design challenges of photocalorimeters are complex, primarily because light power is being introduced to the calorimeter which can thus both saturate the amplifiers and swamp the response of the sample. Careful instrument design is thus paramount. The aim of this work was to develop a robust, compact, and easy to use photocalorimeter with the immediate focus of developing photostability assays for pharmaceuticals. The final instrument design, arrived at through a series of iterative design modifications, is based on a twin differential heat-conduction principle and achieves an average base line deflection of -0.04 ± 0.11 μW with light irradiating the sample cell. The performance capabilities of the instrument were demonstrated using a model system; the photodegradation of 2-nitrobenzaldehyde in solution. © *2007 American Institute of Physics.*
[DOI: 10.1063/1.2670220]

I. INTRODUCTION

There are a number of reasons why assessment of photostability is desirable; to quantify the stability of a molecule or product under "white light" conditions, to determine stability as a function of wavelength (which may give mechanistic information on the degradation reaction), to develop packaging materials that can ameliorate the effects of photodegradation, and (pharmaceutically) to estimate the *in vivo* photosensitizing potential of a drug from its *in vitro* photostability (photolabile drugs are often used for chemotherapy, for instance).

In spite of the existence of the International Conference on Harmonisation (ICH) Q1B guideline on photostability testing, there are in practice a number of methods in existence practically to perform a photostability test. Most methods irradiate samples separately from the analytical instrument used to quantify any degradation that does occur. It is also difficult to quantify photostability of multicomponent products because the analyte(s) must be isolated prior to measurement. Photocalorimetry (the measurement of the heat change when a sample is irradiated) offers a direct method with which to assess photostability, because the data recorded (power as a function of time) are acquired in real time, in a noninvasive manner, and are easily interpreted in (at least) a qualitative fashion (although quantitative interpretation is also achievable).

Although the principle of photocalorimetry has been known for many decades,[1] the design challenges inherent

[a]Author to whom correspondence should be addressed; FAX: +44 (0)20 7753 5942; electronic mail: simon.gaisford@pharmacy.ac.uk
[b]Present address: Department of Pharmacy and Pharmacology, University of Bath, Bath, BA2 7AY, United Kingdom.

when introducing light (a power source) into an extremely sensitive calorimetric cell are considerable and it is currently the case that no isothermal photocalorimeters are commercially available (although a photocalorimetric accessory for differential scanning calorimeters is available from Mettler-Toledo). Here we report the development and early trials of an isothermal heat-conduction photocalorimeter; the design brief was to produce a robust, compact, easy to use instrument, capable of yielding data open to qualitative and ideally quantitative interpretations. The ideal instrument would also be able to deal with solid samples as well as those in the liquid state.

II. MATERIALS AND METHODS

2-nitrobenzaldehyde (2-NB) (>98%) and ethylenediamine tetra-acetic acid (EDTA) were purchased from Sigma. Ethanol (>99.5%) was purchased from Hayman Ltd. Deionized water was used throughout. All materials were used as received.

The 300 W Xe arc lamp, O_2-free (model 6258), and liquid light guides (model 77554) were purchased from LOT-Oriel UK Ltd. Optical components (38 mm^2 polka-dot mirror, Part No. A46-461; first surface mirror, Part No. A31-422; plano-convex lens, UV-AR coated, 25.4 mm, Part No. A46-267; and plano-concave lenses, 25.4 mm, Part No. A08-026) were purchased from Edmund Optics Ltd.

A. Preparation of the actinometric solutions

2-NB (1.5211 g) was accurately weighed and crushed in a pestle and mortar. The solid was dissolved in a 1:1 v/v water:ethanol mixture by stirring for 1 h. The solution was then made up to 100 ml using the same solvent. The final concentration of 2-NB was thus 0.1*M*.

B. Photocalorimetry

Calorimetric data were recorded with a 2277 thermal activity monitor (TAM) (Thermometric AB, Sweden) at 25 °C. The TAM works on a heat-conduction principle; the sample is surrounded by a heat sink which is maintained at a constant temperature. Any heat released (or absorbed) by the sample is quantitatively exchanged with the heat sink via a series of thermocouples (a thermopile). The thermopile produces a voltage signal which is amplified and converted to a power signal. Each channel comprises a sample and a reference side; the sides are connected in opposition and hence the output data are the differential response of the sample and reference thermopiles. The instrument was fitted with 20 ml calorimetric channels into which the photocalorimeter was designed to fit. Although it underwent a number of detail changes, the overarching design was common and consisted of light from an external source (a Xe arc lamp set to an output power of 240 W) being directed into sample and reference cells. Data were recorded with the dedicated software package DIGITAM 4.1 and experiments were run at least in triplicate. The instrument was calibrated periodically by the electrical substitution method and was set to an amplifier range of 300 μW. Data are presented throughout with a standard deviation (calculated as σ_{n-1}).

The photocalorimeter was zeroed before use by setting the light intensity on the sample side to a predetermined level (determined with an external radiometer) and adjusting the light power on the reference side until the TAM reported a zero signal. Prior to any measurement the Xe arc lamp was allowed to warm up for 1 h. Stainless steel (20 ml) calorimetric cells were used throughout. The sample cell was charged with 2-NB solution (0.1*M*, 4 ml) and the reference cell with 1:1 v/v water:ethanol (4 ml). The apparatus was allowed to equilibrate in the TAM before the commencement of sample irradiation.

C. *p*H determination

The 2-NB solution was set up in the photocalorimeter as noted above, although temperature control was ensured by using a temperature-controlled block rather than by the TAM, and irradiated for various periods of time (10 min increments to a total irradiation time of 3 h). The *p*H of the solution was determined after each period of irradiation with a *p*H meter (Hamilton glass electrode). Experiments were conducted in the presence and absence of EDTA (50 mg per 100 ml).

III. INSTRUMENT DESIGN

The principle of photocalorimetry is not new, first being recorded by Magee *et al.*[1] who studied the quantum efficiency of photosynthesis in algae (*Chlorella pyrenoidosa or Chlorella vulgaris*) and subsequently by Seybold *et al.*,[2] Olmsted,[3,4] and Adamson *et al.*[5] However, these instruments all had quartz windows to facilitate the photochemical measurement and were hence cumbersome and not particularly sensitive. More modern instrument designs obviate the need for transparent windows by using optical light guides to introduce light into the ampoules. These enable the calorimetric cell to be fully enclosed in a thermostat and to be made of a single material. Schaarschmidt and Lamprecht[6] first described the use of light guides in photocalorimetry in developing photocalorimeters for the study of living yeast cells. Cooper and Converse[7] transformed a LKB batch calorimeter into a photocalorimeter by fitting it with quartz optical fiber light guides for their study of the photochemistry of rhodopsin.

Teixeira and Wadsö[8] developed a differential photocalorimeter utilizing two twin calorimeters (i.e., employing four vessels, two samples with two corresponding references). Fiber-optic bundles guided light from a 100 W tungsten lamp through a monochromator before being split equally into the two sample vessels. One vessel, a stirred perfusion/titration vessel, was used for the measurement of the thermal power during a photochemical reaction. The other served as a photoinert reference. The differential signal was recorded for each of the two twin calorimetric vessels. Subsequent work by Dias *et al.*[9] utilized a similar design, but the two light guides were fed into the sample and reference channels of one twin calorimeter. The reference side was photoinert, quantitatively transforming the entire incident light. The position of the optical fibers was adjusted to maintain a stable

base line with and without illumination. In such conditions, the same heat output is measured in both vessels and thus the net output is zero.

Such an arrangement forms the basis of the photocalorimeter described here. The instrument directs light from a single point source (a Xe arc lamp, set to an output of 240 W) into sample and reference cells. The cells are housed in a TAM. The reference cell is connected in opposition to the sample cell, which means that any heat introduced to the sample cell by the incident light should be automatically compensated for by the same quantity of light entering the reference cell. The design process that resulted in the final apparatus configuration was iterative and resulted in the construction of two principal instruments. These iterative steps and the experimental observations that refined the initial apparatus design to the design described here are discussed below.

A. Design 1

In the initial configuration light was directed from the lamp through a collimating lens and IR filter into a fiber-optic bundle. The bundle was trifurcated: one branch directed light to the sample cell, one to the reference cell, and the third to an external actinometer. A significant problem with this arrangement was that it proved impossible to get a repeatable base line signal with the light on or off (the average base line value recorded was 74.1 ± 8.1 μW).

B. Design 2

Dealing with the inability to attain a zero base line first, the primary problem was the fixed geometry of the sample and reference cells relative to each other. Unless aligned perfectly with the TAM, it was always the case with Design 1 that one cell would sit higher in its channel than the other. The original reason for fixing the geometry was to keep the fiber-optic bundles in a consistent position because of their fragility. Switching to liquid-filled light guides obviated this need. In addition, because liquid light guides are flexible, it was possible to raise and lower each cell from the TAM individually, removing the need for the trolley and making the apparatus more compact. This change resulted in an average base line value of 0.5 ± 0.3 μW.

The remaining issue was to attain a zero base line signal with the light on. This was achieved by incorporating a beam splitter between the lamp and the liquid light guides. The beam splitter, the basic design of which is represented in Fig. 1, uses a polka-dot and front-surface mirror to divide the light into two equal beams (50% of the light is reflected through 90°, while the remaining 50% continues straight through; a second mirror then reflects this light through 90° into the reference ampoule). The beams can then be further adjusted in intensity using a number of focusing and shuttering assemblies.

Using the beam splitter and liquid light guides allows a simple, but very controllable experimental strategy to be adopted when setting up the photocalorimeter. The light power introduced to the sample cell is adjusted until a specific value is obtained; the precise value can be quantified

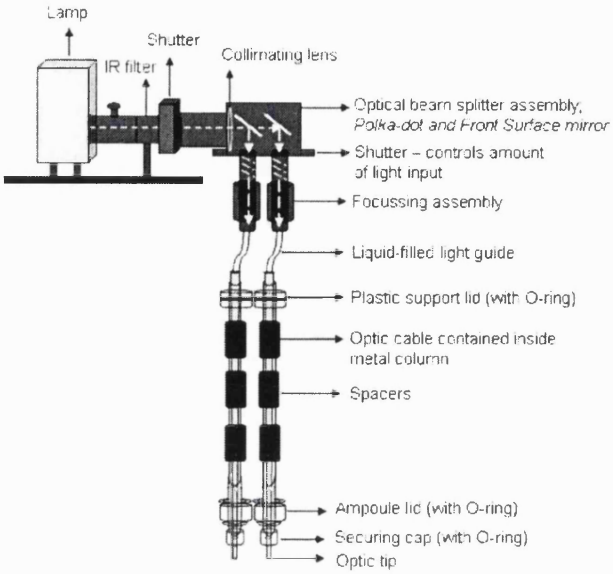

FIG. 1. A schematic of the final instrument design.

using an external radiometer and the value can be altered for individual experiments. Calorimetric data are then recorded, while the preset light power enters the sample cell and the shuttering and focusing assemblies are adjusted on the reference side until the calorimetric power signal reduces to zero. In effect, during setup the calorimeter itself is used as a null-adjust balance to ensure parity between the sample and reference sides.

Two important points arise from using this methodology. First, attainment of a zero base line signal does not mean that the light powers being introduced to the sample and reference cells are equal; it means that the differential power signal recorded by the calorimeter is zero. Necessarily, small instrumental differences (such as in the geometry of the channels, the fit of the cells in the channel, the electronic circuitry, and so on) act to produce different output signals for the same input. However, this is not relevant when the instrument is used for quantitative work on real samples (and is, indeed, the principal reason why differential calorimeter designs are adopted). The only relevant factor is the light power irradiating the sample and that is known exactly from the radiometry data. Second, the approach ensures equivalence in the operating performance of multiple instruments because, as noted above, the light power irradiating the sample is precisely set and quantified. This means that the exact conditions under which data have been recorded can be defined and, more importantly, repeated in subsequent measurements. This is an essential quality if validation and calibration routines are to be developed.

Note also that with further development of a suitable actinometric reference material, it will be possible to use the calorimeter for quantifying the light power introduced to the sample ampoule, obviating the need for an external radiometer.

Typical data showing the base lines attained with and without light are shown in Fig. 2. The effects on the calorimetric output when undertaking the steps described above

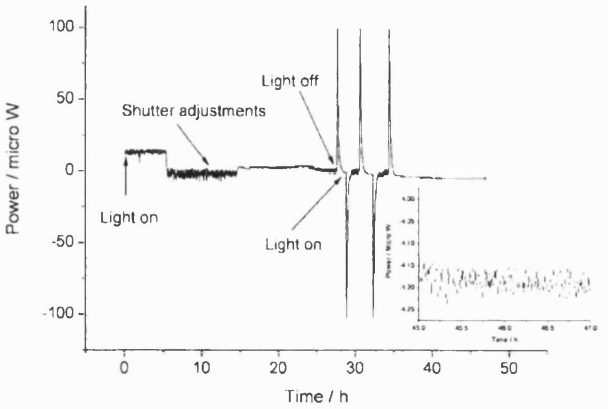

FIG. 2. The effect on the base line of adjustment by the focusing and shuttering assemblies of the beam splitter (Inset graph: an expanded view of the base line postadjustment).

are evident and the base line signals in the presence and absence of light are almost equal (-0.04 ± 0.11 and 0.07 ± 0.06 μW, respectively) and compare favorably with the manufacturer's stated base line noise (±0.2 μW). A schematic representation of the final instrument design is given in Fig. 1.

C. Chemical actinometry

As we have noted previously[10] there are many reasons why the *in situ* validation of instrumental performance is preferable to external calibration. For photodegradation a substance that can act as a chemical actinometer is required. There are a number of guidelines that deal with photostability testing and chemical actinometry but, at present, there is no uniformly accepted system. ICH guideline Q1B (photostability testing of new active substances and medicinal products) indicates a chemical actinometer based on quinine, while International Union of Pure and Applied Chemists (IUPAC) indicates the use of potassium ferrioxalate.[11] The use of quinine is hampered by the fact that the quantum yield of the reaction is unknown. Potassium ferrioxalate must be prepared in the dark under an inert atmosphere and our experience makes us feel that this system is therefore not robust enough to be useful as a general test and reference reaction. Hence, for this initial investigation, we decided to look at the suitability of an alternative system; the photodegradation of 2-NB. 2-NB has been suggested as a chemical actinometer for photostability testing as it is convenient and easy to prepare/handle.[12,13]

Typical data for the irradiation of 2-NB are shown in Fig. 3. The data shows that the photocalorimeter is sensitive to photodegradation and that the magnitude of the signal is much greater than the base line response. A zero-order response was expected (ideally a constant deflection from zero) but it can be seen that this was not observed, there being a non-zero-order region extending for ca. 5 h following the start of irradiation. In order to understand the cause of this discrepancy, it was decided to follow the progress of the photodegradation by monitoring the changes in *p*H as the photodegradation product, 2-nitrosobenzoic acid (2-NBA), was formed. The concentration of product formed versus irradiation time profile is shown in Fig. 4. Here, unlike the calorimeter, the technique is only sensitive to a change in acidic or basic components; it can be seen that over the initial period the *p*H remains constant before increasing linearly with time. This implies that an additional event is occurring prior to photodegradation. Suspecting that an oxidation process was responsible, the experiment was repeated with the addition of a small quantity of EDTA (which chelates any free metal ions and prevents them catalyzing oxidative processes). These data showed pseudo-zero-order kinetics for the duration of measurement, Fig. 4, although a small break point still appears at ca. 100 min. Although, at this stage, it is not possible to define the oxidation event, the data suggest that this is the likely cause for the non-zero-order region observed in the calorimeter. Repeating the calorimetric experiment with the inclusion of EDTA produced a notably different response, although, as noted in the *p*H data, the data were still not truly zero order, Fig. 3. Since an exhaustive study of the photodegradation of 2-NB was not the objective of the present study, further discussion of this system will not

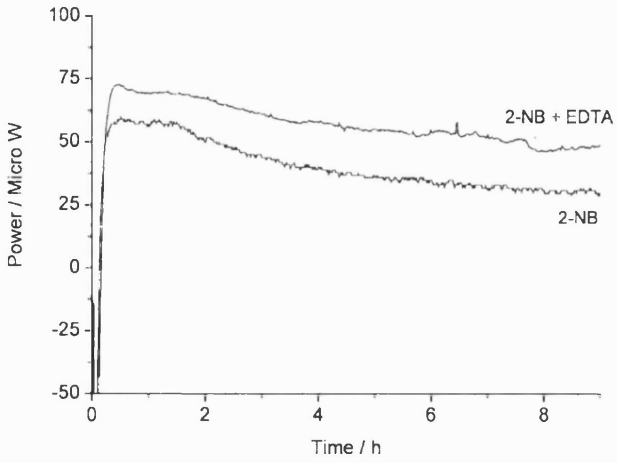

FIG. 3. Power-time data for the photodegradation of 2-NB, showing a non-zero-order phase immediately after the commencement of irradiation and for the photodegradation of 2-NB with EDTA.

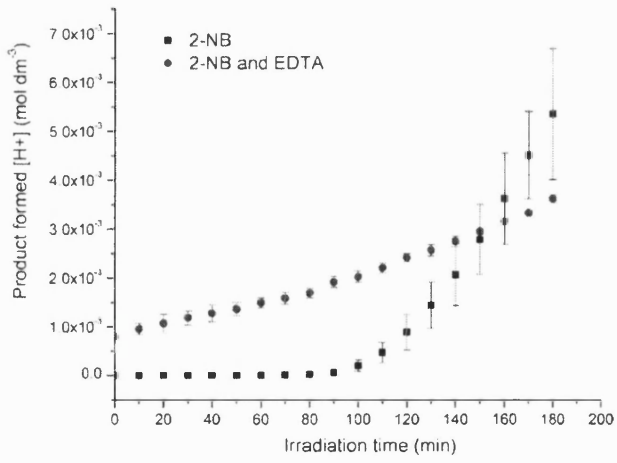

FIG. 4. *p*H data for the photodegradation of 2-NB, in the presence and absence of EDTA.

be presented here. However, we simply note that the degradation of 2-NB appears to be very sensitive to the method of preparation and will return to the subject of its use as a test and reference material for photocalorimeters in a future publication.

IV. SUMMARY

A photocalorimeter has been developed based on a twin differential heat-conduction design. The instrument is robust, compact, and gives a zero calorimetric signal when light is irradiating the sample and reference cells; the design brief was thus met. In the course of the development several factors were found to be critical to ensuring proper operation of the instrument: the geometry of the sample and reference cells relative to each other and, more importantly, to the calorimeter; the nature of the light guides used to direct light to the cells; and the need for systems to adjust the light intensity of the sample and reference sides. In particular, the adjustability of the light intensity means that a novel strategy for zeroing the instrument could be implemented; the power on the sample side is set to a predetermined level, while that of the reference side is adjusted until the calorimeter reports a zero signal. Thus, the calorimeter itself is used as a null adjuster to ensure (thermal) equivalence between the sample and reference cells.

The performance of the instrument was tested using 2-NB as a model system, specifically because it has been proposed as a chemical actinometer for photostability assays.[12,13] Although a zero-order response was expected, the initial data exhibited non-zero-order behavior. Subsequent investigation of the system using a *p*H assay suggested that the likely explanation of this was an additional oxidation event which occurred prior to photodegradation of 2-NB. Subsequent experiments with a 2-NB solution containing EDTA to inhibit oxidation produced results that more closely followed a zero-order pathway, both by *p*H measurement and by utilizing the photocalorimeter. A discussion of the relative merits of 2-NB as a chemical actinometer for photocalorimeters will thus form the basis of a future investigation.

[1] J. L. Magee, T. W. DeWitt, E. C. Smith, and F. Daniels, J. Am. Chem. Soc. **61**, 3529 (1939).
[2] P. G. Seybold, M. Gouterman, and J. Callis, Photochem. Photobiol. **9**, 229 (1969).
[3] J. Olmsted III, Rev. Sci. Instrum. **50**, 1256 (1979).
[4] J. Olmsted III, J. Am. Chem. Soc. **102**, 66 (1980).
[5] A. W. Adamson, A. Vogler, H. Kunkely, and R. Wachter, J. Am. Chem. Soc. **100**, 1298 (1978).
[6] B. Schaarschmidt and I. Lamprecht, Experientia **29**, 505 (1973).
[7] A. Cooper and C. A. Converse, Biochemistry **15**, 2970 (1976).
[8] C. Teixeira and I. Wadsö, J. Chem. Thermodyn. **22**, 703 (1990).
[9] P. B. Dias, C. Teixeira, and A. R. Dias, J. Organomet. Chem. **482**, 111 (1994).
[10] A. E. Beezer *et al.*, Thermochim. Acta **380**, 13 (2001).
[11] I. Wadsö and R. N. Goldberg, Pure Appl. Chem. **73**, 1625 (2001).
[12] J. M. Allen, S. K. Allen, and S. W. Baertschi, Photochem. Photobiol. **69**, 17s (1999).
[13] J. M. Allen, S. K. Allen, and S. W. Baertschi, J. Pharm. Biomed. Anal **24**, 167 (2000).

Application of Chemometric Analysis to Complexity in Isothermal Calorimetric Data

Michael A.A. O'Neill,*,† Anthony E Beezer,‡ John Tetteh,§ Simon Gaisford,‡ and Meena Dhuna‡

Department of Pharmacy and Pharmacology, University of Bath, Claverton Down, Bath BA2 7AY, U.K., School of Pharmacy, University of London, 29-39 Brunswick Square, London WC1N 1AX, U.K., and University of Greenwich, School of Sciences, Central Avenue, Chatham Maritime, ME4 4TB, U.K.

Received: January 5, 2007; In Final Form: April 16, 2007

The interpretation of complexity in isothermal calorimetric data is demanding. The observed power signal is a composite of the powers arising from each of the individual events occurring (which can involve physical, as well as chemical, change). The challenge, therefore, lies in deconvoluting the observed data into their component parts. Here, we discuss the potential use of chemometric analysis, because it offers the significant advantage of being model-free, using principal component analysis to deconvolute data. Using model data, we discovered that the software required a minimum trivariate data matrix to be constructed. Two variables, power and time, were available from the raw data. Selection of a third variable was more problematic, but it was found that by running multiple experiments the small variation in the number of moles of compound in each experiment was sufficient to allow a successful analysis. In general we noted that it required a minimum $2n + 2$ repeat experiments to allow analysis (where n is the number of reaction processes). The data outputted from the chemometric software were of the form intensity (arbitrary units) versus time, reflecting the fact that the software was written for analysis of spectroscopic data. We provide a mathematical treatment of the data that allows recovery of both reaction enthalpy and rate constants. The study demonstrates that chemometric analysis is a promising approach for the interpretation of complex calorimetric data.

Introduction

Quantitatively analyzing isothermal calorimetric data is not straightforward when more than one event contributes to the measured signal, because heat is ubiquitous and the calorimeter simply measures the net heat change. In some instances experimental design can be used to isolate (and hence investigate) each process, but increasingly it is desirable to study "whole" systems. Thus, methods of dealing with complexity in calorimetric data must be developed.

We have proposed a number of methods for quantitative analysis of complexity, both in solution[1-3] and solid states.[4] We have also discussed a method for the direct calculation of reaction parameters in complex systems.[5] However, these approaches shared the common drawback of requiring knowledge of the reaction mechanism. An alternative approach to the problem of complexity in data is the application of chemometric procedures via techniques such as principal component analysis (PCA).[6-7] Chemometric analyses are well established for spectroscopic data, and there are many commercially available software packages for this purpose (from, for example, DiKnow Ltd, U.K. and Infometrix Inc, U.S.A.). Chemometric analysis has been applied to the interpretation of non-isothermal calorimetric data (in particular to solid-state systems) where the complexity arises from the underlying (applied) change in temperature over the course of the experiment as well as any multistep chemical/physical processes. Such analyses are designed to recover the "kinetic trilogy" (rate constant, k, reaction order, n, and activation energy, E_a). Debate exists as to the best chemometric approach for the analysis of scanning calorimetric data, with a study dedicated to the comparison of the different methods being available: the ICTAC Kinetics Project.[8-13] However, currently there exists no chemometric package written specifically for the analysis of isothermal calorimetric data; addressing this significant knowledge gap is the focus of this paper.

We discuss here the potential application of chemometric analysis for interpretation of complex isothermal calorimetric data. The primary issue to be addressed is to determine unequivocally the number of reaction processes; since there is no (direct) molecular information in isothermal calorimetric data there is a need to find a matrix that can yield the number of processes and the reaction order. Subsequent analysis can be performed to recover kinetic and thermodynamic parameters. As a check on the appropriateness of analysis, there is a requirement that all reaction orders are integral. This paper is concerned with showing that this analysis is possible. For the purposes of discussion, this paper focuses on consecutive reaction schemes, but we will return to the subject of more complex pathways in a future publication.

Experimental Methods

Chemometric Analysis. The measured power from the calorimeter is the sum of the power outputs for each constituent reaction at defined times. The initial purpose of a meaningful chemometric analysis must then be to determine the *number* of reaction processes that comprise the overall data. A test of such deconvolution is that the reaction order of each process is *integral*. Once the number and orders of individual processes

* Corresponding author. E-mail: mon20@bath.ac.uk. Telephone: +44 (0) 1225 386797. Fax: +44 (0) 1225 386114.
† University of Bath.
‡ University of London.
§ University of Greenwich.

10.1021/jp0700985 CCC: $37.00
Published on Web 06/22/2007

are known, then reaction parameters can be recovered by classical analyses such as those we have already proposed.[1-4]

From the perspective of pattern analysis, each component in the system will exhibit a unique maximum during the course of the reaction at a defined time which suggests that the data may be analyzed by a multivariate method if a suitable matrix can be generated. Multivariate data are easily generated in spectroscopic systems[14] (for instance, intensity as a function of wavenumber, time, pH, temperature, etc.). Calorimetric data recorded at a fixed temperature are univariate, and there is, therefore, the need to engineer a third (intensity, or S) factor of the matrix. S could, for instance, be obtained from replicate runs of the same experiment. These runs may be designed such that each one varies from the other in the total power output (for example, variation in sample loading or weight for repeated experiments provides S sets of data). A system in which X species evolve after time t will require at least $2X + 2$ replicate runs (i.e., $S = 2X + 2$) to create a suitable matrix, M, which can then be analyzed to determine the rank of the data through multivariate data decomposition.

In the work reported here, factor analysis was used to deconvolute the data matrix on the assumption that (i) the power signal at time t is a linear sum of all species present at that moment and (ii) that the power signal is proportional to the sample load in the calorimeter. The data deconvolution and further treatments required to furnish the underlining evolution profile of a suitably simulated experimental data set are presented in the data analysis section of this paper. The algorithms and methods are embodied in software called InSight[15] coded in Matlab.[16] All chemometric data analysis was performed through this software.

Principles of Analysis. Calorimetric power−time data, at a fixed temperature, for the same sample with variable weights generate a data matrix M whose rows, in the work reported in this paper, represent the time (t) points. The columns represent variation in sample weight (w), and it is assumed that the reaction's kinetic parameters are not changed by sample size and that the instrument exhibits random noise for each sample run (S, 1 to m; m is the number of runs). The deconvolution of M without prior knowledge will at least provide a basic understanding of the underlying factors or species in the reaction over a time period, t. In this work, we used a modified target factor analysis (TFA) technique to analyze the data. TFA is used to determine whether or not a hypothetical vector, gleaned from chemical principles or heuristic intuition, lies inside the factor space and thus contributes to the phenomenon.[17-18] The analytical strength of target testing lies in the fact that each hypothetical vector can be tested individually for significance in the presence of a host of other unknown factors. When a data matrix has been deconvoluted into abstract factors (also known as principal components) in the row and column space of the data M and the numbers of significant factors have been determined, these significant factors can be subjected to various forms of mathematical scrutiny to determine if they have real chemical or physical meaning. In this work the mathematical technique of singular value decomposition (SVD)[19]was used for the deconvolution process involved in the TFA process.

Equations 1−6 summarize the mathematical principles used to deconvolute the "spectral" data, M. The principal factor matrices describing the row and column information are R and C respectively. R and C are the significant components of the matrix after excluding E, the error or noise added to the data from the instrument to data, M. Recombination of the significant row and columns R and C produces a new matrix M_x, eq 2. X_t are hypothetical j sets of vectors that are considered fully to describe the data M_x. Various schemes have been proposed to determine X_t. In this paper the so-called needle search method (fully described elsewhere[14-15]) was employed. Essentially, initial hypothetical test vectors are generated by setting all time points to zero except those points that show significant power intensity for each of the j factors identified. From these test vectors, prototype profiles are generated after target testing. An iterative or interactive method is then used to select the unique set of X_t that best describes the data. Operating the pseudoinverse of R, i.e. R^+ with X_t yields T, the transformation matrix indicated in eq 3. This parameter, T, is used to obtain X_j and Y. The parameter X_n represents the predicted test matrix based on the X_t (see eq 4) and describes the row domain real information, which are the predicted evolution profiles for each of the significant j factors identified in the data matrix, M. Y is the column domain real information matrix, equivalent to the predicted power output profiles obtained from eq 5. Recombination of X_n and Y produces M_n the significant part of the data matrix, M. The differences between M_n and M_x are minimized. An extended treatment of theory and applications of TFA can be found elsewhere.[14-15]

$$M = [RC] + E \tag{1}$$

$$M_x = RC \tag{2}$$

$$T = R^+X_t \tag{3}$$

$$X_n = RT \tag{4}$$

$$Y = T^+C \tag{5}$$

$$M_n = X_n\mathrm{Y} \tag{6}$$

Data Simulation. Simulated data were created to allow exploration of the range of applicability of the proposed method. Simulated data offer the advantage that the reaction mechanism and reaction parameters are known unequivocally. It was regarded as essential for success that the methods described herein should require no information other than the sample load placed into the calorimeter and the associated power-time outputs observed over a reasonable time period (24 h in this instance). Thus, no model was imposed on the data during chemometric analysis for interpretation of mechanism. The first objective was to determine whether the analysis could correctly identify the number of processes involved in the reaction and their concentration profiles. Values for the target parameters (first-order rate constant, k, and reaction enthalpy ΔH) were selected for a consecutive reaction system (A to B to C to D). The power outputs as a function of time for each component reaction were then calculated using eqs 7−9[20]

$$P_{A\rightarrow B} = H_1k_1A_0\,\mathrm{e}^{-k_1t} \tag{7}$$

$$P_{B\rightarrow C} = H_2\left[A_0k_1\mathrm{k}_2\frac{(-\mathrm{e}^{k_1t} + \mathrm{e}^{-k_2t})}{(k_1 - k_2)}\right] \tag{8}$$

$$P_{C\rightarrow D} = \Delta H_3\left[A_0k_1k_2k_3\left(\frac{\mathrm{e}^{-k_1t}}{(k_2 - k_1)(k_3 - k_1)} + \frac{\mathrm{e}^{-k_2t}}{(k_1 - k_2)(k_3 - k_2)} + \frac{\mathrm{e}^{-k_3t}}{(k_1 - k_3)(k_2 - k_3)}\right)\right] \tag{9}$$

where P (J s^{-1}) is the calorimetric output (power) and A_0 is the initial quantity of reactant (mol). The subscripted numbers denote the reaction step.

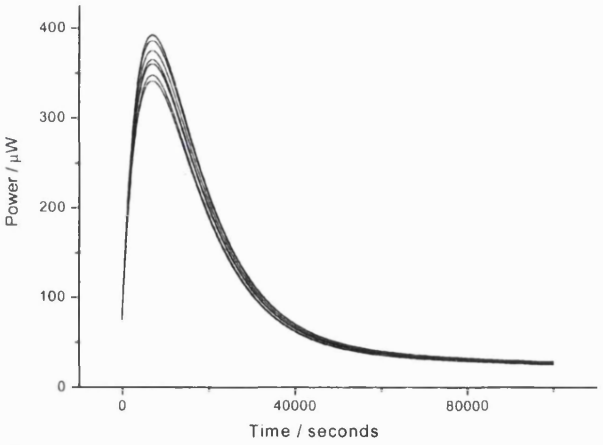

Figure 1. Set of simulated data entered into the chemometric software for PCA analysis.

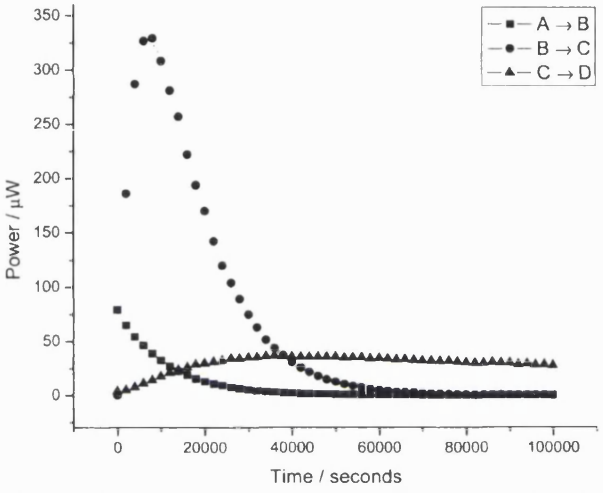

Figure 2. Component steps of the simulated data shown in Figure 1.

The simulated observed calorimetric output is then simply a summation of these reaction steps.

It was noted earlier that successful chemometric analysis usually requires a multi- (at least tri-) variate data matrix. The raw calorimetric data (power and time) provide two variables, and hence, a third parameter must be generated. Since in reality there is a contribution to the calorimetric signal from inherent noise within the system (electrical, thermal etc) as well as slight variations in experimental parameters (variations in sample weighing for instance), we opted to add a random error function to the simulated data as the third variable. This was achieved by (i) adding a random noise value to the enthalpy value used when creating data and (ii) varying the value of A_0 between data sets.

The final data matrix thus consisted simply of files of power-time data for 8 different (arbitrary) initial concentration values of A_0 with overlaid noise; an example data set can be seen in Figure 1. The set of individual power-time data which comprise the "overall" simulated data can be found in Figure 2. Only the overall data files were submitted to the chemometric program; thus, as noted above, no information on mechanism was provided prior to analysis.

The k values used to generate the simulated data for the three reaction steps were 9×10^{-5} s^{-1}, 2×10^{-4} s^{-1}, and 5×10^{-6} s^{-1} respectively. The ΔH values used for the simulation were 10, 80 and 90 kJ mol^{-1} (the percentage variation imposed was a random value between +2% and −2% of the enthalpy value) respectively. The values of A_0 ranged from 7.5×10^{-5} to 9×10^{-5} moles.

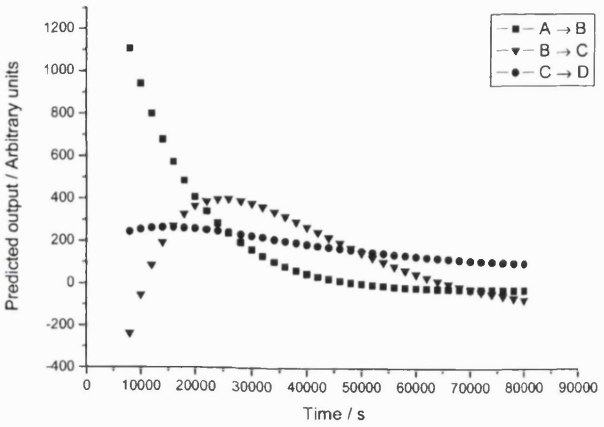

Figure 3. Three principal components outputted from the chemometric analysis (further factors were indistinguishable from noise, data not shown).

Results/Discussion

The simulated data were entered into the InSight program and subjected to PCA analysis. The first test of the software was the determination of the number of reaction steps (or principal components). In order to effect this statistical examination three criteria were used; the statistical F-test, the percentage cumulative variance in the data and a visual examination of the factors in both row and column domains. The InSight software package performs the statistical tests as part of the deconvolution process and comprehensively described three principal factors, co-incident with the model used to generate the data. Additional factors were indistinguishable from noise. This was further confirmed by visual inspection of the output, which also revealed three principal factors (shown in Figure 3). Thus, the first objective stated earlier, the ability of the software to determine the number of principal components, was demonstrated (note that although we have used a three-step model as an example, similar analyses of other consecutive data sets with varying numbers of steps always produces the correct number of principal factors; data not shown).

The next step was to confirm that each process identified by the analysis was integral order because, as noted above, this acts to demonstrate appropriateness of the output. There are several ways to accomplish this but we opted to use the data pairing technique derived by Willson.[21] In brief this algorithm takes pairs of data points and uses the derived ratios to predict an order of reaction. While this works perfectly with simulated data (i.e., integral numbers are returned for the predicted order of reaction) for our data set we returned values for reaction orders which were not integral but did return values for each step of 1 ± 0.2, i.e., the returned order values could be rounded up or down with reasonable confidence. It is perhaps unsurprising that this is so as real data have an element of random noise interspersed within the signal. This has the effect of introducing some uncertainty to the returned order values. Moreover the returned chemometric data sets do not reflect a "real" calorimetric output but are a composite response of the number of repeat data sets submitted to the software. Hence it is likely that further error will be incorporated into the analysis. Thus far we have demonstrated that complex isothermal calorimetric data are amenable to chemometric analysis to yield,

as a minimum, the number of reaction processes and their respective reaction orders. Once these values are known it is possible to select an appropriate reaction mechanism and analyze the original calorimetric data using the techniques we have already established.[1-4,22]

One interesting, and unexpected, issue that arose from this study is that the deconvoluted data had no defined *y*-axis units (the software plots the principal components as an arbitrary intensity; a result of the fact that the software package used was designed for spectroscopic analyses). This is a consequence of a deconvolution process in which no calibration curve is used (it is impossible to generate such a curve for calorimetric data). Although it is possible, once the mechanism is known, to return to the original data and analyze them using established techniques, it is interesting to consider whether quantitative reaction parameters can be determined from the chemometric output, both from an academic standpoint and because the values obtained would give good estimates for further analyses. While the rate constant values should be easy to ascertain (because they are time dependent, and the time axis is unaffected by chemometric deconvolution) the enthalpy values are not (because they are power dependent). One approach is to consider analysis based on fractional extents of reaction, since this normalizes the *y*-axis data. We show below a method for determining both parameters, considering up to three reaction steps; extension to longer schemes is easily achieved by following the same principles.

Calculation of Rate Constants. The determination of k_1 is straightforward; a plot of ln(intensity) versus time for the first principal component should be linear, and the slope gives the rate constant. An alternative, approximate, method would be to plot ln(power) versus time (i.e., the observed calorimetric data) and take the slope over the initial few hours of data (where the reaction *A* to *B* predominates).

In the case of a two-step reaction, the value of k_2 can be calculated as follows because there is only one intermediate compound. The concentration of product *C* as a function of time is given by

$$[C] = A_0\left[1 + \frac{1}{k_1 - k_2}(k_2\, e^{-k_1 t} - k_1\, e^{-k_2 t})\right] \qquad (10)$$

Assuming that all of *A* will degrade to *C*, then when 50% of the reaction has occurred

$$[C] = \frac{A_0}{2} \qquad (11)$$

and hence

$$F = 0.5 = 1 + \frac{1}{k_1 - k_2}[(k_2\, e^{-k_1 t_{50}}) - (k_1\, e^{-k_2 t_{50}})] \qquad (12)$$

where *F* is the fraction of reaction that has occurred and t_{50} is the time at which 50% of reaction has occurred. (t_{50} can be calculated a number of ways; if the reaction has progressed to completion during the experimental time frame then fractional areas suffice. Alternatively, the amount of degradation that has occurred during the experiment can be quantified post measurement by a complementary analysis. Note also that there is no requirement for 50% to be the required fraction of reaction; the method is equally valid for any fraction of reaction.) The value of k_2 is then easily calculated by iteration.

If there are more than two consecutive steps, then an alternative method must be used to determine the rate constants, although the rate constant for the final step can be obtained as above (if one remembers to substitute the appropriate rate constants and concentration terms). Here, it is required that the time for maximum rate (t_{max}) to be attained is known; this corresponds to the peak power output in the power-time curve. It can be shown from classical reaction kinetics that

$$\frac{k_1\, e^{-k_1 t_{max}}}{k_2 - k_1} + \frac{k_2\, e^{-k_2 t_{max}}}{k_1 - k_2} = 0 \qquad (13)$$

As before, the value of k_2 is easily determined by iteration.

Calculation of Reaction Enthalpies. Once the rate constants are determined, reaction enthalpies are easily calculated. We present two methods: one based upon two power−time data and one upon two heat−time data. While the two methods are equivalent when applied to simulated data, it is likely that, in practice, the heat−time method will be more robust, because it averages data over the time range selected.

Calculation of Reaction Enthalpies from Two Power−Time Points. The power output for a reaction that proceeds through two consecutive, first-order steps is given by summation of eqs 7 and 8

$$\frac{dq}{dt} = k_1 H_1 A_0\, e^{-k_1 t} + k_1 k_2 H_2 A_0 \frac{e^{-k_1 t} - e^{-k_2 t}}{k_2 - k_1} \qquad (14)$$

It is therefore possible to select from the experimental data the instantaneous power outputs (P_1 and P_2) at two respective time points (t_1 and t_2) and write

$$P_1 = k_1 H_1 A_0\, e^{-k_1 t_1} + k_1 k_2 H_2 A_0 \frac{e^{-k_1 t_1} - e^{-k_2 t_1}}{k_2 - k_1} \qquad (15)$$

$$P_2 = k_1 H_1 A_0\, e^{-k_1 t_2} + k_1 k_2 H_2 A_0 \frac{e^{-k_1 t_2} - e^{-k_2 t_2}}{k_2 - k_1} \qquad (16)$$

Rewriting eq 15 to make H_1 the subject

$$H_1 = \frac{P_1(k_2 - k_1) - k_1 k_2 A_0 H_2(e^{-k_1 t_1} - e^{-k_2 t_1})}{k_1 A_0 (k_2 - k_1)\, e^{-k_1 t_1}} \qquad (17)$$

Substituting eq 17 into eq 16 and rearranging for H_2 gives

$$H_2 = \frac{(k_2 - k_1)(P_1\, e^{-k_1 t_2} - P_2\, e^{-k_1 t_1})}{k_1 k_2 A_0 (e^{-k_1 t_1 - k_2 t_2} - e^{-k_1 t_2 - k_2 t_1})} \qquad (18)$$

Thus, eq 18 can be used to calculate the value of H_2. Knowledge of H_2 then allows H_1 to be calculated. If t_1 is selected to be zero, then P_1 becomes equal to the initial power output of the reaction, and eq 18 reduces to

$$H_2 = \frac{(k_2 - k_1)(P_1\, e^{-k_1 t_2} - P_2)}{k_1 k_2 A_0 (e^{-k_2 t_2} - e^{-k_1 t_2})} \qquad (19)$$

A further discussion of the practicality of the use of t_0 as a reference point can be found below.

Calculation of Reaction Enthalpies from Two Heat−Time Points. In this case, the heat outputs (q_1 and q_2) at two time points (t_1 and t_2) are required. The heats correspond to the area under the curve up to the two time points and can easily be determined using a mathematical analysis package (such as Origin, Microcal Software Inc.). However, in order to show the derivation of this approach, it is necessary to consider the

mathematical equations that give these values; these are the integrals of eq14 between t_i and t_1 and t_i and t_2 (where t_i is some initial time which does not have to be zero) and are represented by

$$q_1 = A_0H_1(k_1\,e^{-t_1k_1} - k_2\,e^{-t_1k_1} + k_2\,e^{-t_ik_1} - k_1\,e^{-t_ik_1}) + A_0H_2(k_1\,e^{-t_1k_2} - k_1\,e^{-t_ik_2} + k_2\,e^{-t_1k_1} - k_2\,e^{-t_1k_1})/(k_2 - k_1) \quad (20)$$

$$q_2 = A_0H_1(k_1\,e^{-t_2k_1} - k_2\,e^{-t_2k_1} + k_2\,e^{-t_ik_1} - k_1\,e^{-t_ik_1}) + A_0H_2(k_1\,e^{-t_2k_2} - k_1\,e^{-t_ik_2} + k_2\,e^{-t_ik_1} - k_2\,e^{-t_2k_1})/(k_2 - k_1) \quad (21)$$

Rewriting eq 20 to make H_1 the subject gives

$$H_1 = \left[\frac{q_1(k_2 - k_1)}{A_0} - H_2k_2\,e^{-t_ik_1} + H_2k_1\,e^{-t_ik_2} + H_2k_2\,e^{-t_1k_1} - H_2k_1\,e^{-t_1k_2}\right]/(-k_2\,e^{-t_1k_1} + k_1\,e^{-t_1k_1} + k_2\,e^{-t_ik_1} - k_1\,e^{-t_ik_1}) \quad (22)$$

Substituting eq 22 into eq 21 and rearranging for H_2 gives

$$H_2 = -q_2[(-e^{-t_ik_1} + e^{-t_1k_1})(k_2 - k_1)] - q_1[((k_2 - k_1)\,e^{-2t_ik_1}) + ((k_1 - k_2)\,e^{-(t_i + t_2)k_1})]/A_0(k_2\alpha + k_1\beta) \quad (23)$$

where

$$\alpha = e^{-t_2k_1} - e^{-k_1(2t_i + t_2)} - e^{-t_ik_1} + e^{-3t_ik_1} \quad (24)$$

and

$$\beta = e^{-t_ik_1 - t_ik_2 - t_1k_1} + e^{-t_1k_2 - t_ik_1 - t_2k_1} + e^{-2t_ik_1 - t_2k_2} - e^{-t_2k_2 - t_ik_1 - t_1k_1} - e^{-t_1k_2 - 2t_ik_1} - e^{-t_ik_1 - t_ik_2 - t_2k_1} \quad (25)$$

Thus, eq 23 can be used to calculate the value of H_2. Knowledge of H_2, as before, allows H_1 to be calculated from eq 14. In the special case where $t_i = t_0$ (i.e., the time at which the reaction was initiated), eq 23 reduces to

$$H_2 = \frac{-q_2[(e^{-t_1k_1} - 1)(k_2 - k_1)] - q_1[(k_2 - k_1) + (k_1 - k_2)\,e^{-t_2k_1}]}{A_0k_1(e^{-t_1k_1} + e^{-t_1k_2 - t_2k_1} + e^{-t_2k_2} - e^{-t_2k_2 - t_1k_1} - e^{-t_1k_2} - e^{-t_2k_1})} \quad (26)$$

In most calorimetric experiments there is a time delay between the initiation of reaction and the commencement of data measurement, commensurate with the fact that ampules are usually prepared externally from the calorimeter. However, it is also usually the case that the percentage of data lost is negligible (for long-term reactions) or that the data can be extrapolated to the initiation time (for short-term reactions). We have shown previously[5,22] using simulated data for single-step processes that extrapolation to t_0 by fitting the measured data to a suitable exponential or polynomial equation returns a value that is entirely consistent with that expected. In either case, eq 19 or 26 can be used to determine H_2.

Summary

The purpose of this study was to ascertain whether PCA analysis was capable of analyzing complex data where it was difficult to construct a trivariate data matrix. By incorporating small differences in the quantity of material studied we have shown that PCA does indeed have merit. In particular, it is clear that the deconvolution process reveals the correct number of processes, although it is also apparent that the deconvoluted data do not mimic exactly those that were generated initially (they are however, very close). The reasons for this are unclear although several possibilities present themselves; the output from the chemometric deconvolution is an average of the data sets (8 in this case) inputted and hence do not exactly describe any one of them individually; another reason may be scarcity of the data. Nevertheless, the fact remains that the software allows distinction of the contributing factors to the calorimetric signal. At the very least this reduces the burden on any further kinetic/thermodynamic analysis of the data by allowing an appropriate kinetic model to be employed in an iterative analysis. From the successful deconvolution of simulated data there is an increased confidence in any results returned from data that describe a real system. Although this discussion has centered on consecutive reaction schemes, and we have proposed methods for quantitative analysis of such data, we do not envisage problems with extending the methodology to other, more complex schemes.

References and Notes

(1) Willson, R. J.; Beezer, A. E.; Mitchell, J. C.; Loh, W. *J. Phys. Chem. B* **1995**, *99*, 7108.

(2) O'Neill, M. A. A. *Curr. Pharm. Biotechnol.* **2005**, *6*, 251.

(3) Skaria, C. V.; Gaisford, S.; O'Neill, M. A. A.; Buckton, G.; Beezer, A. E. *Int. J. Pharm.* **2005**, *292*, 127.

(4) O'Neill, M. A. A.; Beezer, A. E.; Morris, A. C.; Urakami, K.; Willson, R. J.; Connor, J. A. *J. Therm. Anal. Calorim.* **2003**, *73*, 709.

(5) Beezer, A. E.; Morris, A. C.; O'Neill, M. A. A.; Willson, R. J.; Hills, A.; Mitchell, J. C.; Connor, J. A. *J. Phys. Chem. B* **2001**, *105*, 1212.

(6) Galwey, A. K. *Thermochim. Acta* **2003**, *407*, 93.

(7) Dias, M.; Hadgraft, J.; Raghavan, S. L.; Tetteh, J. *J. Pharm. Sci.* **2004**, *93*, 186.

(8) Brown, M. E.; Galwey, A. K.; *Thermochim. Acta* **2000**, *387* 173.

(9) Brown, M. E.; Maciejewski, M.; Vyazovkin, S.; Nomen, R.; Sempere, J.; Burnham, A.; Opfermann, J.; Strey, R.; Anderson, H. L.; Kemmler, A.; Keuleers, R.; Janssens, J.; Desseyn, H. O.; Chao-Rui Li.; Tang, T. B.; Roduit, B.; Malek, J.; Mitsuhashi, T. *Thermochim. Acta* **2000**, *355*, 125.

(10) Maciejewski, M. *Thermochim. Acta* **2000**, *355*, 145.

(11) Vyazovkin, S. *Thermochim. Acta* **2000**, *355*, 155.

(12) Burnham, A. K. *Thermochim. Acta* **2000**, *355*, 165.

(13) Roduit, B. *Thermochim. Acta* **2000**, *355*, 171.

(14) Geladi, P. *Spectrochim. Acta, Part B* **2003**, *58*, 767.

(15) InSight User Manual; DiKnow Ltd.: London, 2000.

(16) Matlab User Manual; Mathworks Inc. U.S.A., 1999.

(17) Malinowski, E. *Factor Analysis in Chemistry*, 2nd ed.; Wiley: New York, 1991.

(18) Tetteh, J. Enhanced Target Factor Analysis and Radial Basis Function Neural Network for Analytical Spectroscopy. Ph.D. Thesis, University of Greenwich, London, U.K., 1997.

(19) Johnson, R. M. *Psychometrika* **1963** *28, 259.*

(20) Gaisford, S.; Hills, A. K.; Beezer, A. E.; Mitchell, J. C. *Thermochim. Acta* **1999**, *328, 39.*

(21) Willson, R. J.; Beezer, A. E. *Thermochimica Acta* **2003**, *402*, 75.

(22) O'Neill, M. A. A. Ph.D. Thesis, University of Greenwich, London, U.K., 2002.